Analysis of Protein Transport to the Inner Nuclear Membrane

Dissertation
for the award of the degree
“Doctor rerum naturalium”
of the Georg-August-Universität Göttingen

within the doctoral program “Molecular Biology of Cells”
of the Georg-August University School of Science (GAUSS)

submitted by
Marina Blenski

from Bobingen

Göttingen 2019

Thesis Committee / Examination Board

Prof. Dr. Ralph H. Kehlenbach (1st referee)
Department of Molecular Biology
University Medical Center Göttingen
Georg-August-Universität Göttingen

Prof. Dr. Michael Meinecke (2nd referee)
Department of Cellular Biochemistry
University Medical Center Göttingen

Prof. Dr. Steven Johnsen
Clinic for General, Visceral and Pediatric Surgery
University Medical Center Göttingen

Further members of the Examination Board

Prof. Dr. Blanche Schwappach
Department of Molecular Biology
University Medical Center Göttingen
Georg-August-Universität Göttingen

Prof. Dr. Heike Krebber
Department of Molecular Genetics
Institute for Microbiology and Genetics
Georg-August-Universität Göttingen

Dr. Alexander Stein
Membrane Protein Biochemistry
Max Planck Institute for Biophysical Chemistry, Göttingen

Date of oral examination: **25th June 2019**

Statutory declaration

I hereby declare that I have written this PhD thesis independently with no other sources and aids than clearly stated.

This thesis was not submitted in the same or in a substantially similar version to any other authority to achieve an academic grading and was not published elsewhere.

Göttingen, May 2019

Marina Blenski

Contents

Abstract

The eukaryotic cell is divided into different compartments. The biggest compartment is the nucleus which is formed by one lipid bilayer folded into two membranes: the outer nuclear membrane (ONM) and the inner nuclear membrane (INM). The ONM is continuous with the endoplasmic reticulum (ER) membrane and merges with the INM at a curved piece of membrane at the level of the nuclear pore complex (NPC). The NPC controls the exchange of proteins or other molecules between the cytoplasm and the nuclear compartment. While the active transport of soluble proteins via the NPC mediated by transport factors is well studied, less is known about the targeting of membrane proteins to the INM.

Most membrane proteins are first inserted into the ER-membrane before they are targeted to their destination. A nascent polypeptide chain can be inserted into the ER-membrane during translation in a co-translational manner or post-translationally after termination of translation. The best described route of post-translational insertion into the ER-membrane of tail-anchored proteins, which are membrane proteins with a very short C-terminus, is the TRC (transmembrane domain-recognition complex) pathway. In this study, the insertion mechanism of the single-pass membrane protein LRRC59 (leucine-rich repeat-containing protein 59) into the ER-membrane is analyzed by *in vitro* microsome integration assays. LRRC59 is shown to be a tail-anchored protein, which can be post-translationally inserted independently of the TRC pathway.

In former studies, LRRC59 was found at the ER-membrane and the nuclear envelope, a localization that was suggested to depend on the nuclear transport factor importin β. In this thesis, by usage of rapamycin-induced dimerization assays, a localization to the INM could be confirmed. However, INM targeting of LRRC59 is independent of importin β. Additionally, the extraluminal region of LRRC59 does not contain a nuclear localization signal. Instead, the efficiency of INM targeting of LRRC59 was shown to depend on the size of the extraluminal domain, suggesting passive diffusion of LRRC59 to the INM by peripheral channels of the NPC.

In addition to LRRC59, the ER located integral membrane proteins Sec61β, DDOST and Ube2j1 were shown to reach the INM mainly by passive diffusion. The INM targeting of these proteins were not only dependent on the size of the extraluminal domain but also on the geometry of the inserted tags in the rapamycin-induced dimerization assay. These results suggest that some ER-membrane proteins might reach the INM by diffusion as long as they fulfill the size restriction to pass the peripheral channels of the NPC.

1 Introduction

One of the main characteristic features of a eukaryotic cell is its compartmentalization. The biggest compartment is the nucleus, which contains the majority of genetic material. The nucleus spatially separates transcription of DNA into mRNA from translation, the process of protein synthesis, which occurs in the cytoplasm (Moog and Maier, 2017). The division of the cell into a nuclear region and the cytoplasm requires an active transport mechanism between these two compartments (Wente and Rout, 2010; Purves et al., 2006b). The following chapter of the introduction will focus on the structure of the nucleus and its nuclear pore complexes (NPCs) mediating a regulated active transport together with transport factors. Additionally, an overview is given about insertion of membrane proteins into the endoplasmic reticulum (ER) membrane and the current status in research about nuclear targeting of some of these membrane-embedded proteins to the inner nuclear membrane. This chapter will introduce the model protein LRRC59 and outline the aims of this thesis.

1.1 The Nucleus and the Nuclear Envelope

The nucleus is formed by a single phospholipid bilayer, which is folded into two membranes, an outer nuclear membrane (ONM) and an inner nuclear membrane (INM). The ONM is continuous with the ER-membrane and also merges with the INM at a curved piece of membrane adjacent to the nuclear pore complex (NPC). The INM and the ONM are separated by 10-50 nm with a luminal/perinuclear space (Moog and Maier, 2017; Gruenbaum, 2015; Schooley et al., 2012). The membrane protein composition of the ONM is different from the INM. While the ONM and the membrane of the rough ER share many membrane proteins with the exception of specific ONM protein complexes, the INM contains a specific set of membrane proteins (Lusk et al., 2007). Some of these INM proteins can directly interact with chromatin or peripheral associated INM proteins (Katta et al., 2014; Ungricht and Kutay, 2015; Murthi and Hopper, 2005; Lai et al., 2009).

The nuclear envelope (NE) is defined as the ONM and INM, the luminal space and the sum of the NPCs (Ungricht and Kutay, 2017) (figure 1). The interior of the nucleus, also called the nucleoplasm, stores the majority of genetic material of the cell and is organized in several membraneless suborganelles e.g. the nucleolus, which contains ribosomal genes and is the place of ribosomal biogenesis (Tsekrekou et al., 2017). The DNA containing genetic information is organized in euchromatin and heterochromatin. While euchromatin is defined as DNA-regions in a less-condensed form, heterochromatin is highly condensed (Solovei et al., 2016). Underneath the INM, intermediate filaments or lamins, form a meshwork. Within this meshwork, there are different types of lamins, A-type (lamins A and C) and B-type lamins (lamins B1 and B2), which overlap each other. Lamins maintain and stabilize the nuclear shape and anchor chromatin to the NE as well as the membrane-embedded NPCs. Lamins are peripheral associated INM proteins and can be bound by INM proteins such as emerin (Burke and Stewart, 2013; Schooley et al., 2012; Shimi et al., 2010). The LINC (linker of nucleoskeleton and cytoskeleton) complex, consisting of SUN (Sad1-UNC-84 homology) domain containing proteins, interacts with the lamins resulting in an indirect connection of nuclear and cytoplasmic architecture (Schooley et al., 2012; Starr and Fridolfsson, 2010; Burke, 2012).

Within the NE, many NPCs are embedded in the concentric membrane-bilayer (in U2OS cells: 3000 ± 1000 NPC (Beck et al., 2011)) and control the import of proteins from the cytoplasm into the nucleus and export from the nucleus into the cytoplasm (Beck and Hurt, 2017). The NPC acts as a highly selective bidirectional gatekeeper, which inhibits free diffusion of proteins with a molecular mass higher than ~40 kDa from one compartment to the other (Wente and Rout, 2010). Therefore, an active transport mechanism for cargos mediated by transport factors is needed in eukaryotic cells. Proteins with a smaller molecular mass, ions, water and small metabolites can enter the nucleus through the NPC using passive diffusion (Beck and Hurt, 2017; Terry and Wente, 2009). For further information about nuclear import of soluble proteins see section 1.1.2. For a schematic overview of the NE see figure 1.

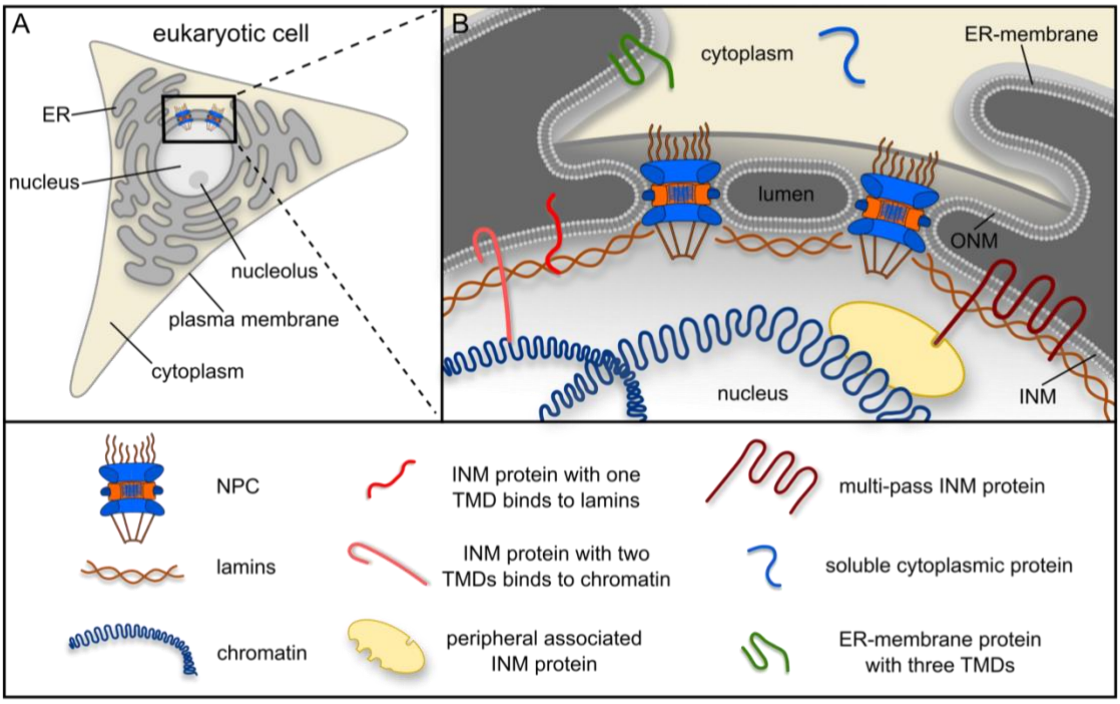

Figure 1: Schematic overview of a eukaryotic cell with focus on the NE.
(A) The simplified overview of a eukaryotic cell shows the endoplasmic reticulum (ER), the nucleus, the nucleolus, the cytoplasm and the plasma membrane. The rectangle indicates the area of interest for (B). (B) The scheme shows the nuclear pore complexes (NPCs) embedded into the inner (INM) and outer (ONM) nuclear membrane. In the membranes of ER and nucleus, different types of membrane proteins containing at least one transmembrane domain (TMD) are represented by various examples in the scheme. Located in the INM, these proteins can interact with lamins, chromatin or peripheral associated INM proteins. For instance, the LEM (LAP2, emerin, MAN1) domain containing proteins emerin or LAP2β (lamina-associated polypeptide 2β) interact with BAF (barrier of autointegration factor), a peripheral chromatin-associated protein (Lee et al., 2001; Shumaker et al., 2001). In addition, soluble proteins can be found in all compartments of the eukaryotic cell. Scheme inspired by Schooley et al., 2012.

1.1.1 Nuclear Pore Complex

In mammalian cells, the NPC has a molecular mass of around 120 MDa (Beck and Hurt, 2017) and is so far the largest identified protein complex. In contrast to ion channels or translocons, which permeate the membrane via a hydrophobic stretch, the NPC perforates the double lipid bilayer of ONM and INM creating pores of 100 nm diameter in the membrane (Weberruss and Antonin, 2016). This special way of membrane embedding leads to the curvature of the nuclear membrane next to the NPC. Within the NE, the number and density of embedded NPCs can vary between organisms of different species, but also within one organism according to the cell type, phase of the cell cycle and the developmental stage of a cell (Grossman et al., 2012). For instance, cells of vertebrates contain around 10-20 pores/µm^2 each nucleus (2000-5000 pores/nucleus), while *Xenopus laevis* oocytes have ~60 pores/µm^2 and yeast cells have 12 pores/µm^2 (Winey et al., 1997; Görlich and Kutay, 1999; Fabre and Hurt, 1997; Grossman et al., 2012; Beck et al., 2011).

The main function of the NPC is the controlled exchange of proteins or other molecules between the cytoplasm and the nuclear compartment (Beck and Hurt, 2017; Christie et al., 2016). The nucleocytoplasmic transport occurs via the central channel of the NPC, which is around 50 nm in diameter, while the overall dimensions of the NPC itself is approximately 120 nm in width and around 85 nm in height (Grossman et al., 2012). In addition to the central channel of the NPC, lateral channels, also called peripheral channels, with a diameter of 5-10 nm have been identified by electron microscopy to be adjacent to the membrane (Hinshaw et al., 1992; Beck et al., 2007; Maimon et al., 2012). In addition to nucleocytoplasmic transport, the NPC is also involved in regulation of gene expression (Ptak

et al., 2014; Van de Vosse et al., 2011) and cell cycle (Capelson et al., 2010), chromatin organization (Krull et al., 2010) and DNA repair (Therizols et al., 2006).

Schematic subdivision of the NPC

With the progression in transmission electron microscopy, the understanding of the structure of the NPC has increased. It could be shown that the NPC consists of only approximately 30 different components (Cronshaw et al., 2002; Schwartz, 2016). These proteins are named nucleoporins (Nups) and have a molecular mass up to 358 kDa. The high molecular mass of the NPC is due to (multiple) 8-fold copies (8-64) of the conserved Nups within a single NPC (Beck and Hurt, 2017; von Appen and Beck, 2016). In a view on top of the pore, the NPC is assembled of eight asymmetric spokes. In a side view (figure 2), each spoke is composed of a cytoplasmic and a nucleoplasmic half, connected at the equator of the NPC (Hinshaw et al., 1992; Akey and Radermacher, 1993). The structural motives of the Nups dictate their localization within these spokes. Nucleoporins can therefore be divided into three classifications (Grossman et al., 2012; Weberruss and Antonin, 2016): membrane anchored Nups contain a transmembrane domain (TMD), barrier Nups are defined by the presence of phenylalanine-glycine-rich (FG) repeats, and scaffold Nups, which form three parts, an outer and an inner ring and a linker. The scaffold is reflected at the equator of the NPC, one copy is facing the cytoplasm (cytoplasmic ring) and the second is located at the nuclear side (nucleoplasmic ring). In addition to these symmetric parts, the NPC also comprises asymmetric segments: the cytoplasmic filaments assembled by FG-repeat containing Nups and nuclear Nups forming a basket-like structure (Grossman et al., 2012; Suntharalingam and Wente, 2003; Alber et al., 2007) (figure 2).

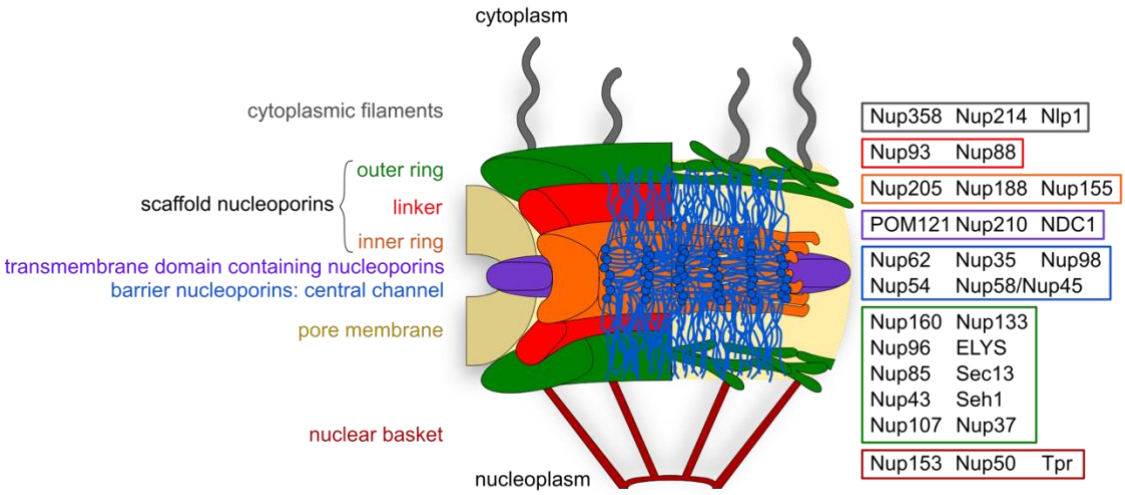

Figure 2: Several proteins assemble into the large protein complex of the NPC.
Schematic sideview of the NPC dividing the complex into several structural parts. The symmetric part of the NPC is assembled by scaffold, transmembrane domain containing and barrier nucleoporins. The asymmetric segments are comprised of cytoplasmic filaments and nuclear nucleoporins forming a basket-like shape. The different nucleoporins are assigned to the classifications by color. Scheme modified according to Weberrus and Antonin, 2016, Wente and Rout, 2010 and Grossman et al., 2012.

The main function of the **scaffold nucleoporins** is to connect the TMD-containing Nups to the barrier Nups for stabilization of the NPC (Grossman et al., 2012). Most Nups of the scaffold structure are incorporated in the NPC for the entire life span of nondividing cells (D'Angelo et al., 2009). The outer ring of the scaffold Nups is formed by copies of the Nup107-Nup160 complex, also called the Y-complex, which consists of the ten nucleoporins Nup160, Nup37, ELYS, Nup96, Sec13, Nup85, Seh1, Nup43, Nup107 and Nup133 (Hoelz et al., 2016). A conformational change within the Y-complex seems to allow the passage of large cargos through the NPC (Nagy et al., 2009; Grossman et al., 2012). The inner ring and the linker are formed by the assembly of Nup205, Nup188, Nup155, Nup93 and Nup88, which

connects FG-containing nucleoporins to membrane-associated Nups (Vollmer and Antonin, 2014; Weberruss and Antonin, 2016; Grossman et al., 2012).

Three Nups are classified as **TMD-containing nucleoporins**, which anchor the NPC to the NE and interact with the nuclear membrane: Pom121, NDC1 and Nup210, also called gp210 (Weberruss and Antonin, 2016; Grossman et al., 2012; Lusk et al., 2007).

The nuclear transport is restricted and regulated by the **barrier nucleoporins**. They localize to the central channel of the NPC with expansions towards the cytoplasm and nucleoplasm. These Nups are mainly anchored to the inner ring or the linker and are comprised of multiple FG-repeats with the following combinations: GLFG, FxFG, PxFG or SxFG, with F representing the amino acid phenylalanine, G glycine, L leucine, P proline, S serine and x any amino acid (Frey and Görlich, 2007; Aramburu and Lemke, 2017). Nups with FG-repeats directly interact with transport receptors with a low affinity to enable nucleocytoplasmic transport. (Radu et al., 1995a; Radu et al., 1995b; Katahira et al., 1999; Aramburu and Lemke, 2017; Grossman et al., 2012). However, the network of FG-containing Nups provides a diffusion barrier (Ribbeck and Görlich, 2002; Li et al., 2016; Kabachinski and Schwartz, 2015).

Barrier, TMD- and scaffold Nups are assembled in a symmetric manner, while the structures of the NPC facing the nucleoplasm and the cytoplasm differ from each other. The **cytoplasmic filaments** are structurally unordered elongated peptides, which can interact with transport complexes (Beck and Hurt, 2017; Marelli et al., 2001; Suntharalingam and Wente, 2003). The **nuclear basket** facing the nucleoplasm is also able to interact with transport factors. This structure is assembled of Nup153, Nup50 and Tpr, which form eight elongated filaments from the nucleoplasmic ring (Goldberg and Allen, 1992; Grossman et al., 2012). These nucleoporins are involved in export of mRNA, retention of non-spliced RNA, spindle pole assembly and telomere organization (Xu et al., 2007; Frosst et al., 2002; Grossman et al., 2012). In contrast to the scaffold Nups, nucleoporins constituting the nuclear basket are continuously renewed (D'Angelo et al., 2009).

1.1.2 Transport of soluble cargos into the nucleus

The NPC is a barrier for biomolecules entering or leaving the nucleus. Formerly, molecules smaller than 40 kDa or 5 nm in diameter, ions, water and metabolites were suggested to pass this gatekeeper by passive diffusion (Akey and Radermacher, 1993; Keminer and Peters, 1999). For larger proteins and molecules like RNA, ribosomal subunits or viral particles, an active transport mechanism is required (Cautain et al., 2015; Wente and Rout, 2010; Grossman et al., 2012). However, latest findings indicate that the passage of the NPC is also determined by the surface properties of the cargo protein. While hydrophobic residues, cysteine, histidine and positively charged arginine promote transport through the NPC, negative residues and lysine inhibit passage through the pore (Frey et al., 2018). As cargos need to be targeted from the cytoplasm into the nucleus (import) and, at the same time, nuclear cargos have to be exported into the cytoplasm (export), a bidirectional transport system is necessary (Feldherr et al., 1984) (figure 3).

The β-karyopherin family

A family of β-karyopherins consisting of at least 20 proteins in humans mediates nucleocytoplasmic transport of cargo proteins (Kim et al., 2017). These proteins have an NPC-binding domain, which mediates the interaction with the FG-repeat containing Nups, a cargo-binding site and a binding domain at the N-terminus for the small Ras-like GTPase Ran (Wente and Rout, 2010). The members of this protein family are also termed transport receptors/factors or, more specific, importins or exportins depending on the direction of transport they are mediating (Görlich et al., 1994; Stade et al., 1997; Cautain et al., 2015). They are able to recognize special signal sequences within a cargo protein, which are required for transport. These signals are termed nuclear localization signal (NLS) (Kalderon et al., 1984; Lanford and Butel, 1984; Robbins et al., 1991) necessary for nuclear import or nuclear export signal (NES) required for export events (Fornerod et al., 1997; Fukuda et al., 1997; Ossareh-Nazari et al., 1997; Stade et al., 1997). After the binding of the karyopherin to the signal within the cargo protein, the assembled complex is able to cross the NPC (Tetenbaum-Novatt and Rout, 2010).

One of the best studied members of the β-karyopherin family is importin β (also known as karyopherin β1). It was first described to bind via the adaptor protein importin α to cargo proteins containing a basic classical nuclear localization signal (cNLS) as, for instance, the monopartite NLS of SV40 T antigen or the bipartite NLS of nucleoplasmin (Görlich et al., 1995; Dingwall et al., 1988; Radu et al., 1995a; Chi et al., 1995; Imamoto et al., 1995). A monopartite NLS is a cluster of three to five positively charged amino acids, while a bipartite NLS contains an additional small cluster of lysine/arginine residues in a distance of 10 to 12 amino acids to the monopartite-like sequence (Dingwall and Laskey, 1991; Dingwall et al., 1988). These cNLSs are bound by the adaptor protein importin α (also termed karyopherin α), which is then bound by importin β (Oka and Yoneda, 2018; Miyamoto et al., 2016). Importin α contains an importin β binding (IBB) domain at the N-terminus followed by an NLS binding domain (Cook et al., 2007). Upon binding of importin α to the NLS within the cargo, the C-terminus of importin β assembles with the IBB domain completing the import complex. The import mechanism via the importin α/importin β pathway is often termed the classical import pathway. However, importin β was shown to be able to interact directly with some of its cargo proteins without the need of the adaptor protein (Kim et al., 2017; Görlich and Kutay, 1999; Miyamoto et al., 2016). Another protein of the β-karyopherin family is transportin, which was shown to assemble into an import complex with the mRNA binding protein hnRNPA1 via the binding of its M9 sequence. This sequence is an NLS of 38 amino acids providing a positive charge, which interacts with the C-terminus of transportin (Pollard et al., 1996; Aitchison et al., 1996).

Transport of the cargo-karyopherin complex through the NPC

After the assembly of an import complex, the protein of the β-karyopherin family interacts with the FG-repeat containing nucleoporins of the NPC. These Nups provide binding sites for the transport receptors with low affinity. Several models are discussed on how this interaction mediates the transport of the import complexes through the NPC (Grünwald et al., 2011; Grossman et al., 2012; Walde and Kehlenbach, 2010; Hayama et al., 2017). For instance, in a polymer brush model, the cytoplasmic, fishing polymers containing the FG-repeats collapse after binding of a karyopherin to the FG-repeats resulting in a pulling motion into the channel. In the central channel, the import complex is passed from the cytoplasmic to the nuclear side of the pore by the assembly and disassembly of karyopherin-FG-repeat interactions (Lim et al., 2007). Another model, called the selective phase/hydrogel model, assumes that the FG-FG interactions within the Nups form a hydrogel, which only opens the mesh upon low affinity interactions of the cargo-carrying karyopherin with the FG-repeats. Within the hydrogel, the import complex passes the NPC through a solubility-diffusion process. Molecules, which are not able to interact with the FG-repeats, cannot permeate the hydrogel (Frey et al., 2006; Frey and Görlich, 2007, 2009; Ribbeck and Görlich, 2002).

Disassembly of the cargo-karyopherin complex in the nucleus

When the import complex passes the NPC and reaches the nucleus, binding of RanGTP to the N-terminus of β-karyopherins disassembles the complex resulting in the release of the cargo protein or the cargo-bound adaptor protein (Cavazza and Vernos, 2015; Cook et al., 2007). The 24 kDa protein Ran belongs to the Ras superfamily of small GTPases and has a guanine nucleotide-binding domain (G domain) (Bischoff and Ponstingl, 1991b; Drivas et al., 1990; Macara et al., 1996; Görlich and Kutay, 1999; Cook et al., 2007). RanGTP is primarily found in the nucleoplasm, while the hydrolyzed form RanGDP is mostly in the cytoplasm (Cavazza and Vernos, 2015). The concentration gradient of RanGTP between the nucleus and the cytoplasm dictates the directionality of the karyopherin-mediated transport (Melchior et al., 1993a; Moore and Blobel, 1993). RanGDP is imported into the nucleus by NTF2 (nuclear transport factor 2) (Ribbeck et al., 1998; Smith et al., 1998). The nuclear RanGDP is then converted to a GTP-bound form catalyzed by the chromatin-bound Ran guanine nucleotide exchange factor (RanGEF) RCC1 (regulator of chromosome condensation 1) (Bischoff and Ponstingl, 1991a, b; Ohtsubo et al., 1987; Ohtsubo et al., 1989; Klebe et al., 1995; Moore, 2001; Kim et al., 2017). Within the cytoplasm, the RanGTPase-activating protein (RanGAP) and the coactivators RanBP1 and RanBP2

stimulate the GTP hydrolysis of Ran (Bischoff et al., 1994; Bischoff et al., 1995a; Bischoff et al., 1995b; Becker et al., 1995; Hopper et al., 1990; Mahajan et al., 1997; Matunis et al., 1996; Melchior et al., 1993b; Richards et al., 1995; Wu et al., 1995; Yokoyama et al., 1995; Görlich and Kutay, 1999). Nucleotide hydrolysis is the energy providing step of the nucleocytoplasmic transport. The translocation of transport complexes through the NPC itself is energy independent and is mediated by diffusion (Schwoebel et al., 1998). In addition to RanGTP, the β-karyopherin family member CAS/CSE1L seems to be involved in the release of cargos bound by the adaptor protein importin α, transported by importin β. Only after cargo release, RanGTP bound importin β as well as the importin α-CAS complex can be recycled back into the cytoplasm. The GTP hydrolysis in the cytoplasm mediates a conformational change within Ran, which results in the release of the transport receptors and CAS/importin α, which can be reused for the next import event (Solsbacher et al., 1998; Oka and Yoneda, 2018) (figure 3).

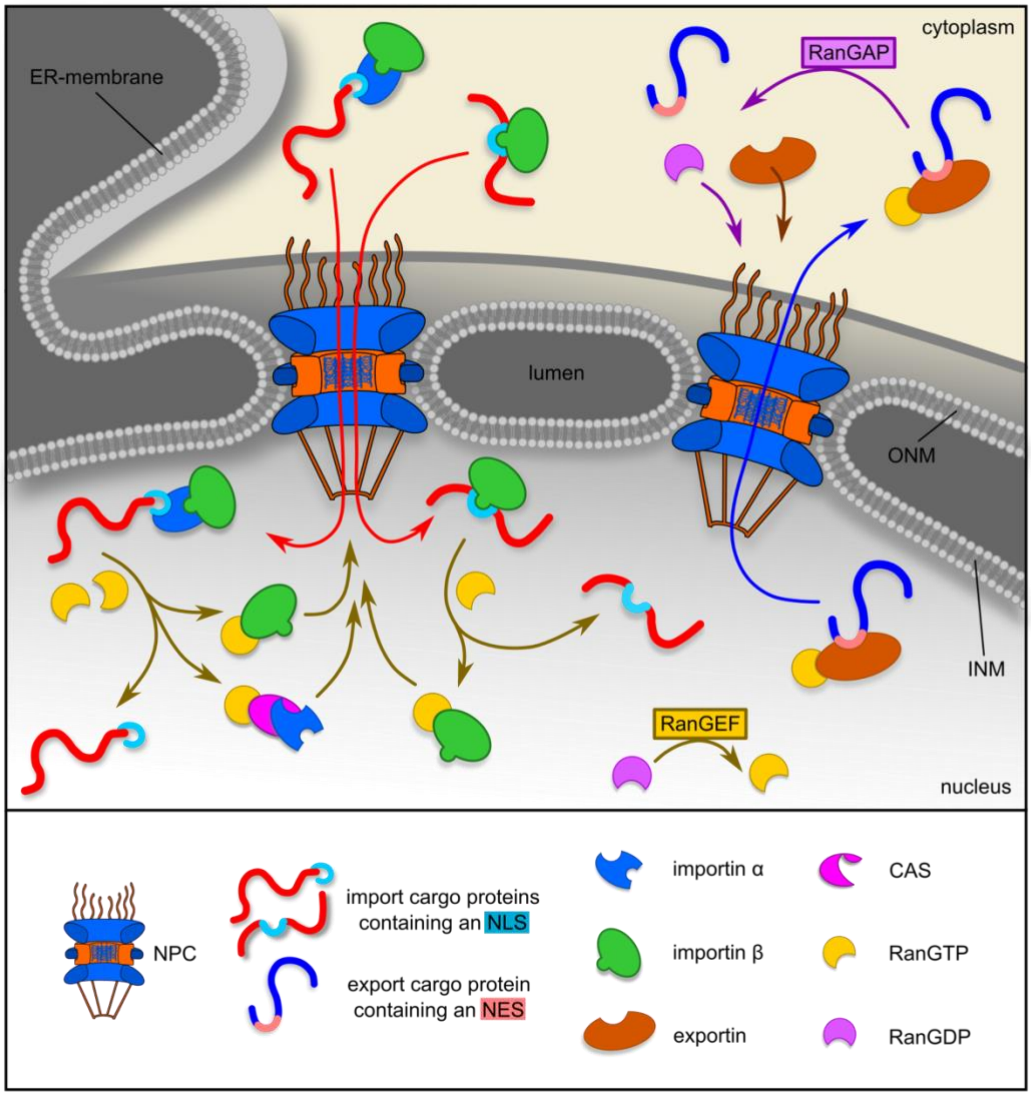

Figure 3: The nucleocytoplasmic transport of soluble cargos.
Nuclear import mechanism (red arrows). A soluble import cargo protein containing a nuclear localization signal (NLS) is transported into the nucleus upon recognition and binding by importin α/importin β or directly by importin β. The complexes are transported via the central channel of the nuclear pore complex (NPC). After import, binding of RanGTP to importin β disassembles the complexes and releases the import cargo proteins. Importin β in its RanGTP bound form and importin α bound by CAS-RanGTP are recycled back into the cytoplasm for another import event. Nuclear export mechanism (blue arrow). The binding of RanGTP increases the binding affinity of an exportin to a nuclear export signal (NES) containing export cargo protein. After export complex assembly, the complex is targeted through the NPC. In the cytoplasm, the hydrolysis of RanGTP to

RanGDP catalyzed by RanGAP (RanGTPase-activating protein) mediates the complex disassembly. The exportin is recycled back into the nucleus. RanGDP is imported into the nucleus by NTF2 (nuclear transport factor 2, not illustrated). RanGEF (Ran guanine nucleotide exchange factor) and NTF2 maintain the RanGTP concentration difference between the nucleus and the cytoplasm. Scheme inspired by Grossman et al., 2012, Oka and Yoneda, 2018, Wente and Rout, 2010 and Caley et al., 2015.

Nuclear export

The RanGTP gradient between the cytoplasm and the nucleus is also the driving force of protein export. RanGTP binding increases the affinity of exportins, for instance Crm1 (chromosome region maintenance 1), to the cargo proteins containing an NES, which is rich in hydrophobic residues (Fornerod et al., 1997; Stade et al., 1997). After the export complex has translocated through the NPC and has reached the cytoplasm, RanGTP hydrolysis causes the dissociation of the export complex (Stade et al., 1997; Fornerod et al., 1997; Cavazza and Vernos, 2015) (figure 3). Afterwards, RanGDP is reimported into the nucleus by NTF2 (Kim et al., 2017).

The nucleocytoplasmic transport is highly efficient

Every NPC consists of approximately 200 FG-containing Nups within the central channel, each containing 5-50 FG-repeats. These provide potentially more than 1000 transport factor binding sites per pore, enabling 100-500 translocation events per second (Wente and Rout, 2010; Yang et al., 2004; Kubitscheck et al., 2005; Yang and Musser, 2006; Ribbeck and Görlich, 2001; Riddick and Macara, 2005; Grossman et al., 2012). The NPC is able to translocate artificial substrates up to 39 nm in diameter due to its high flexibility and dynamics (Pante and Kann, 2002). For the transport of large complexes, such as ribosomal subunits, the NPC is suggested to undergo large structural changes to enable transport within the cellular compartments of the nucleus and cytoplasm (Stoffler et al., 1999; Pante and Kann, 2002; Fried and Kutay, 2003; Grossman et al., 2012).

1.2 Membrane proteins

In contrast to the nuclear import of soluble proteins, targeting to the INM of proteins containing transmembrane domain(s) (TMD(s)) is yet not well understood (Zuleger et al., 2012; Laba et al., 2014; Katta et al., 2014). The following chapter gives an overview of classes and the biogenesis of membrane proteins which are inserted into the ER-membrane.

1.2.1 Classes of membrane proteins

Proteins embedded in the phospholipid bilayer of a membrane are termed integral or intrinsic membrane proteins. They contain amino acids with hydrophobic side chains which are able to interact with fatty acyl groups of the membrane phospholipids. The membrane spanning domains comprise approximately 20 residues which permeate and anchor the protein to the membrane. These domains form either α-helices or a β-barrel consisting of multiple β-strands (Shao and Hegde, 2011b; Lodish et al., 2000). A membrane embedded protein containing one TMD is termed bitopic, proteins with two or more TMD are referred to as polytopic (Arkin, 2002; Bocharov et al., 2017; Ott and Lingappa, 2002). Membrane proteins can be divided into five classes (figure 4): (1) bitopic type I membrane proteins have their C-terminus oriented to the cytoplasm, (2) type II membrane proteins, also single-pass TMD-containing proteins, orient their N-terminus towards the cytoplasm, (3) multi-pass transmembrane proteins with several TMDs, (4) lipid chain-anchored membrane proteins and (5) GPI (glycosylphosphatidylinositol)-anchored membrane proteins (Chou and Elrod, 1999; Chou and Cai, 2005). In addition, external proteins can be peripherally attached to the membrane. These peripheral membrane proteins do not span the phospholipid bilayer. They interact directly with the lipid polar head groups or are indirectly bound to integral membrane proteins for their membrane attachment (Whited and Johs, 2015; Lodish et al., 2000; Chou and Cai, 2005).

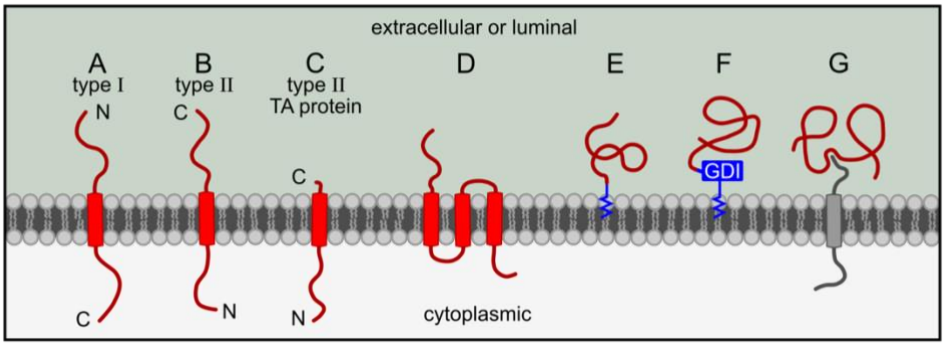

Figure 4: Classification of membrane proteins.
(A) Bitopic type I membrane protein with its N-terminus in the lumen. (B) Bitopic type II membrane protein with its N-terminus in the cytoplasm. (C) A special type II membrane protein: a tail-anchored (TA) membrane protein with a very short C-terminus in the lumen of the ER. (D) Example of a multi-spanning membrane protein. (E) Example of a lipid-anchored membrane protein. (F) GPI (glycosylphosphatidylinositol)-anchored membrane protein. (G) Protein peripherally attached to a membrane inserted protein. Inspired by Chou and Cai, 2005.

1.2.2 Overview of membrane protein biogenesis

The biogenesis of membrane proteins requires several steps to ensure successful membrane insertion. First, the nascent chain is targeted to the ER-membrane. Afterwards, the TMD(s) is/are translocated into the ER-lumen for recognition and correct orientation. Then, the TMD(s) is/are integrated into the phospholipid bilayer of the ER-membrane and, if applicable, followed by the assembly of multimeric complexes (Ott and Lingappa, 2002). The first critical step of membrane insertion, the targeting of the polypeptide to the ER-membrane, is mediated by a **signal sequence** that differentiates membrane proteins from cytoplasmic proteins. Signal sequences for ER-targeting can be subdivided into cleavable and uncleavable ("signal-anchor") sequences.

Cleavable signals are proteolytically removed from the mature protein after targeting of the protein to the ER-membrane. For membrane anchoring, the polypeptide contains an additional stop-transfer sequence, which acts as a TMD. The C-terminus of signal peptide containing proteins faces the cytoplasm (type I membrane proteins) (Shao and Hegde, 2011b; Ott and Lingappa, 2002).

Uncleavable signals act as targeting sequences to the ER-membrane and at the same time as the TMD, the "signal anchor" of the membrane protein to the phospholipid bilayer. Proteins with this kind of targeting signal can be type I or type II membrane proteins. The orientation of the protein within the membrane is determined by the distribution of charged amino acid residues that flank the hydrophobic core of the signal-anchor sequence. A special type of signal-anchor containing membrane proteins are tail-anchored (TA) proteins, which have their signal located at the very C-terminus of the amino acid sequence (figure 4) (Shao and Hegde, 2011b; Ott and Lingappa, 2002). This special localization within the protein requires a post-translational membrane insertion mechanism independent of the ribosome (High and Laird, 1997; Kutay et al., 1993). See section 1.2.4 for further explanations.

1.2.3 Co-translational ER-membrane insertion via the Sec61 translocon

Secretory and ER-membrane proteins with a cleavable or uncleavable signal sequence can be inserted into the ER-membrane during translation of the nascent peptide chain. This insertion pathway for poly- and bitopic membrane proteins is therefore called co-translational insertion and is highly conserved in all organisms (figure 5A) (Mandon et al., 2013; Grudnik et al., 2009; Shao and Hegde, 2011b). During translation, the signal sequence (cleavable or uncleavable) emerges from the ribosome. The hydrophobic stretch is recognized and bound sequence-independently by the signal recognition particle (SRP), which can localize at the exit tunnel of the ribosome (Halic et al., 2004; Walter and Blobel, 1980, 1982). Upon binding, the Alu domain of SRP, which binds close to the elongation factor binding site of the ribosome, slows down the translation process (Siegel and Walter, 1986; Lipp et al., 1987; Walter and Blobel, 1981; Halic et al., 2004). This allows the ribosome-SRP complex to be targeted to the ER-membrane and therefore prevents additional hydrophobic stretches of the nascent peptide chain

from emerging out of the ribosome into the cytosol (Lakkaraju et al., 2008; Mason et al., 2000). By binding of the SRP to the SRP receptor, which is located within the ER-membrane, the ribosome is targeted to the ER-membrane and results in the exposure of a part of the ribosome exit tunnel to the Sec61 complex (Akopian et al., 2013; Shao and Hegde, 2011b). This complex, also termed the translocon, is a heterotrimeric complex assembled by three subunits α, β and γ. The Sec61 subunit α forms a dynamic translocon channel, which enables the movement of substrates in two dimensions: TMDs can be laterally inserted into the ER-membrane or peptide sequences can be translocated into the lumen of the ER (Hanein et al., 1996; Denks et al., 2014; Van den Berg et al., 2004). Therefore, the usage of the Sec61 complex is also the conserved route for translocation of proteins lacking a TMD or signal sequence into the ER-lumen (Ott and Lingappa, 2002). Upon GTP hydrolysis, the nascent chain is transferred from SRP to the Sec61 complex, the SRP-SRP receptor complex is then disassembled (Mandon et al., 2013) and the translocon forms a continuous channel with the ribosome exit tunnel (Beckmann et al., 1997; Prinz et al., 2000; Shao and Hegde, 2011b). As translation proceeds, the nascent chain continues to enter the translocon channel. The TMD(s) is/are oriented and inserted into the phospholipid bilayer by the lateral opening of the translocon channel (Martoglio et al., 1995; Shao and Hegde, 2011b).

Some proteins have been identified to associate with the translocon: For the cleavage of N-terminal signal sequences, signal peptidases were shown to interact with the translocon. The oligosaccharyl transferase (OST) is Sec61 complex-associated for N-linked sugar addition to the nascent chain (Evans et al., 1986; Kelleher et al., 1992). The ER-lumen located chaperone BiP (Binding immunoglobulin protein) binds to the nascent chain upon translocation through the Sec61 complex channel to prevent back-sliding (Denks et al., 2014).

1.2.4 Post-translational ER-membrane insertion via the TRC pathway

Tail-anchored (TA) proteins are a class of bitopic, type II membrane proteins, which have their N-terminal region in the cytosol. The single TMD consisting of approximately 20 hydrophobic amino acids is located at or very close to the C-terminus and acts as a signal-anchor (Shao and Hegde, 2011b; Kutay et al., 1993; High and Laird, 1997). Approximately 300-400 membrane proteins (3-5% of membrane inserted proteins) in eukaryotic cells are defined as TA proteins (Beilharz et al., 2003; Kalbfleisch et al., 2007; Shao and Hegde, 2011b; Wattenberg and Lithgow, 2001). TA proteins have been identified in archaea, bacteria and eukaryotes (Beilharz et al., 2003; Kalbfleisch et al., 2007; Kriechbaumer et al., 2009; Borgese and Righi, 2010) and are involved in vesicular trafficking, protein translocation, apoptosis, protein maturation, degradation, organelle structure and lipid homeostasis (Borgese et al., 2003; Johnson et al., 2013; Borgese and Fasana, 2011; Shao and Hegde, 2011b; Ungar and Hughson, 2003; Osborne et al., 2005; Hockenbery et al., 1990). To fulfill these diverse functions, correct membrane insertion is important. However, ER-membrane insertion of TA proteins and very short TMD-containing proteins is problematic: Their hydrophobic TMDs emerge from the ribosome after termination of translation. As the SRP targets membrane proteins during their translation to the ER-membrane, this class of membrane proteins requires a post-translational membrane insertion mechanism, such as the TRC (TMD-recognition complex) pathway (figure 5B) (Borgese and Fasana, 2011; Shao and Hegde, 2011b; Hegde and Keenan, 2011; Kutay et al., 1993; Johnson et al., 2013). Most components of this insertion pathway are conserved between mammals and *Saccharomyces cerevisiae*, in which it is termed GET (guided entry of tail-anchored proteins) pathway (Schuldiner et al., 2008; Mateja and Keenan, 2018; Shao and Hegde, 2011b; Chartron et al., 2012). For homologues proteins of mammals and *S. cerevisiae* of these pathways see table 1 (Denic, 2012; Denic et al., 2013; Mateja and Keenan, 2018; Chio et al., 2017).

Table 1: Overview of components of the mammalian TRC pathway and the yeast GET pathway

Organism	Pre-targeting complex				ATPase	Membrane receptors	
Mammal	Bag6	Ubl4A	TRC35	SGTA	TRC40	CAML	WRB
S. cerevisiae	Not present	Get5	Get4	Sgt2	Get3	Get2*	Get1

* no sequence but function equivalence

In the TRC pathway (Mateja and Keenan, 2018; Chio et al., 2017; Johnson et al., 2013), SGTA binds to the TMD of the TA protein in a pre-targeting complex together with Bag6, TRC35 and Ubl4A (Leznicki et al., 2010; Winnefeld et al., 2006; Mariappan et al., 2010; Chang et al., 2010; Mateja and Keenan, 2018) (SGTA: small glutamine-rich tetratricopeptide repeat-containing protein alpha; Bag6: large proline-rich protein BAG6, also termed Bat3; TRC35: Golgi to ER traffic protein 4 homolog; Ubl4A: Ubiquitin-like protein 4A). Afterwards, the TA protein is transferred to TRC40 (TMD recognition complex of 40 kDa or Asna1) (Mariappan et al., 2010; Hegde and Keenan, 2011). Cytosolic TRC40 was shown to interact with several TA proteins in crosslinking experiments (Stefanovic and Hegde, 2007). The homodimer TRC40 is an ATPase, which binds as a chaperone to the TMD of TA proteins and undergoes conformational changes in a nucleotide-dependent manner. In its ATP-bound form, TRC40 has a closed conformation which provides a hydrophobic groove able to bind to the hydrophobic TMD of TA proteins. Upon binding of the TA protein to TRC40, the pre-targeting complex disassembles and TRC40 delivers the TA protein to the ER-membrane due to interaction with the ER-membrane embedded receptor composed of the proteins WRB (tryptophan-rich basic protein) and CAML (calcium-modulating cyclophilin ligand). In its TA protein bound form, TRC40 hydrolyzes ATP followed by interaction with CAML. Upon the release of ADP, TRC40 is in an open conformation enabling the interaction with WRB and the release of the TA protein (Chio et al., 2017; Hegde and Keenan, 2011). While the TA protein is inserted by the WRB-CAML complex (Schuldiner et al., 2008; Vilardi et al., 2011; Vilardi et al., 2014; Yamamoto and Sakisaka, 2012; Wang et al., 2014; Shao and Hegde, 2011b), TRC40 is recycled into the cytosol in a closed conformation upon ATP-binding (Hegde and Keenan, 2011).

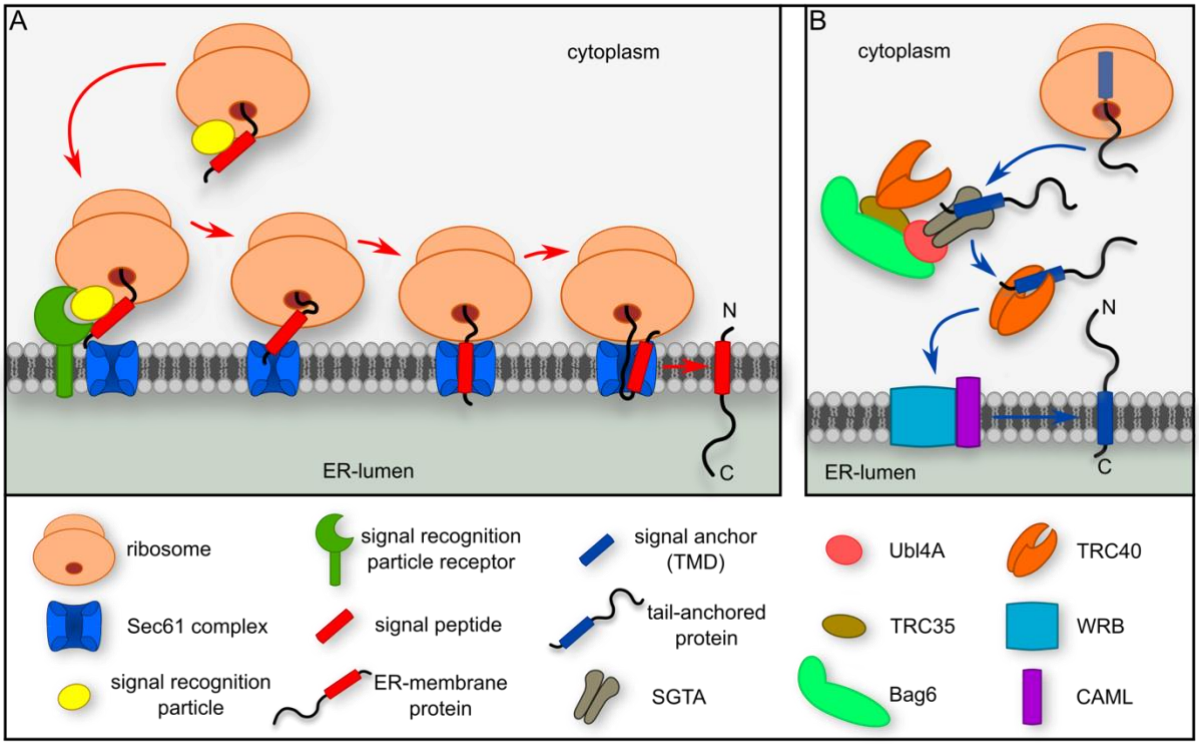

Figure 5: Co- and post-translational ER-membrane insertion.
(A) Co-translational membrane insertion. During translation, the nascent polypeptide chain containing a signal peptide exits the ribosome. The signal peptide is bound by the signal recognition particle (SRP), which targets the ribosome to the SRP receptor at the ER-membrane. After transfer of the nascent chain from the SRP-SRP receptor complex to the Sec61 translocon, translation continues and the transmembrane domain (TMD) is correctly oriented and laterally inserted into the membrane by the translocon. (B) Post-translational membrane insertion. After the translation of the protein is completed, the tail-anchored (TA) protein is bound by a pre-targeting complex assembled by SGTA, TRC35, Ubl4A and Bag6. After transfer of the signal anchor (TMD) onto TRC40, the TA protein is targeted to the ER-membrane embedded receptors WRB and CAML, which insert the TA protein into the ER-membrane. Inspired by Johnson et al., 2013, Shao and Hegde, 2011, Hegde and Keenan, 2011, Van Puyenbroeck and Vermeire, 2018, Rivera Monroy, 2017.

1.2.5 Further insertion mechanisms

In addition to the classical co- and post-translational insertion pathways described above, further membrane targeting and insertion mechanisms have been identified in the past years. Many TA proteins have been shown to be able to insert into the ER-membrane in the absence of the TRC or GET pathway, however, with reduced efficiency (Hegde and Keenan, 2011). This observation might be explained by the diversity of additional targeting mechanisms for TA proteins to the ER-membrane (Chio et al., 2017; Rabu et al., 2009; Borgese and Fasana, 2011; Ast and Schuldiner, 2013), introduced in the following paragraphs. The discovery of alternative routes to the ER-membrane has demonstrated the complexity in membrane targeting of TA proteins.

Crosslinking studies discovered that **SRP** is also able to bind the TMD of some TA proteins in a **post-translational manner**. The TA protein is released from the ribosome after translation termination and is bound by SRP. The complex of SRP and TA protein is targeted to the ER-membrane in a ribosome-unassociated but GTP- and SRP receptor-dependent manner for membrane insertion via the Sec61 translocon (Abell et al., 2004; Abell et al., 2003).

The chaperones **Hsp40 and Hsc70** were able to bind the TMD of TA proteins indicating an ATP-dependent **chaperone-mediated route**. In *in vitro* studies, Hsp40 and Hsc70 were shown to mediate membrane insertion of some TA proteins with a low hydrophobic TMD in the absence of other cytosolic factors (Abell et al., 2007; Rabu et al., 2008). How this alternative pathway mediates targeting to and insertion into the ER-membrane still needs to be examined (Ast and Schuldiner, 2013).

An additional insertion mechanism parallel to the SRP and TRC pathways was recently described as the **SND pathway** (SRP-independent targeting). By a visual screen in *S. cerevisiae*, the proteins Snd1, Snd2 and Snd3 were identified to be involved in the ER-membrane targeting of the model protein Gas1 (Aviram et al., 2016), a protein which is known to be inserted independently of SRP (Ast et al., 2013) and partially GET-independent (Ng et al., 1996). While Snd1 is located in the cytosol and might interact with hydrophobic TMDs, Snd2 and Snd3 are located in the ER-membrane and form a complex together with the translocon. The SND pathway was shown to be a backup insertion mechanism, if the functionality of the SRP and GET pathway was lost (Aviram et al., 2016). In human cells, the membrane-embedded protein hSnd2 (also termed TMEM208, yeast Snd2 ortholog) enables membrane-targeting of TMD-containing proteins (Hassdenteufel et al., 2017). The TRC pathway was shown to be not essential for the insertion of TA proteins (Rivera-Monroy et al., 2016). The SND pathway could be an alternative route, also in mammalian cells (Hassdenteufel et al., 2017; Casson et al., 2017).

For membrane insertion of small secretory proteins and TA proteins with a moderate hydrophobic TMD, an insertion pathway dependent on **calmodulin** and the **ER-membrane protein complex** (EMC) assembled by six proteins was shown. Calmodulin can bind to signal peptides and preserves the TMD-containing proteins from aggregation or degradation. Afterwards, the EMC seems to insert the TMD into the ER-membrane (Jonikas et al., 2009; Guna et al., 2018; Shao and Hegde, 2011a; Mateja and Keenan, 2018; Johnson et al., 2013; Chitwood et al., 2018).

The mammalian TA protein cytochrome b5 was shown to insert into the ER-membrane in an **unassisted insertion** manner. This protein has a TMD with a low hydrophobicity which is inserted post-translationally but independent of the TRC pathway (Favaloro et al., 2008; Favaloro et al., 2010; Stefanovic and Hegde, 2007). The membrane insertion of cytochrome b5 could require cytosolic proteins (Colombo et al., 2009; Yabal et al., 2003), perhaps the chaperones Hsp40 and Hsc70 (Rabu et al., 2008), but is not dependent on any membrane protein (Brambillasca et al., 2006; Brambillasca et al., 2005; Yabal et al., 2003; Rabu et al., 2009).

1.3 Proteins of the inner nuclear membrane

1.3.1 Identification of inner nuclear membrane proteins and their importance in human diseases

In 2002, less than 20 confirmed membrane proteins of the INM were identified. Most of them were shown to interact with lamins and/or chromatin (Burke and Stewart, 2002) suggesting a function in nuclear structure, organization and anchoring (Mekhail and Moazed, 2010; Katta et al., 2014). Until then, a connection between some human diseases and mutations in genes coding for nuclear-lamina and lamina-associated proteins was observed. These diseases were therefore called laminopathies (Burke and Stewart, 2002). One example of laminopathies is the Emery-Dreifuss muscular dystrophy (EDMD), which appears in weakness of skeletal and cardiac muscles (Emery and Dreifuss, 1966; Emery, 1989). This was the first described disease resulting from NE-specific defects (Bione et al., 1994; Nagano et al., 1996). Defects can be caused in two different ways, either by the mutation of the INM protein emerin leading to X-linked EDMD or by mutations in the gene coding for lamin A and C (LMNA) causing an autosomal-dominant form of the disease (Burke and Stewart, 2002; Bonne and Quijano-Roy, 2013). Emerin is a TA protein of 29 kDa (UniProt ID P50402) and has a LEM (LAP2, emerin, MAN1) domain which locates in the nucleoplasm and interacts with BAF (barrier of autointegration factor). BAF itself binds to chromatin. In addition, emerin interacts with A-type lamins. Together, these interactions are suggested to contribute to stabilization and organization of the nucleus. In the X-linked EDMD, emerin is lost from the NE due to nonsense or in-frame deletions of the emerin gene (Bione et al., 1994; Manilal et al., 1996; Nagano et al., 1996; Bonne and Quijano-Roy, 2013). Autosomal EDMD is caused by different mutations of LMNA, which lead to loss of function of lamin A and lamin C proteins due to folding defects.

Several other human diseases have been linked to mutations coding for INM proteins or lamins, pointing out an important function of INM proteins (Bonne et al., 1999; Bonne and Quijano-Roy, 2013). A comparative study using MALDI-TOF mass spectrometry analysis (MALDI: matrix-assisted laser desorption/ionization; TOF: time of flight) identified 19 new membrane proteins of the NE (Dreger et al., 2001). By multidimensional protein identification method (MudPIT) in a subtractive study of proteins detected in microsomal membranes or NE of rat liver, 67 uncharacterized proteins of the INM were identified. The identified proteins were suggested to be type II or multi-spanning membrane proteins with a cytoplasmic N-terminus. Confirmed INM proteins were termed “NET” proteins (nuclear envelope transmembrane protein; NET3, NET4, NET8, NET26, NET31, NET39, NET51, NET56). Twenty-three of the identified INM proteins were highlighted and mapped within chromosome regions, connecting them to different human diseases (Schirmer et al., 2003). Additional 87 potential INM proteins were identified with MudPIT by the comparison of NE proteins of leukocytes in two different states (resting and phytohemagglutinin activated state) followed by the confirmation of the INM localization of eleven of these identified proteins (Korfali et al., 2010). Another MudPIT study using fractions of rat skeletal muscles also identified several new NET proteins (Wilkie et al., 2011). Further screens identified hundreds of potential INM proteins in total, partially evaluated, whose composition is tissue specific (Malik et al., 2010; Korfali et al., 2012; Gomez-Cavazos and Hetzer, 2012; de Las Heras et al., 2013). Some of these INM proteins are involved in transcription, DNA repair and replication, recombination and signaling cascades (Ungricht and Kutay, 2015; Schirmer and Gerace, 2005) and were connected to further human diseases, underlining their importance in the NE (Chatzifrangkeskou et al., 2015; Dauer and Worman, 2009).

1.3.2 Targeting to the reassembled inner nuclear membrane at the end of open mitosis

Even though many INM proteins have been identified, the mechanism of their targeting to the INM still raises questions. In general, two ways to the INM can be distinguished with respect to the phase of the cell cycle. Membrane proteins can reach the INM at the end of **mitosis**, but also have to be targeted to the INM in **interphase** cells (Antonin et al., 2011).

The cell cycle can be divided into two main segments, interphase and mitosis. During the interphase, DNA is replicated and other cellular components are produced to prepare for the division of the cell into two daughter cells. Interphase can be subdivided into the gap phase 1 (G1), the synthesis phase (S), which is the phase of chromosome replication, and the gap phase 2 (G2). After interphase, the cell undergoes mitosis (M), the phase of the cell cycle when the NE is dispersed, the synthesized material is rearranged and two spatially separated nuclear membranes are rebuilt around the divided genetic material. Subsequently, the cell can undergo cytokinesis, the division of the cytoplasm. After mitosis and cytokinesis, two daughter cells are equipped for cell growth of the interphase (McIntosh, 2016; Purves et al., 2006a).

Depending on the organism and cell type, eukaryotic cells can undergo an open or closed **mitosis**. Most fungi undergo closed mitosis in which the NE stays intact as the mitotic spindle, which segregates the duplicated chromosomes, is assembled inside the nucleus. In contrast, an open mitosis, which can be found in cells of plants and animals, is characterized by the disassembly of the NE before and a reassembly after the segregation of the chromosomes. In open mitosis, the NE is disassembled in the NE breakdown process which enables the accessibility of chromatin by the cytoplasmic mitotic spindle and its microtubules (Boettcher and Barral, 2013; Ungricht and Kutay, 2017).

For the NE breakdown, protein interactions within NPCs, lamins, INM proteins and chromatin are disrupted by phosphorylation (Ungricht and Kutay, 2017). The NPC loses its barrier properties when Nup98 is phosphorylated by CDK1 (Cyclin-dependent kinase 1) (Dultz et al., 2008; Laurell et al., 2011). Chromatin is detached from phosphorylated INM and INM-associated proteins. For instance, the protein-protein interactions of BAF, which interacts with INM proteins containing a LEM domain and also with chromatin, are disrupted by its phosphorylation mediated by VRK1 (vaccinia-related kinase 1) (Molitor and Traktman, 2014; Gorjanacz et al., 2007). Also, lamins are phosphorylated by CDK1 and PKC (protein kinase C) during NE breakdown. Thereby, they lose their connection to the NE and chromatin, which leads to the solubilization of A-type lamins while B-type lamins are shifted to the ER-membrane (Gerace and Blobel, 1980; Goss et al., 1994; Peter et al., 1990; Heald and McKeon, 1990). Due to the disruption of the retention in the INM, membrane proteins are retracted in the ER-membrane (Ungricht and Kutay, 2017).

After separation of the sister chromatids, the NE has to be rebuilt. The phosphorylating enzymes are inhibited and counteracting protein phosphatases are activated, which enable new protein-protein interactions between NPC, lamins, chromatin, INM and INM-associated proteins. Due to the binding of INM proteins, which are located in the mitotic ER-membrane, to chromatin, the ER-membrane is wrapped around the chromatin reforming the NE (Ellenberg et al., 1997; Yang et al., 1997; Ulbert et al., 2006; Anderson et al., 2009; Haraguchi et al., 2008; Yang et al., 2017). The formation of NPCs into the new NE differs from NPC assembly of interphase cells and is relatively fast. During the NE breakdown, nucleoporins are bound by importin β for solubilization. When chromatin and NE come in close proximity during NE reassembly, the chromatin-associated RanGEF RCC1 provides high concentration of RanGTP at the rebuilding NE causing a disassembly of importin β and the nucleoporins. These Nups, which may form subcomplexes, assemble into new NPCs. For the recruitment of the Y-complex to the assembling pore the Nup ELYS has been shown to be important (Wandke and Kutay, 2013; Hampoelz et al., 2019).

1.3.3 Targeting to the inner nuclear membrane during interphase of the cell cycle

Cells in **interphase**, as well as cells that undergo a closed mitosis, need to have a mechanism for targeting membrane proteins to the INM when the NE is intact (Antonin et al., 2011). Depending on the protein, several models are currently discussed for INM targeting of integral membrane proteins (Katta et al., 2014; Laba et al., 2014; Antonin et al., 2011; Burns and Wente, 2012; Ungricht and Kutay, 2015; Gonzalez and Andres, 2011; Tapley et al., 2011).

Transport factor dependent INM targeting

One proposed route for INM targeting of membrane proteins is the active transport-based model. Ohba and colleagues showed that the INM trafficking of TMD-containing reporters in a live cell assay was ATP- and temperature dependent (Ohba et al., 2004). Later, the NE proteins Heh1 and Heh2 of *S. cerevisiae* were shown to reach the INM in a transport factor- and energy-dependent manner. Heh1 and Heh2 (homologues of metazoan MAN1 and LEM2, respectively) contain two TMDs each and localize to the INM, as shown by immunoelectron microscopy. In yeast strains where GTP binding and hydrolysis in the GTPase Ran were disrupted nuclear import of Heh1 and Heh2 was inhibited. Additionally, the dependency of INM targeting on the karyopherin Kap95 (yeast homolog of human importin β) and Kap60 (yeast homolog of human importin α) was shown for both INM proteins in deletion stains. Direct binding of Heh2 to Kap60 was demonstrated by pulldown experiments indicating an NLS in the N-terminus. When Nup170, an inner nuclear ring nucleoporin, was depleted, the INM localization of Heh1 and Heh2 was completely lost (King et al., 2006). To further analyze whether Heh2 passes the central channel of the NPC on its way to the INM, Meinema and colleagues created a protein containing the bipartite NLS, the linker region and the first TMD of Heh2 and analyzed its way through the pore by a trapping system (Meinema et al., 2011). They could trap the artificial protein in the central channel of the NPC, suggesting interactions with FG-containing Nups. They emphasized the importance of the length of the linker for INM targeting and that transient openings within the NPC have to exist to enable membrane-inserted proteins to pass the central channel in a karyopherin-bound form (Meinema et al., 2011; Meinema et al., 2013). However, in a later experiment, the artificial protein could also be trapped at nucleoporins which are close to the membrane but not part of the central channel. Further, when the NLS or the linker was removed, the protein could still be trapped at the NPC. Consequently, the assay was assessed to be unable to clarify the route of the membrane protein through the NPC. The Heh2 import was proposed to be closer to the membrane, but still suggested to be dependent on transport factors and the Ran GTPase cycle (Laba et al., 2015).

Based on these findings, a **transport factor mediated model** for INM targeting of membrane proteins was suggested (figure 6A). To reach its destination in the nucleus, a membrane protein contains an NLS, which is bound by a karyopherin in the cytoplasm. After complex formation, the karyopherin shuttles the membrane-bound protein through the central channel of the NPC presuming a short-term disruption of the pore itself. A certain length of the linker, the amino acids between the TMD and the NLS, is an important requirement to bridge the distance between the central channel of the pore and the membrane. In the nucleus, the binding of RanGTP to karyopherin releases the cargo and the membrane protein accumulates in the INM against a concentration difference compared to the ONM (Katta et al., 2014; Ungricht and Kutay, 2015).

Sorting motive mediated INM targeting

Many INM proteins have been shown to contain potential NLS, but so far, their need for INM targeting could not be certainly clarified (Katta et al., 2014). For LBR (lamin B receptor) and nurim, an INM-sorting motive (INM-SM), a positively charged amino acid sequence adjacent to the TMD, was suggested to bind to importin-α-16. This truncated version of importin α lacks the IBB domain and is membrane associated in proximity to Sec61α. In a **sorting motive-mediated model** (not illustrated), importin-α-16 binds to the INM-SM directly after translation and remains bound to the membrane protein after membrane insertion by the translocon. For targeting to the NPC, it was suspected that the complex of importin-α-16 and the INM-SM containing membrane protein interacts directly or indirectly with cellular motor proteins or that importin-α-16 mediates interaction with FG-repeats of the NPC. Further, it was suggested that importin-α-16 could dissociate from the INM-SM containing membrane protein before or after targeting to the INM via peripheral channels. Alternatively, importin-α-16 was suggested to be required for ONM accumulation of the membrane protein which is then bound by importin α and importin β for INM targeting (Braunagel et al., 2007; Saksena et al., 2006; Katta et al., 2014).

INM targeting via vesicles

In a **vesicle-mediated model** (not illustrated), the ONM is suggested to bud into the perinuclear space. The bud contains the membrane proteins and fuses with the INM followed by the diffusion of the integral proteins into the INM (Katta et al., 2014; Laba et al., 2014; Burns and Wente, 2012). This NPC-independent model could not be demonstrated so far for INM targeting. The model is based on a reverse pathway, the vesicular transport of herpesvirus from the nucleus into the cytoplasm. Upon infection of a cell by the herpesvirus, the nucleocapsids are transported to an NPC and the viral DNA is released and imported into the nucleus via the NPC. In the nucleus, the viral genome is replicated and packed into nucleocapsids, which are approximately 120 nm in diameter and consequently too big for export via the NPC (Hellberg et al., 2016; Ungricht and Kutay, 2017). Therefore, the nucleocapsids leave the nucleus through the nuclear membrane. First, nuclear lamins are dissolved due to phosphorylation by the viral kinase pUS3 and the cellular kinase PKC (Park and Baines, 2006; Muranyi et al., 2002). Then, the viral nuclear egress complex (NEC) is assembled and mediates the vesicle formation of the INM into the perinuclear space (Reynolds et al., 2001; Klupp et al., 2007; Bigalke and Heldwein, 2015; Hagen et al., 2015) enclosing nucleocapsids. Afterwards, the bud is fused with the ONM and releases the capsids (Ungricht and Kutay, 2017). Another egress pathway from the INM to the ONM has been shown for the export of messenger ribonucleoprotein particles in *Drosophila melanogaster* (Speese et al., 2012).

Diffusion and retention mediated INM targeting

As the ER-membrane is continuous with the ONM, membrane proteins are suggested to diffuse freely after insertion into the ER-membrane to the NE. Several studies compared the mobility of INM proteins between the ER-membrane and at the NE and found that the mobility was rapidly decreased when the membrane proteins reached the NE. By FRAP (fluorescence recovery after photobleaching) experiments, Wu and colleagues showed that MAN1 is relatively immobile when localized to the NE compared to MAN1 in the ER-membrane (Wu et al., 2002). In mitotic cells, LBR is located in the ER-membrane during NE breakdown and is highly mobile. However, in interphase, when localized to the NE, LBR seems to be immobilized by binding to lamins compared to a rapidly diffusing and mobile subpopulation of LBR in the ER-membrane (Ellenberg et al., 1997). In FRAP and FLIP (fluorescence loss in photobleaching) experiments, emerin and BAF were shown to diffuse rapidly to the NE, but their mobility is decreased when located in the INM by binding to interaction partners in the nucleus (Shimi et al., 2004; Ostlund et al., 1999). The loss of mobility of integral membrane proteins after reaching the INM was suggested to be caused by interactions with lamins or chromatin (Katta et al., 2014; Ungricht and Kutay, 2015). An additional retention mechanism was shown for the INM proteins containing a luminal SUN domain. These proteins interact with the perinuclear space located tail of KASH (Klarsicht, ANC-1, Syne homology) domain proteins, specific ONM proteins. As KASH domain proteins bind to actin, microtubules and filaments in the cytoplasm, this interaction connects the nucleus to the cytoplasmic cytoskeleton as part of the LINC complex (Schooley et al., 2012; Starr and Fridolfsson, 2010; Burke, 2012; Wilson and Foisner, 2010). The immobility of SUN domain containing INM proteins is therefore not only mediated by the interaction with lamins, but also due to anchoring to ONM proteins (Wilson and Foisner, 2010).

For several proteins, when the cytoplasmic/nucleoplasmic region was increased to approximately 60 kDa, the INM targeting was slowed down or was completely blocked, suggesting a size-dependency of INM localization of membrane proteins (Soullam and Worman, 1993, 1995; Wu et al., 2002; Ohba et al., 2004; Zuleger et al., 2011; Antonin et al., 2011; Katta et al., 2014; Ungricht and Kutay, 2015). For instance, reporter proteins with an extraluminal domain of 60-75 kDa were not able to reach the INM, while reporters with smaller cytoplasmic/nucleoplasmic regions did rapidly diffuse to the INM (Ohba et al., 2004). This size-dependency could be shown for all human INM proteins no matter whether they contain a predicted NLS or not (Boni et al., 2015; Ungricht et al., 2015; Ungricht and Kutay, 2015). The NPC is able to transport soluble proteins of a few megadaltons (Grossman et al., 2012) and artificial substrates up to a diameter of 39 nm via its central channel (Pante and Kann, 2002). As the sizes of the extraluminal domains of the examined INM proteins fall below this limit and the existence of an NLS was

mostly not crucial (Boni et al., 2015; Ungricht et al., 2015), the majority of INM proteins are suggested to reach the INM by passive diffusion. INM proteins are supposed to diffuse from the ONM to the INM by passing the NPC at peripheral channels, which are lateral gateways of approximately 10 nm in width adjacent to the NPC membrane (Maimon et al., 2012; Hinshaw et al., 1992; Beck et al., 2007; Reichelt et al., 1990; Ohba et al., 2004; Holmer and Worman, 2001; Katta et al., 2014; Ungricht and Kutay, 2015). Peripheral channels are suggested to be the bottleneck of the NPC, which restricts diffusion into the INM depending on the cytoplasmic/nucleoplasmic size of the membrane protein. Interestingly, when nucleoporins of the inner ring of the NPC or the transmembrane nucleoporin NDC1 were depleted, the size restriction in INM targeting was abolished and membrane proteins with enlarged extraluminal domains could freely diffuse into the INM (Theerthagiri et al., 2010; Boni et al., 2015; Ungricht et al., 2015; Ungricht and Kutay, 2015). INM proteins with larger extraluminal regions or more TMDs reach the INM slower than membrane proteins with smaller cytoplasmic/nucleoplasmic regions, which could be explained by a more time-consuming threading and funneling into the peripheral channel (Ungricht and Kutay, 2015).

Based on these discoveries, a **diffusion and retention-mediated model** for membrane protein targeting to the INM was suggested (figure 6B). A TMD-containing protein which needs to be targeted to the INM diffuses freely to the ONM after membrane insertion into the ER-membrane. The membrane protein passes the NPC by using the peripheral channels of the pore and further diffuses into the INM. The integral membrane protein can be retained in the INM upon interaction of its binding domains with lamins or chromatin. The diffusion into the INM via the peripheral channels is dependent on the size of the extraluminal region of the membrane protein (Katta et al., 2014; Ungricht and Kutay, 2015; Burns and Wente, 2012; Powell and Burke, 1990; Holmer and Worman, 2001).

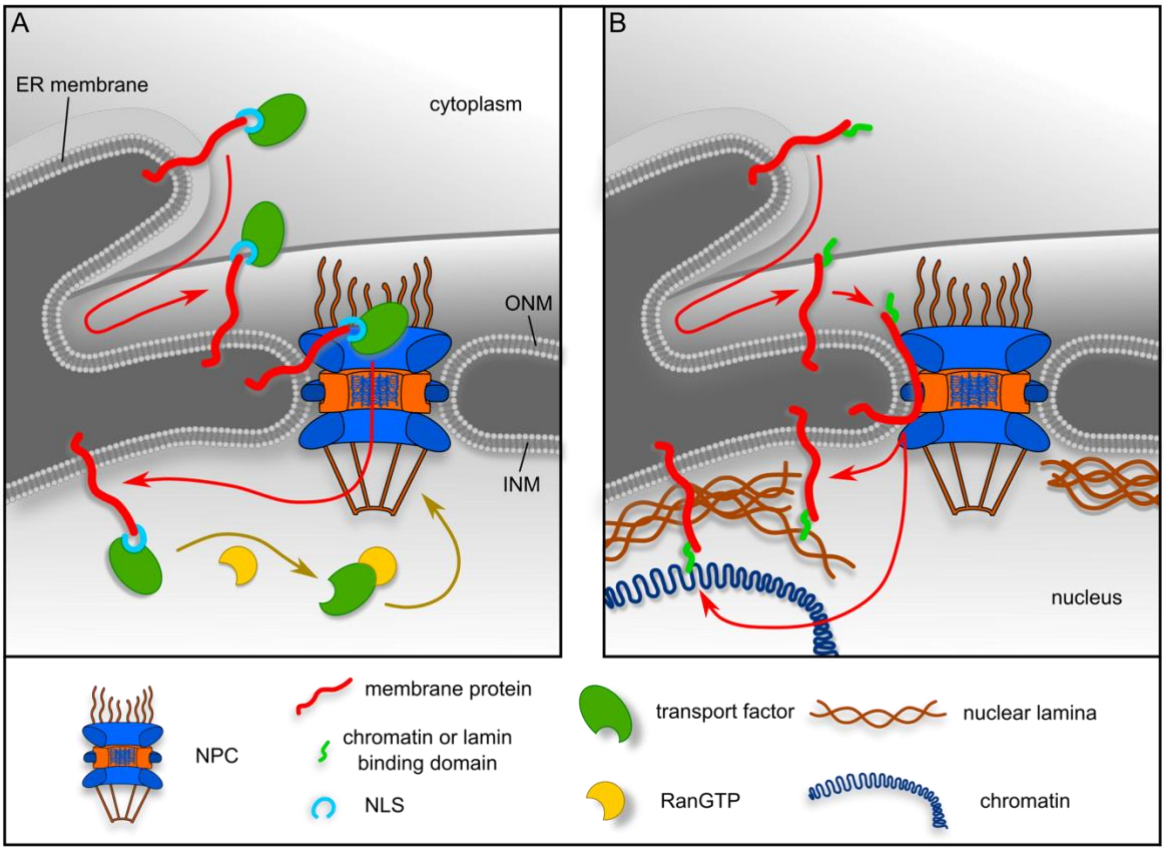

Figure 6: Models for INM targeting of integral membrane proteins.
(A) Active-transport based model. The integral membrane protein exposes a nuclear localization signal (NLS) into the cytoplasm after insertion into the endoplasmic reticulum (ER). This NLS can be recognized by transport factors, which mediate the targeting from the outer nuclear membrane (ONM) to the inner nuclear membrane (INM). When the complex passed the central channel of the nuclear pore complex (NPC) and reached the INM, binding of nuclear RanGTP mediates dissociation of the complex. (B) Diffusion-and-retention based model. An integral membrane protein passively diffuses

from the ONM to the INM through peripheral channels of the NPC. At the INM, the membrane protein can interact with chromatin and/or the nuclear lamina. Inspired by Katta et al., 2014, Ungricht and Kutay, 2015. See also Blenski and Kehlenbach, 2019.

Controversy in the discussion of membrane protein targeting to the INM

With the current state of knowledge, a general mechanism for INM targeting of membrane proteins could not yet be identified. Most experimental results suggest that diffusion is the main targeting mechanism of integral membrane proteins to the INM. The integral membrane protein is then kept in the INM through interactions with lamins or chromatin (Ungricht and Kutay, 2015). However, there are experimental results, which suggest the possibility for other targeting mechanisms or intermediate variants. For instance, the INM localization of the SUN domain-containing protein UNC-84 (*Caenorhabditis elegans*), which has an extraluminal domain of approximately 59 kDa, cannot only be explained by a diffusion mechanism if the peripheral channels restrict INM targeting in a size-dependent manner (Tapley et al., 2011; Katta et al., 2014; Ungricht and Kutay, 2015). Several motives in the extraluminal domain of UNC-84 were identified which are important for INM targeting. When all motives were disrupted, UNC-84 lost its NE localization (Tapley et al., 2011). Furthermore, the INM targeting of reporters in a live cell assay was shown to be ATP-dependent (Ohba et al., 2004), which is not in line with the energy-independent diffusion and retention model. Also, the INM targeting of Heh1 and Heh2 was shown to be RanGTPase dependent (King et al., 2006). Additionally, the INM targeting of LBR was inhibited upon expression of RanQ69L (Zuleger et al., 2011), a dominant negative mutant of the GTPase Ran, which fails to hydrolyze GTP (Klebe et al., 1995). These results were taken as evidence for a different targeting mechanism other than the diffusion and retention model.

However, also the active transport factor-dependent import of the *S. cerevisiae* protein Heh2 is questionable. Yeast lacks nuclear lamins, and therefore the retention of integral membrane proteins in the INM is suggested to occur via interaction with chromatin or other proteins. It is not known how Heh2 is retained at the INM. Therefore, it is possible that the INM localization of Heh2 is dependent on a nuclear retention partner, which could be dependent on Kap60, Kap95 and RanGTPase for its nuclear import. The observed dependency of Heh2 INM targeting on transport factors and RanGTPase activity is likely an indirect effect. Furthermore, the experimental implementation cannot exclude a nuclear import of Heh2 as a soluble protein followed by integration into the INM (Ungricht and Kutay, 2015). Also, the ATP dependency in INM targeting of membrane proteins could be explained by effects on the mobility of the ER itself upon ATP-depletion, which could influence the INM targeting indirectly. Overexpression of RanQ69L might also affect the INM targeting of membrane proteins in an indirect manner, as soluble binding partners could be inhibited in their nuclear transport resulting in a lack of retention of the membrane proteins at the INM (Boni et al., 2015; Ungricht et al., 2015; Ungricht and Kutay, 2015).

In mammals, the SUN domain-containing protein SUN2 was shown to contain a cNLS, which was suggested to be bound by importin α and importin β. A cluster of four arginine residues in its N-terminus acts as an ER localization signal preventing accumulation in the Golgi. The cNLS was sufficient to target heterogenous proteins into the nucleus. However, it cannot be excluded that the cNLS works as a retention motif rather than an import signal for the importin α/importin β pathway (Turgay et al., 2010). For the N-terminal extraluminal region of LBR, a direct Ran-sensitive interaction with importin β, but independent of importin α, could be detected (Ma et al., 2007). However, in semi-permeabilized cells the NE targeting of SUN2 and LBR was shown to be independent of transport factors or central FG-repeats of the NPC (Ungricht et al., 2015).

For some INM proteins, one sole model might explain their nuclear trafficking mechanism. However, for other proteins, various elements of different models could be suitable to explain their INM targeting. Consequently, further integral membrane proteins have to be analyzed for their INM targeting mechanism.

1.4 The membrane protein LRRC59

LRRC59 was first described as p34 (ribosome-binding protein p34), a protein of 34.9 kDa, which was suggested to bind to ribosomes in rough microsomes (Tazawa et al., 1991; Ichimura et al., 1993). p34 was shown to consist of 307 amino acids and contains a large cytosolic N-terminal domain followed by a single TMD and a short C-terminus facing the lumen of the ER (figure 7). It is a non-glycosylated type II signal-anchor membrane protein with a highly conserved sequence (Protein sequence BLAST tool of NCBI: at least 94% sequence identity of LRRC59 of *Homo sapiens*, *Mus musculus*, *Rattus norvegicus* and *Bos taurus*) and with a wide expression in different tissues (Skjerpen et al., 2002; Ohsumi et al., 1993). At the N-terminus, a leucine-rich repeat (LRR) domain with five repeats was identified (Ohsumi et al., 1993) (UniProt ID Q96AG4, Gene name: LRRC59, ORF name: PRO1855). Due to these repeats and the refutation of the potential function as a ribosome receptor (Ohsumi et al., 1993; Kalies et al., 1994), p34 was termed LRRC59, leucine-rich repeat-containing protein 59. In general, leucine-rich repeats (LRR) are suggested to mediate reversible protein-protein interactions (Buchanan and Gay, 1996). LRRC59 was identified in some large-scale screens as a potential interaction partner of several proteins (interaction with human MT_1 melatonin receptor (Daulat et al., 2007); interaction with MPG (DNA-3-methyladenine glycosylase) and other proteins but with low confidence (Ewing et al., 2007); crosslinking to mitochondrial DNA (Bogenhagen et al., 2008); interaction with RRP1B (ribosomal RNA processing 1 homolog B) by tandem affinity purification analysis (Crawford et al., 2009)). However, these identifications were not further analyzed and do not indicate what the biological function of LRRC59 could be. In addition to the LRR domain, the cytosolic region contains a coiled-coil domain, which is in general known to assist in the assembly of dimers and higher multimers (Lupas, 1996). Later, the ability of LRRC59 to form dimers and trimers has been shown in crosslinking experiments (Skjerpen et al., 2002).

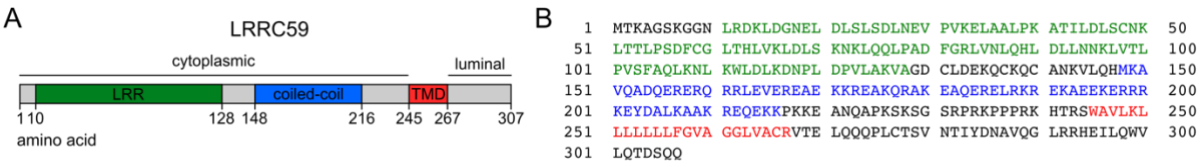

Figure 7: The amino acid sequence of LRRC59, a single-pass type II membrane protein.
(A) Scheme of full-length LRRC59 with the leucine rich repeat region (LRR, green) containing five repeats, the putative coiled-coil domain (blue) and the transmembrane domain (TMD, red). (B) Amino acid sequence of LRRC59 with the LRR region (green), the coiled-coil domain (blue) and the single TMD (red). See UniProt ID Q96AG4 and Zhen et al., 2012.

Furthermore, LRRC59 was shown to interact with the ER-membrane protein UNC93B1 (uncoordinated 93 homolog B1) upon stimulation of cells with certain nucleic acids independent of toll-like receptors (TLRs). By direct interaction, UNC93B1 is involved in the trafficking of nucleic acid-sensing TLRs from the ER to the Golgi or endosomes. The endosomal localization of TLR3 was decreased upon LRRC59 depletion, suggesting that LRRC59 may be involved in the translocation of nucleic acid-sensing TLRs from the ER after infection by the interaction with UNC93B1 (Tatematsu et al., 2015).

In a yeast two hybrid screen, LRRC59 was identified to interact with the oncoprotein CIP2A (cancerous inhibitor of PP2A), an inhibitor of the tumor suppressor PP2A (protein phosphatase 2A). CIP2A promotes mitotic progression and tumorigenesis after its nuclear translocation. LRRC59 was suggested to bind CIP2A during the G1/S phase of the cell cycle independent of PP2A and promotes nuclear import of CIP2A at G2/M of the cell cycle, as nuclear localization of CIP2A was decreased by 80% upon knockdown of LRRC59 (Pallai et al., 2015).

LRRC59 was demonstrated to localize to the ER-membrane and the NE. The luminal localization of the C-terminus was confirmed by the addition of a glycosylation site and SDS-PAGE analysis (Zhen et al., 2012; Skjerpen et al., 2002). LRRC59, was shown to interact with FGF1 (fibroblast growth factor 1)

via its coiled-coil domain (Skjerpen et al., 2002; Zhen et al., 2012). Fibroblast growth factors are involved in stimulation of cell proliferation after translocation into the nucleus (Maddaluno et al., 2017; Ornitz and Itoh, 2015). FGF1 and FGF2 do not diffuse freely into the nucleus, even though they have a low molecular mass. Two NLS have been identified within the amino acid sequence of FGF1, which are required for its nuclear import (Imamura et al., 1990; Wesche et al., 2005). Additionally, the nuclear import of exogenous FGF1, but not FGF2, was shown to be dependent on LRRC59. Depletion of LRRC59 blocked the transport of FGF1 into the nucleus but did not affect its translocation from endosomes into the cytosol. Also, the nuclear import of FGF1 was shown to be Ran-, importin α- and importin β-dependent. For LRRC59, the cytoplasmic region containing the coiled-coil domain in a soluble GFP-tagged version was located in the nucleus, indicating a potential NLS within the amino acid sequence. In U2OS cells, the knockdown of importin β resulted in a total loss of the NE localization of endogenous LRRC59. This suggests that the nuclear import of LRRC59 itself depends on importin β. Together, exogenous FGF1 is supposed to bind to the coiled-coil domain of LRRC59 after uptake by the cell in endosomes and transfer into the cytosol. After binding of importin α and importin β to the coiled-coil domain of LRRC59, the complex was suggested to be targeted into the nucleus in a Ran-dependent manner (Zhen et al., 2012).

1.5 Aim of the study

The nucleocytoplasmic transport of soluble cargo proteins is a well-studied research field. By contrast, there is not much known about the nuclear import of membrane proteins to the INM after their insertion into the ER-membrane. In this thesis, the INM targeting of membrane proteins is examined with special focus on LRRC59 as a model protein.

First, the mechanism how LRRC59 is inserted into the ER-membrane will be studied. LRRC59 contains a single TMD at its C-terminus followed by 40 amino acids facing the lumen of the ER. The TMD at the C-terminus suggests that LRRC59 is a potential TA protein (Kutay et al., 1993), which could be a substrate for post-translational membrane insertion via the TRC pathway. By *in vitro* microsome integration assays and cell-culture based experiments, the potential involvement of the TRC pathway in ER-membrane insertion of LRRC59 will be studied.

In immunofluorescence experiments, LRRC59 was shown to localize mainly to the ER, but also to the NE, a localization which was suggested to be dependent on the transport factor importin β (Zhen et al., 2012). In this study, the mechanism of INM targeting of LRRC59 will be examined in more detail. Not much is known about the biological function of LRRC59. Therefore, the protein will be analyzed for potential interaction partners using proximity labeling.

To get a more general impression of INM targeting of proteins containing a single TMD, seven additional proteins will be analyzed in terms of INM localization using rapamycin-induced dimerization assays and in terms of the mechanism in which some of them they are targeted into the nucleus.

Overall, the aim of this thesis is to gain a deeper understanding in INM targeting of LRRC59 and other single TMD-containing proteins. This will potentially contribute to solve the question of how membrane proteins are targeted to the INM in general.

2 Material and Methods

For basic methods and buffer composition, see Current Protocols in Molecular Biology, Luttmann et al. (2014), Mülhardt (2013), Rehm and Letzel (2010), Schmitz (2011) and Shackleton et al. (2016).

2.1 Material

2.1.1 Software

Table 2: Software

Software	Company
AxioVision (LE) Rel. 4.8.1	Carl Zeiss
Gene 5 plate reader software	BioTek
EndNote X9	Clarivate Analytics
Image Reader LAS-3000	Fujifilm
ImageJ 1.52a	NIH
Inkscape™	Open Source Scalable Vector Graphics Editor
ImageStudio, ImageStudio Lite 5.2.5	LI-COR
LSM 510 Release Version 4.0 SP2	Zeiss
LSM Image Browser	Zeiss
Microsoft Office	Microsoft
NanoDrop 2000 Software	Thermo Fisher Scientific
Perseus Software version 1.5.6.0	Max Planck Institute for Biochemistry, Martinsried, Germany
Serial Cloner 2.6.1	SerialBasics

2.1.2 Technical equipment

Table 3: Technical equipment

Equipment	Company
3 Channel Display Clock Timer WB388	Oregon Scientific
Agarose gel documentation GelSTICK touch	INTAS Science Imaging Instruments
Agarose gel documentation printer P93D	Mitsubishi
Agarose gel running chamber	Home-made, Workshop, UMG
Airflow-Control EN14275	Weidner
Autoclave Sterilizer DX-200	Systec
BioPhotometer	Eppendorf
Cell culture hood Herasafe™ KS	Thermo Fisher Scientific
Cell culture incubator HeracII™ 150i	Thermo Fisher Scientific
Cell culture incubator Cytoperm 2	Heraeus Instruments
Centrifuge 5414R	Eppendorf
Centrifuge 5424	Eppendorf
Centrifuge Sigma	Sigma-Aldrich
Centrifuge Allegra® X-15R with rotor SX4750	Beckman Coulter
Centrifuge Allegra® X-22 with rotor SX4250	Beckman Coulter
Centrifuge Avanti™ J-30I with rotor JA30.50Ti	Beckman Coulter
Centrifuge J6-MI with rotor JS 4.2	Beckman Coulter
Centrifuge Optima MAX-XP with rotor TLA 120.1	Beckman Coulter
Compact disc Digital radio Player	TCM
Confocal microscope LSM 510 meta	Zeiss
Cryo System 750	MVE
Developer machine CURIX60	Agfa
Dual Gel Caster for Mini Vertical Units	Hoefer
Documentation system LAS-3000	Fujifilm
DPU-414 Thermal Printer	Seiko Instruments Inc.
Electrophoresis Power Supply EPS 301	Amersham Bioscience

Equipment	Company
Emulsiflex-C3	BD Bioscience
Falcon tube roller	Home-made, Workshop, UMG
Fluorescence microscope Axioskop 2	Zeiss
Hera freeze -80 °C	Thermo Electron Corporation
Heating plate Type 12801	MEDAX
HP Laser Jet 1320n	HP
Ice machine	Ziegra Eismaschinen GmbH
iMac	Apple
Incubator Haraeus function line	Haraeus
Incubator Shaker INNOVA 4430	New Brunswick Scientific
Incubation/Inactivation Water Bath Model 1003	GFL
Isotherm liquid nitrogen storage	KGW
IMPRESSA J9.3 One Touch TFT	Jura
MacBook Pro	Apple
Magnetic stirrer H+P Variomag Power direct	VWR
Magnetic stirrer HR Hei-Mix L	Heidolph
Magnetic stirrer IKA – Combimag RCT	Bachhofer
Micro centrifuge model IR 220 VAC	Roth
Microwave oven	Ciatronic
Mini Trans-Blot® Cell	Bio-Rad
Milli-Q®	Millipore
Odyssey® Sa Infrared Imaging System	LI-COR
Odyssey® CLx Imaging System	Li-COR
Olympus CK40 Culture Microscope	Olympus
OptiPlex 7050	Dell
pH 522	Bodo Schmidt
Pipet 2.5 µl	Eppendorf
Pipet aid	Drummond
Pipetman 10, 20, 100, 200, 1000 µl	Gilson
Plate reader BioTek Synergy HT	BioTek
Premium No Frost Freezer	Liebherr
Profi Line Fridge	Liebherr
Pump	KNF Lab Laboport
Rocker Rocking Shaker	ELMI
Rocker Sky Sine Shaker DRS-12	ELMI
Rocker Duomax 1030	Heidolph
Scale	Kern EW
Scale PE 3600 Delta Range	Mettler
SE250 Mighty Small II Mini Vertical Electrophoresis Unit	Hoefer
Spectra/Por 1 Dialysis membrane Standard RC tubing 6-8 kDa	Spectrum
Spectrophotometer NanoDrop 2000c	Thermo Fisher Scientific
Spinning wheel	LABINCO
Standard Power Pack P25	Biometra
Syntec DX-200 autoclave	Syntec
Thermocycler FlexCycler^2	Analytik Jena AG
Thermocycler T professional	Biometra
Thermomixer comfort	Eppendorf
Thermomixer compact	Eppendorf
UV (ultraviolet) sterilizer	Biometra
UV (ultraviolet) transilluminator	Uvitec
Vacuum sealer Vacupack	Krups
Vortexer MS2 Minishaker	IKA
VortexGenie2	Suedlabor

2.1.3 Consumables

Table 4: Consumables

Consumable	Company
96 well micro test plate	Sarstedt
96 well micro test plate lid	Sarstedt
Amersham Hybond ECL Nitrocellulose Blotting Membrane	GE Healthcare
Amersham Hyperfilm™ ECL	GE Healthcare
Amersham Protran 0.45 µm NC Nitrocellulose Blotting Membrane	GE Healthcare
Autoclave bag	Sarstedt
Beakers	VWR, Labsolute
Bottle Top Filter, 0,1 µm, 500 ml	Sarstedt
Bottle Top Filter,0,2 µm, 500 ml	Sarstedt
Cell culture dish 10 cm	Sarstedt
Cell scratcher 25 cm	Sarstedt
Centrifuge Bottle Assembly, Polycarbonate 50 ml	Beckman Coulter
Centrifuge tube, thick wall, Polycarbonate 500 µl	Beckman Coulter
Centrifuge tubes 500 ml	Heinemann
Cryotubes (Nunc)	Thermo Fisher Scientific
cuvette	Sarstedt
Disposable scalpel	Bayha
Erlenmeyer flask	Schott
Fabric tape	Roth
Falcon 15 ml	Sarstedt
Falcon 50 ml	Sarstedt
Filter tips 10, 20, 300, 1250 µl	Greiner
Glass bottles 50, 100, 250, 500, 1000, 2000 ml	Schott
Inoculation spreader	Sarstedt
Inoculation spreader glass beads	Thermo Fisher Scientific
Labeling tapes	Pdc Precision dynamic corporation
Magnetic stirrer	VWR
Measuring cup	VWR
Measuring cylinder	VWR
Medix XBU medical X-ray film	FOMA Bohemia
Microscope coverslips (12 mm ∅)	Menzel-Glaeser
Microscope slides	Menzel-Glaeser
Mini Protean TGX Precast gels (4-20%)	Bio-Rad
Minisart RC 15, single use syringe filters (0.45 µm, 0.20 µm)	Sartorius
Minisart single use filter units (0.45 µm)	Sartorius
Neubauer chamber advanced 0.100 mm	Brand
Parafilm “M”	Bemis Company, Inc
Pasteur pipets	Brand
PBS	AppliChem
PD-10 desalting columns	GE Healthcare
Petri dish 10 cm	Sarstedt
pH indicator strips	Macherey-Nagel
Plastic Pipet tips 5 ml, 10 ml, 25 ml	Greiner
Polystyrene Round-Bottom tubes 13 ml	Sarstedt
Reaction tubes (1.5 ml, 2 ml)	Sarstedt
Reaction tubes safe lock (0.2 ml, 0.5 ml)	Eppendorf
Reaction tubes safe lock (1.5 ml, 2 ml)	Sarstedt
Spray bottle	VWR, Kautex
Starlab comfort gloves S	Starlab
Storage box for reaction tubes	Sarstedt
Syringe filter 0,2 µm	Th. Geyer
Syringe filter 0,45 µm	Th. Geyer

Consumable	Company
Syringes and needles	B. Braun, Servoprax
TC-Plate 24 well standard F	Sarstedt
Tweezers	LI-COR
Weighing pan	Th. Geyer
Western blot incubation boxes	LI-COR
Whatman gel blotting paper	GE Healthcare

2.1.4 Kits

Table 5: Kits

Kit	Company
NucleoBond™ Xtra Midi	Macherey-Nagel
NucleoSpin® PCR clean-up/Gel extraction	Macherey-Nagel
NucleoSpin® Plasmid	Macherey-Nagel
Pierce® BCA Protein Assay Kit	Thermo Fisher Scientific
RNeasy Mini Kit	Qiagen
SuperScript III Reverse Transcriptase	Thermo Fisher Scientific
TnT® Quick Coupled Transcription/Translation System	Promega

2.1.5 Chemicals, reagents, enzymes

All used chemicals and reagents were obtained from AppliChem GmbH (Darmstadt), Carl Roth GmbH + Co. KG (Karlsruhe), Serva Electrophoresis GmbH (Heidelberg), Sigma-Aldrich (Taufkirchen) or Merck (Darmstadt).

Table 6: Chemicals and Reagents

Reagent	Company
β-Mercaptoethanol	Roth
Acetic acid	Roth
Acrylamide 4K Solution (30%)	AppliChem
Adenosine 5'-triphosphate disodium salt hydrate (A3377)	Sigma-Aldrich
Advanced protein assay reagent 5x	Cytoskeleton Inc.
Agarose PeqGold	VWR
Amylose Resin High Flow	New England BioLabs
Aluminum-sulfate-(14-18)-hydrate	AppliChem
Ampicillin	Roth
Ammonium persulfate	Sigma-Aldrich
Aprotinin	Roth
Biotinphenol	Iris Biotech
Bovine Serum Albumin (BSA) 20 mg/ml	Thermo Fisher Scientific
Bromophenol blue	Serva
BSA, fraction V	AppliChem
Calcium chloride ($CaCl_2$)	Sigma-Aldrich
Chloramphenicol	Sigma-Aldrich
Coomassie Brilliant Blue (CBB)-G250	Serva
DAPI (D9542)	Sigma-Aldrich
Desthiobiotin	Sigma-Aldrich
Dithiothreitol (DTT)	AppliChem
Dulbecco's Modified Eagle Medium (DMEM), high glucose, pyruvate	Thermo Fisher Scientific
Dulbecco's Modified Eagle Medium (DMEM), high glucose, no glutamine, no lysine, no arginine	Thermo Fisher Scientific
Digitonin	Calbiochem
Disodium hydrogen phosphate (Na_2HPO_4)	Sigma-Aldrich

Reagent	Company
dNTP Set, 100 mM solutions	Thermo Fisher Scientific
Ethanol (analytical grade)	Roth
Ethylenediaminetetraacetic acid (EDTA)	AppliChem
Ethyleneglycol-bis (β-aminoethyl ether)-N,N,N',N'-tetraacetic acid (EGTA)	AppliChem
Fetal bovine serum (FBS) Superior	Biochrom
Formaldehyde Solution min. 37%	Millipore
GeneRuler 100bp DNA Ladder	Thermo Fisher Scientific
GeneRuler 100bp DNA Ladder Plus	Thermo Fisher Scientific
GeneRuler 1kb DNA Ladder	Thermo Fisher Scientific
Gibco® Dulbecco's Modified Eagle Medium (DMEM; 1x)	Thermo Fisher Scientific
Gibco® Penicillin Streptomycin	Thermo Fisher Scientific
Glycerol 87%	AppliChem
Glycine	Roth
Glutathione Sepharose 4 Fast Flow	GE Healthcare
Heavy $^{13}C_6{}^{15}N_2$-L-lysine	Silantes
Heavy $^{13}C_6{}^{15}N_4$-L-arginine	Silantes
HEPES	AppliChem
Hydrochloric acid (HCl)	AppliChem
Hydrogen peroxide (H_2O_2)	Sigma-Aldrich
Imidazole	Roth
Immobilon™ Western Chemiluminescent HRP Substrate	Millipore
IPTG	Thermo Fisher Scientific
Kanamycin sulfate	Roth
LB medium	AppliChem
LB Agar	AppliChem
L-Glutamine 200 mM	Roth
Leupeptin	Roth
LiCl	Merck
Light $^{12}C_6{}^{14}N_2$-L-lysine	Sigma-Aldrich
Light $^{12}C_6{}^{14}N_4$-L-arginine	Sigma-Aldrich
Magnesium acetate ($Mg(OAc)_2$)	Roth
Magnesium Chloride ($MgCl_2$)	Roth
Methanol (technical grade)	Roth
Mowiol ® 4-88	Calbiochem
NeutrAvidin® Agarose	Thermo Fisher Scientific
Ni-NTA Agarose	Qiagen
Nonidet P-40 (NP-40)	AppliChem
Oligonucleotides	Sigma-Aldrich
Ortho-Phosphoric acid 85% p.A.	AppliChem
Ovalbumin	AppliChem
PageRuler Prestained Protein Ladder	Thermo Fisher Scientific
PageRuler Unstained Protein Ladder	Thermo Fisher Scientific
Pepstatin	Roth
Phenylmethane sulfonyl fluoride (PMSF)	AppliChem
Pierce Coomassie Plus Protein Assay Reagent	Thermo Fisher Scientific
Ponceau S	Sigma-Aldrich
Potassium acetate (KOAc)	Roth
Potassium chloride (KCl)	AppliChem
Potassium dihydrogen phosphate (KH_2PO_4)	Roth
Powdered milk	Roth
Protein-A-Sepharose 4 Fast Flow	GE Healthcare
Puromycin dihydrochloride from *Streptomyces alboniger* (P8833)	Sigma-Aldrich
Rapamycin Ready Made Solution, 2.5 mg/ml in DMSO (dimethyl sulfoxide) (2.74 mM), from *Streptomyces hygroscopicus*	Sigma-Aldrich

Reagent	Company
RNase free water	Santa Cruz Biotechnology
SafeView™ Classic (DNA stain)	Applied Biological Materials Inc.
Sodium acetate (NaOAc)	Roth
Sodium ascorbate	AppliChem
Sodium azide (NaN_3)	Merck
Sodium chloride (NaCl)	Roth
Sodium deoxycholate	Merck
Sodium dodecyl sulfate (SDS), powder	Roth
Sodium dodecyl sulfate (SDS), 20% liquid	AppliChem
Streptavidin HRP	Jackson ImmunoResearch
TEMED	Roth
Tris (buffer grade)	AppliChem
Triton-X100	Sigma-Aldrich
Trolox	Sigma-Aldrich
Trypan blue solution 0.4%	Sigma-Aldrich
Tween	Roth
Xylene cyanole	Abcam

Table 7: Enzymes

Enzyme	Company
Creatine phosphokinase, Rabbit Skeletal Muscle	Calbiochem
DNase I	Roth
Fast alkaline phosphatase (FastAP)	Thermo Fisher Scientific
Pfu Ultra II polymerase	Agilent
Phusion High-Fidelity DNA Polymerase	Thermo Fisher Scientific
Restriction enzymes	Thermo Fisher Scientific
T4 DNA ligase	Thermo Fisher Scientific
Gibco® Trypsin/EDTA 0.25% (1x)	Thermo Fisher Scientific
Peptide-N-Glycosidase F (PNGase F)	New England BioLabs

2.1.6 Buffers, stock solutions, media

Table 8: Buffers and Solutions

Buffer	Composition
Binding buffer	50 mM Tris pH 7.4, 200 mM NaCl, 1 mM $MgCl_2$, 5% (v/v) glycerol, 1 mM DTT, 20 mg/ml ovalbumin
$CaCl_2$ buffer	250 mM in H_2O
Coomassie fixing solution	40% (v/v) ethanol, 10% (v/v) acetic acid
Coomassie staining	5% (w/v) aluminum sulfate-(14-18)-hydrate, 10% (v/v) ethanol, 2% (v/v) ortho-phosphoric acid, 0.02% (w/v) CBB-G250
DNA loading buffer (6x)	0.2% (w/v) bromophenol blue, 0.2% (w/v) xylene cyanole, 60% (v/v) glycerol, 60 mM EDTA
G7 reaction buffer (10x)	0.5 M sodium phosphate pH 7.5
Glycoprotein Denaturing buffer (10x)	5% SDS, 0.4 M DTT
2x HEPES buffer	50 mM HEPES, 250 mM NaCl, 1.5 mM Na_2HPO_4, pH 6.94
Laemmli running buffer (10x)	250 mM Tris, 1.92 M glycine, 0.5% (v/v) SDS
Medium salt buffer	50 mM HEPES, 300 mM KOAc, 10 mM $Mg(OAc)_2$, 10% (v/v) glycerol, 4 mM β-mercaptoethanol, 1 µg/ml leupeptin, 1 µg/ml pepstatin, 1 µg/ml aprotinin
Mowiol mounting medium	13.3% (w/v) Mowiol 4-88, 33.3% (w/v) glycerol, 133 mM Tris-HCl, pH 8.5, (1 µg/ml DAPI)
PBS (10x)	1.37 M NaCl, 27 mM KCl, 100 mM Na_2HPO_4, 18 mM KH_2PO_4, pH 7.5
Ponceau S staining solution	0.5% (w/v) Ponceau S in 1% (v/v) acetic acid

Buffer	Composition
Pulldown buffer	50 mM Tris pH 7.4, 200 mM NaCl, 1 mM $MgCl_2$, 5% (v/v) glycerol, 1 mM DTT
Quenching buffer	5 mM Trolox, 10 mM NaN_3, 10 mM sodium ascorbate, in 1x PBS
RIPA buffer	50 mM Tris, (pH 7.4), 5 mM Trolox, 0.5% (w/v) sodium deoxycholate, 150 mM NaCl, 0.1% (w/v) SDS, 1% (v/v) Triton X-100, 1 mM PMSF, 10 mM NaN_3, 10 mM sodium ascorbate, 1 µg/ml aprotinin, 1 µg/ml leupeptin and 1 µg/ml pepstatin
SDS sample buffer (4x)	125 mM Tris pH 6.8, 4% (v/v) SDS, 0.02% (w/v) Bromophenol blue, 10% (v/v) glycerol
TBST	50 mM Tris pH 7.5, 150 mM NaCl, 0.05% (v/v) Tween-20
TAE buffer (50x)	2 M Tris, 0.05 M EDTA, 5.71% (v/v) acetic acid
Transport buffer (10x)	200 mM HEPES, 1.1 M KOAc, 20 mM $Mg(OAc)_2$, 10 mM EGTA, pH 7.3
Washing buffer 1	50 mM HEPES (pH 7.4), 0.1% (w/v) sodium deoxycholate, 1% (v/v) Triton X-100, 500 mM NaCl, 1 mM EDTA
Washing buffer 2	50 mM Tris (pH 8.0), 250 mM LiCl, 0.5% (v/v) NP-40, 0.5% (w/v) sodium deoxycholate, 1 mM EDTA
Washing buffer 3	50 mM Tris (pH 7.4), 50 mM NaCl
Western blot transfer buffer (10x)	250 mM Tris, 1.93 M glycerol, 0.2% (v/v) SDS
Western blot transfer buffer	25 mM Tris, 193 mM glycine, 0.02% (v/v) SDS, 20% (v/v) methanol

Table 9: Stock Solutions

Solution	Composition
1,4-Dithiothreitol (DTT)	1 M in H_2O
4',6-Diamidin-2-phenylindol (DAPI)	1 mg/ml in H_2O
Ammonium persulfate	10% ammonium persulfate in H_2O
Ampicillin	100 mg/ml in H_2O
Aprotinin	1 mg/ml in 20 mM HEPES pH 7.4
Adenosine triphosphate (ATP)	100 mM ATP in 100 mM $Mg(OAc)_2$, 20 mM HEPES (pH 7.4)
Calcium Chloride ($CaCl_2$)	1 M in H_2O
Chloramphenicol	30 mg/ml
Creatine Phosphate	80 mg/ml in H_2O
Digitonin	10% (w/v) in DMSO (dimethyl sulfoxide)
Ethylenediaminetetraacetic acid (EDTA)	0.5 M in H_2O, pH 8
Ethyleneglycol-bis (β-aminoethyl ether)-N,N,N',N'-tetraacetic acid (EGTA)	0.5 M in H_2O, pH 8
HEPES	1 M in H_2O, pH 7.4
Isopropyl β-D-1-thiogalactopyranoside (IPTG)	10 M in H_2O
Kanamycin	60 mg/ml in H_2O
Leupeptin/Pepstatin	1 mg/ml each, in DMSO (dimethyl sulfoxide)
Magnesium acetate ($Mg(OAc)_2$)	1 M in H_2O
Magnesium chloride ($MgCl_2$)	1 M in H_2O
Sodium chloride (NaCl)	5 M in H_2O
Phenylmethylsulfonyl fluoride (PMSF)	100 mM in 2-propanol
Potassium acetate (KOAc)	1 M in H_2O
Potassium acetate (KOAc)	3 M in H_2O
Potassium chloride (KCl)	3 M in H_2O
Puromycin	10 mg/ml in H_2O
Sodium acetate	1 M in H_2O
Tris pH 6.8	1 M in H_2O
Tris pH 7.4	1 M in H_2O
Tris pH 8.8	2 M in H_2O

Table 10: Bacterial media

Medium	Composition
LB	1% (w/v) bacto-tryptone, 0.5% (w/v) yeast extract, 1% (w/v) NaCl, pH 7.0
LB ampicillin	LB medium supplemented with 100 mg/l Ampicillin
LB kanamycin	LB medium supplemented with 60 mg/l Kanamycin
LB chloramphenicol	LB medium supplemented with 30 mg/l Chloramphenicol
LB agar plates	LB supplemented with 1.5% (w/v) bacto-agar
LB agar plates with ampicillin	LB supplemented with 1.5% (w/v) bacto-agar, 80 mg/l Ampicillin
LB agar plates with kanamycin	LB supplemented with 1.5% (w/v) bacto-agar, 60 mg/l Kanamycin
LB agar plates with chloramphenicol	LB supplemented with 1.5% (w/v) bacto-agar, 1.5 mg/l Chloramphenicol
SOC	2% (w/v) tryptone, 0.5% (w/v) yeast extract, 10 mM NaCl, 2.5 mM KaCl, 10 mM $MgCl_2$, 10 mM $MgSO_4$, 0.36% (w/v) glucose, pH 7.0

Table 11: Mammalian cell media

Medium	Composition
Cell culture medium	Dulbecco´s Modified Eagle Medium (DMEM), 10% (v/v) FBS, 2 mM L-glutamine, 100 U/ml penicillin, 100 µg/ml streptomycin
Heavy isotopes labelling medium	Dulbecco´s Modified Eagle Medium (high glucose, no glutamine, no lysine, no arginine), 10% (v/v) dialyzed FBS, 6 mM L-glutamine, 100 U/ml penicillin, 100 µg/ml streptomycin, 0.4 mM $^{13}C_6{}^{15}N_2$-L-lysine, 0.2 mM $^{13}C_6{}^{15}N_4$-L-arginine
Light isotopes labelling medium	Dulbecco´s Modified Eagle Medium (high glucose, no glutamine, no lysine, no arginine), 10% (v/v) dialyzed FBS, 6 mM L-glutamine, 100 U/ml penicillin, 100 µg/ml streptomycin, 0.4 mM $^{12}C_6{}^{14}N_2$-L-lysine, 0.2 mM $^{12}C_6{}^{14}N_4$-L-arginine

2.1.7 Cell lines

Table 12: Cell lines

Cell line	Specification	Origin
HeLa P4	Human adenocarcinoma cell line; modified expressing CD4; adherent; derived from the cervix of a 31-year old woman	NIH AIDS Reagent Program; Charneau et al. (1994)
U2OS	Human osteosarcoma cell line; adherent; derived from a moderately differentiated sarcoma of the tibia of a 15-year-old girl	ATCC® HTB96

2.1.8 *Escherichia coli* strains

Table 13: *E. coli* strains

E. coli strain	Specification and genotype
DH5α	F- Φ80lacΔZ M15 Δ(lacZYA-argF) U169 recA1 endA1 hsdR17 (rK-, mK+) phoA supE44 λ- thi-1 gyrA96 relA1
Rosetta 2	F^- ompT $hsdS_B(r_B{}^- m_B{}^-)$ gal dcm (DE3) pRARE2 (Cam^R)

2.1.9 Antibodies

Table 14: Primary antibodies

Name	Species	Origin	Application*	Dilution	Number
α-alpha tubulin	rabbit	Proteintech, 11224-1-AP	IF/WB	1:500/1:1000	Ab081
α-c-Myc	mouse	Santa Cruz Biotechnology, sc-40	IF	1:200	Ab191
α-calnexin	rabbit	Enzo, ADI-SPA-860	WB	1:1000	Ab220
α-CAML	guinea pig	Synaptic Systems, 359004	WB	1:1000	Ab0069**
α-emerin	rabbit	Proteintech, 10351-1-AP	IF/WB	1:500/1:1000	Ab083
α-emerin	mouse	Santa Cruz Biotechnology, sc-81552	IF/WB	1:200/1:1000	Ab301
α-FLAG	mouse	Sigma-Aldrich, F3165	IF	1:3000	Ab013

Name	Species	Origin	Application*	Dilution	Number
α-GFP	rat	ChromoTek, 3h9-100	WB	1:1000	Ab015
α-GST	goat	Amersham, 27-4577-50	WB	1:2000	Ab127
α-HA	mouse	Covance, MMS-101P	IF/WB	1:1000/1:1000	Ab186
α-His	mouse	Qiagen, 34660	WB	1:1000	Ab140
α-IgG	rabbit	Sigma Aldrich	Depletion	1.5 µg/20 µl Protein A Sepharose, 120 µl reticulocyte lysate	Ab001
α-importin β	rabbit	Frohnert et al. (2014)	IF/WB	1:500/1:1000	Ab208b
α-importin β	mouse	Steve Adam/Thermo Fisher Scientific, MA3-070	IF/WB	1:1000/1:1000	Ab025/ Ab248
α-lamin A/C	mouse	Abcam, ab40567	IF/WB	1:250/1:1000	Ab095
α-lamin A/C	rabbit	Cell Signaling, #2032	IF/WB	1:100/1:1000	Ab089
α-LRRC59	rabbit	Sigma-Aldrich, HPA030829	IF/WB	1:100/1:250	Ab090
α-MBP	mouse	New England BioLabs, E8032S	IF/WB	1:500/1:1000	Ab214
α-opsin	mouse	Adamus et al. (1991)	WB	1:1000	Ab092
α-PDI	rabbit	Cell Signaling, 3501	WB	1:1000	Ab0640**
α-TRC40	mouse	Sigma-Aldrich, WH0000439M3-100UG	WB	1:1000	Ab222
α-TRC40	rabbit	Favaloro et al. (2010)	Depletion	15 µl/20 µl Protein A Sepharose, 120 µl reticulocyte lysate	Ab0405**

*Abbreviation of application: WB: Western Blot, IF: immunofluorescence
** Laboratory of Prof. Dr. Blanche Schwappach

Table 15: Secondary antibodies

Name	Species	Origin	Application*	Dilution
IRDye 680 CW α-mouse	donkey	LI-COR	WB	1:10,000
IRDye 800 CW α-mouse	donkey	LI-COR	WB	1:10,000
IRDye 800 CW α-mouse	goat	LI-COR	WB	1:10,000
IRDye 680 CW α-rabbit	donkey	LI-COR	WB	1:10,000
IRDye 800 CW α-rabbit	donkey	LI-COR	WB	1:10,000
IRDye 680 CW α-goat	donkey	LI-COR	WB	1:10,000
IRDye 800 CW α-goat	donkey	LI-COR	WB	1:10,000
IRDye 800 CW α-guinea pig	donkey	LI-COR	WB	1:10,000
α-mouse HRP	goat	Jackson ImmunoResearch	WB	1:10,000
α-rabbit HRP	goat	Jackson ImmunoResearch	WB	1:10,000
α-goat HRP	donkey	Jackson ImmunoResearch	WB	1:10,000
α-rat HRP	goat	Jackson ImmunoResearch	WB	1:10,000
α-mouse Alexa Fluor 488 conjugated	donkey	Molecular Probes	IF	1:1000
α-mouse Alexa Fluor 594 conjugated	donkey	Molecular Probes	IF	1:1000
α-mouse Alexa Fluor 647 conjugated	goat	Molecular Probes	IF	1:1000
α-rabbit Alexa Fluor 488 conjugated	donkey	Molecular Probes	IF	1:1000
α-rabbit Alexa Fluor 594 conjugated	donkey	Molecular Probes	IF	1:1000
α-rabbit Alexa Fluor 647 conjugated	donkey	Molecular Probes	IF	1:1000

*Abbreviation of application: WB: Western Blot, IF: immunofluorescence

2.1.10 siRNAs

RNA interference (RNAi) or small interfering RNA (siRNA) was discovered by Fire et al. (1998). Further information can be found in Kim and Rossi (2008). Lyophilized siRNAs were diluted with RNase-free water to a 100 µM stock solution for long time storage at -80°C. As working stock solution stored at -20°C, siRNAs were diluted further to 20 µM.

Table 16: siRNA sequences and supplier

Name	siRNA sequence 5'→3'	Target	Company
control siRNA (non-targeting)	UGGUUUACAUGUCGACUAA	Scrambled sequence	Dharmacon, ON-TARGETplus Non-targeting siRNA #1, D-001810-01-50
importin β 1 siRNA	ACAGUGCCAAGGAUUGUUA	importin β	Eurofins Genomics
Importin β 2 siRNA	CUGGAAUCGUCCAGGGAUUAA	importin β	Sigma-Aldrich
lamin A/C siRNA	GGUGGUGACGAUCUGGGCU	lamin A/C	Dharmacon, siGENOME Lamin A/C Control siRNA (Human/Mouse/Rat), D-001050-01-05
LRRC59 siRNA	GGAGUAUGAUGCCCUCAAAG	LRRC59	Sigma-Aldrich

2.1.1 Oligonucleotides

All oligonucleotides were obtained from Sigma-Aldrich, a Merck subcompany, in a concentration of 100 µM in water solution. The synthesis scale was 0.025 µmol and the purification grade "desalted".

Design of oligonucleotides for PCR cloning

For design of oligonucleotide primers for PCR, the software Serial Cloner 2.6.1 was used. According to cloning strategy, the sequence of the selected restriction enzyme was added to the 5' end of the oligonucleotide together with 3 to 6 upstream base pairs facilitating cleavage close to the end of DNA fragments. The number of upstream base pairs was selected specifically for each restriction enzyme as recommended by the enzyme supplier Thermo Fisher Scientific. The primers were designed with a primer melting temperature of 56 °C to 62 °C.

Table 17: Oligonucleotides for cloning

Number	Name	Sequence (5`→ 3`)
G1379	LRRC59 Forward XhoI	TTTCTCGAGATGACCAAGGCCGGTAGC
G1453	LRRC59 rev EcoRI	TTTGAATTCTCACTGCTGAGAGTCGGTC
G1468	LRRC59_dTMD_EcoRI_fwd2	AAAAGAATTCATGACCAAGGCCGGTAGCAAG
G1469	LRRC59_dTMD_SalI_rev2	TTTGTCGACTCAGTGATGGTGATGGTGATGGGAACGAGTGTGCTTCCGGG
G1560	LRRC59 AS1-137_SalI_His_rev	TTTGTCGACTCAGTGATGGTGATGGTGATGACACTGCTTCTCATCCAAGCAGT
G1561	LRRC59 AS138-244_EcoRI_fwd	AAAAGAATTCATGAAGCAGTGTGCAAACAAGGTGTTACA
G1713	P_For_HA-Emerin_BamHI	AAAAGGATCCATGTACCCATACGATGTTCCAGATTACGCTATGGACAACTACGCAGATCTTT
G1715	P_For_HA-LRRC59_EcoRI	AAAAAGAATTCATGTACCCATACGATGTTCCAGATTACGCTATGACCAAGGCCGGTAGC
G1716	P_Rev_HA-LRRC59_XhoI	AAAACTCGAGCTGCTGAGAGTCGGTCTG
G1717	P_Rev_HA-Emerin_ohne His_XhoI	AAAACTCGAGCTAGAAGGGGTTGCCTTCTT
G1718	P_Rev_HA-LRRC59_ohne His_XhoI	AAAACTCGAGTCACTGCTGAGAGTCGGTC
G1719	P_Rev_HA-LRRC59 AS1-267_XhoI	AAAACTCGAGTCACCGACAAGCAACCAGCC
G1720	P_Rev_HA-LRRC59 AS1-278_XhoI	AAAACTCGAGTCAGGTGCAGAGGGGCTGC
G1773	SND2 cDNA_fw_BamHI_with HA	AAAAGGATCCATGTACCCATACGATGTTCCAGATTACGCTATGGCGCCCAAGGGCAAA
G1774	SND2 cDNA_rv_XhoI_wo HA	AAAACTCGAGCTATAACCGCTTCATCTGCC
G1775	SND2 cDNA_fw_BamHI_wo HA	AAAAGGATCCAAATGGCGCCCAAGGGCAA
G1776	SND2 cDNA_rv_XhoI_with HA	AAAACTCGAGCTAAGCGTAATCTGGAACATCGTATGGGTATAACCGCTTCATCTGCCG
G1777	MBP_fw_XhoI	AAAACTCGAGATGAAAATCGAAGAAGGTAAACTG
G1778	MBP_rv_XhoI	AAAACTCGAGATTGTTATTGTTGTTGTTGTTCGAG
G1779	LRRC59_fw_EcoRI	AAAAAGAATTCAATGACCAAGGCCGGTAGC

Number	Name	Sequence (5`→ 3`)
G1780	LRRC59dTM_rv_XbaI	AAAATCTAGATTAGGAACGAGTGTGCTTCCG
G1792	G1792_Emerin_BamHI_fw	AAAAGGATCCATGGACAACTACGCAGATCTTT
G1793	G1793_Emerin_XhoI_rv with HA	AAAACTCGAGTCAAGCGTAATCTGGAACATCGTATGGGTAGAAGGGGTTGCCTTCTTCA
G1794	G1794_LRRC59_EcoRI_fw	AAAAGAATTCATGACCAAGGCCGGTAGC
G1795	G1795_LRRC59-HA_XhoI_rv with HA	AAACTCGAGTCAAGCGTAATCTGGAACATCGTATGGGTACTGCTGAGAGTCGGTCTG
G1796	G1796_LRRC59 AA1-267-HA_XhoI_rv with HA	AAAACTCGAGTCAAGCGTAATCTGGAACATCGTATGGGTACCGACAAGCAACCAGCC
G1797	G1797_LRRC59 AA1-278-HA_XhoI_rv_with HA	AAAACTCGAGTCAAGCGTAATCTGGAACATCGTATGGGTAGGTGCAGAGGGGCTGC
G1798	G1798_LRRC59AA1-267+EmerinAA244-254-HA_XhoI_rv	AAAACTCGAGTCAAGCGTAATCTGGAACATCGTATGGGTAGAAGGGGTTGCCTTCTTCAGCCTGCATGAAGTGCCGACAAGCAACCAGCC
G1802	G1802_EcoRI-NES-BFP_fw	AAAAAGAATTCATGCTACCACCACTAGAACGACTGACACTAATGGTGTCTAAGGGCGAAGA
G1803	G1803_BFP-Stop-XhoI_rv	AAAACTCGAGTCAATTAAGCTTGTGCCCCAGTTT
G1804	G1804_BFP-NLS-Stop-XhoI_rv	AAAACTCGAGTCAAACTTTCCTCTTTTTCTTTGGATTAAGCTTGTGCCCCAGTTT
G1805	G1805_MBP-Stop-XhoI_rv	AAAACTCGAGTCAATTGTTATTGTTGTTGTTGTTCGAG
G1806	G1806_EcoRI-Nesrev-MBP_fw	AAAAAGAATTCATGCTACCACCACTAGAACGACTGACACTAATGAAAATCGAAGAAGGTAAACTG
G1807	G1807_MBP-NLS-XhoI_rv	AAAACTCGAGTCAAACTTTCCTCTTTTTCTTTGGATTGTTATTGTTGTTGTTGTTCGAG
G1808	G1808_AgeI-BFP_fw	AAAACCGGTATGGTGTCTAAGGGCGAAGA
G1809	G1809_BFP-XhoI_rv (BFP-MCS)	AAAACTCGAGATTAAGCTTGTGCCCCAGTTT
G1811	G1811_XhoI-LRRC59_fw	AAAACTCGAGAAATGACCAAGGCCGGTAGC
G1812	G1812_LRRC59-XbaI_rv	AAAATCTAGATCACTGCTGAGAGTCGGTC
G1813	G1813_XhoI_LRRC59 AA1_frame1_fw	AAAACTCGAGAAATGACCAAGGCCGGTAGC
G1814	G1814_LRRC59 AA -137_EcoRI_rv	AAAAAGAATTCTCAACACTGCTTCTCATCCAAGC
G1815	G1815_LRRC59 AA -140-EcoRI_rv	AAAAAGAATTCTCAACACTGCTTACACTGCTTCTC
G1816	G1816_LRRC59 AA -235-EcoRI_rv	AAAAAGAATTCTCACTTGCGGGGACGGGAG
G1817	G1817_LRRC59 AA -244-EcoRI_rv	AAAAAGAATTCTCAGGAACGAGTGTGCTTCCG
G1818	G1818_XhoI-LRRC59 AA138-_frame 1_fw	AAAACTCGAGAAATGAAGCAGTGTGCAAACAAGGTG
G1819	G1819_XhoI-LRRC59 AA 141-_frame1_fw	AAAACTCGAGAAATGGCAAACAAGGTGTTACAGCAC
G1866	G1866_Primer_LRRC59 AA-216-EcoRI_rv	AAAAAGAATTCTCATTTCTTCTCCTGCTCCCG
G1867	G1867_Primer_LRRC59 AA-225-EcoRI_rv	AAAAAGAATTCTCACGGGGCCTGATTTGCTTC
G1868	G1868_Primer_LRRC59 AA-231-EcoRI_rv	AAAAAGAATTCTCAGGAGCCAGACTTAGATTTCG
G1869	G1869_Primer_XhoI-LRRC59 AA217-_fw	AAAACTCGAGAAATGCCTAAGAAGGAAGCAAATCAG
G1900	G1900_Primer_BamHI-Emerin_F1_fw	AAAAGGATCCATGGACAACTACGCAGATCTTTCGG
G1901	G1901_Primer_Emerin-AA222-His-HindIII_rv	AAAAAAGCTTTCAGTGATGGTGATGGTGATGCTGGCGATCCTGGCCCAGC
G1902	G1902_Primer_HindIII-HA-Emerin_fw	AAAAAAGCTTATGTACCCATACGATGTTCCAGATTACGCTATGGACAACTACGCAGATCTTTC
G1903	G1903_Primer_Emerin-BamHI_rv	AAAAGGATCCCTAGAAGGGGTTGCCTTCTTC

Number	Name	Sequence (5`→ 3`)
G1904	G1904_Primer_Emerin-AA222-STOP-BamHI_rv	AAAAGGATCCTCACTGGCGATCCTGGCCCAG
G1905	G1905_Primer_XhoI-ALG1_fw	AAAACTCGAGATGGCGGCCTCATGCTTGGTC
G1906	G1906_Primer_ALG1-SalI_rv	AAAAGTCGACTTATGTGTCCATAACCAAAGGGAGCAC
G1907	G1907_Primer_XhoI-ALG14_fw	AAAACTCGAGATGGTGTGCGTTCTCGTTCTAGC
G1909	G1909_Primer_XhoI-BET1_fw	AAAACTCGAGATGAGGCGTGCAGGCCTGGG
G1911	G1911_Primer_XhoI-LMAN2_fw	AAAACTCGAGATGGCGGCGGAAGGCTGGATTTG
G1912	G1912_Primer_LMAN2-SalI_rv	AAAAGTCGACTCAGTAGAAGCGCTTGTTCCGCTCC
G1913	G1913_Primer_XhoI-PIGK_fw	AAAACTCGAGATGGCCGTCACCGACAGCC
G1917	G1917_Primer_XhoI-TMED2_fw	AAAACTCGAGATGGTGACGCTTGCTGAACTGC
G1919	G1919_Primer_XhoI-TMED10_fw	AAAACTCGAGATGTCTGGTTTGTCTGGCCCAC
G1920	G1920_Primer_TMED10-SalI_rv	AAAAGTCGACTTACTCAATCAATTTCTTGGCCTTGAAG
G1923	G1923_Primer_HindIII-ALG5_fw	AAAAAAGCTTATGGCTCCGCTTCTGTTGCAGC
G1924	G1924_Primer_ALG5-SalI_rv	AAAAGTCGACCTAATTCATTTTCCGAGTTTGCTCAAGC
G1925	G1925_Primer_XhoI-BET1L_fw	AAAACTCGAGATGGCGGACTGGGCTCGGG
G1926	G1926_BET1L-SalI_rv	AAAAGTCGACTCACGTCCTTGCCCTGGACAAG
G1927	G1927_XhoI-SEC61B_fw	AAAACTCGAGATGCCTGGTCCGACCCCCAG
G1959	G1959_Primer_XhoI-Sec22B_fw	AAAACTCGAGATGGTGTTGCTAACAATGATCGCCCG
G1961	G1961_Primer_EcoRI-mTagBFP2_fw	AAAAAGAATTCATGGTGTCTAAGGGCGAAGA
G1962	G1962_Primer_XhoI-Syne1B aa1639-1989_fw	AAAACTCGAGATGGCCTGGCTAGGAGAGACAG
G1963	G1963_Primer_Syne1B aa1639-1989-HindIII_rv	AAAAAAGCTTTCAGAGTGGAGGAGGACCGTTG
G1968	G1968_Primer_BET1-EcoRI_rv	AAAAAGAATTCTCACCTCAGTTTAATAATCCAATAAATGATAAAAAAG
G1969	G1969_Primer_BET1L-EcoRI_rv	AAAAAGAATTCTCACGTCCTTGCCCTGGACAAG
G1971	G1971_Primer_Sec61B-EcoRI_rv	AAAAAGAATTCCTACGAACGAGTGTACTTGCCCCA
G1975	G1975_Primer_Sec22B-EcoRI_rv	AAAAAGAATTCTCACAGCCACCAGAATCGGACATACA
G1977	G1977_Primer_SalI-FRB_fw	AAAAGTCGACATGTGGCATGAAGGCCTGG
G1978	G1978_Primer_FRB-AgeI_rv	AAAAACCGGTAACTTTGAGATTCGTCGGAACAC
G1991	G1991_Primer_AGL14-HindIII_woStop_rv	AAAAAAGCTTTAACAATTCGCCCAAGGTACAC
G1992	G1992_Primer_LMAN2-HindIII_woStop_rv	AAAAAAGCTTTGTAGAAGCGCTTGTTCCGCTCCTGCCGC
G1993	G1993_Primer_PIGK-HindIII_woStop_rv	AAAAAAAGCTTTAAAAATGAACTTCATATGCTTAATTCC
G1998	G1998_Primer_TMED2-EcoRI_woStop_rv	AAAAAGAATTCAAAACAACTCTCCGGACTTCAAAAAATC
G1999	G1999_Primer_TMED10-EcoRI_woStop_rv	AAAAAGAATTCAACTCAATCAATTTCTTGGCCTTGAAG
G2002	G2002_Primer_XhoI-DDOST_fw	AAAACTCGAGATGGGGTACTTCCGGTGTGCAGG
G2003	G2003_Primer_DDOST-HindIII_woStop_rv	AAAAAAGCTTTGTCGGACTTCTCCTTCTCCTTCATG
G2004	G2004_Primer_XhoI-UBE2J1_fw	AAAACTCGAGATGGAGACCCGCTACAACCTGAA
G2005	G2005_Primer_UBE2J1-SalI_wStop_rv	AAAAGTCGACTTATAACTCAAAGTCAAATATGTATTCGTT
G2006	G2006_Primer_HindIII-UBE2J2_fw	AAAAAAGCTTATGAGCAGCACCAGCAGTAAGAG
G2007	G2007_Primer_UBE2J2-EcoRI_wStop_rv	AAAAAGAATTCTCACTCCTGCGCGATGCTCC
G2032	G2032_XhoI-Sec22b_AA1-194_fw	AAAACTCGAGAAATGGTGTTGCTAACAATGATCG
G2033	G2033_Sec22b_AA1-194-EcoRI_ST_rv	AAAAGAATTCTCAGGCATAAGTGGAACGCATGT
G2034	G2034_XhoI-Sec61B_AA1-70_fw	AAAACTCGAGAAATGCCTGGTCCGACCCCC

Number	Name	Sequence (5`→ 3`)
G2035	G2035_Sec61B_AA1-70-EcoRI_St_rv	AAAAGAATTCTCAAGGGCCAACTTTGAGCCCAG
G2036	G2036_XhoI-UBE2J1_AA1-285_fw	AAAACTCGAGAAATGGAGACCCGCTACAACC
G2037	G2037_UBE2J1_AA1-285-BamHI-St_rv	AAAAGGATCCTCAACCATGATCAGTGTGGTTGTC
G2038	G2038_EcoRI-UBE2J2_AA1-226_fw	AAAAGAATTCAATGAGCAGCACCAGCAGTAAG
G2039	G2039_UBE2J2_AA1-226-BamHI_St_rv	AAAAGGATCCTCAGTGGTGCCGGTTGGCCTG
G2040	G2040_HindIII-HA-FKBP12_fw	AAAAAGCTTATGTACCCATACGATGTTCCAGATTACGCTATGGCTAGCGGAGTGCAGG
G2041	G2041_FKBP12-EcoRV_rv	AAAAAGATATCTTCCAGTTTTAGAAGCTCCACATC
G2042	G2042_EcoRV-(PmlI-AgeI-NotI)-Nup62_fw	AAAAAGATATCCACGTGACCGGTGCGGCCGCAAGCGGGTTTAATTTTGGAGGC
G2043	G2043_Nup62*-XhoI_rv	AAAACTCGAGTCAGTCAAAGGTGATCCGGA
G2044	G2044_EcoRI-(SalI-AgeI-NheI)-FKBP12_fw	AAAAAGAATTCGTCGACACCGGTGCTAGCATGGCTAGCGGAGTGCAGG
G2045	G2045_FKBP12-HA*-EcoRV_rv	AAAAAGATATCTCAAGCGTAATCTGGAACATCGTATGGGTATTCCAGTTTTAGAAGCTCCACATC
G2056	G2056_EcoRI-SUN1_fw	AAAAAGAATTCATGAGTGGCGTGGAGCAGCAGGTGGCC
G2057	G2057_SUN1-opsin*-HindIII_rv	AAAAAGCTTTCAGCCCGTCTTGTTGGAGAAAGGCACGTAGAAGTTTGGGCCTCACTTGACAGGTTCGCCATGAACTCTGAACCG
G2077	G2077_NotI-(BamHI)-Nup54_fw	AAAAAGCGGCCGCGGATCCATGGCCTTCAATTTTGGGGCTC
G2078	G2078_Nup54*-XhoI_rv	AAAACTCGAGTTAACTAAAGACACCACCTCTGATG
G2083	G2083_HindIII-Nup58	AAAAAGCTTATGTCCACAGGGTTCTCCTTCGGGTC
G2084	G2084_Nup58-BamHI_rv	AAAAAGGATCCAATCTTTTTCCTCTTTTGTTTCCAGCTGGAGGTTT
G2089	G2089_HindIII-NEGFP_fw	AAAAAGCTTATGGTGAGCAAGGGCGAGGAGC
G2090	G2090_NEGFP-FLAG-BamHI_rv	AAAGGATCCCTTGTCGTCATCGTCTTTGTAGTCGGTACCAGCGCTGTTTAAACACTGCTTGTCGGCCATGATATAGACG
G2105	G2105_Nup54_pre-PCR_fw	ATGGCCTTCAATTTTGGGGCTCCCTCGGGCACCTCCGGTA
G2106	G2106_Nup54_pre-PCR_rv	TTAACTAAAGACACCACCTCTGATGTGGATGGTTTCATTC
G2107	G2107_Nup58_pre-PCR_fw	ATGTCCACAGGGTTCTCCTTCGGGTCCGGGACTCTGGGCT
G2108	G2108_Nup58_pre-PCR_rv	TTATCTTTTTCCTCTTTTGTTTCCAGCTGGAGGTTTCTTC
G2129	G2129_HindIII-MBP_fw	AAAAAGCTTTAATGAAAATCGAAGAAGGTAAAC
G2130	G2130_MBP-EcoRI_rv	AAAAAGAATTCAAATTGTTATTGTTGTTGTTGTTCG
G2131	G2131_MBP-HindIII_rv	AAAAAGCTTTATTGTTATTGTTGTTGTTGTTCG
G2132	G2132_HindIII-MBP_fw	AAAAAGCTTATGAAAATCGAAGAAGGTAAAC
G2133	G2133_MBP-HindIII_rv	AAAAAGCTTATTGTTATTGTTGTTGTTGTTCG
G2159	G2159_NcoI-Nup210AA1830-_fw	AAACCATGGAAATGACTGTCTGCACGCCCCG
G2160	G2160_Nup210AA-1887*-EcoRI_rv	AAAAAGAATTCTCAGTGGGAGGCATAGGCTGGG
G2161	G2161_SUN1-opsin*-HindIII_rev	AAAAAGCTTTCAGCCCGTCTTGTTGGAGAAAGGCACGTAGAAGTTTGGGCCCTTGACAGGTTCGCCATGAACTCTGAACCGATACA
G2176	G2176_XhoI-MBP_fw	AAAAACTCGAGAAATGAAAATCGAAGAAGGTAAACTG
G2177	G2177_MBP-HindIII_rv	AAAAAGCTTATTGTTATTGTTGTTGTTGTTCGAG
G2178	G2178_HindIII-M9_fw	AAAAAGCTTATGGGGAATTACAACAATCAGTCTTC
G2179	G2179_M9-EcoRI_rv	AAAAAGAATTCATAGCCACCTTGGTTTCGTG
G2180	G2180_EcoRI-FKBP12_fw	AAAAAGAATTCATGGCTAGCGGAGTGCAGG
G2181	G2181_FKBP12-BamHI_rv	AAAGGATCCTCATTCCAGTTTTAGAAGCTCCACATC

Number	Name	Sequence (5`→ 3`)
G2182	G2182_BamHI-FLAG-BiMAX2_fw	AAAGGATCCATGGACTACAAAGACGATGACGACAAGATGCGGAGGAGACGACGGAGAA
G2183	G2183_BiMAX2-EcoRI_rv	AAAAAGAATTCTCAGTCCAGCCTTCTCCGCTTC
G2187	G2187_BspOI-MBP_fw	AAAGCTAGCATGAAAATCGAAGAAGGTAAACTGG
G2188	G2188_MBP-GGGGS-EcoRV_rv	AAAAAGATATCGCTTCCTCCTCCTCCATTGTTATTGTTGTTGTTCGAGC
G2189	G2189_EcoRV-mCh_fw	AAAAAGATATCATGGTGAGCAAGGGCGAGG
G2190	G2190_mCherry-GGGGS-AgeI_rv	AAAACCGGTGCTTCCTCCTCCTCCCTTGTACAGCTCGTCCATGC
G2191	G2191_AgeI-FRB_fw	AAAACCGGTATGTGGCATGAAGGCCTGG
G2192	G2192_FRB-GGGGS-HindIII_rv	AAAAAAGCTTGCTTCCTCCTCCTCCCTTTGAGATTCGTCGGAACAC
G2193	G2193_HindIII-MBP_fw	AAAAAAGCTTATGAAAATCGAAGAAGGTAAACTGGT
G2194	G2194_MBP-GGGGS-XhoI_rv	AAAACTCGAGGCTTCCTCCTCCTCCATTGTTATTGTTGTTGTTCGAGC
G2195	G2195_XhoI-LRRC59_fw	AAAACTCGAGATGACCAAGGCCGGTAGCAA
G2196	G2196_LRRC59*-EcoRI_rv	AAAAAGAATTCTCACTGCTGAGAGTCGGTCT
G2197	G2197_BspOI-mCh_fw	AAAGCTAGCATGGTGAGCAAGGGCGAGG
G2198	G2198_mCherry-GGGGS-EcoRV_rv	AAAAAGATATCGCTTCCTCCTCCTCCCTTGTACAGCTCGTCCATGC
G2199	G2199_FRB-HindIII-GGGGS-XhoI_rv	AAAACTCGAGGCTTCCTCCTCCTCCAAGCTTCTTTGAGATTCGTCGGAACAC
G2200	G2020_mCherry-EcoRV-GGGGS-AgeI_rv	AAAACCGGTGCTTCCTCCTCCTCCGATATCCTTGTACAGCTCGTCCATGCC
G2212	G2212_EcoRI-P2X2_fw	AAAAAGAATTCATGGTCCGGCGCTTGGCCCG
G2213	G2213_P2X2-HindIII*_rv	AAAAAGCTTTCAAAGTTGGGCCAAACCTTTGGGGTC
G2225	G2225_XhoI-GST_fw	AAAACTCGAGATGTCCCCTATACTAGGTTATTG
G2226	G2226_GST-XhoI_rv	AAAACTCGAGTTTTGGAGGATGGTCGCCAC
G2227	G2227_HindIII-GST_fw	AAAAAGCTTATGTCCCCTATACTAGGTTATTG
G2228	G2228_GST-HindIII_rv	AAAAAGCTTTTTTGGAGGATGGTCGCCAC
G2229	G2229_HindIII-GST+2bp_fw	AAAAAGCTTATATGTCCCCTATACTAGGTTATTG
G2230	G2230_GST-EcoRI+2bp_rv	AAAAAGAATTCATTTTTGGAGGATGGTCGCCAC
G2231	G2231_GST-HindIII+2bp_rv	AAAAAGCTTTTTTTGGAGGATGGTCGCCAC

* indicates a stop codon

Design of oligonucleotides for mutagenesis PCR cloning

Mutagenesis was performed using the site-directed mutagenesis method (Weiner et al., 1994) with primers containing the mutated sequence surrounded by 10-15 additional base pairs upstream and downstream of the mutation. The forward and reverse primer were designed with an identical sequence, but antiparallel, with a length up to 45 base pairs. Plasmid DNA sequence changes with the result of up to seven amino acids in the expressed protein were performed using one primer pair.

Table 18: Oligonucleotides for mutagenesis

Number	Name	Sequence (5`→ 3`)
G1711	P_For_siRNA resistent Importin beta	GTGAAAAACAGCGCCAAAGATTGCTATCCTGCTGTCCAG
G1712	P_Rev_siRNA resistent Importin beta	CTGGACAGCAGGATAGCAATCTTTGGCGCTGTTTTTCAC
G1870	G1870_Primer_LRRC59 AA226 228 mut_fw	CAGGCCCCGGCATCTGCGTCTGGCTC
G1871	G1871_Primer_LRRC59 AA226 228 mut_rev	GAGCCAGACGCAGATGCCGGGGCCTG
G1872	G1872_Primer_LRRC59 AA232 234 235 mut_fw	TGGCTCCGCTCCCGCCGCGCCACCA

Number	Name	Sequence (5`→ 3`)
G1873	G1873_Primer_LRRC59 AA232 234 235 mut_rv	TGGTGGCGCGGCGGGAGCGGAGCCA
G1874	G1874_Primer_LRRC59 AA239 240 243 mut_fw	ACCACCCGCGGCGCACACTGCTTCCTGAGA
G1875	G1875_Primer_LRRC59 AA239 240 243 mut_rv	TCTCAGGAAGCAGTGTGCGCCGCGGGTGGT
G1876	G1876_Primer_LRRC59 mut 157 159 161 162 zu Alanin_fw	GGCAGATCAGGAGGCGGAGGCGCAGGCGG CGCTGGAAGTAGAAC
G1877	G1877_Primer_LRRC59 mut 157 159 161 162 zu Alanin_rv	GTTCTACTTCCAGCGCCGCCTGCGCCTCCGC CTCCTGATCTGCC
G1878	G1878_Primer_LRRC59 mut 171 172 173 176 178 zu Alanin_fw	GTGAGGCAGAGGCGGCGGCTGAGGCTGCGC AGGCAGCTAAGGAAG
G1879	G1879_Primer_LRRC59 mut 171 172 173 176 178 zu Alanin_rv	CTTCCTTAGCTGCCTGCGCAGCCTCAGCCGC CGCCTCTGCCTCAC
G1880	G1880_Primer_LRRC59 mut 185 188 189 190 192 zu Alanin_fw	GCTCAGGAGGCGGAACTGGCGGCGGCGGAG GCGGCGGAAGAGAAG
G1881	G1881_Primer_LRRC59 mut 185 188 189 190 192 zu Alanin_rv	CTTCTCTTCCGCCGCCTCCGCCGCCGCCAGT TCCGCCTCCTGAGC
G1882	G1882_Primer_LRRC59 mut 196 198 199 200 201 zu Alanin_fw	GGCGGAAGAGGCGGAGGCCGCGGCAGCGG AGTATGATGCCC
G1883	G1883_Primer_LRRC59 mut 196 198 199 200 201 zu Alanin_rv	GGGCATCATACTCCGCTGCCGCGGCCTCCG CCTCTTCCGCC
G1884	G1884_Primer_LRRC59 mut 210 211 215 216 zu Alanin_fw	CTCAAAGCAGCCGCGGCGGAGCAGGAGGCG GCACCTAAGAAGG
G1885	G1885_Primer_LRRC59 mut 210 211 215 216 zu Alanin_rv	CCTTCTTAGGTGCCGCCTCCTGCTCCGCCGC GGCTGCTTTGAG
G1955	G1955_Primer_fw_LRRC mut 207 210 211 215 216 218 219	GATGCCCTCGCAGCAGCCGCGGCGGAGCAG GAGGCGGCACCTGCGGCGGAAGCAAATC
G1956	G1956_Primer_rv_LRRC mut 207 210 211 215 216 218 219	GATTTGCTTCCGCCGCAGGTGCCGCCTCCTG CTCCGCCGCGGCTGCTGCGAGGGCATC
G1957	G1957_Primer_fw_LRRC mut 210 211 215 216 218 219	CAAAGCAGCCGCGGCGGAGCAGGAGGCGGC ACCTGCGGCGGAAGCAAATC
G1958	G1958_Primer_rv_LRRC mut 210 211 215 216 218 219	GATTTGCTTCCGCCGCAGGTGCCGCCTCCTG CTCCGCCGCGGCTGCTTTG
G2028	G2028_DDOST-K450A-K452A-K454A_fw	CTTCTTGCACATGGCGGAGGCGGAGGCGTC CGACAAAGC
G2029	G2029_DDOST-K450A-K452A-K454A_rv	GCTTTGTCGGACGCCTCCGCCTCCGCCATGT GCAAGAAG
G2030	G2030_LMAN2-mut347-354_fw	GTGGTGTTCCAGGCGGCGCAGGAGGCGAAC GCGGCCTTCTACAAAGCTTCG
G2031	G2031_LMAN2-mut347-354_rv	CGAAGCTTTGTAGAAGGCCGCGTTCGCCTCC TGCGCCGCCTGGAACACCAC
G2096	G2096_LRRC59 mut 239-243_-244-SalI_rv	TTTGTCGACTCAGTGATGGTGATGGTGATGG GAAGCAGTGTGCGCCGCGG
G2172	G2172_LRRC59 S227A S229A S231A_fw	CAGGCCCCGAAAGCTAAGGCTGGCGCCCGT CCCCGCAAGC
G2173	G2173_LRRC59 S227A S229A S231A_rv	GCTTGCGGGGACGGGCGCCAGCCTTAGCTT TCGGGGCCTG
G2174	G2174_LRRC59 T242A S244A_fw	CCACCCCGGAAGCACGCTCGTGCCTGGGCT GTGCTGAAGC
G2175	G2175_LRRC59 T242A S244A rev	GCTTCAGCACAGCCCAGGCACGAGCGTGCTT CCGGGGTGG

Design of oligonucleotides for sequencing

Sequencing primers were mainly used from the sequencing supplier GATC, a subcompany of Eurofins Genomics. If these primers were not sufficient for sequencing of long constructs, additional primers were sent in a concentration of 10 µM together with the sample. Individual primers were synthesized by Sigma-Aldrich and listed in the oligonucleotide list of the laboratory of Prof. Dr. Ralph H. Kehlenbach designed by different group members.

Table 19: Oligonucleotides for sequencing

Number	Name	Sequence (5→3`)
G12	EF-For	GAGTAGCACCCACCAAGGCA
G13	EF-Rev	CCCAAGAACCCAAGGAACAA
G364	pEYFP-C1 5'	CGAGAAGCGCGATCACAT
G694	Syne1_aa355_NcoI_f	TTTTCCATGGCCGCCTGGCTAGGAGAGACAG
G695	Syne1_NotI_r	TTTTGCGGCCGCGAGTGGAGGAGGACCGTT
G718	Nup358_aa806_NotI_f	TTTTGCGGCCGCGGATCAGAATTCTTTACTGAAAATG
G719	Nup358_aa1306_SpeI_r	TTTTACTAGTTTTTAAAATGCTCTGGGC
G1440	Hzz_EcoRI_for	TTTGAATTCATGCACCACCATCACCATCAC
G1453	LRRC59 rev EcoRI	TTTGAATTCTCACTGCTGAGAGTCGGTC
G1473	FRB NcoI fwd	TTTCCATGGAAGAGATGTGGCATGAAGGC
G1474	FRB EcoRI rev	TTTGAATTCTGCTTTGAGATTCGTCGGAA
G1487	pmCherry-C1_rev	GCATTCATTTTATGTTTCAGGTTCAG
G1622	FRB_forward_BglII	GAAGATCTGAGATGTGGCATGAAGGCC
G1716	P_Rev_HA-LRRC59_XhoI	AAAACTCGAGCTGCTGAGAGTCGGTCTG
G1724	Importin B Sequencing_Forward	GTGTGCTGGGCTTTCTC
G1905	G1905_Primer_XhoI-ALG1_fw	AAAACTCGAGATGGCGGCCTCATGCTTGGTC
G1913	G1913_Primer_XhoI-PIGK_fw	AAAACTCGAGATGGCCGTCACCGACAGCC
G1921	G1921_Primer_XhoI-TMEM214_fw	AAAACTCGAGATGGCGACCAAGACGGCGG
G1923	G1923_Primer_HindIII-ALG5_fw	AAAAAAGCTTATGGCTCCGCTTCTGTTGCAGC
G1929	G1929_Primer_XhoI-SORT1_fw	AAAACTCGAGATGGAGCGGCCCTGGGGAG
G1971	G1971_Primer_Sec61B-EcoRI_rv	AAAAAGAATTCCTACGAACGAGTGTACTTGCCCCA
G1975	G1975_Primer_Sec22B-EcoRI_rv	AAAAAGAATTCTCACAGCCACCAGAATCGGACATACA
G1978	G1978_Primer_FRB-AgeI_rv	AAAAACCGGTAACTTTGAGATTCGTCGGAACAC
G2005	G2005_Primer_UBE2J1-SalI_wStop_rv	AAAAGTCGACTTATAACTCAAAGTCAAATATGTATTCGTT
G2007	G2007_Primer_UBE2J2-EcoRI_wStop_rv	AAAAAGAATTCTCACTCCTGCGCGATGCTCC
G2042	G2042_EcoRV-(PmlI-AgeI-NotI)-Nup62_fw	AAAAAGATATCCACGTGACCGGTGCGGCCGCAAGCGGGTTTAATTTTGGAGGC
G2043	G2043_Nup62*-XhoI_rv	AAAACTCGAGTCAGTCAAAGGTGATCCGGA
G2046	G2046_HindIII-Nup210_fw	AAAAAGCTTATGGCGGCGCGGGGCCGGGG
G2047	G2047_Nup210-EcoRI_rv	AAAAAGAATTCGTGGGAGGCATAGGCTGGGCTCCAC
G2056	G2056_EcoRI-SUN1_fw	AAAAAGAATTCATGAGTGGCGTGGAGCAGCAGGTGGCC
G2057	G2057_SUN1-opsin*-HindIII_rv	AAAAAGCTTTCAGCCCGTCTTGTTGGAGAAAGGCACGTAGAAGTTTGGGCCTCACTTGACAGGTTCGCCATGAACTCTGAACCG
G2109	G2109_Nup210-seq_bp800_fw	CAGAAGATCAGGCAAGGG
G2110	G2110_Nup210-seq_bp1600_fw	GTATGTGATCGAGCCCC
G2111	G2111_Nup210-seq_bp2400_fw	GGTTCGACAACTTCAGCTC
G2112	G2112_Nup210-seq_bp3200_fw	GCTGGACAGAGAATCAAC
G2113	G2113_Nup210-seq_bp4000_fw	GTTCCAGTTGTGCATGTTG
G2114	G2114_Nup210-seq_bp4800_fw	GAAGTCATCCAGGCCTTG
G2130	G2130_MBP-EcoRI_rv	AAAAAGAATTCAAATTGTTATTGTTGTTGTTGTTCG
G2131	G2131_MBP-HindIII_rv	AAAAAGCTTTATTGTTATTGTTGTTGTTGTTCG
G2190	G2190_mCherry-GGGGS-AgeI_rv	AAAACCGGTGCTTCCTCCTCCTCCCTTGTACAGCTCGTCCATGC

Number	Name	Sequence (5→3`)
G2191	G2191_AgeI-FRB_fw	AAAACCGGTATGTGGCATGAAGGCCTGG
G2192	G2192_FRB-GGGGS-HindIII_rv	AAAAAAGCTTGCTTCCTCCTCCTCCCTTTGAGATTCGTC GGAACAC
G2193	G2193_HindIII-MBP_fw	AAAAAAGCTTATGAAAATCGAAGAAGGTAAACTGGT
G2194	G2194_MBP-GGGGS-XhoI_rv	AAAACTCGAGGCTTCCTCCTCCTCCATTGTTATTGTTGTT GTTGTTCGAGC
G2195	G2195_XhoI-LRRC59_fw	AAAACTCGAGATGACCAAGGCCGGTAGCAA
G2199	G2199_FRB-HindIII-GGGGS-XhoI_rv	AAAACTCGAGGCTTCCTCCTCCTCCAAGCTTCTTTGAGA TTCGTCGGAACAC
G2212	G2212_EcoRI-P2X2_fw	AAAAAGAATTCATGGTCCGGCGCTTGGCCCG
GATC	BGH-Reverse	TAGAAGGCACAGTCGAGG
GATC	CMV-F	CGCAAATGGGCGGTAGGCGTG
GATC	EBV-RP	GTGGTTTGTCCAAACTCATC
GATC	M13-RP	CAGGAAACAGCTATGACC
GATC	pcDNA3.1-FP	CTCTGGCTAACTAGAGAAC
GATC	pcDNA3.1-RP_1	CAAACAACAGATGGCTGGC
GATC	pEGFP_C2-FP	GATCACATGGTCCTGCTG
GATC	pEGFP-FP	TTTAGTGAACCGTCAGATC
GATC	pET-RP	CTAGTTATTGCTCAGCGG
GATC	pGEX5-FP	AACGTATTGAAGCTATCCC
GATC	pMalE	TCAGACTGTCGATGAAGC
GATC	pRSET-RP	ATGCTAGTTATTGCTCAGC
GATC	SP6	ATTTAGGTGACACTATAGAA
GATC	T7	TAATACGACTCACTATAGGG
GATC	pEGFP-RP	AACAGCTCCTCGCCCTTG

2.1.2 Synthesized Genes

Synthesized genes were ordered at Thermo Fisher Scientific, cloned into pMA-RQ vector for GeneArt™ Gene Synthesis or sent as DNA fragments for further costumer cloning as GeneArt™ Srings™ Fragments. The sequence of the synthesized genes can be found in appendix A.

Table 20: Overview of synthesized genes

Name	Type	Company	Product
LRRC59_mut_210-243	Cloned into plasmid #2003	Thermo Fisher Scientific	GeneArt™ Gene Synthesis
Nup210_AA1830-1887	Cloned into vector #36	Thermo Fisher Scientific	GeneArt™ Strings™ DNA Fragments
EcoRI-P2X2-HindIII	Cloned into plasmid #1239	Thermo Fisher Scientific	GeneArt™ Strings™ DNA Fragments

2.1.3 Vectors

Table 21: Available vectors

Number	Name	Tag	Resistance*	Application	Source
3	pET-23b	His (C-terminus)	Amp	Expression	Novagen
29	pMal-C2	MBP	Amp	Expression	New England BioLabs
30	pEGFP-C1	EGFP (N-terminus)	Kana	Transfection	Clontech
34	pcDNA3	untagged	Amp	Transfection	Invitrogen
36	pETM30	GST, His (N-terminus)	Kana	Expression	EMBL
37	pETM41	His, MBP (N-terminus), His (C-terminus)	Kana	Expression	EMBL
65	pmCherry-N1	mCherry (C-terminus)	Kana	Transfection	Clontech
75	pMal-PreScission	MBP (N-terminus)	Amp	Expression	Sarah Port

Number	Name	Tag	Resistance*	Application	Source
AO2005	p415Met25_mTagBFP2	mTagBFP2	Amp	Expression	Laboratory of Prof. Dr. Schwappach

*Abbreviation of resistance: Amp: ampicillin, Kana: kanamycin

Table 22: Generated vectors

Number	Name	Cloning
89	pEGFP-(without EGFP)-mTagBFP2-MCS	PCR mTagBFP2 (AO2005, laboratory of Prof. Dr. Blanche Schwappach, G1808, G1809) cloned into vector #30 (AgeI, XhoI)

pEGFP-(without EGFP)-mTagBFP2-MCS

The EGFP-coding fragment of the vector pEGFP-C1 was replaced by mTagBFP2, which was PCR amplified using G1808 and G1809 as primers and AO2005 (laboratory of Prof. Dr. Blanche Schwappach) as template, via the restriction sites of AgeI and XhoI (figure 8).

Figure 8: Multiple cloning site of pEGFP-(without GFP)-mTagBFP2-MCS

2.1.4 Plasmids

Table 23: Available plasmids

Number	Name	Resistance*	Application	Source
23	pRSETb-His-Importin alpha	Amp	Expression	Laboratory of Ralph H. Kehlenbach
26	pET30a-S-His-Importin beta	Kana	Expression	Laboratory of Ralph H. Kehlenbach
293	pdEGFP-GST	Kana	Transfection	Christiane Spillner
294	pdEGFP-C1	Kana	Transfection	Laboratory of Ralph H. Kehlenbach
297	pdEGFP-GST-cNLS	Kana	Transfection	Sonja Neimanis
476	pEF-HA-Importin beta	Amp	Expression	Hutten et al. (2008)
552	pEF-myc-Importin beta	Amp	Expression	Sarah Hutten
762	pCS2+MT-Syne1B aa1639-1989 (*mus musculus*)	Amp	Transfection	Dan Starr
812	pCS2plus-Importin beta-FLAG	Amp	Expression	Detlef Doenecke (pJK255)
1052	pET328-HZZ-tev-emerin-opsin	Amp	Expression	Ralph H. Kehlenbach
1219	LRRC59-pcDNA3	Amp	Transfection	Antoni Wiedlocha
1224	pET328-HZZ-tev-LRRC59-opsin	Amp	Expression	Imke Baade
1230	pdEGFP-GST-cNLS-FKBP12	Kana	Transfection	Janine Pfaff, Kalpana Rajanala
1231	mCherry-FRB	Kana	Transfection	Kalpana Rajanala
1232	mCherry-FRB-Emerin	Kana	Transfection	Kalpana Rajanala
1239	pET328-His-ZZ-tev	Amp	Expression	Fabio Vilardi
1247	Sec61beta-opsin-pcDNA3.1	Amp	Transfection	Fabio Vilardi
1424	mCherry-FRB-LRR59	Kana	Transfection	Kalpana Rajanala
1425	WRB-FRB-HA	Amp	Transfection	Kalpana Rajanala
1458	pGEX-6P1-Nup62	Amp	Expression	Sarah Port, Sarina Norell
1469	pdEGFP-GST-FKBP12	Kana	Transfection	Kalpana Rajanala
1544	pMAL-PP-LRRC59 AA1-244-His	Amp	Expression	Cara Jamieson
1546	pmCherry-FRB-GST-LRRC59	Kana	Transfection	Cara Jamieson
1580	pGEM3Z-emerin-opsin	Amp	Expression	Fabio Vilardi
1603	pdEGFP-GST-M9-FKBP12	Kana	Transfection	Janine Pfaff, Christiane Spillner
1610	pcDNA3-FKBP12-EGFP-APEX2	Amp	Transfection	Marret Müller

Number	Name	Resistance*	Application	Source
1648	pEGFP-(without EGFP)-HA-FRB-Importin 13	Kana	Transfection	Marret Müller, Elif Günyüz
1684	pEGFP-Bimax2	Kana	Transfection	Kosugi et al. (2008); Dorothee Dormann
1720	pGEM3Z-Preprolactin-HA	Amp	Expression	Fabio Vilardi, laboratory of Prof. Dr. Blanche Schwappach, AO2045
1721	pGEM3Z-Preprolactin-myc	Amp	Expression	Fabio Vilardi, laboratory of Prof. Dr. Blanche Schwappach, AO2026
2105	pcDNA3.1(-)-cMyc-TRC40 WT	Amp	Transfection	Coy-Vergara et al. (2019)
2106	pcDNA3.1(-)-cMyc-TRC40 D74E	Amp	Transfection	Coy-Vergara et al. (2019)
2157	pET328-HZZ-tev-cytochrome b5-opsin	Amp	Expression	Favaloro et al. (2010)

*Abbreviation of resistance: Amp: ampicillin, Kana: kanamycin

Table 24: Generated plasmids

Number	Name	Cloning
1608	pMAL-PP-LRRC59 AA1-137-His	PCR EcoRI-LRRC59 AA1-137-SalI (#1219, G1468, G1560) cloned into vector #75 (EcoRI, SalI)
1609	PMAL-PP-LRRC59 AA138-244-His	PCR EcoRI-LRRC59 AA138-244-SalI (#1219, G1469, G1561) cloned into vector #75 (EcoRI, SalI)
1716	pET23b-HA-Emerin	PCR BamHI-HA-Emerin-XhoI (#1232, G1713, G1717) cloned into vector #3 (BamHI, XhoI)
1717	pET23b-HA-LRRC59	PCR EcoRI-HA-LRRC59-XhoI (#1424, G1715, G1718) cloned into vector #3 (EcoRI, XhoI)
1718	pET23b-HA-LRRC59 AA1-267	PCR EcoRI-HA-LRRC59-XhoI AA1-267 (#1424, G1715, G1719) cloned into vector #3 (EcoRI, XhoI)
1719	pET23b-HA-LRRC59 AA1-278	PCR EcoRI-HA-LRRC59 AA1-278-XhoI (#1424, G1715, G1720) cloned into vector #3 (EcoRI, XhoI)
1722	pEF-HA-Importin-β siRNA resistant	mutagenesis (G1711, G1712) on plasmid #476
1723	pEF-myc-Importin-β siRNA resistant	mutagenesis (G1711, G1712) on plasmid #552
1724	pCS2-FLAG-Importin-β siRNA resistant	mutagenesis (G1711, G1712) on plasmid #812
1821	pET23b-Preprolactin-HA	Fragment SacI-Preprolactin-HA-HindIII from plasmid #1720 cloned into vector #3 (SacI, HindIII)
1822	pET23b-Preprolactin-myc	Fragment SacI-Preprolactin-myc-HindIII from plasmid #1721 cloned into vector #3 (SacI, HindIII)
1844	pcDNA3-HA-SND2	PCR BamHI-HA-SND2-XhoI (HeLa P4 cDNA, G1773, G1774) cloned into vector #34 (BamHI, XhoI)
1845	pcDNA3-SND2-HA	PCR BamHI-SND2-HA-XhoI (HeLa P4 cDNA, G1775, G1776) cloned into vector #34 (BamHI, XhoI)
1846	dEGFP-GST-LRRC59 AA1-244	PCR EcoRI-LRRC59 AA1-244-XbaI (#1219, G1779, G1780) cloned into plasmid #1469 (EcoRI, XbaI)
1848	pmCerry-FRB-MBP-LRRC59	PCR XhoI-MBP-XhoI (vector #29, G1777, G1778) cloned into plasmid #1424 (XhoI)
1863	pET23b-Emerin-HA	PCR BamHI-Emerin-HA-XhoI (#1232, G1792, G1793) cloned into vector #3 (BamHI, XhoI)
1864	pET23b-LRRC59-HA	PCR EcoRI-LRRC59-HA-XhoI (#1424, G1794, G1795) cloned into vector #3 (EcoRI, XhoI)
1865	pET23b-LRRC59 AA1-267-HA	PCR EcoRI-LRRC59 AA1-267-HA-XhoI (#1424, G1794, G1796) cloned into vector #3 (EcoRI, XhoI)
1866	pET23b-LRRC59 AA1-278-HA	PCR EcoRI-LRRC59 AA1-278-HA-XhoI (#1424, G1794, G1797) cloned into vector #3 (EcoRI, XhoI)

Number	Name	Cloning
1867	pET23b-LRRC59 AA1-267-Emerin AA244-254-HA	PCR EcoRI-LRRC59 AA1-267-Emerin AA244-254-HA-XhoI (#1424, G1794, G1798) cloned into vector #3 (EcoRI, XhoI)
1884	pEGFP-LRRC59 AA1-235	PCR XhoI-LRRC59 AA1-235-EcoRI (#1219, G1813, G1816) cloned into vector #30 (XhoI, EcoRI)
1885	pEGFP-LRRC59 AA1-244	PCR XhoI-LRRC59 AA1-244-EcoRI (#1219, G1813, G1817) cloned into vector #30 (XhoI, EcoRI)
1886	pEGFP-LRRC59 AA1-137	PCR XhoI-LRRC59 AA1-137-EcoRI (#1219, G1813, G1814) cloned into vector #30 (XhoI, EcoRI)
1887	pEGFP-LRRC59 AA1-140	PCR XhoI-LRRC59 AA1-140-EcoRI (#1219, G1813, G1815) cloned into vector #30 (XhoI, EcoRI)
1888	pEGFP-LRRC59 AA138-235	PCR XhoI-LRRC59 AA138-235-EcoRI (#1219, G1816, G1818) cloned into vector #30 (XhoI, EcoRI)
1889	pEGFP-LRRC59 AA138-244	PCR XhoI-LRRC59 AA138-244-EcoRI (#1219, G1817, G1818) cloned into vector #30 (XhoI, EcoRI)
1890	pEGFP-LRRC59 AA141-235	PCR XhoI-LRRC59 AA141-235-EcoRI (#1219, G1816, G1819) cloned into vector #30 (XhoI, EcoRI)
1891	pEGFP-LRRC59 AA141-244	PCR XhoI-LRRC59 AA141-244-EcoRI (#1219, G1817, G1819) cloned into vector #30 (XhoI, EcoRI)
1892	pcDNA3-NES-mTagBFP2	PCR EcoRI-NES-mTagBFP2-XhoI (AO2005, laboratory of Prof. Dr. Blanche Schwappach, G1802, G1803) cloned into vector #34 (EcoRI, XhoI)
1893	pcDNA3-NES-mTagBFP2-cNLS	PCR EcoRI-NES-mTagBFP2-cNLS-XhoI (AO2005, laboratory of Prof. Dr. Blanche Schwappach, G1802, G1804) cloned into vector #34 (EcoRI, XhoI)
1894	pcDNA3-NES-MBP	PCR EcoRI-NES-MBP-XhoI (vector #29, G1805, G1806) cloned into vector #34 (EcoRI, XhoI)
1895	pcDNA3-NES-MBP-cNLS	PCR EcoRI-NES-MBP-cNLS-XhoI (vector #29, G1806, G1807) cloned into vector #34 (EcoRI, XhoI)
1905	pEGFP-(without EGFP)-HA-FRB-LRRC59	PCR XhoI-LRRC59-XbaI (#1219, G1811, G1812) cloned into plasmid #1648 (XhoI, XbaI)
1923	pEGFP-LRRC59 AA138-216	PCR EcoRI-LRRC59 AA138-216-XhoI (#1219, G1818, G1866) cloned into vector #30 (EcoRI, XhoI)
1924	pEGFP-LRRC59 AA138-225	PCR EcoRI-LRRC59 AA138-225-XhoI (#1219, G1818, G1867) cloned into vector #30 (EcoRI, XhoI)
1925	pEGFP-LRRC59 AA138-231	PCR EcoRI-LRRC59 AA138-231-XhoI (#1219, G1818, G1868) cloned into vector #30 (EcoRI, XhoI)
1926	pEGFP-LRRC59 AA 217-244	PCR EcoRI-LRRC59 AA217-244-XhoI (#1219, G1817, G1869) cloned into vector #30 (EcoRI, XhoI)
1927	pEGFP-LRRC59 AA138-244 K226A K228A	Mutagenesis (G1870, G1871) on plasmid #1889
1928	pEGFP-LRRC59 AA138-244 R232A R234A K235A	Mutagenesis (G1872, G1873) on plasmid #1889
1929	pcDNA3-HA-LRRC59	Fragment EcoRI-HA-LRRC59-XhoI from plasmid #1717 cloned into vector #34 (EcoRI, XhoI)
1930	pEGFP-LRRC59 AA138-244 R239A K240A R243A	Mutagenesis (G1874, G1875) on plasmid #1889
1932	pEGFP-LRRC59 AA138-244 R157A R159A R161A R162A	Mutagenesis (G1876, G1877) on plasmid #1889
1933	pEGFP-LRRC59 AA138-244 K171A K172A R173A K176A R178A	Mutagenesis (G1878, G1879) on plasmid #1889
1934	pEGFP-LRRC59 AA138-244 R185A R188A K189A R190A K192A	Mutagenesis (G1880, G1881) on plasmid #1889
1935	pEGFP-LRRC59 AA138-244 K196A R198A R199A R200A K201A	Mutagenesis (G1882, G1883) on plasmid #1889

Number	Name	Cloning
1936	pEGFP-LRRC59 AA138-244 K210A R211A K215A K216A	Mutagenesis (G1884, G1885) on plasmid #1889
1946	pcDNA3-HA-Emerin	PCR HindIII-HA-Emerin-BamHI (#1232, G1902, G1903) cloned into vector #34 (HindIII, BamHI)
1947	pcDNA3-HA-Emerin AA1-222	PCR HindIII-HA-Emerin AA1-222-BamHI (#1232, G1902, G1904) cloned into vector #34, (HindIII, BamHI)
1948	pMAL-PP-Emerin AA1-222-His	PCR BamHI-Emerin AA1-222-His-HindIII (#1232, G1900, G1901) cloned into vector #75 (BamHI, HindIII)
1968	pcDNA3-HA-LRRC59 AA1-244	PCR EcoRI-HA-LRRC59 AA1-244-EcoRI (#1219, G1715, G1817) cloned into vector #34 (EcoRI)
1974	pEGFP-LRRC59 AA 138-244 K207A K210A R211A K215A K216A K218A K219A	Mutagenesis (G1955, G1956) on plasmid #1936
1975	pEGFP-LRRC59 AA 138-244 K210A R211A K215A K216A K218A K219A	Mutagenesis (G1957, G1958) on plasmid #1936
1976	pEGFP-LRRC59 AA 138-225 K210A R211A K215A K216A K218A K219A	Mutagenesis (G1957, G1958) on plasmid #1924
1977	pmCherry-FRB-ALG5	PCR HindIII-ALG5-SalI (HeLa P4 cDNA, G1923, G1924) cloned into plasmid #1231 (HindIII, SalI)
1982	pEGFP-LRRC59 AA138-225 K207A K210A R211A K215A K216A K218A K219A	Mutagenesis (G1955, G1956) on plasmid #1976
1983	pmCherry-FRB-ALG1	PCR XhoI-ALG1-SalI (HeLa P4 cDNA, G1905, G1906) cloned into plasmid #1231 (XhoI, SalI)
1984	pmCherry-FRB-LMAN2	PCR XhoI-LMAN2-SalI (HeLa P4 cDNA, G1911, G1912) cloned into plasmid #1231 (XhoI, SalI)
1985	pmCherry-FRB-TMED10	PCR XhoI-TMED10-SalI (HeLa P4 cDNA, G1919, G1920) cloned into plasmid #1231 (XhoI, SalI)
1986	pET23b-Emerin AA1-222-His	PCR BamHI-Emerin AA1-222-His-HindIII (#1948, G1900, G1901) cloned into vector #3 (BamHI, HindIII)
1987	pcDNA3-mTagBFP2-cNLS	PCR EcoRI-mTag-BFP2-cNLS-XhoI (#1893, G1804, G1961) cloned into vector #34 (EcoRI, XhoI)
1994	pmCherry-FRB-SYNE1B AA1639-1989	PCR XhoI-SYNE1B AA1639-1989-HindIII (#762, G1962, G1963) cloned into plasmid #1231 (XhoI, HindIII)
1995	pEGFP-LRRC59 AA138-244 K210A R211A K215A K216A K218A K219A R239A K240A R243A	Mutagenesis (G1874, G1875) on plasmid #1975
1996	pFRB-mCherry	PCR AgeI-FRB-SalI (#1424, G1977, G1978) cloned into vector #65 (AgeI, SalI)
1997	pEGFP-LRRC59 AA138-244 K207A K210A R211A K215A K216A K218A K219A R239A K240A R243A	Mutagenesis (G1955, G1956) on plasmid #1995
1998	pmCherry-FRB-BET1	PCR XhoI-BET1-EcoRI (HeLa P4 cDNA, G1909, G1968) cloned into plasmid #1424 (XhoI, EcoRI)
1999	pmCherry-FRB-BET1L	PCR XhoI-BET1L-EcoRI (HeLa P4 cDNA, G1925, G1969) cloned into plasmid #1424 (XhoI, EcoRI)
2000	pmCherry-FRB-SEC61B	PCR XhoI-SEC61B-EcoRI (#1247, G1927, G1971) cloned into plasmid #1424 (XhoI, EcoRI)
2001	pTMED2-FRB-mCherry	PCR XhoI-TMED2-EcoRI (HeLa P4 cDNA, G1917, G1998) cloned into plasmid #1996 (XhoI, EcoRI)
2002	pTMED10-FRB-mCherry	PCR XhoI-TMED10-EcoRI (#1985, G1919, G1999) cloned into plasmid #1996 (XhoI, EcoRI)
2003	pmCherry-FRB-SEC22B	PCR XhoI-SEC22-EcoRI (HeLa P4 cDNA, G1959, G1975) cloned into plasmid #1424 (XhoI, EcoRI)

Number	Name	Cloning
2004	ALG14-FRB-mCherry	PCR XhoI-ALG14-HindIII (HeLa P4 cDNA, G1907, G1991) cloned into plasmid #1996 (XhoI, HindIII)
2005	LMAN2-FRB-mCherry	PCR XhoI-LMAN2-HindIII (#1984, G1911, G1992) cloned into plasmid #1996 (XhoI, HindIII)
2006	PIGK-FRB-mCherry	PCR XhoI-PIGK-HindIII (HeLa P4 cDNA, G1913, G1993) cloned into plasmid #1996 (XhoI, HindIII)
2007	DDOST-FRB-mCherry	PCR XhoI-DDOST-HindIII (HeLa P4 cDNA, G2002, G2003) cloned into plasmid #1996 (XhoI, HindIII)
2008	mCherry-FRB-UBE2J1	PCR XhoI-UBE2J1-SalI (HeLa P4 cDNA, G2004, G2005) cloned into plasmid #1424 (XhoI, SalI)
2009	mCherry-FRB-UBE2J2	PCR HindIII-UBE2J2-EcoRI (HeLa P4 cDNA, G2006, G2007) cloned into plasmid #1424 (HindIII, EcoRI)
2017	DDOST K450A K452A K454A -FRB-mCherry	Mutagenesis (G2028, G2029) on plasmid #2007
2018	LMAN2 K347A R348A R351A K353A R354A -FRB-mCherry	Mutagenesis (G2030, G2031) on plasmid #2005
2019	pEGFP-SEC22B AA1-194	PCR XhoI-SEC22B AA1-194-EcoRI (#2003, G2032, G2033) cloned into vector #30 (XhoI, EcoRI)
2020	pEGFP-SEC61B AA1-70	PCR XhoI-SEC61B AA1-70-EcoRI (#2000, G2034, G2035) cloned into vector #30 (XhoI, EcoRI)
2021	pEGFP-UBE2J1 AA1-285	PCR XhoI-UBE2J1 AA1-285-BamHI (#2008, G2036, G2037) cloned into vector #30 (XhoI, BamHI)
2022	pEGFP-UBE2J2 AA1-226	PCR EcoRI-UBE2J2 AA1-226-BamHI (#2009, G2038, G2039) cloned into vector #30 (EcoRI, BamHI)
2023	pcDNA3-HA-FKBP12	PCR HindIII-HA-FKBP12-EcoRV (#1603, G2040, G2041) cloned into vector #34 (HindIII, EcoRV)
2024	pcDNA3-FKBP12-HA	PCR EcoRV-FKBP12-HA-EcoRI (#1603, G2044, G2045) cloned into vector #34 (EcoRV, EcoRI)
2025	pmCherry-FRB-LRRC59 K210A R211A K215A K216A K218A K219A R239A K240A R243A	PCR XhoI-LRRC59 K210A R211A K215A K216A K218A K219A R239A K240A R243A-EcoRI (GeneArt™ Gene Synthesis LRRC59_mut_210-243, G1379, G1453) cloned into #2003 (XhoI, EcoRI)
2026	pET328-HZZ-tev-SUN1	PCR EcoRI-SUN1-HindIII (HeLa P4 cDNA, G2056, G2057) cloned into plasmid #1239 (EcoRI, HindIII)
2030	pMAL-PP-LRRC59 AA138-244 K210A R211A K215A K216A K218A K219A R239A K240A R243A	PCR EcoRI-LRRC59 AA138-244 K210A R211A K215A K216A K218A K219A R239A K240A R243A-SalI (#2025, G1561, G2096) cloned into plasmid #1544 (EcoRI, SalI)
2031	pMAL-PP-LRRC59 AA1-244 K210A R211A K215A K216A K218A K219A R239A K240A R243A	PCR EcoRI-LRRC59 AA1-244 K210A R211A K215A K216A K218A K219A R239A K240A R243A-SalI (#2025, G1468, G2096) cloned into plasmid #1608 (EcoRI, SalI)
2042	pcDNA3-HA-FKBP12-Nup62	PCR EcoRV-Nup62-XhoI (#1458, G2042, G2043) cloned into plasmid #2023 (EcoRV, XhoI)
2045	pcDNA3-NEGFP-FLAG	PCR HindIII-NEGFP-FLAG-BamHI (vector #30, G2089, G2090) cloned into vector #34 (HindIII, BamHI)
2046	pcDNA3-HA-FKBP12-Nup54	Pre-PCR Nup54 (HeLa P4 cDNA, G2105, G2106), PCR on Pre-PCR NotI-Nup54-XhoI (G2077, G2078) cloned into plasmid #2023 (NotI, XhoI)
2047	pcDNA3-Nup58-HA-FKBP12	Pre-PCR Nup54 (HeLa P4 cDNA, G2107, G2108), PCR on Pre-PCR HindIII-Nup54-BamHI (G2083, G2084) cloned into plasmid #2024 (HindIII, BamHI)
2090	pETM30-Nup210 AA1830-1887	PCR NcoI-Nup210 AA1830-1887-EcoRI (GeneArt™ Gene Synthesis Nup210_AA1830-1887) cloned into vector #36 (NcoI, EcoRI)
2091	pET328-HZZ-SUN1-opsin	PCR EcoRI-SUN1-opsin-HindIII (plasmid #2026, G2056, G2161) cloned into plasmid #2026 (EcoRI, HindIII)

Number	Name	Cloning
2092	pdEGFP-MBP-M9-FKBP12	PCR 1 XhoI-MBP-HindIII (plasmid #1848, G2176, G2177), PCR 2 HindIII-M9-EcoRI (plasmid #1603, G2178, G2179), PCR 3 EcoRI-FKBP12-BamHI (plasmid #1603, G2180, G2181) cloned into plasmid #294 (XhoI, BamHI)
2093	pcDNA3-FLAG-BiMAX2	PCR BamHI-FLAG-BiMAX2-EcoRI (plasmid #1684, G2182, G2183) cloned into vector #34 (BamHI, EcoRI)
2094	pmCherry-FRB-LRRC59 S227A S229A S231A	Mutagenesis (G2172, G2173) on plasmid #1424
2102	pmCherry-FRB-LRRC59 (containing GGGGS linker)	PCR 1 BspOI-mCherry-AgeI (plasmid #1424, G2197, G2200), PCR 2 AgeI-FRB-XhoI (plasmid #1424, G2191, G2199), PCR 3 XhoI-LRRC59-EcoRI (plasmid #1424, G2195, G2196) cloned into plasmid #1424 (BspOI, EcoRI)
2103	pmCherry-FRB-MBP-LRRC59 (containing GGGGS linker)	PCR 1 BspOI-mCherry-AgeI (plasmid #1424, G2197, G2200), PCR 2 AgeI-FRB-HindIII (plasmid #1424, G2191, G2192), PCR 3 HindIII-MBP-XhoI (plasmid #1848, G2193, G2194), PCR 4 XhoI-LRRC59-EcoRI (plasmid #1424, G2195, G2196) cloned into plasmid #1424 (BspOI, EcoRI)
2104	pmCherry-FRB-LRRC59 S227A S229A S231A T242A S244A	Mutagenesis (G2174, G2175) on plasmid #2094
2107	pmCherry-mCherry-FRB-LRRC59 (containing GGGGS linker)	PCR 1 BspOI-mCherry-EcoRV (plasmid #1424, G2197, G2198), PCR 2 EcoRV-mCherry-AgeI (plasmid #1424, G2189, G2190), PCR3 AgeI-FRB-XhoI (plasmid #1424, G2191, G2199), PCR4 XhoI-LRRC59-EcoRI (plasmid #1424, G2195, G2196) cloned into plasmid #1424 (BspOI, EcoRI)
2108	pmCherry-mCherry-FRB-MBP-LRRC59 (containing GGGGS linker)	PCR1 BspOI-mCherry-EcoRV (plasmid #1424, G2197, G2198), PCR2 EcoRV-mCherry-AgeI (plasmid #1424, G2189, G2190), PCR3 AgeI-FRB-HindIII (plasmid #1424, G2191, G2192), PCR4 HindIII-MBP-XhoI (plasmid #1848, G2193, G2194), PCR5 XhoI-LRRC59-EcoRI (plasmid #1424, G2195, G2196) cloned into plasmid plasmid #1424 (BspOI, EcoRI)
2109	pMBP-mCherry-FRB-MBP-LRRC59 (containing GGGGS linker)	PCR1 BspOI-MBP-EcoRV (plasmid #1848, G2187, G2188), PCR2 EcoRV-mCherry-AgeI (plasmid #1424, G2189, G2190), PCR3 AgeI-FRB-HindIII (plasmid #1424, G2191, G2192), PCR4 HindIII-MBP-XhoI (plasmid #1848, G2193, G2194), PCR5 XhoI-LRRC59-EcoRI (plasmid #1424, G2195, G2196) cloned into plasmid #1424 (BspOI, EcoRI)
2110	pET328-HZZ-tev-P2X2	PCR EcoRI-P2X2-HindIII (GeneArt™ Gene Synthesis EcoRI-P2X2-HindIII, G2212, G2213) cloned into plasmid #1239 (EcoRI, HindIII)
2111	pET328-HZZ-tev-Preprolactin-HA	Fragment SacI-Preprolactin-HA-HindIII from plasmid #1821 cloned into vector #1239 (SacI, HindIII)
2112	pET328-HZZ-tev-Preprolactin-myc	Fragment SacI-Preprolactin-myc-HindIII from plasmid #1822 cloned into vector #1239 (SacI, HindIII)
2119	mCherry-FRB-MBP-Sec61ß	PCR XhoI-MBP-XhoI (plasmid #1848, G1777, G1778) cloned into plasmid #2000 via XhoI
2120	LMAN2-MBP-FRB-mCherry	PCR HindIII-MBP-EcoRI (plasmid #1848, G2129, G2130) cloned into plasmid #2005 via HindIII, EcoRI
2121	DDOST-MBP-FRB-mCherry	PCR HindIII-MBP-HindIII (plasmid #1848, G2129, G2131) cloned into plasmid #2007 via HindIII
2122	mCherry-FRB-MBP-UBE2J2	PCR HindIII-MBP-HindIII (plasmid #1848, G2132, G2133) cloned into plasmid #2009 via HindIII
2123	mCherry-FRB-MBP-Sec22ß	PCR XhoI-MBP-XhoI (plasmid #1848, G1777, G1778) cloned into plasmid #2003 via XhoI

Number	Name	Cloning
2124	mCherry-FRB-MBP-UBE2J1	PCR XhoI-GST-XhoI (plasmid #1848, G1777, G1778) cloned into plasmid #2008 via XhoI
2125	mCherry-FRB-GST-Sec61ß	PCR XhoI-GST-XhoI (plasmid #1546, G2225, G2226) cloned into plasmid #2000 via XhoI
2126	mCherry-FRB-GST-Sec22ß	PCR XhoI-GST-XhoI (plasmid #1546, G2225, G2226) cloned into plasmid #2003 via XhoI
2127	LMAN2-GST-FRB-mCherry	PCR HindIII-GST-EcoRI (plasmid #1546, G2229, G2230) cloned into plasmid #2005 via HindIII, EcoRI
2128	DDOST-GST-FRB-mCherry	PCR HindIII-GST-HindIII (plasmid #1546, G2229, 2231) cloned into plasmid #2007 via HindIII
2129	mCherry-FRB-GST-UBE2J1	PCR XhoI-GST-XhoI (plasmid #1546, G2225, G2226) cloned into plasmid #2008 via XhoI
2130	mCherry-FRB-GST-UBE2J2	PCR HindIII-GST-HindIII (plasmid #1546, G2227, G2228) cloned into plasmid #2009 via HindIII

2.2 Molecular Biology Methods

2.2.1 RNA Isolation from Cellular Extracts

Total RNA was isolated from HeLa P4 cells, growing on a 10 cm cell culture dish with a density of $1x10^7$ cells, using the RNeasy Mini Kit (Qiagen). The protocol "Purification of Total RNA from Animal Cells using Spin Technology" was performed according to the instructions of the manufacturer. For RNA elution, two times 30 µl RNase-free water was used. Before storage at -20 °C, RNA purity was determined by measurement of the A_{260}/A_{280} ratio with the spectrophotometer NanoDrop 2000c. Samples with an A_{260}/A_{280} ratio of 1.8-2.0 were considered as pure RNA.

2.2.2 cDNA synthesis

Complementary DNA (cDNA) is an artificially synthesized DNA from mRNA as template using the enzyme reverse transcriptase. For cDNA synthesis from isolated RNA, the SuperScirpt III reverse transcriptase of Thermo Fisher Scientific was used according to manufacturer's recommendation. 2 µg of RNA was mixed with 1 µl of 100 µM oligo(dT)-primer, 1 µl of 10 mM dNTPs and an appropriate volume of RNAse-free water for a final volume of 13 µl. After 5 minutes of incubation at 65 °C, the solution was cooled on ice for 1 minute. For synthesis of cDNA, 4 µl of 5x First-Strand buffer, 1 µl of 0.1 M DTT (dithiothreitol), 1 µl of RiboLock RNase Inhibitor (40 U/µl) and 1 µl of SuperScript III reverse transcriptase (100 U/µl) were added to the reaction. Reactions were performed after careful mixing of all components at 50 °C for 60 minutes before enzyme inactivation at 70 °C for 15 minutes. cDNA was stored at -20 °C.

2.2.3 Polymerase Chain Reaction (PCR)

Polymerase chain reaction is an *in vitro* method for amplification of a selected, specific DNA sequence using a DNA template, two oligonucleotide primers, dNTPs and a thermostable DNA polymerase under different temperature phases (Mullis and Faloona, 1987; Saiki et al., 1988). For amplification of specific DNA segments, the Phusion High-Fidelity DNA Polymerase (Thermo Fisher Scientific) was used according to manufacturer's instructions. The amplification was performed using 1-2 µl of cDNA or 100 ng of plasmid DNA as template. For a 50 µl reaction, the template was mixed with high-fidelity buffer, 0.2 µM of forward and reverse primer, respectively, 0.2 mM of dNTPs, 1 U of proof-reading Phusion polymerase and an appropriate volume of ddH_2O. The amplification was performed in a three-temperature step reaction using a thermocycler. For the denaturation of complexes of DNA and primers, the mixture was heated to 98 °C for 10 seconds, followed by an annealing phase for 15 seconds at 56-62 °C according to the melting temperature of the primers, and an elongation step at 72 °C adjusted to the number of base pairs of the amplified DNA segment with 30 seconds/1000 base pairs.

This cycle was repeated 35 times. The PCR product was mixed with 6x DNA loading buffer and analyzed by preparative agarose gel-electrophoresis (see section 2.2.5)

2.2.4 Site-directed mutagenesis

Site-directed mutagenesis is a PCR-based method to change single base pairs of a DNA sequence introducing the sequence change via primers. The used protocol is based on the publication of Weiner et al. (1994). For the mutagenesis PCR of 50 µl volume, 1 µg of plasmid DNA was added to Pfu buffer, 0.2 µM for forward and reverse primers, 0.2 mM dNTPs, 2.5 U Pfu Ultra II DNA polymerase (Agilent) and filled up with ddH_2O. For the denaturation step of the PCR, a temperature of 98 °C for 30 seconds was chosen, followed by annealing of primers and single strand DNA at 60 °C for 30 seconds and an elongation phase at 72 °C for a time adjusted to the number of base pairs of the plasmid DNA by 1000 base pairs/minute. This amplification cycle was repeated 35 times. Afterwards, the template plasmid DNA was digested by the addition of 2 µl of DpnI (Thermo Fisher Scientific) at 37 °C for 3 h, as this restriction enzyme cleaves only the methylated template DNA. 25 µl of the digested PCR product was then transformed into chemically competent *E. coli* DH5α (see section 2.2.10). The bacteria were plated onto LB agar plates containing appropriate antibiotics and incubated at 37 °C over night. At least three colonies were picked for inoculation of 6 ml of LB media supplemented with antibiotics at 37 °C over night. Plasmid DNA was isolated from 5 ml of the culture using NucleoSpin® Plasmid Isolation Kit of Macherey-Nagel (see section 2.2.11).

2.2.5 Agarose gel electrophoresis

Agarose gel electrophoresis is a method for DNA fragment separation using an electric field to move the charged molecules through an agarose matrix. The used protocol is based on the publication of Lee et al. (2012), with adjustments in buffer compositions and usage of a non-toxic nucleic acid stain instead of ethidium bromide. For visualization of the DNA fragments, the 1-2% agarose gels were supplemented with SafeView™ Classic DNA stain (Applied Biological Materials Inc.) according to the instructions of the manufacturer. Agarose was dissolved in 1x TAE (Tris/Acetate/EDTA) buffer by boiling in a microwave oven. After the solution was cooled down to 60 °C, SafeView™ Classic DNA stain was added (7.5 µl/100 ml agarose gel solution) prior to casting of the gel. DNA samples were supplemented with 6x DNA loading buffer and loaded onto the gel next to a DNA standard for size comparison (GeneRuler 100bp DNA Ladder, GeneRuler 100bp DNA Ladder Plus, GeneRuler 1kb DNA Ladder, Thermo Fisher Scientific). The gel run in 1x TAE buffer at 100 V for 20 to 40 minutes depending on the size of the DNA fragments to be separated and the gel size. DNA fragments determined for further cloning were identified and cut out on a UV (ultraviolet) transilluminator using a scalpel, followed by purification using the NucleoSpin® PCR clean-up/Gel extraction kit (Macherey-Nagel) according to the recommendation of the manufacturer. For analytical agarose gel electrophoresis of DNA fragments resulting from plasmid DNA digestion, size separation was documented using Agarose gel documentation GelSTICK touch.

2.2.6 Quantification of double stranded DNA

Concentration and purity of DNA was determined using the NanoDrop 2000c (Thermo Fisher Scientific) by measurement of the UV absorbance at 260 nm and 280 nm. Samples with an A_{260}/A_{280} ratio of 1.7 to 2 were considered as double stranded DNA and further processed.

2.2.7 Restriction enzyme digest

Restriction digestion is a technique for cleavage of DNA at specific sites of the sequence using restriction endonucleases. With this tool, DNA fragments can be removed from a plasmid and further inserted into another linearized plasmid, cut with the same enzymes. For planning of the cloning strategy, the enzyme ratio and the best buffer conditions of the digest, the Double Digest Calculator from Thermo Fisher Scientific was used.

Preparative digest of PCR products and plasmids

For plasmid DNA digestion, 3 µg of plasmid was cut using 2 U of restriction enzyme in a total reaction volume of 40 µl, supplemented with 1x buffer, suitable for the enzyme combination, and ddH_2O. PCR products were extracted from agarose gels using PCR clean-up/Gel extraction Kit and eluted in 25 µl of buffer NE. For a digestion reaction volume of 40 µl, 1 U of restriction enzyme each, ddH_2O and recommended 1x buffer was added. The reactions were incubated at 37 °C for 2 h. Digested plasmid DNA was supplemented with 6x DNA loading buffer after dephosphorylation (see section 2.2.8) and analyzed by agarose gel electrophoresis followed by isolation, while digested PCR products were purified using the PCR clean-up protocol of PCR clean-up/gel extraction Kit of Macherey-Nagel.

Analytical digest of isolated plasmid DNA

For the analysis of cloning success, 300-500 ng of plasmid DNA were digested in a total reaction volume of 20 µl, 0.5 U of each restriction enzyme and 1x buffer, suitable for the enzyme combination. DNA was digested at 37 °C for 2 hours prior to analytic agarose gel electrophoresis.

2.2.8 Dephosphorylation of vectors

After restriction digest, the phosphate groups of the 5'-ends of the cleaved DNA-strands were removed using Fast alkaline phosphatase to avoid recirculation during ligation of the plasmid cut by just one enzyme. 1 U of FastAP (Thermo Fisher Scientific) was added to 40 µl of the digestion reaction and incubated at 37 °C for 10 minutes. Afterwards, plasmid DNA was analyzed in a preparative way by agarose gel electrophoresis.

2.2.9 Ligation of DNA Fragments

To ligate DNA fragments cut with one or two identical restriction enzymes, T4 DNA ligase (Thermo Fisher Scientific) was used, which joins the DNA fragment ends by the formation of two covalent phosphodiester bonds between the 3'-hydroxyl end of one with the 5'-phosphate end of another DNA terminus. In a reaction volume of 10 µl, 100 ng of digested, dephosphorylated and purified plasmid was mixed with 5x molar excess of the DNA fragment to be inserted, 1 µl of 100 mM ATP, 1 µl of 10x T4 ligase buffer, 0.2 µl of T4 DNA ligase (1 U/µl) and ddH_2O. The reaction solution was incubated at room temperature for 1-2 hour(s) and partially transformed into *E. coli* DH5α (see section 2.2.10).

2.2.10 Transformation of plasmid DNA into *E. coli* DH5α

Bacterial transformation is a method to introduce foreign plasmid DNA into a bacterium (modified from Seidman and Struhl (2001), Froger and Hall (2007)). Chemically competent *E. coli* DH5α cells were thawed on ice for 10 minutes, before 5 µl of ligation reaction, 0.3 µg of plasmid DNA or 25 µl of mutagenesis-PCR was added for 30 minutes. Cells were heat shocked at 42 °C for 90 seconds prior to 2 minutes incubation on ice followed by addition of 500 µl SOC-medium and soft shaking of 400 rpm in a Thermomixer at 37°C for 60 minutes. Afterwards, cells were spun down at 300 xg for 3 minutes, 450 µl of the supernatant was removed, the pellet was resuspended in the remaining media and plated on LB agar plates containing the appropriate antibiotic using 10-20 glass beads. The bacteria were incubated at 37 °C over night.

2.2.11 Small Scale Plasmid DNA Isolation

For the isolation of the plasmid DNA, the NucleoSpin® Plasmid Miniprep Kit according to Macherey-Nagel's instruction was used which is based on the protocol of Birnboim and Doly (1979). Individual bacteria colonies were picked using a pipet tip and used for inoculation of 6 ml of LB-medium supplemented with appropriate antibiotics. After growing at 37 °C at 150 rpm for 16 h, 5 ml of the bacteria solution was pelleted in several steps in a 2 ml reaction tube at 11,000 xg for 1 minute. From this bacteria pellet, the plasmid DNA was isolated following the protocol "Isolation of high-copy plasmid DNA from *E. coli*" or "Isolation of low-copy plasmid DNA from *E. coli*" of the kit.

2.2.12 Large Scale Plasmid DNA Isolation

After successful DNA-sequencing (see section 2.2.13) of a newly cloned plasmid, plasmid DNA was isolated from *E. coli* DH5α in a large scale using NucleoBond™ Xtra Midi Kit (Macherey-Nagel, based on Birnboim and Doly (1979)) according to instructions of the manufacturer. For the protocol "High-copy plasmid purification" 200 ml of LB-medium supplemented with antibiotic was inoculated with 1 ml of bacteria culture containing the sequenced plasmid, while 400 ml of LB-medium was used for the protocol "Low-copy plasmid purification". The bacteria culture was incubated at 37 °C at 150 rpm over night and pelleted at 5250 xg at 4 °C for 20 minutes. After the purification, the DNA-concentration was adjusted to 1 mg/ml with ddH_2O.

2.2.13 Sequencing

All newly cloned plasmids were sequenced by GATC Biotech, a subcompany of Eurofins Genomics. Either GATC-standard primers were selected for sequencing or costumer specific primers (table 19) at a concentration of 10 pmol/µl in 20 µl volume were sent together with the samples to be analyzed. The company performs sequencing based on Sanger et al. (1977).

2.3 Biochemical Methods

2.3.1 SDS-PAGE

Sodium dodecyl sulfate (SDS) polyacrylamide gel electrophoresis (PAGE) is a method for separation of charged molecules by their molecular mass in an electric field, described first by Laemmli (1970), performed here with modifications according to Harlow and Lane (1988) and Sambrook and Russell (2006). Two-parted gels consisting of a resolving gel containing 10-15% acrylamide and a stacking gel with 5% acrylamide were prepared in the Dual Gel Caster for Mini Vertical Units of Hoefer. Protein samples or cell lysate were supplemented with SDS sample buffer, boiled at 95 °C for 5 minutes and centrifuged at 15,000 xg for 5 minutes prior to loading of the gel. For protein molecular mass comparison, the protein standard PageRuler Prestained Protein Ladder or PageRuler Unstained Protein Ladder (Thermo Scientific Fisher) was loaded next to the samples. Gel running was performed in the SE250 Mighty Small II Mini Vertical Electrophoresis Unit of Hoefer using 1x Laemmli running buffer at 20-25 mA per gel until the required separation was reached. For better visualization of protein samples of small and large molecular mass, Mini Protean TGX Precast gels (4-20%, Bio-Rad) were used for SDS-PAGE of RAPIDS experiments (see section 2.6.4). Gels were either used for visualization of proteins with Coomassie staining or for immunodetection after Western blotting.

2.3.2 Coomassie staining of SDS-PAGE gels

Proteins of pulldown experiments or purifications separated via SDS-PAGE were visualized using Coomassie staining, as Coomassie dye interacts with amino and carboxyl groups of proteins. The gel was incubated in ddH_2O for 10 minutes prior to fixation using Coomassie fixing solution for 5-60 minutes and staining with Coomassie staining solution over night. Gels were rinsed with ddH_2O shortly before documentation with LAS3000 (Fujifilm) followed by image analysis using ImageJ. The Coomassie staining protocol was modified from Neuhoff et al. (1988) and Kang et al. (2002).

2.3.3 Western Blotting

For the immunodetection of proteins, the proteins separated by SDS-PAGE were blotted under wet conditions onto an Amersham Protran 0.45 µm NC Nitrocellulose Blotting Membrane (GE Healthcare). For blotting, the Mini Trans-Blot® Cell of Bio-Rad filled with cold 1x Western blot transfer buffer and a cooling pack was used. The SDS-gel was placed without air bubbles onto the nitrocellulose membrane surrounded by Whatman gel blotting paper and fiber pads to both sides in a gel holder cassette. The transfer was performed at 100 V for 1.5 h. Blotting onto nitrocellulose membrane was first described by Towbin et al. (1979).

2.3.4 Ponceau S staining

After blotting of proteins onto nitrocellulose membrane, they were optionally stained by incubation with Ponceau S staining solution for 1 minute (Salinovich and Montelaro, 1986). Excess of staining solution was removed by several washing steps with 0.1% acetic acid. For documentation of the stained proteins, LAS-3000 (Fujifilm) was used, followed by image processing in ImageJ.

2.3.5 Immunodetection of proteins

The immunodetection of proteins is based on the method described by Gallagher et al. (2004) and the recommendation of LI-COR, the developer company of the Odyssey System. The nitrocellulose membrane was incubated with 5% milk powder dissolved in 1x TBST buffer for 30 minutes at room temperature on a rocking plate after blotting was completed. The membrane was cut into smaller pieces using the PageRuler prestained protein Ladder for orientation. Each piece was incubated with appropriate antibodies diluted in 5% TBST-milk at 4 °C over night. Unbound antibodies were removed by three washing steps with 1x TBST at room temperature on the rocker plate for 10 minutes each. After that, the membrane was incubated with appropriate fluorescence- or HRP- (Schneppenheim et al., 1991) coupled secondary antibodies (1:10,000 in 1x TBST-milk) for at least 1 hour at room temperature. After three washing steps with 1x TBST for 10 minutes on a rocker plate, the fluorescence-coupled antibodies were visualized using the Odyssey® Sa Infrared Imaging System or Odyssey® CLx Imaging System of LI-COR. For HRP-coupled secondary antibody detection, the membrane was incubated with Immobilon™ Western Chemiluminescent HRP Substrate (Millipore) for 1 minute, before the emitted luminescence light was detected using the LAS3000 (Fujifilm) or by putting the membrane into a light-protected cassette and exposing it to Medix XBU medical X-ray film (FOMA Bohemia), followed by film development in the developer machine CURIX60 (Agfa).

2.3.6 Protein purification

Purified GST (glutathione S-transferase) was available in the common laboratory stock.

For *in vitro* binding assays, recombinant proteins were expressed in *E. coli* Rosetta 2. For the cultivation of *E. coli* Rosetta 2, 30 mg/l chloramphenicol and, according to transformed plasmid for protein expression, 100 mg/l ampicillin or 60 mg/l kanamycin were added to the LB medium. After transformation of 0.2 µg of plasmid DNA (pETM41 for expression of His-MBP-His, pMAL-PP-LRRC59 aa1-244 for expression of MBP-LRRC59 aa1-244-His and pETM30-Nup210 aa1830-1887 for expression of His-GST-Nup210 aa1830-1887) into bacteria, cells were distributed using glass beads onto LB agar plates with appropriate antibiotics and 1.5 µg of chloramphenicol per plate and incubated at 37 °C over night. On the next day, 6 ml LB medium containing antibiotics was inoculated with 25 colonies picked from the LB agar plate. This preculture was cultivated at 37 °C for 4 hours prior to inoculation of an overnight preculture of 250 ml LB medium supplemented with appropriate antibiotics. The overnight preculture was used on the next morning to inoculate 3 to 9 l of LB medium supplemented with appropriate antibiotics starting with an OD_{600} of 0.03-0.06 (optical density at a wavelength of 600 nm). The culture was incubated at 37 °C with 120 rpm until reaching an OD_{600} of 0.6. Prior to the addition of 0.3 mM IPTG to start overexpression of proteins, a 30 µl sample (“before induction”) was taken and supplemented with 30 µl of SDS sample buffer. For protein expression, cultures were incubated for 4 hours at 25 °C. 30 µl of bacteria culture was supplemented with 30 µl of SDS sample buffer referred to as “after induction”. For cell harvest, cells were centrifuged at 4200 rpm (Beckman Coulter, centrifuge J6-MI with rotor JS 4.2) and 4 °C for 30 minutes. The cell pellet was resuspended in 25 ml of cold PBS and transferred into 50 ml Falcon tubes. Cells were centrifuged at 4750 xg and 4 °C for 15 minutes before the supernatant was removed and the pellet was frozen in liquid nitrogen for storage at -80 °C.

For purification, a pellet from 2 l of bacteria culture, was resuspended in 35 ml medium salt buffer prior to cell lysis using an EmulsiFlex-C3 (BD Bioscience). A sample of 30 µl referred to as “EmulsiFlex homogenate” was supplemented with 30 µl of SDS sample buffer. For clearing, the lysate was

centrifuged at 100,000 xg and 4 °C for 30-60 minutes. 30 µl of the cleared lysate was mixed with SDS sample buffer for workflow control and referred to as “total fraction”. For 35 ml of cleared lysate, 700 µl of NI-NTA Agarose (Qiagen) was equilibrated in 50 ml medium salt buffer and spun down at 800 xg and 4 °C for 3 minutes. The supernatant was removed and the cleared cell lysate was added to the beads and incubated at 4 °C for 2 hours on a spinning wheel. After binding of proteins to the beads, the mixture was centrifuged at 800 xg, 4 °C for 3 minutes (sample “unbound”) before three or four washing steps using 50 ml of medium salt buffer supplemented with 20 mM imidazole. After each centrifugation step, a sample of the supernatant was taken referred to as “washing 1-4”. The beads were transferred into an empty column and proteins were eluted from the beads using medium salt buffer supplemented with 300 mM imidazole (“non-dialyzed eluate”). To remove imidazole from the eluate, the eluted sample was desalted with medium salt buffer using PD-10 Desalting Columns (GE Healthcare). Fractions containing the highest amount of protein were identified using Pierce Coomassie Plus Protein Assay Reagent (Thermo Fisher Scientific) and pooled. After dialysis, the eluate was aliquoted and frozen in liquid nitrogen for storage at -80 °C (dialyzed eluate). For protein concentration determination, SDS-PAGE followed by Coomassie staining was performed with increasing amounts of purified proteins. The concentration was calculated relative to a BSA-standard using an LAS3000-picture of the Coomassie stained gel, lane scanning with ImageJ and analysis by Microsoft Excel.

2.3.7 Binding assay

For analysis of protein binding of LRRC59 aa1-244 and Nup210 aa1830-1887, pulldown experiments were performed immobilizing either MBP-LRRC59 aa1-244-His and His-MBP-His as control on amylose beads or His-GST-Nup210 aa1830-1887 or GST as control on glutathione beads. 75 µl of Amylose Resin High Flow (BioLabs) or Glutathione Sepharose High Performance (GE Healthcare) was equilibrated in pulldown buffer (Port et al., 2016) in 500 µl reaction tubes. Beads were centrifuged at 500 xg, 4 °C for 3 minutes followed by removal of the supernatant. For each immobilized protein, 200 pmol was added to the beads together with 500 µl of pulldown buffer prior to incubation at 4 °C on a spinning wheel for 60 minutes. After immobilization of the proteins, beads were washed twice with binding buffer. After washing, 500 µl of binding buffer was added to the beads followed by 5 minutes of incubation on ice and addition of 600 pmol of MBP-LRRC59 aa1-244 to the immobilized GST or His-GST-Nup210 aa1830-1887 and 600 pmol of His-GST-Nup210 aa1830-1887 to the immobilized His-MBP-His or MBP-LRRC59 aa1-244-His, respectively. After 60 minutes of incubation at 4 °C on a spinning wheel, beads were washed four times using pulldown buffer. After total removal of the supernatant of the last washing step, beads were mixed with 50 µl of SDS sample buffer, vortexed, boiled at 95 °C for 5 minutes and spun down at 15,000 xg for 5 minutes. The binding was analyzed by 12% SDS-PAGE followed by Coomassie staining or Western blotting and immunodetection. For Coomassie staining, 10% of the used input of immobilized and added protein was separated by SDS-PAGE, while for Western Blot analysis 1% of the used protein amounts was analyzed.

2.3.8 Microsome integration assay

The microsome integration assay is a method to observe the membrane insertion of an *in vitro* transcribed and translated integral membrane protein. The terminus of the membrane protein which is facing the lumen is tagged with a 13 amino acid long opsin-tag, which is glycosylated upon membrane insertion of the integral membrane protein. This glycosylation can be observed by SDS-PAGE and immunoblotting.

For the insertion of proteins into rough microsomes, the protein of interest was cloned into a T7-promotor containing plasmid (pET328-HZZ or pGEM3) with a C-terminal opsin tag. These constructs were used for a coupled *in vitro* transcription and translation reaction using the TnT Quick Coupled Transcription/Translation system (Promega) (Pelham and Jackson, 1976; Jagus and Beckler, 2003; Favaloro et al., 2010; Vilardi et al., 2011) according to the protocol of the manufacturer. For the reaction, 1 µl of 200 ng/µl plasmid DNA was mixed with 8.8 µl of rabbit reticulocyte lysate and 0.2 µl methionine (1 mM stock solution). As transcription/translation control for specific protein expression, the translation

inhibitor puromycin at a final concentration of 2.5 mM was added to the mixture at time point 0 minutes. The reaction was taking place at 30 °C in a Thermomixer for 90 minutes until the addition of puromycin at a final concentration of 2.5 mM for 10 minutes (Favaloro et al., 2010). After 10 minutes of incubation with puromycin, 1 µl of dog pancreas rough microsomes (Walter and Blobel, 1983) were added to the reaction for 60 minutes at 30 °C. Reactions were stopped by addition of 50 µl SDS sample buffer, heating at 95 °C for 5 minutes and centrifugation at 15,000 xg for 5 minutes. Protein expression and membrane insertion monitored by the N-glycosylation of the opsin-tag (Adamus et al., 1991) was analyzed by loading 10-25% of the samples onto 12% SDS-PAGE followed by Western blotting and immunodetection. For quantification, lane scans were performed using ImageJ. The membrane insertion efficiencies were calculated as the percentage of the glycosylated protein compared to the sum of the glycosylated and the non-glycosylated form. Values were normalized to the control reaction for the transcribed and translated protein for rough microsome treatment. The mean and the standard deviation for each treatment condition were calculated from five or six individual experiments.

PNGase F treatment

For confirmation of specific N-glycosylation of the inserted opsin-tag, a deglycosylation reaction after the microsome integration assay was performed. The protocol was modified from Pfaff et al. (2016). 25% of the insertion reaction was mixed with 1 µl glycoprotein denaturing buffer and filled up with ddH_2O to a final volume of 13 µl. The proteins were denatured at 100 °C for 10 minutes. Afterwards, the solution was chilled on ice for 1 minute and centrifuged for 10 seconds. For the specific cleavage of N-linked oligosaccharides from glycoproteins, either 500 U of peptide-N-Glycosidase F (PNGase F, New England BioLabs) or ddH_2O as a control was added to the reaction supplemented with 1% NP-40 (Nonidet P-40), 1x G7 reaction buffer and ddH_2O added to a final volume of 20 µl. After the deglycosylation reaction at 37 °C for 60 minutes, 12 µl of 4x SDS sample buffer was added and 50% of the reaction was analyzed by SDS-PAGE and immunoblotting.

Microsome integration assay using trypsin-treated rough microsomes

The microsome integration assay was performed as described above with addition of 1 µl of trypsin- (Favaloro et al., 2010) or EDTA and high salt-treated microsomes instead of rough microsomes. The treatment of rough microsomes with trypsin leads to the removal of receptor proteins of the membranes while preparation of microsomes with washing steps using EDTA and high salt leads to removal of peripheral attached proteins to the membrane serving as control treatment. For proof of receptor removal, 1 µl of trypsin- and EDTA/high salt-treated microsomes were supplemented with SDS sample buffer followed by analysis using SDS-PAGE and immunoblotting.

Microsome integration assay with addition of MBP-WRBcc or GST-CAML-N

For proof of membrane insertion of examined protein via the TRC pathway receptors WRB and CAML, the microsome integration assay was performed as described above with the addition of the dominant negative inhibitory fragments MBP-WRBcc (Vilardi et al., 2011; Pfaff et al., 2016) or GST-CAML-N (Yamamoto and Sakisaka, 2012; Pfaff et al., 2016). Instead of puromycin addition after 90 minutes of transcription and translation reaction, 5 or 10 µM of purified MBP-WRBcc or GST-CAML-N was added 10 minutes prior to supplemental of 1 µl rough microsomes. After additional 60 minutes of reaction, 50 µl of SDS sample buffer was added and the samples were analyzed using 12% SDS-PAGE and immunoblotting. Purified MBP-WRBcc and GST-CAML-N was a kind gift of Dr. Jhon Rivera-Monroy, member of the laboratory of Prof. Dr. Blanche Schwappach.

Immunodepletion of rabbit reticulocyte lysate

The immunodepletion of TRC40 from rabbit reticulocyte lysate was described previously by Leznicki et al. (2010). Shortly, rabbit reticulocyte lysate was immunodepleted using anti-TRC40 antibodies (laboratory of Prof. Dr. Blanche Schwappach, Ab0405) (Favaloro et al., 2010) in 1.5 ml reaction tubes. 20 µl of Protein A Sepharose 4 Fast Flow (GE Healthcare) were washed in 1 ml cold 1x PBS buffer followed by a centrifugation step at 500 xg, 4 °C for 2 minutes and removal of the

supernatant. After that, 15 µl of rabbit anti-TRC40 (Favaloro et al. (2010); TRC40 depletion) or 1.5 µg of rabbit IgG (Sigma-Aldrich; mock depletion) was added and the tube was filled up with 500 µl of cold 1x PBS. For binding of the antibody or IgG to the Protein A Sepharose, the reaction tubes were put onto a spinning wheel at 4 °C for 60 minutes. After a washing step with cold 1x PBS and centrifugation at 500 xg, 4 °C for 2 minutes, 120 µl of rabbit reticulocyte lysate was added to the immobilized antibodies. The immunodepletion was performed in the reaction tubes put into a 50 ml Falcon tube, rotating at 4 °C for 60 minutes. The solution was spun down at 13,000 xg, 4 °C for 1 minute, the supernatant was transferred into a new reaction tube and used for the microsome integration assay as described above. To check for the efficiency of the immunodepletion of TRC40, 2 µl of anti-TRC40 or the IgG-treated rabbit reticulocyte lysate was analyzed using 12% SDS-PAGE, Western blotting, Ponceau S staining and immunodetection after mixing with SDS sample buffer.

2.4 Cell Biology Methods

2.4.1 Cultivation of adherent cells

The adherent cell lines HeLa P4 (Charneau et al., 1994) and U2OS (ATCC® HTB96) were cultivated in Dulbecco's Modified Eagle Medium (DMEM) supplemented with 10% (v/v) fetal bovine serum (FBS) Superior (Biochrom) (v/v), 2 mM L-glutamine (Roth), 100 U/ml penicillin and 100 µg/ml streptomycin (Thermo Fisher Scientific). Cells were grown in 10 cm cell culture dishes at 37 °C and 5% CO_2 in a humid atmosphere. Cells were checked for contamination with mycoplasma on a regular basis. When cells reached a density of 80%, the cells were passaged and diluted for further growing. Medium was removed and the cells were washed with 1x PBS. Cells were supplemented with 1 ml of Gibco® Trypsin/EDTA 0.25% and placed onto a heating plate (Type 12801, MEDAX) at 37 °C. By addition of 9 ml of FBS containing DMEM growth medium, the digestion was inhibited and the cells were separated from each other by pipetting using a 1 ml pipet. For HeLa P4, 750 µl of cells suspension was added to 9.25 ml of cell culture medium in a new 10 cm cell culture dish (splitting 1:15). U2OS cells were split in a ratio 1:7 (1.5 ml of cell suspension mixed with 8.5 ml of cell culture medium). Both cell lines were split twice a week. All cell culture work was performed under a tissue culture hood.

2.4.2 Determination of cell concentration

For the determination of the number of cells growing in a 10 cm dish, the hemocytometer Neubauer chamber advanced 0.1 mm (Brand) was used. 25 µl of cell suspension was mixed with 75 µl of 0.4% Trypan blue solution (Sigma-Aldrich) and added to both counting grids of the Neubauer chamber. In each counting grid, cells in the four corner quadrates of the 3x3 counting quadrates of 1 mm edge length were counted. The mean of the cell number of these eight counted quadrates was calculated and multiplied by four to consider the dilution with Trypan blue solution. The received value multiplied by 10,000 corresponded to the number of cells in 1 ml cell culture medium.

2.4.3 Seeded cell number for different experiments

For transient transfection of HeLa P4 cells, 24 well cell culture plates were equipped with 12 mm coverslips and a 120,000 cells/ml cell suspension was prepared. In each well, 500 µl of cell suspension was added (60,000 cells/well). The next morning, cells were transfected using the calcium-phosphate method (see section 2.4.4). For the transfection of U2OS cells with siRNAs, 30,000 cells were seeded per well (500 µl cell suspension) in a 24 well cell culture plate. For immunostaining of endogenous proteins without transfection, HeLa P4 cells were seeded in a 24 well cell culture plate with a number of 120,000 cells/well and stained the next day. For RAPIDS experiments (see section 2.6), 1,650,000 cells/10 ml were seeded onto 10 cm cell culture dishes containing one coverslip per plate for immunofluorescence analysis. For selective permeabilization of cells in solution using digitonin, 5,000,000 cells were seeded onto a 10 cm cell culture dish containing 10 ml of cell culture medium, while several coverslips were distributed over the plate for immunofluorescence staining.

2.4.4 Transient transfection of mammalian cells with DNA and siRNAs using calcium-phosphate

For transient transfection of HeLa P4 or U2OS cells with plasmid DNA and/or siRNAs, the calcium-phosphate method (Chen and Okayama, 1987) was modified and used for cells seeded one day before treatment. For microscopy-based cell assays (24 well cell culture plates), 20 µl of $CaCl_2$ (250 mM) was added to a final concentration of 0.2-1.5 µg of plasmid DNA and/or 100 nM siRNAs per well provided in a 1.5 ml reaction tube before the mixture was vortexed at full power for 5 seconds. Afterwards, 20 µl of 2x HEPES were added prior to 10 second vortexing and 25 minutes of incubation time at room temperature. As a master mix, transfection reactions for up to six wells were performed in one tube. After 40 µl of the mixture was added to the cells in one well drop by drop, cells were incubated at 3% CO_2 for 6 hours. The next day, the media was replaced after two washing steps with 1x PBS.

For the transfection of HeLa P4 cells with plasmid DNA used for RAPIDS experiments (10 cm dishes), 500 µl of $CaCl_2$ (250 mM) was added to 10 µg of plasmid pmCherry-FRB-LRRC59 and 7 µg of plasmid pcDNA3-FKBP12-EGFP-APEX2 for each plate followed by 5 seconds of full speed vortexing. After the addition of 500 µl of 2x HEPES, the mixture was vortexed with full speed for 10 seconds. After 25 minutes at room temperature, the reaction mixtures (one per 10 cm dish) were united and 1 ml was added to the cells of each dish. Cells were incubated at 3% CO_2 for 6 hours. After two washing steps with 1x PBS, the medium was replaced by medium containing the appropriate isotopes on the next day.

2.4.5 Differential permeabilization of cells

Semi-permeabilization of the plasma membrane was first described by Adam et al. (1990) using the glycoside digitonin. Digitonin selectively permeabilizes the plasma membrane due to its high concentration of cholesterol, but the intracellular membranes stay intact (Adam, 2016). For microscopy-based experiments, HeLa P4 cells were grown on coverslips in a 10 cm cell culture dish with 5,000,000 cells seeded the day before. For permeabilization of attached cells using digitonin, cells were washed twice with 1x PBS and coverslips were moved onto a parafilm positioned on a metal block on ice. Cells were washed twice with transport buffer supplemented with 1 µg/ml leupeptin and pepstatin, 1 µg/ml aprotinin and 0.1 mM PMSF (phenylmethane sulfonyl fluoride) followed by digitonin permeabilization using 60 µl of 0.001% digitonin diluted in transport buffer for 5 minutes. After removal of the permeabilization solution, cells were washed three times (2x shortly, 1x for 2 minutes) using transport buffer. After a washing step with 1x PBS on the ice block, the wet coverslips were transferred quickly into a humidity/dark chamber on top of a parafilm positioned on a wet tissue paper. After an additional washing step with 1x PBS, the cells were fixed with 3.7% formaldehyde diluted in 1x PBS. If necessary, cells were subjected to indirect immunofluorescence staining for protein detection (see section 2.4.6).

For permeabilization of HeLa P4 cells in solution, 5,000,000 cells were seeded on a 10 cm dish for 24 hours before washing with 1x PBS. Coverslips for immunostaining of proteins were removed before further procedure. Cells were detached using 1 ml of Gibco® Trypsin/EDTA 0.25% for enzymatic digest of cell attaching proteins. After detachment of the cells, 9 ml of cell culture medium was added. Cells were pelleted with 300 xg at room temperature for 3 minutes prior to washing with 2 ml of 1x PBS. Cell number was determined using the Neubauer chamber. The volume containing 1,000,000 cells was transferred into a new tube, cells were pelleted with 300 xg at room temperature for 3 minutes. PBS was removed and cells were resuspended in 2 ml of transport buffer. From this cell suspension, 1 ml was transferred into a new tube supplemented with SDS sample buffer (input) while the other 1 ml was mixed with 12 µl of 1% digitonin incubated for 5 minutes on ice. Permeabilized cells were centrifuged at 16,000 xg and 4 °C for 30 minutes. The supernatant was transferred into a new tube and mixed with SDS sample buffer while the pellet remained in the tube for mixing with SDS sample buffer. All samples were boiled at 95 °C for 10 minutes and centrifuged at 15,000 xg for 5 minutes prior to analysis by SDS-PAGE, Western blotting and immunodetection.

2.4.6 Indirect immunofluorescence for protein detection

For the detection of endogenous or HA-, FLAG- or c-Myc-tagged proteins, cells were subjected to indirect immunofluorescence staining. Cells were grown on coverslips and, if necessary, transiently transfected with plasmid DNA or siRNAs. After 48 hours of knockdown and/or overexpression, cells were washed twice with 1x PBS and the coverslips were transferred into a humidity/dark chamber using tweezers. In the chamber, the coverslips were positioned onto a parafilm on top of a wet tissue paper. Whenever possible, the humidity/dark chamber was closed to protect fluorescently labeled proteins from light exposure. Cells were fixed with 3.7% formaldehyde diluted in 1x PBS at room temperature for 15 minutes. After two washing steps with 1x PBS, the cells were permeabilized using 0,5% Triton X-100 for 5 minutes (Koley and Bard, 2010) followed by three washing steps with 1x PBS. For reduction of unspecific antibody binding, cells were incubated with blocking solution (3% BSA diluted in 1x PBS) for 20 minutes. After removal of the blocking solution, primary antibody appropriately diluted in blocking solution was added to the cells (50 µl/coverslip) for 1-1.5 hours. For endogenous staining of LRRC59, primary antibody incubation time was extended to 2.5 hours and the blocking solution was supplemented with Triton X-100 in a final concentration of 0.05%. Cells were washed three times with 1x PBS prior to addition of secondary antibody diluted in blocking solution for 1 hour. For LRRC59 staining, the blocking solution was supplemented with 0.05% Triton X-100 and the incubation time extended to 1.5 hours. After two washing steps with 1x PBS and one with H_2O, coverslips were transferred onto a Whatman paper for drying and protected from light. The coverslips were placed onto Mowiol mounting medium, if necessary supplemented with 1 µg/ml DAPI (Sigma-Aldrich) on microscopy slides prior to microscopy analysis. A list of primary and secondary antibodies used in this work can be found in table 14 and 15.

2.4.7 Confocal microscopy

For the analysis of directly or indirectly fluorescent labeled proteins, the Zeiss LSM 510 meta confocal microscope base on the Axiovert 200M was used. Images were taken with the 63x Plan-Neofluar 1.3 NA water-corrected objective with appropriate filter settings. For detection of DAPI or NES-mTagBFP2-cNLS at 405 nm, a Diode-laser was used. For detection of EGFP-tagged or Alexa Fluor 488 conjugated secondary antibody stained proteins, an Argon488 laser was used. For detection of mCherry-tagged or Alexa Fluor 594 stained proteins, a HeNe543 or HeNe594 laser was used, while Alexa Fluor 633 and 647 was detected with a HeNe633 laser. For reduction of bleaching time, scanning with Diode-laser and HeNe543 or Argon488 and HeNe633 were performed in one scanning process. Dependent on the fluorescence signal, laser power was adjusted for signal detection. The pinhole was set to a diameter of 0.8 airy units for all used channels. Background level was controlled by Amplifier Offset adjustment. All settings were controlled with the help of the range indicator function in the palette tool. Generally, four images were averaged at a data depth of 8 bit. For processing of microscopy images in ImageJ 1.52a, channels were separated followed by brightness and contrast adjustment. The image type was changed to RGB color prior to saving as tiff file.

Note: Where indicated, the Zeiss microscope Axioskop2 mot plus, an upright, non-confocal light microscope was used as an alternative. For images, the AxioVision 4.8.1 software was used with the AxioCam MRm TV2/3”C 0,63x with the objective Plan-Neofluar 100x/1,30 Oil. The exposure time for each channel was appropriately adjusted and kept for all taken images of an experiment.

2.5 Rapamycin-induced dimerization assay

For the verification of INM localization of a membrane protein, a rapamycin-based dimerization assay, was used (Pfaff et al., 2016; Ohba et al., 2004; Haruki et al., 2008). Detailed information about the dimerization mechanism can be found in section 3.2.2.

Cells were transiently transfected with the plasmid coding for the nuclear reporter $EGFP_2$-GST-M9-FKBP12 or $EGFP_2$-MBP-M9-FKBP12 and the protein of interest. This protein contains a membrane

domain and is tagged with a FRB domain and a HA- or mCherry-tag on its cytoplasmic localizing terminus. An overview of all used constructs and plasmid DNA concentrations for transient transfection used in the rapamycin-based dimerization assay can be found in table 25. After 48 hours of overexpression, cells were washed twice with 1x PBS. The coverslips were transferred into the humidity/dark chamber using tweezers onto a parafilm on top of a wet tissue paper. Cells were treated with 200 nM rapamycin diluted in 1x PBS at room temperature for 1-30 minutes to allow the dimerization between the FKBP12- and the FRB-domain mediated by rapamycin. When the incubation time was over, rapamycin-PBS was removed and cells were immediately fixed with 3.7% formaldehyde diluted in PBS. If necessary, immunofluorescence staining was performed prior to fluorescence microscopy.

The rapamycin-induced dimerization assay was performed with simultaneous knockdown of importin β. Cells were transfected with 100 nM control siRNA or 50 nM importin β siRNA 1 + 50 nM importin β siRNA 2 and 0.3 µg $EGFP_2$-GST-M9-FKBP12, 0.5 µg mCherry-FRB-LRRC59 and, optionally, 0.7 µg NES-mTagBFP2-cNLS (per well). For rapamycin-induced dimerization assay with simultaneous expression of Bimax2 or a control, the cells were transfected with 0.3 µg $EGFP_2$-GST-M9-FKBP12, 0.5 µg mCherry-FRB-LRRC59, 1 µg NES-mTagBFP2-cNLS and 1 µg FLAG-Bimax2 or the vector pcDNA3 (per well).

For the analysis of rapamycin induced reporter response, at least 100 cells were counted per condition and experiment and categorized as “responding” or “not responding”. A “responding” cell was defined as a cell which showed a reporter recruitment to the NE indicated as a green rim, while the reporter of a “not responding” cell was distributed all over the nucleus without aggregation at the NE.

Table 25: Plasmids used for transfection of HeLa P4 cells in a 24 well cell culture plate

Rapamycin assay constructs with FRB domain			**Reporter with FKBP12 domain**		
Number	**Name**	**[µg/well]**	**Number**	**Reporter**	**[µg/well]**
1232	mCherry-FRB-emerin	0.5	1603	$EGFP_2$-GST-M9-FKBP12	0.3
1424	mCherry-FRB-LRRC59	0.4/0.5	1603	$EGFP_2$-GST-M9-FKBP12	0.3
1424	mCherry-FRB-LRRC59	0.4/0.5	2092	$EGFP_2$-MBP-M9-FKBP12	0.2
1425	WRB-FRB-HA	0.5	1603	$EGFP_2$-GST-M9-FKBP12	0.3
1546	mCherry-FRB-GST-LRRC59	1	2092	$EGFP_2$-MBP-M9-FKBP12	0.2
1848	mCherry-FRB-MBP-LRRC59	1	1603	$EGFP_2$-GST-M9-FKBP12	0.3
1848	mCherry-FRB-MBP-LRRC59	1	2092	$EGFP_2$-MBP-M9-FKBP12	0.2
1905	HA-FRB-LRRC59	1	1603	$EGFP_2$-GST-M9-FKBP12	0.3
2000	mCherry-FRB-Sec61β	0.5	1603	$EGFP_2$-GST-M9-FKBP12	0.3
2000	mCherry-FRB-Sec61β	1.5	2092	$EGFP_2$-MBP-M9-FKBP12	0.166
2003	mCherry-FRB-Sec22β	0.5	1603	$EGFP_2$-GST-M9-FKBP12	0.3
2005	LMAN2-FRB-mCherry	0.5	1603	$EGFP_2$-GST-M9-FKBP12	0.3
2007	DDOST-FRB-mCherry	0.5	1603	$EGFP_2$-GST-M9-FKBP12	0.3
2007	DDOST-FRB-mCherry	1.5	2092	$EGFP_2$-MBP-M9-FKBP12	0.166
2008	mCherry-FRB-UBE2J1	1	1603	$EGFP_2$-GST-M9-FKBP12	0.3
2008	mCherry-FRB-UBE2J1	1.5	2092	$EGFP_2$-MBP-M9-FKBP12	0.166
2009	mCherry-FRB-UBE2J2	1	1603	$EGFP_2$-GST-M9-FKBP12	0.3
2102	mCherry-FRB-LRRC59 (containing GGGGS linker)	0.7	1603	$EGFP_2$-GST-M9-FKBP12	0.3
2103	mCherry-FRB-MBP-LRRC59 (containing GGGGS linker)	0.7	1603	$EGFP_2$-GST-M9-FKBP12	0.3
2119	mCherry-FRB-MBP-Sec61β	1.5	2092	$EGFP_2$-MBP-M9-FKBP12	0.166
2121	DDOST-MBP-FRB-mCherry	1.5	2092	$EGFP_2$-MBP-M9-FKBP12	0.166
2124	mCherry-FRB-MBP-UBE2J1	1.5	2092	$EGFP_2$-MBP-M9-FKBP12	0.166
2125	mCherry-FRB-GST-Sec61β	1.5	2092	$EGFP_2$-MBP-M9-FKBP12	0.166
2128	DDOST-GST-FRB-mCherry	1.5	2092	$EGFP_2$-MBP-M9-FKBP12	0.166
2129	mCherry-FRB-GST-UBE2J1	1.5	2092	$EGFP_2$-MBP-M9-FKBP12	0.166

2.6 Rapamycin- and APEX-dependent identification of proteins by SILAC (RAPIDS)

The rapamycin- and APEX-dependent identification of proteins by SILAC (RAPIDS) is an experimental approach to identify proteins in close proximity to a membrane protein. The experimental protocol was established by Dr. Marret Müller in the laboratory of Prof. Dr. Ralph H. Kehlenbach, and performed with adjustments for the protein LRRC59 in plasmid DNA concentration usage and overexpression time of 52 hours instead of 24 hours.

2.6.1 Dialyzing FBS

FBS (100 ml) was dialyzed against PBS using a dialysis membrane with a molecular mass cut-off of 6-8 kDa (Spectra/Por 1 Dialysis membrane Standard RC tubing 6-8 kDa, Spectrum) while stirring at 4 °C. PBS (2 l) was exchanged after 1 hour before dialysis over night. On the next day, 1x PBS was again exchanged followed by 1 hour dialysis and transfer of the FBS into two 50 ml Falcon tubes. Dialyzed FBS was stored at -20 °C until usage. 50 µl of the dialyzed FBS was added to 2 ml of DMEM medium in a 2 cm cell culture dish and observed for bacterial contamination.

2.6.2 SILAC labeling

For SILAC (stable isotope labeling of amino acids in cell culture) experiments (Ong et al., 2002), HeLa P4 cells were grown in medium containing heavy or light isotopes of arginine and lysine. Cells were cultivated in high glucose DMEM lacking glutamine, lysine and arginine (Thermo Fisher Scientific) supplemented with 10% (v/v) dialyzed FBS, 6 mM L-glutamine, 100 U/ml penicillin, 100 µg/ml streptomycin and either heavy or light labeled isotopes. For “heavy media” 0.4 mM $^{13}C_6{}^{15}N_2$-L-lysine and 0.2 mM $^{13}C_6{}^{15}N_4$-L-arginine, for “light media” 0.4 mM $^{12}C_6{}^{14}N_2$-L-lysine and 0.2 mM $^{12}C_6{}^{14}N_4$-L-arginine were added. To ensure a sufficient incorporation of heavy amino acids of ≥ 97%, cells were passaged five to seven times in SILAC medium before the biotinylation experiment. The incorporation rate was analyzed by mass spectrometry analysis and was higher than 98% for all performed experiments. Cells were grown at 37 °C and 5% CO_2 and passaged when reaching 80% confluency.

2.6.3 Rapamycin-dependent biotinylation assay

After cultivation of HeLa P4 cells in either heavy or light isotope labeled medium for five to seven passages, 1,650,000 cells/10 cm dish, seeded the day before, were transiently transfected with plasmids coding for mCherry-FRB-LRRC59 and FKBP12-EGFP-APEX2. For cells grown in light medium, six 10 cm dishes were prepared, while for cells of heavy medium seven 10 cm dishes were used, as one plate was for incorporation analysis. For microscopic analysis of the cells, one coverslip per plate was added. 24 hours after transfection, cells were washed using 1x PBS prior to medium replacement. After 52 hours of overexpression, the biotinylation experiment was performed. Cells for incorporation analysis were only harvested in RIPA buffer as described below prior to determination of the protein concentration. In the forward experiment, medium of cells cultivated in light medium was replaced with light medium supplemented with 500 µM biotinphenol (Iris Biotech) and 200 nM rapamycin, while cells grown in heavy medium were incubated with heavy medium containing 500 µM biotinphenol lacking rapamycin. For the reverse experiment, rapamycin addition to the cells in appropriate medium was switched. Incubation of the cells with biotinphenol with or without rapamycin was performed at 37 °C, 5% CO_2 for 30 minutes. Subsequently, 1 mM H_2O_2 was added to each 10 cm dish at room temperature for 1 minute. The medium was immediately removed and cells were supplemented with 10 ml of quenching buffer. After an additional washing step with 10 ml quenching buffer, cells were washed with 1x PBS. The coverslip of each plate was taken out with tweezers and placed into a humidity/dark chamber for fixation of the cells with 3.7% formaldehyde in PBS for 15 minutes. Coverslips were placed onto microscopy slides with Mowiol mounting medium containing DAPI for microscopy analysis. The PBS in the cell culture dishes was removed and 1,4 ml of RIPA buffer was added prior to cell harvest using a cell scraper. The cell suspension was transferred into 2 ml reaction tubes and kept on ice until all plates were processed. The cell lysate was centrifuged at 16,000 xg, 4 °C for 10 minutes.

The protein concentrations of cell lysates coming from heavy or light isotope labeled medium were determined using Pierce 660 nm Protein Assay (Thermo Fisher Scientific) analyzed with the plate reader BioTek Synergy HT and a BSA dilution series for comparison and adjusted to each other. 40 µl of both cell lysates were mixed with 40 µl of SDS sample buffer ("total lysate"). For Western blot analysis, 2.8 ml of each cell lysate was transferred into two 1.5 ml reaction tubes. For mass spectrometry analysis, equal protein amounts of cell lysates cultivated in heavy or light medium, were mixed in a ratio 1:1 (total volume: 11.2 ml) and transferred into eight 1.5 ml reaction tubes. Each reaction tube contained 130 µl of NeutrAvidin Agarose Resin (Thermo Fisher Scientific), equilibrated in RIPA buffer. For protein binding to the NeutrAvidin beads, the mixtures were incubated on a rotation wheel at 4 °C over night. The mixtures were centrifuged at 800 xg, 4 °C for 1 minute and the supernatant was removed. Beads were washed once using washing buffer 1 on a spinning wheel at 4 °C for 8 minutes followed by one additional washing step using washing buffer 2 and two washing steps with washing buffer 3. After the last washing, supernatant was removed and beads were dried using a compressed loading tip to avoid sucking off of beads. Proteins bound to the beads from different tubes were eluted by incubation with in total 110 µl (mass spectrometry samples) or 80 µl (Western blot samples) SDS sample buffer supplemented with 5 mM desthiobiotin (Sigma Aldrich) at 95 °C for 5 minutes. The RAPIDS experiment was performed twice to have four independent replicates.

2.6.4 Protein analysis using SDS-PAGE and Western blotting

The biotinylated proteins of samples of RAPIDS experiments prepared for SDS-PAGE and Western blotting were analyzed using Mini Protean TGX Precast gels, 4-20% (BioRad) in Laemmli running buffer prior to transfer onto Nitrocellulose Blotting Membrane. Biotinylated proteins were detected using HRP-coupled streptavidin (1:20,000 in 3% BSA in 1x TBST).

2.6.5 Mass spectrometry analysis

The mass spectrometry analysis for the samples of RAPIDS experiments was performed by Thierry Wasselin, Dr. Christof Lenz and Dr. Henning Urlaub (Core Facility Proteomics, University Medical Center Göttingen). The submitted samples were separated using 4-12% NuPAGE Novex Bis-Tris Minigels (Invitrogen) followed by Coomassie Blue staining. Each lane was sliced into 11-12 pieces, all equal in size, washed and reduced with DTT. Afterwards, proteins in gel pieces were alkylated with 2-iodoacetaminde and digested with trypsin overnight followed by peptide extraction and drying in a SpeedVac. Afterwards, the peptides were reconstituted in 2% acetonitrile and 0.1 formic acid (v/v) and analyzed as described in Atanassov and Urlaub (2013) using a nanoLC-MS/MS on a hybrid quadrupole/orbitrap mass spectrometer (Q Exactive, Thermo Fisher Scientific). The raw data processing was performed using MaxQuant Software version 1.5.7.4 (Max Planck Institute for Biochemistry, Martinsried, Germany). For analysis of proteins, peptides were identified by comparison to the human reference proteome (v2017.02) considering a set of common laboratory contaminations. For the relative protein quantification, Arginine R10 and Lysine K8 labels including the "Re-quantify" option were used.

For the statistic evaluation, Perseus Software version 1.5.6.0 (Max Planck Institute for Biochemistry, Martinsried, Germany), was used. For information about the Matrix workflow see table S 8. The results of two forward and two reverse RAPIDS experiments were analyzed together for statistical evaluation of relative protein quantification values and a two-sided Significance B test (Cox and Mann, 2008) using normalized $\log_2$ ratios. In Significance B testing, Benjamini Hochberg False Discovery Rate was used for truncation with a threshold value of 0.05.

3 Results

In this study, the ER- and NE-localizing protein LRRC59 was examined with respect to its ER-membrane insertion mechanism using microsome integration and cell culture-based assays (see section 3.1). Detailed information about LRRC59 can be found in section 1.4. Additionally, the INM targeting of LRRC59 using cell culture-based techniques and rapamycin-induced dimerization assays was studied (see section 3.2). By the performance of RAPIDS (rapamycin- and APEX-dependent identification of proteins by SILAC) experiments, proteins in close proximity to LRRC59 were identified and further analyzed. RAPIDS experiments combine biotinylation of proteins by the rapamycin-dependent targeting of APEX2 with stable isotope labeling of amino acids in cell culture (SILAC) (see section 3.3). Beyond this, further ER- and NE-localizing proteins were identified as INM proteins and examined for their INM targeting by rapamycin-induced dimerization assays (see section 3.4).

3.1 Membrane insertion of LRRC59

LRRC59 is a protein of 34.9 kDa (UniProt ID Q96AG4) and has a single TMD at its C-terminus followed by additional 40 amino acids. Its N-terminus is oriented towards the cytoplasm, while the C-terminus is facing the lumen of the ER. LRRC59 has no signal sequence, but a hydrophobic segment (signal anchor) near the C-terminus. These properties classify LRRC59 as a potential tail-anchored (TA) protein (Kutay et al., 1993), which could be post-translationally inserted into ER-membranes using the classical insertion mechanism for TA proteins, the TRC pathway (Stefanovic and Hegde, 2007). To examine the membrane insertion mechanism of LRRC59, *in vitro* microsome integration assays were performed (Favaloro et al., 2010; Vilardi et al., 2011). In these assays, the well analyzed TA protein emerin, which is inserted via the TRC pathway into the microsomal membranes, served as control (Pfaff et al., 2016).

3.1.1 Post-translational membrane insertion of LRRC59

For microsome integration assays, an *in vitro* transcription and translation reaction is coupled with a membrane insertion reaction using purified dog pancreas rough microsomes (Walter and Blobel, 1983; Favaloro et al., 2010; Vilardi et al., 2011). For this, the cDNA sequences of LRRC59 and emerin were cloned into the T7-promotor containing plasmids pET328-HZZ or pGEM3. An additional 13 amino acid long opsin-tag (Adamus et al., 1991) was added to the C-terminus of LRRC59. This opsin-tag is N-glycosylated when it is inside the microsomal lumen. The insertion of the transcribed and translated products into rough microsomes were observed by detection of the glycosylation of the opsin-tag by SDS-PAGE, Western blot and immunodetection using a specific opsin-antibody (Adamus et al., 1991).

Microsome integration assay using puromycin

First, LRRC50-opsin or emerin-opsin were produced in rabbit reticulocyte lysate supplemented with the plasmids pET328-HZZ-LRRC59-opsin or pET328-HZZ-emerin-opsin (figure 9A). This transcription/translation reaction was highly specific, as no product could be detected if no DNA was added to the reaction. Upon the addition of rough microsomes (RM), an additional slower migrating band could be observed for LRRC59-opsin and emerin-opsin in the immunoblotting. This slower migrating protein represents the N-linked glycosylated form of opsin-tagged LRRC59 or emerin after insertion into microsomes, as the opsin-tag is specifically modified in the microsomal lumen. To confirm that the additional band is a result of glycosylation of the opsin-tag, 25% of an insertion reaction of LRRC59-opsin was treated with the deglycosylation enzyme PNGase F. This treatment resulted in the loss of the additional band, showing the specific glycosylation of the opsin tag upon membrane insertion (figure 9C). When puromycin, a translation-inhibitor, was added to the transcription/translation reaction before addition of rough microsomes, LRRC59-opsin and emerin-opsin could still be inserted (figure 9A and B). This indicates that both proteins insert post-translationally into microsomal membranes. As a positive control for the inhibitory effect of puromycin, the experiment was carried out with addition of the drug to

the transcription/translation reaction of LRRC59-opsin and emerin-opsin at time point 0 minutes. In these reactions, no production of LRRC59-opsin or emerin-opsin could be observed, showing the efficiency of the drug.

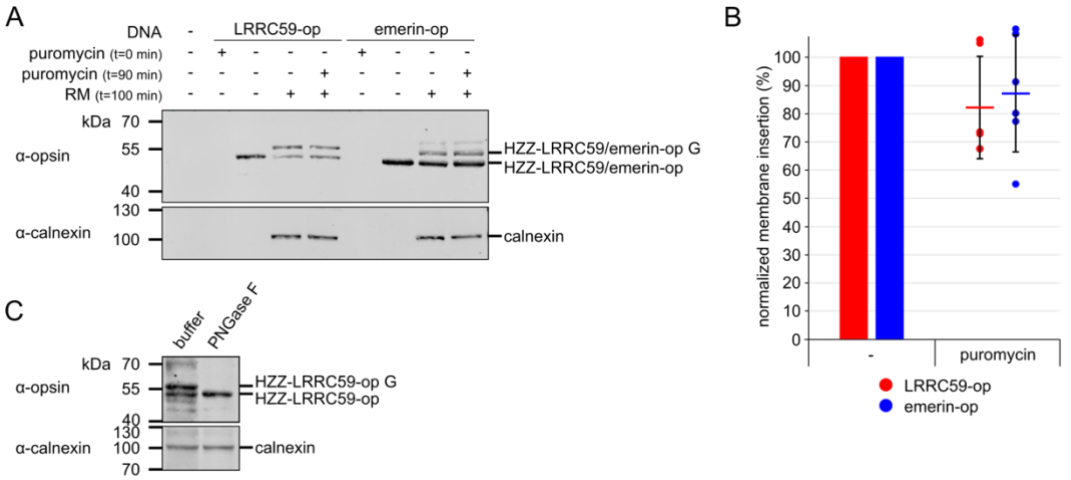

Figure 9: LRRC59 is post-translationally inserted into rough microsomes.
(A) LRRC59 and emerin tagged by opsin (HZZ-LRRC59-op, HZZ-emerin-op) were produced *in vitro* by coupled transcription/translation reactions. As indicated in the figure, the reaction took place in the presence (+) or absence (-) of rough microsomes (RM) and the translation inhibitor puromycin. After SDS-PAGE and Western blotting, the glycosylation of the opsin-tag was analyzed by immunoblotting using antibodies against opsin and calnexin as loading control. HZZ-LRRC59/emerin-op G indicates the glycosylated forms of the proteins. (B) Quantification of the experimental results of (A). The mean and the standard deviation were calculated from six individual experiments. (C) Test for N-linked glycosylation of HZZ-LRRC59-op G. Treatment with PNGase F or buffer of *in vitro* produced protein as described in (A) prior to SDS-PAGE, Western blot and immunodetection analysis using antibodies against opsin and calnexin as loading control. See also Blenski and Kehlenbach, 2019.

Microsome integration assay using trypsin-treated microsomes

Some proteins, such as cytochrome b5, can insert spontaneously into membranes without the involvement of a receptor (Favaloro et al., 2008; Stefanovic and Hegde, 2007; Colombo et al., 2009; Rabu et al., 2009). To examine this possibility for LRRC59, the microsome integration assay was performed as described above but with trypsin- (T-RM) (Favaloro et al., 2010) or high salt/EDTA- (EK-RM) treated microsomes (figure 10). The treatment of rough microsomes with trypsin removes receptor proteins inserted in the membrane, while the control treatment with high salt/EDTA leads to the removal of peripherally attached proteins. As shown in figure 10B, the receptor protein CAML was removed upon the treatment of rough microsomes with trypsin. For both, LRRC59-opsin and emerin-opsin, no membrane insertion was observed with trypsin-treated microsomes (figure 10A), while cytochrome b5-opsin was still able to insert (figure 10C). This result indicates that LRRC59 cannot insert into membranes independently of a receptor protein. Emerin, which is known to insert into the ER-membrane via the TRC pathway using the receptors WRB and CAML (Pfaff et al., 2016), served as control for this experiment.

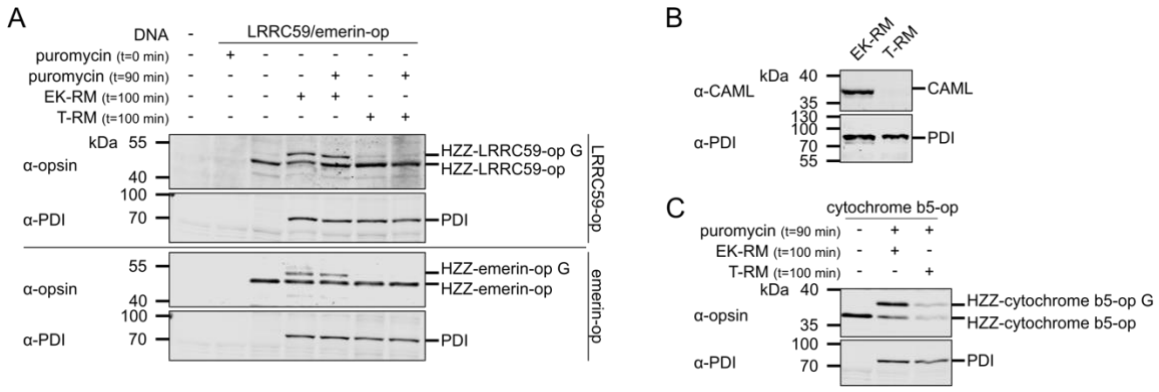

Figure 10: LRRC59 is inserted in a receptor-dependent manner.
(A) The *in vitro* produced HZZ-LRRC59-op or HZZ-emerin-op were tested for membrane insertion into EDTA/high-salt (EK-RM) or trypsin-treated (T-RM) rough microsomes in the presence (+) or absence (-) of puromycin. After separation in SDS-PAGE, the proteins were analyzed by immunoblotting with opsin- and PDI- (loading control) antibodies. HZZ-LRRC59/emerin-op G represents the glycosylated forms of the proteins. (B) For comparison, EK-RM or T-RM were mixed with SDS sample buffer and analyzed by SDS-PAGE, Western blotting and immunodetection using antibodies against CAML or PDI as loading control. (C) After production in an *in vitro* transcription/translation reaction, HZZ-cytochrome b5-opsin was incubated with EK-RM or T-RM in the presence (+) or absence (-) of puromycin. HZZ-cytochrome b5-op G indicates the glycosylated form of the protein. Protein analysis was performed by SDS-PAGE prior to Western blotting and immunodetection with antibodies against the opsin-tag and PDI as loading control. See also Blenski and Kehlenbach, 2019.

3.1.2 Examination of involvement of the TRC pathway in LRRC59 ER-membrane insertion

As LRRC59 was shown to insert into membranes post-translationally in a receptor-dependent manner, the potential involvement of the TRC pathway for LRRC59 membrane insertion was further examined.

Microsome integration assays using dominant negative inhibitory fragments of WRB and CAML

First, the dependency of membrane insertion of LRRC59 on the heteromultimeric receptors WRB and CAML of the TRC pathway was studied.

Pfaff et al. (2016) showed an inhibitory effect for membrane insertion for emerin upon the addition of the dominant negative inhibitory fragments GST-CAML-N or MBP-WRBcc in microsome integration assays. To study the effect on LRRC59, 5 µM or 10 µM of GST-CAML-N (figure 11A) or MBP-WRBcc (figure 11B) were added after 90 minutes of *in vitro* transcription and translation reaction prior to the addition of rough microsomes. For emerin, already the presence of 5 µM of the dominant negative inhibitory fragments resulted in a total loss of membrane insertion. Further experiments showed that the addition of only 1 µM or 3 µM of GST-CAML-N or MBP-WRBcc affected emerin membrane insertion (data not shown). The insertion of LRRC59 into rough microsomes was not affected at all by the addition of the dominant negative inhibitory fragments, not even with 10 µM of receptor fragments. This result indicates that LRRC59 is inserted into the membrane independently of the TRC pathway receptors WRB and CAML.

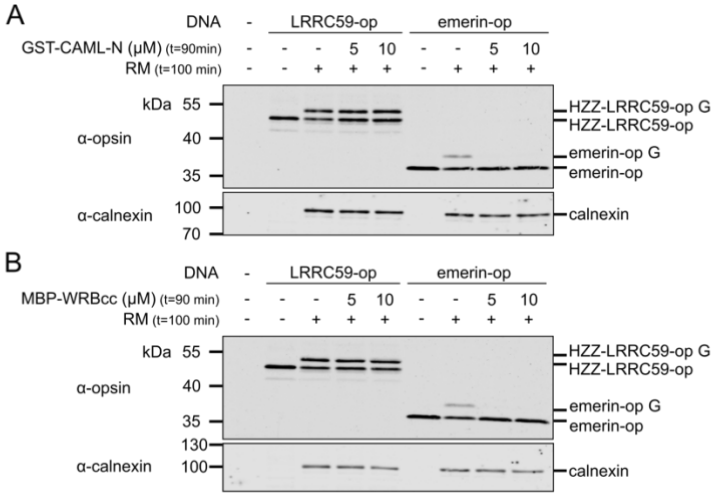

Figure 11: WRB and CAML, the TRC pathway receptors, are not required for LRRC59 microsome insertion.
(A) HZZ-LRRC59-op or emerin-op were produced in an *in vitro* transcription/translation reaction followed by incubation with rough microsomes (RM) without (-) or with 5 or 10 µM of GST-CAML-N. Proteins were analyzed by SDS-PAGE, Western blotting and immunodetection using antibodies against the opsin-tag and calnexin as loading control. In this experiment, the emerin-construct lacks the HZZ-tag at the N-terminus. HZZ-LRRC59-op G and emerin-op G mark the glycosylated form of the proteins. (B) Experimental implementation as (A) using MBP-WRBcc instead of GST-CAML-N. See also Blenski and Kehlenbach, 2019.

Microsome integration assay using TRC40-immunodepleted lysate

The involvement of TRC40 itself in the membrane insertion mechanism of LRRC59 was studied by the performance of microsome integration assays using TRC40 immunodepleted rabbit reticulocyte lysate (figure 12). The reticulocyte lysate was depleted using an antibody against TRC40 (Favaloro et al., 2010) while rabbit IgG served as a control in mock-depletion. The extent of the depletion was controlled with reticulocyte lysate mixed with SDS sample buffer and analyzed by SDS-PAGE and immunoblotting using an alternative TRC40 antibody. Indeed, no TRC40 protein could be detected in the TRC40-depleted lysate, while a Ponceau S staining of the lysate showed equal loading and transfer of the proteins (figure 12C). Using this TRC40-immunodepleted reticulocyte lysate in the microsome integration assay, the membrane insertion of emerin was strongly inhibited to 11.5% ± 12.7 of the value obtained in the mock depleted reaction. For LRRC59, by contrast, only a modest inhibition to 80.9% ± 11.5 was observed (figure 12A and B). This result of the microsome integration assay shows a clear difference in the membrane insertion mechanism regarding the importance of TRC40 for emerin-opsin and LRRC59-opsin.

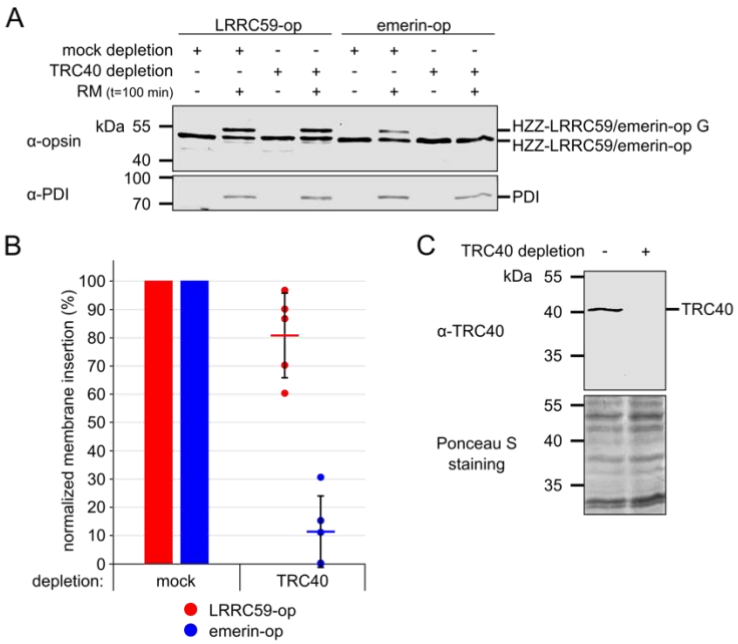

Figure 12: TRC40 is not required for membrane insertion of LRRC59.
(A) HZZ-LRRC59/emerin-op were produced by TRC40- or mock-depleted rabbit reticulocyte lysate and incubated with rough microsomes (RM). Proteins were analyzed with SDS-PAGE prior to Western blotting and immunodetection using antibodies against the opsin-tag and PDI, which served as a loading control. HZZ-LRRC59/emerin-op G indicates the glycosylated proteins. (B) Quantification of five individual experiments as described in (A). Individual values of the reactions with TRC40-depleted lysate were normalized to the reaction with mock-depleted lysate for each experiment. The diagram shows mean and standard deviation of these values. (C) Immunodepletion of the lysate using antibodies against TRC40 (+) or IgG (-) as control used in (A) was analyzed by SDS-PAGE and immunoblotting with antibodies against TRC40 (top) and Ponceau S staining (bottom). See also Blenski and Kehlenbach, 2019.

Subcellular localization of emerin and LRRC59 in TRC40 D74E overexpressing cells

TRC40 is the mammalian homolog of the *S. cerevisiae* ATPase Get3, which has an aspartic acid active site in position 57 (Mateja et al., 2009). In its TA protein bound form, Get3 is recruited to the membrane via its interaction with Get2 (the yeast homolog of CAML). Upon ATP hydrolysis and release of ADP, the TA protein is released from Get3 and is inserted into the ER-membrane by Get2 and Get1 (the yeast homolog of WRB) (Shao and Hegde, 2011b; Yamamoto and Sakisaka, 2012; Hegde and Keenan, 2011). Mariappan and colleagues showed that Get3 is ATPase deficient upon the mutation of aspartic acid in position 57 to asparagine (Get3 D57N). This mutant was able to interact with the TA protein, but the release of the TA protein upon interaction with Get1/2 was not possible (Mariappan et al., 2011). When the aspartic acid was changed to glutamic acid (Get3 D57E), Get3 was also inhibited in its ATPase activity but bound to the TMD of TA proteins (Powis et al., 2013). TRC40 has its aspartic acid active site in amino acid position 74. It was shown, that the mutant TRC40 D74E is still able to bind to different TA proteins, but cannot release them due to its ATPase deficiency. This dominant negative mutant was used to trap TA proteins and analyze them by mass spectrometry to identify substrates which can use the TRC pathway for membrane insertion (Coy-Vergara et al., 2019).

HeLa cells were transfected with plasmids coding for c-Myc-TRC40 WT and c-Myc-TRC40 D74E and immunostained for endogenous LRRC59 and emerin (figure 13). For LRRC59 and emerin, no difference in localization was observed in cells overexpressing c-Myc-TRC40 WT compared to non-transfected cells. In both cases, LRRC59 localized to the ER and NE, while emerin mainly localized to the NE. In contrast to cells overexpressing c-Myc-TRC40 D74E, emerin showed a weaker NE-localization but a diffuse staining in the cytoplasm. This result suggests that TRC40 D74E bound emerin, but could not release it for membrane insertion via the WRB and CAML receptors (also showed by Coy-Vergara et al. (2019)). However, for LRRC59 no difference in localization could be observed in non-transfected cells compared to TRC40 WT or TRC40 D74E overexpressing cells.

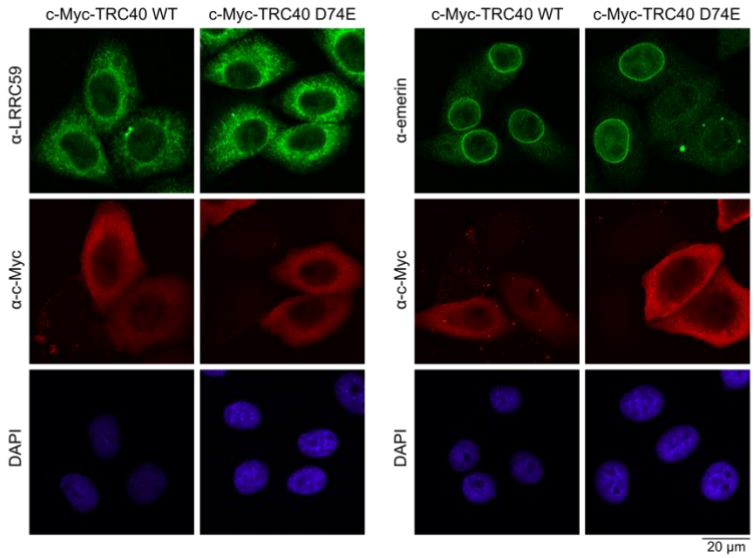

Figure 13: TRC40 D74E inhibits the ER-membrane insertion of emerin but does not seem to affect LRRC59.
HeLa cells were transfected with 1.5 µg of plasmids coding for c-Myc-TRC40 WT or c-Myc-TRC40 D74E. After 48 hours, cells were fixed and immunostained using antibodies against c-Myc and LRRC59 or emerin for confocal microscopy analysis. DAPI marked the nucleic acids in fluorescence microscopy.

The results of the microsome integration assay using TRC40 immunodepleted rabbit reticulocyte lysate and the overexpression of the TRC40 ATPase deficient mutant showing no effect for LRRC59 but for emerin indicate differences in the insertion mechanism of both TA proteins. Further examination is needed to solve the question of which alternative pathway(s) LRRC59 uses for membrane insertion.

3.2 Inner nuclear membrane targeting of LRRC59

The mammalian protein LRRC59 was suggested to dependent on importin β for its NE localization (Zhen et al., 2012). The treatment of U2OS cells with importin β siRNAs resulted in a loss of NE localization of endogenous LRRC59. As a dependency on transport factors and the Ran GTPase cycle for INM targeting could - so far - just be shown for the *S. cerevisiae* proteins Heh1 and Heh2 (King et al., 2006), the INM targeting of LRRC59 was studied in detail.

3.2.1 Subcellular localization of endogenous and overexpressed LRRC59

LRRC59 has previously been shown to localize to the ER-membrane and the NE (Zhen et al., 2012). First, the localization of endogenous LRRC59 in HeLa cells was examined by immunostaining (figure 14A). The specificity of the LRRC59-antibody was confirmed in HeLa cells treated with LRRC59 siRNAs, resulting in a reduction of the signal for LRRC59 in comparison to control knockdown cells (figure S 1). Endogenous LRRC59 localized to the ER and the NE. The NE localization of LRRC59 was indicated by a rim around the nucleus, similar to the localization of lamin A/C, which are proteins peripherally attached to the INM (figure 14A). To examine, whether LRRC59 is mainly membrane-inserted, HeLa cells were semi-permeabilized using digitonin, which permeabilizes the plasma membrane but leaves intracellular membranes intact. Due to digitonin treatment, soluble proteins of the cytoplasm can be washed out of the cell by several washing steps. The digitonin treatment was done for HeLa cells growing on coverslips, followed by immunostaining of LRRC59 (figure S 2A). No difference in LRRC59 staining could be observed between cells treated with digitonin or buffer as a control. Importin β was located in the cytoplasm and at the nuclear membrane in cells incubated with buffer. The localization to the NE is due to the interaction of importin β with the NPC. Upon the treatment with digitonin, however, cytoplasmic importin β is washed out, serving as the control for permeabilization

of cells. Additionally, HeLa cells detached from the cell culture dish were permeabilized using digitonin (figure S 2B). The cells were collected by centrifugation to separate soluble cytoplasmic proteins in the supernatant from membranes and membrane-inserted proteins in the pellet. The supernatant and the pellet were analyzed for LRRC59 by SDS-PAGE and Western blotting. In the insoluble fraction, LRRC59 and the ER-membrane protein calnexin could be detected. LRRC59 could not be detected in the supernatant, which contained soluble proteins of the cytoplasm like alpha-tubulin. This suggests that the major proportion of LRRC59 in HeLa cells was membrane bound and not soluble.

The localization of overexpressed LRRC59 tagged with HA, mCherry or mCherry-FRB was analyzed in HeLa cells. All three, HA-LRRC59, mCherry-LRRC59 and mCherry-FRB-LRRC59 showed a similar localization to the ER and the NE as endogenous LRRC59 (figure 14B).

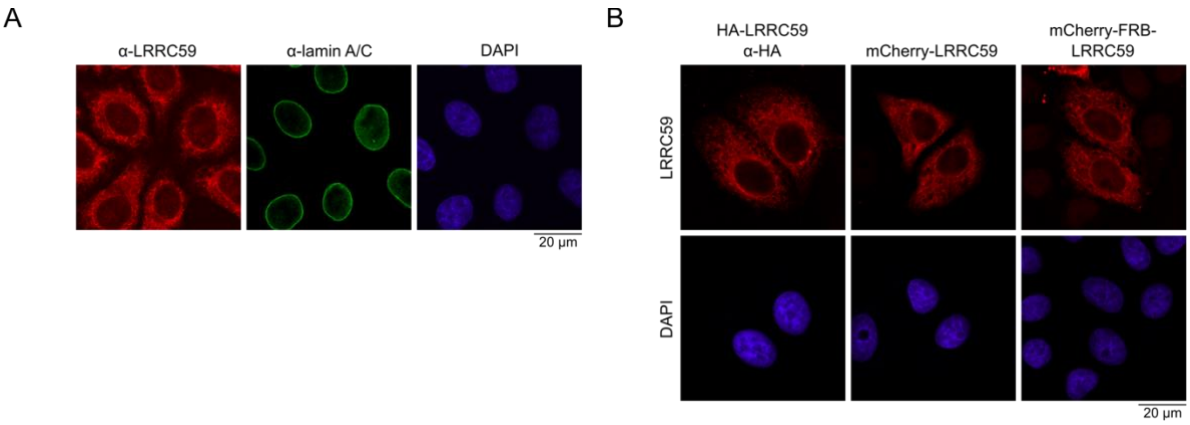

Figure 14: Endogenous or overexpressed LRRC59 localizes to the NE.
(A) For immunofluorescence staining, HeLa cells were grown on coverslips and analyzed with LRRC59- and lamin A/C-antibodies. (B) HeLa cells were transiently transfected for 48 hours with 0.7 µg of plasmids coding for HA-LRRC59, mCherry-LRRC59 and mCherry-FRB-LRRC59. After fixation, the cells were analyzed directly for mCherry-tagged LRRC59 by confocal microscopy or after immunofluorescence staining using antibodies against HA. DAPI marked the nucleic acids in fluorescence microscopy. See also Blenski and Kehlenbach, 2019.

Endogenous LRRC59 was shown to localize to the ER and the NE and is associated with the membrane. The overexpressed protein of differently tagged LRRC59 showed identical localization.

3.2.2 Analysis of inner nuclear membrane localization of LRRC59

With endogenous staining or overexpressed LRRC59, a NE localization could be seen with confocal microscopy. This experimental setup does not discriminate between the localization to the ONM and/or INM. By using a combination of single-point illumination with single-molecule fluorescence recovery after photobleaching (smFRAP), Mudumbi and colleagues could show the localization of nuclear membrane proteins to the INM or ONM with a resolution of <10 nm (Mudumbi et al., 2016). Metal-induced energy transfer (MIET) examined the axial distance between the ONM and INM using the INM protein LAP2β (lamina-associated polypeptide 2β) and the NPC protein Nup358, which faces the cytoplasm (Chizhik et al., 2017). By immunoelectron microscopy, localization of a protein to the INM or ONM is possible, but requires specific antibodies and complex fixation protocols (Yokoyama et al., 1995; Cordes et al., 1997). In general, these super-resolution methods are complex in experimental implementation and technical equipment. Therefore, a fluorescence microscopy based experimental approach was established by Dr. Janine Pfaff in the laboratory of Prof. Dr. Ralph H. Kehlenbach (Pfaff et al., 2016) to indicate the localization of a membrane protein to the INM. The presence in the INM of the protein of interest is shown by a clear change in the subcellular localization of a nuclear reporter upon addition of rapamycin.

Rapamycin, discovered first in 1975 by Vézina C. (1975) and further analyzed by Singh et al. (1979), is a cell permeable antifungal antibiotic produced by *Streptomyces hygroscopicus*. Rapamycin inhibits the lymphokine-dependent proliferation in a moderate way by inhibition of the G1 progression in

the cell cycle and binds with a high affinity (dissociation constant K_d = 0.2 nM) to FK506 binding protein FKBP (Bierer et al., 1990), later named FKBP12 (12 kDa FK506/rapamycin-binding protein). This interaction became interesting for several groups trying to identify rapamycin binding proteins. In yeast-two-hybrid screens, the kinase mTOR or FRAP (FKBP12-rapamycin associated protein) could be identified as a binding partner of FKBP12/rapamycin (Chiu et al., 1994; Brown et al., 1994; Sabatini et al., 1994; Stan et al., 1994). Within FRAP, a 11 kDa FKBP12-rapamycin binding domain could be identified (Chen et al., 1995). This binding domain, later referred to as the FRB (FKBP12-rapamycin-binding) domain, was further characterized by crystal structure analysis. Rapamycin was shown to bind FRB and FKBP12 at the same time via two different hydrophobic pockets, while FRB and FKBP12 are not able to interact among themselves in the absence of rapamycin (Choi et al., 1996). Furthermore, it was shown that FKBP12 binds to rapamycin first due to their high binding affinity, followed by the binding to FRB (Liang et al., 1999; Banaszynski et al., 2005).

The rapamycin-induced dimerization assay

As the dimerization of FRB and FKBP12 in the presence of rapamycin was well established and the binding reaction is specific, the inducible interaction has been used for several experimental approaches addressing localization and targeting questions within the cell. Klemm et al. (1997), for instance, identified an NES within NF-ATc by the localization change of a nuclear reporter to the cytoplasm. Upon the addition of rapamycin, the nuclear reporter Gal4-NLS-$FKBP12_3$ was bound to the potential FRB-tagged NF-ATc NES, resulting in the export of the whole complex from the nucleus into the cytoplasm. Later, Ohba and colleagues used the dimerization of FRB with FKBP12 in the presence of rapamycin to analyze the movement of some membrane proteins from the ONM to the INM in a live cell-based assay. Therefore, they established several FRB and GFP tagged reporters, which accumulate upon the addition of rapamycin within the INM due to binding to a nuclear protein trap tagged with FKBP12. With this approach, they could show a size-dependency in INM targeting for the cytoplasmic domains of their artificial reporters (Ohba et al., 2004). In their “anchor-away technique”, Haruki and colleagues used the rapamycin-based dimerization of FRB and FKBP12 to establish a depletion system in *S. cerevisiae* to deplete proteins from the nucleus (Haruki et al., 2008). Lastly, Pfaff et al. (2016) established a rapamycin-based dimerization assay for the identification of INM proteins, which is used with adaptions in this thesis.

To observe INM localization of a TMD-containing protein by usage of the rapamycin-induced dimerization assay, HeLa cells were transiently transfected with plasmids coding for the reporter $EGFP_2$-GST-M9-FKBP12 and the membrane protein of interest, LRRC59, tagged with mCherry-FRB at its N-terminus (figure 15A). Both proteins were overexpressed for 48 hours. The soluble reporter $EGFP_2$-GST-M9-FKBP12 localized in the nucleus due to nuclear import of the M9 sequence by transportin (Pollard et al., 1996). The reporter contained the FKBP12 domain, which made the dimerization with FRB upon rapamycin addition possible. Additionally, it contained two EGFP- and a GST-tag(s) resulting in a total molecular mass of 99 kDa. As GST is known to dimerize (Bell et al., 2013), $EGFP_2$-GST-M9-FKBP12 probably assembles into dimers of 198 kDa, which should be trapped in the nucleus. The membrane protein of interest, LRRC59, was N-terminally tagged with the FRB domain and the fluorescent tag mCherry. As shown before, mCherry-FRB-LRRC59 is located at the ER-membrane and at the NE (figure 14B, and 15B). If mCherry-FRB-LRRC59 is located at the INM, the soluble reporter $EGFP_2$-GST-M9-FKBP12 will be recruited from its localization all over the nucleus to the NE in the presence of rapamycin (figure 15A). The reporter $EGFP_2$-GST-M9-FKBP12 was located in the nucleus in the rapamycin-induced dimerization assay in the absence of rapamycin. In mCherry-FRB-LRRC59 overexpressing cells incubated with 200 nM rapamycin for 10 minutes, a recruitment of the reporter to the NE resulting in a green rim was observable, while the reporter did not localize to the center of the nucleus (figure 15B). This result indicates that mCherry-FRB-LRRC59 is located in the INM. For emerin, a well-studied INM protein, the reporter was also recruited to the NE upon the addition of rapamycin, confirming the INM localization of emerin (figure 15B). Additionally, WRB, one of the two membrane receptors of the TRC pathway, was examined for INM localization with this approach. As the C-terminus

of WRB is facing the cytoplasm, the protein was tagged C-terminally with FRB and HA. WRB-FRB-HA was localized to the ER and in a rim at the NE, but the localization of the nuclear reporter was not changed by the addition of rapamycin (figure 15B). When the incubation time with rapamycin was increased to 30 minutes, the reporter did still not show any recruitment to the NE in WRB-FRB-HA overexpressing cells (figure S 3). This indicates that WRB-FRB-HA is a protein of the ER and ONM and is not located in the INM. Therefore, this protein serves as a negative control for this assay (figure 15B).

For mCherry-FRB-LRRC59 expressing cells, the reporter recruitment to the NE was comparable for 10 and 30 minutes of rapamycin treatment. Also, for the increased incubation time, when mCherry-FRB-LRRC59 reached the INM, it was bound by rapamycin/EGFP$_2$-GST-M9-FKBP12 and the complex got trapped in the nucleus. It can be excluded that the complex left the nucleus as the reporter retained in the nucleus and was not distributed in the cytoplasm (figure S 3).

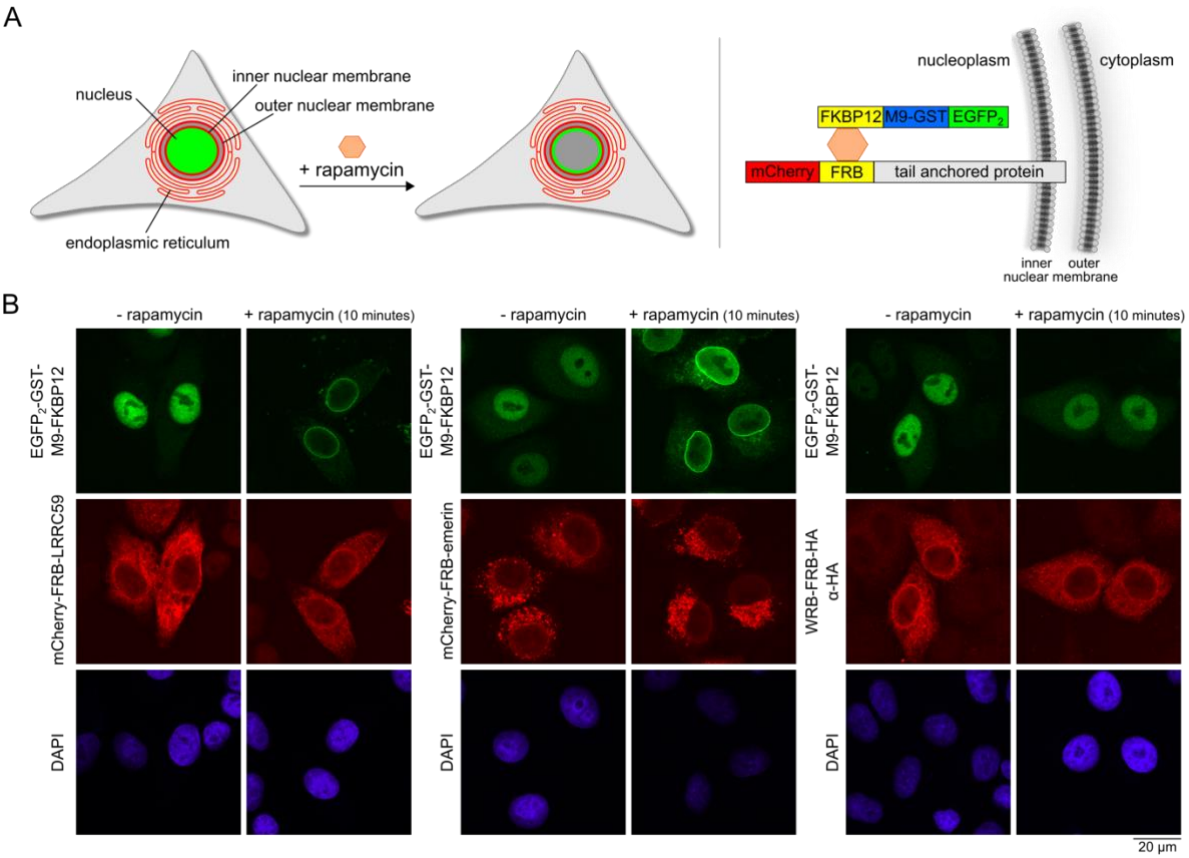

Figure 15: Rapamycin-induced dimerization assay confirms the INM localization of LRRC59. (A) The scheme gives an overview of the rapamycin-induced dimerization assay. Cells are transiently transfected with plasmids coding for the protein of interest tagged with mCherry and FRB (red) and the nuclear reporter EGFP$_2$-GST-M9-FKBP12 (green). Upon the addition of rapamycin (orange hexagon) the FRB- and FKBP12-domains dimerize which leads to a recruitment of the reporter to the NE, if the protein of interest locates to the INM. (B) HeLa cells were transiently transfected with constructs coding for the proteins mCherry-FRB-LRRC59, mCherry-FRB-emerin and WRB-FRB-HA, respectively, and EGFP$_2$-GST-M9-FKBP12. After the treatment of the cells with (+) or without (-) rapamycin for 10 minutes, the cells were fixed and analyzed directly for mCherry-tagged proteins or after immunofluorescence using antibodies against HA (WRB-FRB-HA). DAPI marked the nucleic acids in fluorescence microscopy. For analysis, confocal microscopy was performed. See also Blenski and Kehlenbach, 2019.

The rapamycin-induced dimerization assay identified LRRC59 as a protein of the INM and is a robust and reliable approach to examine the INM localization of LRRC59 and other membrane proteins under different conditions.

Analysis of binding of INM-localized LRRC59 to lamin A/C

The localization of emerin to the INM was shown to depend on its binding partner lamin A/C (Vaughan et al., 2001). As LRRC59 was identified as an INM protein by the rapamycin-induced dimerization assay, it is unclear whether LRRC59 located at the INM is also bound by lamin A/C. HeLa cells were transfected with siRNAs targeting lamin A/C, fixed and immunostained using antibodies against lamin A/C, LRRC59 or emerin. The efficiency of the knockdown was assessed by microscopic (figure 16A) and Western blot analysis (figure 16B). In control depletion cells, emerin was mainly located at the NE, while a knockdown of lamin A/C resulted in a diffuser localization of emerin to the ER with a signal decrease at the NE. This indicates a loss of INM localization of emerin, as it could not bind to lamin A/C for anchoring. LRRC59 localized in control knockdown cells to the ER and the NE. This localization pattern was not changed upon siRNA mediated knockdown of lamin A/C (figure 16A). This result suggests that LRRC59 does not require lamin A/C-binding for its INM localization.

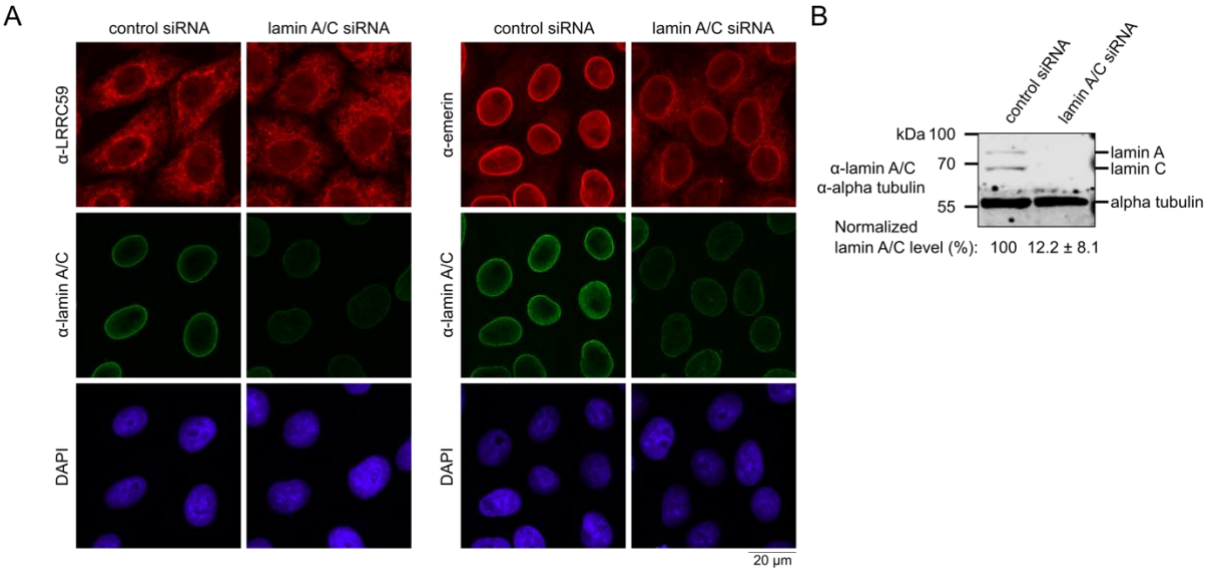

Figure 16: Knockdown of lamin A/C does not affect the NE localization of LRRC59.
(A) HeLa cells were treated with control siRNAs or siRNAs against lamin A/C, fixed after 48 hours and analyzed by indirect immunofluorescence detecting lamin A/C and LRRC59 (left) or emerin (right). DAPI marked the nucleic acids in fluorescence microscopy. Cells were analyzed by confocal microscopy. (B) Cells were treated as in (A) and analyzed by SDS-PAGE followed by Western blotting and immunodetection of lamin A/C and alpha tubulin. The mean and the standard deviation of normalized lamin A/C levels of seven experiments are indicated. For values see table S 1.

3.2.3 Importin β is not required for inner nuclear membrane targeting of LRRC59

It has previously been suggested that the INM targeting of LRRC59 depends on the transport factor importin β. This was based on the observation that the NE localization of endogenous LRRC59 was lost in U2OS cells treated with siRNAs against importin β (Zhen et al., 2012). In this thesis, this observation was re-examined.

NE localization of LRRC59 in importin β knockdown U2OS cells

First, U2OS cells were transiently transfected with two siRNAs against importin β for 48 hours. The cells were fixed and immunostained with an antibody against LRRC59. Cells grown on different coverslips, but treated with the identical transfection solution, were fixed and immunostained with an antibody against importin β. As the LRRC59- and the importin β-antibodies were both raised in rabbits, the staining could not be performed in the same cells. As shown in figure 17, importin β knockdown was successful. The efficiency of the knockdown was also confirmed by Western blot analysis of cell lysate (figure S 4A, table S 2). In control knockdown cells, LRRC59 was located mainly to the ER and to a rim at the NE, as shown in HeLa cells before (figure 14A). In importin β knockdown cells, no difference in

the localization of LRRC59 could be observed (figure 17). This result does not suggest an importin β-dependent NE localization of LRRC59.

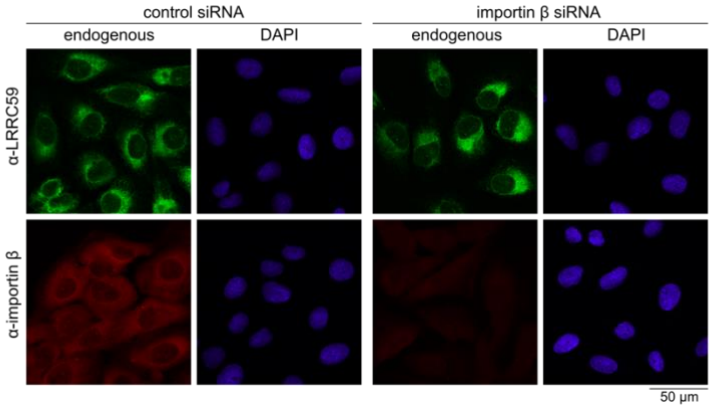

Figure 17: Knockdown of importin β has no effect on NE localization of LRRC59 in U2OS cells. U2OS cells were treated with control or importin β siRNAs. After 48 hours, cells were analyzed by indirect immunofluorescence using antibodies against LRRC59 or, on separate coverslips, importin β. See also Blenski and Kehlenbach, 2019.

Rapamycin-induced dimerization assay in importin β siRNA treated cells

Next, the rapamycin-induced dimerization assay was performed to clarify whether the INM targeting of LRRC59 is affected by an importin β knockdown.

HeLa cells were transiently transfected with siRNAs against importin β and the plasmids coding for $EGFP_2$-GST-M9-FKBP12, mCherry-FRB-LRRC59 and NES-mTagBFP2-cNLS. The protein NES-mTagBFP2-cNLS is a blue fluorescent protein with an N-terminal nuclear export signal (NES) and a C-terminal classical nuclear localization signal (cNLS). A soluble protein containing a cNLS is transported into the nucleus by the importin α/importin β pathway. In control siRNA treated cells, NES-mTagBFP2-cNLS was located in the nucleus while its localization was shifted to the cytoplasm in importin β knockdown cells (figure 18A). The transfection of cells for the rapamycin-induced dimerization assay with the additional construct coding for NES-mTagBFP2-cNLS has two advantages. First, the efficiency of the importin β knockdown could not only be observed by an importin β immunostaining (figure 18A), but also by a shift of NES-mTagBFP2-cNLS from the nucleus to the cytoplasm. Second, importin β was rate limiting for nucleocytoplasmic transport in importin β knockdown cells. The remaining importin β targeted the in excess available cNLS-containing protein to the nucleus. Additionally, the efficiency of the importin β knockdown was controlled by immunostaining of importin β (figure 18A) and Western blot analysis of the cell lysate (figure S 4B).

The reporter $EGFP_2$-GST-M9-FKBP12 used in the rapamycin-induced dimerization assay contained the nuclear localization signal M9. Proteins containing a M9 sequence are targeted to the nucleus by the transport factor transportin (Pollard et al., 1996). Therefore, the nuclear localization of the reporter was not affected by the importin β knockdown (figure 18A). The original used reporter $EGFP_2$-GST-cNLS-FKBP12 of Pfaff et al. (2016) is dependent on the importin α/importin β pathway and therefore could not be used in importin β knockdown cells.

The protein mCherry-FRB-LRRC59 was located to the ER and NE in control and importin β siRNA treated cells (figure 18A). After 10 minutes of rapamycin treatment, the reporter was recruited to the NE in cells of control knockdown, as well as importin β siRNA treated cells (figure 18A). After 10 minutes of drug incubation, no dependency of INM localization of LRRC59 on importin β could be observed. As differences might only be observable in cells with a shorter incubation time with rapamycin, the rapamycin-induced dimerization assay was performed with drug treatment for 1, 1.5, 2, 2.5, 3, 4 and 10 minutes. At least 100 cells per condition and experiment were analyzed with respect to the reporter response. The mean of the responding cells in percent and the standard deviation of 500 (incubation time 1-4 minutes) and 1850 (10 minutes) analyzed cells were plotted against the incubation time (figure

18B, table S 4). After 1 minute of rapamycin treatment, the reporter of 63% ± 5.7 of control siRNA treated cells was recruited to the NE. With the extension of rapamycin addition, more cells responded with a reporter recruitment to the NE until a plateau of 91.2% ± 4.4 responding cells was reached after 3 minutes. For cells treated with siRNA against importin β, the values of rapamycin responding cells were nearly identical to those of cells treated with control siRNA. This result shows that there is no difference in INM targeting of LRRC59 in importin β knockdown cells compared to control siRNA treatment. LRRC59 reaches the INM independently of importin β. Nuclear import of NES-mTagBFP2-cNLS by contrast was clearly affected by the importin β depletion.

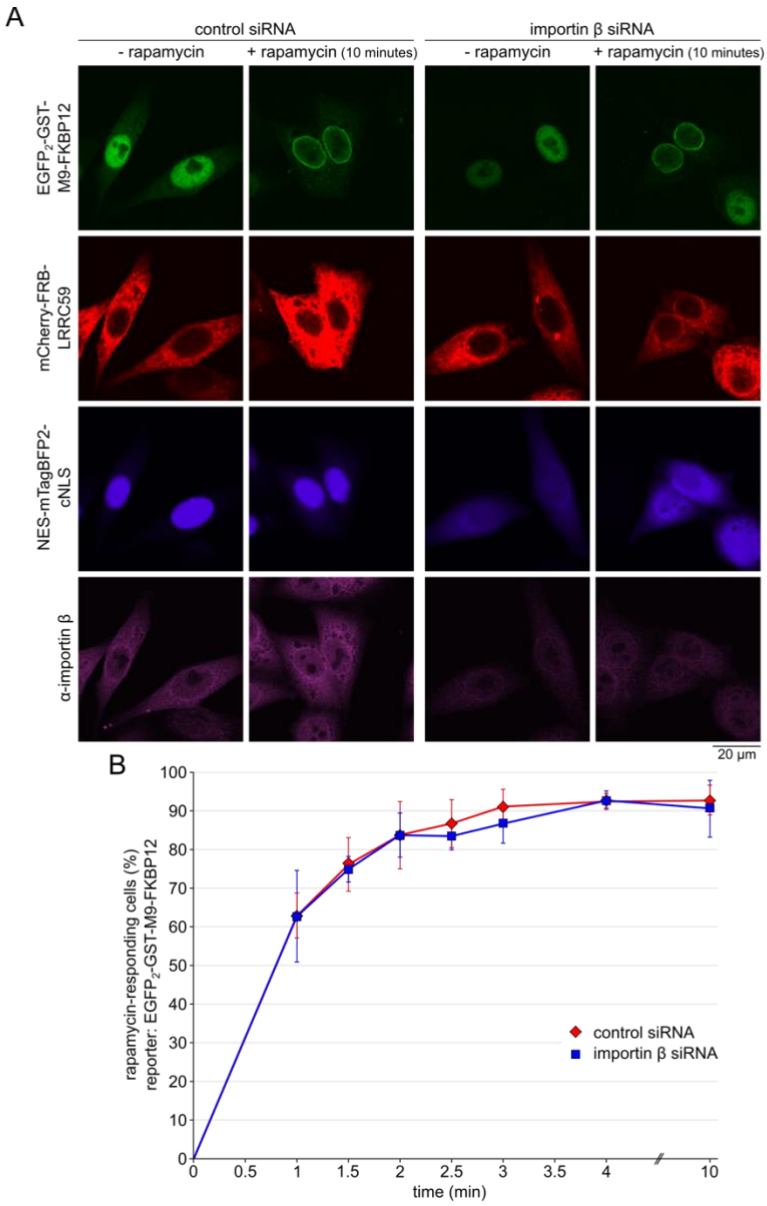

Figure 18: The INM-targeting of LRRC59 is not dependent on importin β.
(A) HeLa cells were transfected with control or importin β siRNAs and plasmids coding for mCherry-FRB-LRRC59, $EGFP_2$-GST-M9-FKBP12 and NES-mTagBFP2-cNLS. After 48 hours, cells were incubated with rapamycin at room temperature for 10 minutes and fixed. After immunostaining using antibodies against importin β, the cells were analyzed by confocal microscopy. DAPI marked the nucleic acids in fluorescence microscopy. (B) Quantification of experiments as in (A) with rapamycin treatment for 1, 1.5, 2, 2.5, 3, 4, and 10 minutes. For values see table S 4. Also see Blenski and Kehlenbach, 2019.

Rapamycin-induced dimerization assay in cells expressing Bimax2

To validate this result in a different experimental setup, the rapamycin-induced dimerization assay was performed by simultaneously overexpression of the plasmid pcDNA3-FLAG-Bimax2 (figure 19A) and the constructs used for the assay before. Bimax2 is a peptide sequence, which inhibits the importin α/importin β nuclear import pathway (Kosugi et al., 2008). This peptide inhibitor binds with a very high affinity to importin α. As importin α bound to Bimax2 can still assemble a complex together with importin β, this complex is imported into the nucleus. Due to the tight binding of Bimax2 to importin α, however, the cargo Bimax2 cannot be released from importin α. As importin α is only exported from the nucleus in a cargo-unbound from, Bimax2-importin α accumulates in the nucleus and cannot be recycled for its contribution to the importin α/importin β import machinery (Kosugi et al., 2008). As shown in figure 19A, NES-mTagBFP2-cNLS was shifted from the nucleus to the cytoplasm in cells expressing FLAG-Bimax2 compared to cells transfected with the control plasmid pcDNA3. This indicates the inhibition of the importin α/importin β import pathway by Bimax2. For the quantification of the rapamycin-induced dimerization assay, cells showing a shift of NES-mTagBFP2-cNLS to the cytoplasm were analyzed for NE recruitment of the reporter $EGFP_2$-GST-M9-FKBP12 after 10 minutes of rapamycin treatment. No difference in rapamycin-response of FLAG-Bimax2-expressing cells could be observed compared to cells transfected with the control plasmid pcDNA3 (figure 19A and B). This result indicates that LRRC59 did reach the INM even if the importin α/importin β pathway was blocked by Bimax2.

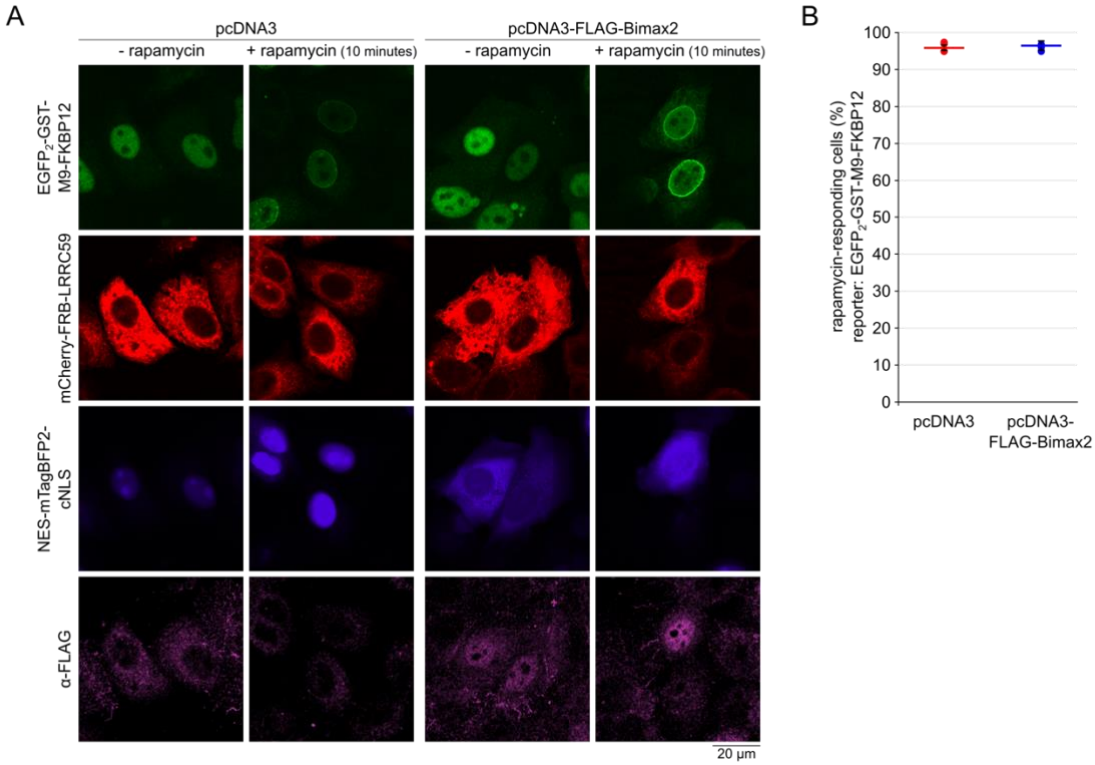

Figure 19: Overexpression of Bimax2 does not influence the nuclear localization of LRRC59. (A) HeLa cells were transiently transfected with plasmids coding for mCherry-FRB-LRRC59, $EGFP_2$-GST-M9-FKBP12, NES-mTagBFP2-cNLS and FLAG-Bimax2 or with the plasmid pcDNA3 as control, respectively. Cells were incubated with rapamycin for 10 minutes prior to fixation and immunofluorescence staining using antibodies against the FLAG-tag. Cells were analyzed by confocal microscopy. DAPI marked the nucleic acids in fluorescence microscopy. (B) Quantification of the rapamycin-induced dimerization assay as described in (B). Diagram contains the mean of the percentage of rapamycin responding cells and the standard deviation of three individual experiments, analyzing 200 cells each. See also Blenski and Kehlenbach, 2019.

Analysis of nuclear targeting of LRRC59 lacking the TMD

The nuclear transport of a protein mediated by the importin α/importin β pathway requires a targeting sequence. If LRRC59 is targeted to the INM in an importin β dependent manner as claimed by Zhen et al. (2012), the cytoplasmic domain of LRRC59 should have a targeting sequence for nuclear import. To examine the cytoplasmic part of LRRC59 for a potential NLS, the amino acids 1-244 before the TMD were cloned into an EGFP containing plasmid resulting in the plasmid pEGFP-LRRC59 aa1-244. The protein EGFP-LRRC59 aa1-244 was overexpressed in cells treated with control or importin β siRNAs. The efficiency of the importin β knockdown was controlled by immunostaining (figure 20A) or immunoblotting of cell lysate (figure 20B). In control knockdown cells, EGFP-LRRC59 aa1-244 localized to the nucleus but not in the cytoplasm. The same localization pattern was observed in cells treated with importin β siRNAs. This result points to an importin β-independent localization of soluble EGFP-LRRC59 aa1-244 to the nucleus. To distinguish between active, transport factor-mediated transport and nuclear retention after passive diffusion, the molecular mass of LRRC59 aa1-244 was increased by a second EGFP and a GST-tag in the construct pEGFP$_2$-GST-LRRC59 aa1-244. With these additional tags, the molecular mass of the overexpressed protein was increased from 55.5 kDa (EGFP-LRRC59 aa1-244) to 109.3 kDa of EGFP$_2$-GST-LRRC59 aa1-244. In addition, the GST-tag leads to dimerization (Bell et al., 2013) of EGFP$_2$-GST-LRRC59 resulting in dimers of 218.6 kDa. If a soluble protein containing an NLS is targeted to the nucleus by the importin α/importin β pathway, the size of the protein should – to a certain degree – not matter for the import machinery. However, EGFP$_2$-GST-LRRC59 aa1-244 was exclusively localized to the cytoplasm (figure 20C), excluding an active transport mechanism. This indicates that EGFP-LRRC59 aa1-244 reached the nucleus by diffusion because of its small molecular mass. To exclude that the localization of EGFP$_2$-GST-LRRC59 aa1-244 could be caused by the EGFP$_2$-GST tag itself, the localization of EGFP$_2$-GST-cNLS was analyzed compared to EGFP-cNLS (figure S 5). EGFP-cNLS localized exclusively to the nucleus, comparable to EGFP-LRRC59 aa1-244. While EGFP$_2$-GST-LRRC59 aa1-244 was not targeted to the nucleus at all and localized only in the cytoplasm, EGFP$_2$-GST-cNLS was mainly found in the nucleus with a weak signal in the cytoplasm. This indicates that the tag EGFP$_2$-GST influenced the localization of cNLS in a weak manner, but was not the reason for the exclusive cytoplasmic localization of EGFP$_2$-GST-LRRC59 aa1-244. The size of this LRRC59 protein seems to be too large to diffuse into the nucleus compared to EGFP-LRRC59 aa1-244. These results show that the cytoplasmic domain of LRRC59 does not contain a nuclear targeting sequence, which could be bound and imported by the importin α/importin β pathway or by any other transport factor.

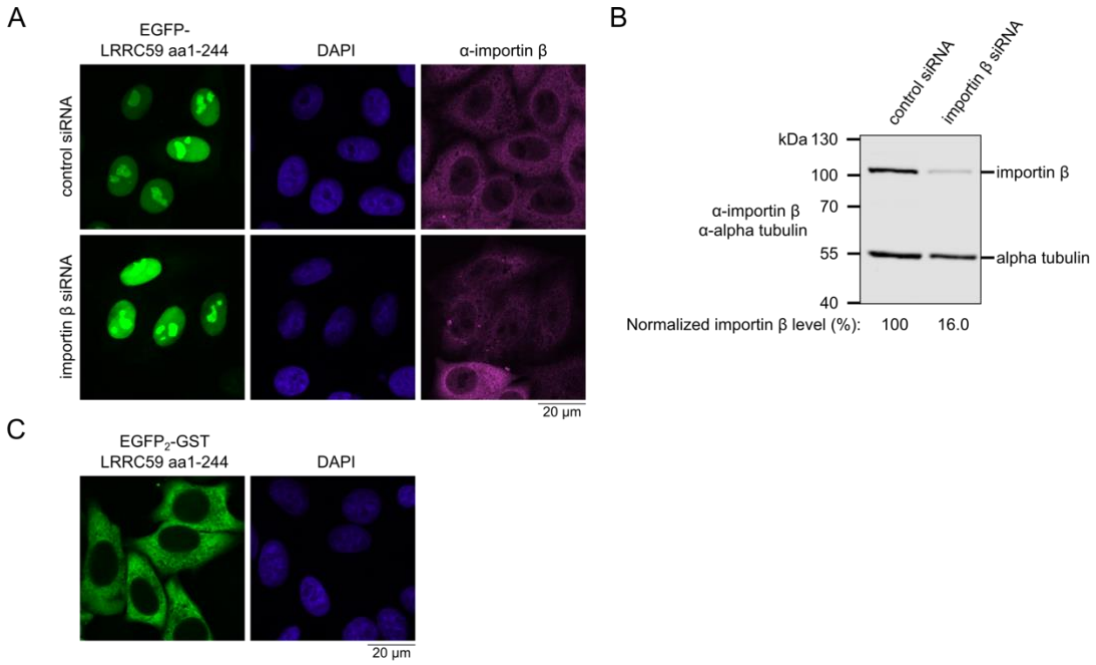

Figure 20: Importin β does not mediate active nuclear import of LRRC59 lacking the TMD.

(A) HeLa cells were transiently transfected with 0.7 µg of plasmid coding for EGFP-LRRC59 aa1-244 and control or importin β siRNAs. After 48 hours, cells were fixed, indirectly immunostained using antibodies against importin β and analyzed by confocal microscopy. (B) Cell lysate of (A) was analyzed by SDS-PAGE and immunoblotting using antibodies against importin β and alpha tubulin. The signal of alpha tubulin served for the normalization of the importin β level. (C) HeLa cells overexpressed 0.7 µg of the plasmid coding for $EGFP_2$-GST-LRRC59 aa1-244 for 48 hours prior to fixation and analysis by confocal microscopy. DAPI marked the nucleic acids in fluorescence microscopy. See also Blenski and Kehlenbach, 2019.

Together, no active transport of LRRC59 to the INM via importin β could be shown. In addition, no importin α/importin β- or importin β-dependent NLS could be found in the cytoplasmic domain of LRRC59. All these results do not point to an importin α/importin β mediated INM targeting of LRRC59.

3.2.4 Size dependency of inner nuclear membrane targeting of LRRC59 on the extraluminal domain

In the literature, two main models for membrane protein targeting to the INM are discussed. In addition to the model of INM targeting of membrane proteins by transport factors, a mechanism by diffusion to and retention at the INM is suggested. In this model, a membrane protein is supposed to diffuse freely from the ER-membrane to the ONM and then to the INM by passing though the NPC via peripheral channels. The NPC seems to have a size limitation for the passage of cytoplasmic domains of membrane proteins dictated by the peripheral channel width. After the INM has been reached, the INM protein could bind to lamins or chromatin using a binding domain in order to remain in the INM, which could lead to a concentration difference between the INM and the ONM (Katta et al., 2014).

For LRRC59, an active transport mechanism using an importin α/importin β- or importin β-dependent pathway could not be shown. To examine whether a diffusion-dependent INM targeting mechanism could apply to LRRC59, the size of the cytoplasmic domain of the proteins used in the rapamycin-induced dimerization assay was changed. The cytoplasmic/nucleoplasmic domain of endogenous LRRC59 has a molecular mass of 27.8 kDa. As the FRB domain is necessary for the rapamycin-induced dimerization assay, this tag had to be cloned into all used constructs for this experimental approach. In addition, the 1.08 kDa small human influenza hemagglutinin (HA)-tag was added to FRB-LRRC59 at the N-terminus to create a protein with a small cytoplasmic domain of 40.8 kDa (HA-FRB-LRRC59). Furthermore, the extraluminal domain was increased in size by adding an MBP-tag between the FRB-tag and the LRRC59 sequence of the pmCherry-FRB-LRRC59 construct creating a plasmid coding for mCherry-FRB-MBP-LRRC59 (cytoplasmic domain: 107.5 kDa, figure 21A). These three constructs were used for a rapamycin-induced dimerization assay with rapamycin incubation times of 1, 1.5, 2, 2.5, 3, 4 and 10 minutes. mCherry-FRB-LRRC59, HA-FRB-LRRC59 and mCherry-FRB-MBP-LRRC59 similarly located to the ER and the NE (figure 21B). The reporter $EGFP_2$-GST-M9-FKBP12 was recruited to the NE upon rapamycin treatment in the majority of cells overexpressing mCherry-FRB-LRRC59 and HA-FRB-LRRC59, respectively. After 3 minutes of rapamycin incubation, a plateau of approximately 92% of rapamycin-responding cells was reached for these two proteins. The values of rapamycin-responding cells of mCherry-FRB-LRRC59 and HA-FRB-LRRC59 overexpressing cells were almost identical for the examined rapamycin incubation times. For mCherry-FRB-MBP-LRRC59, however, only 52.3% ± 6.3 of the cells responded with a reporter recruitment to the NE after 10 minutes of rapamycin treatment. For rapamycin incubation times of 1-10 minutes, a reduction of around 40% for the number of rapamycin-responding cells was observed for cells overexpressing mCherry-FRB-MBP-LRRC59 compared to the proteins with smaller cytoplasmic domains (figure 21C).

The reduction of the cytoplasmic domain from 65.8 kDa of mCherry-FRB-LRRC59 to 40.8 kDa of HA-FRB-LRRC59 did not influence the fast recruitment of the reporter to the NE, confirming the INM localization of both proteins. The increase of the cytoplasmic domain by 41.7 kDa (mCherry-FRB-

LRRC59 compared to mCherry-FRB-MBP-LRRC59), however, reduced the INM localization by approximately 40%.

For the plasmid coding for mCherry-FRB-MBP-LRRC59, the MBP-tag was inserted without additional amino acids into pmCherry-FRB-LRRC59. This insertion could influence the agility of the tags to each other or the accessibility of FKBP12/rapamycin to the FRB-tag. This possibility was excluded by performing a rapamycin-induced dimerization assay with mCherry-FRB-MBP-LRRC59 containing flexible GGGGS-linker (Chen et al., 2013) between each tag and LRRC59. Cells overexpressing the linker-containing protein mCherry-FRB-MBP-LRRC59 showed an identical reduction in rapamycin-responding cells as demonstrated in figure 21 (figure S6). This control experiment demonstrated that the reduction of the reporter recruitment to the NE in rapamycin-responding cells for mCherry-FRB-MBP-LRRC59 was caused by the increase in the cytoplasmic domain. The dependency of INM targeting on the cytoplasmic size points to a diffusion mechanism for nuclear import of LRRC59.

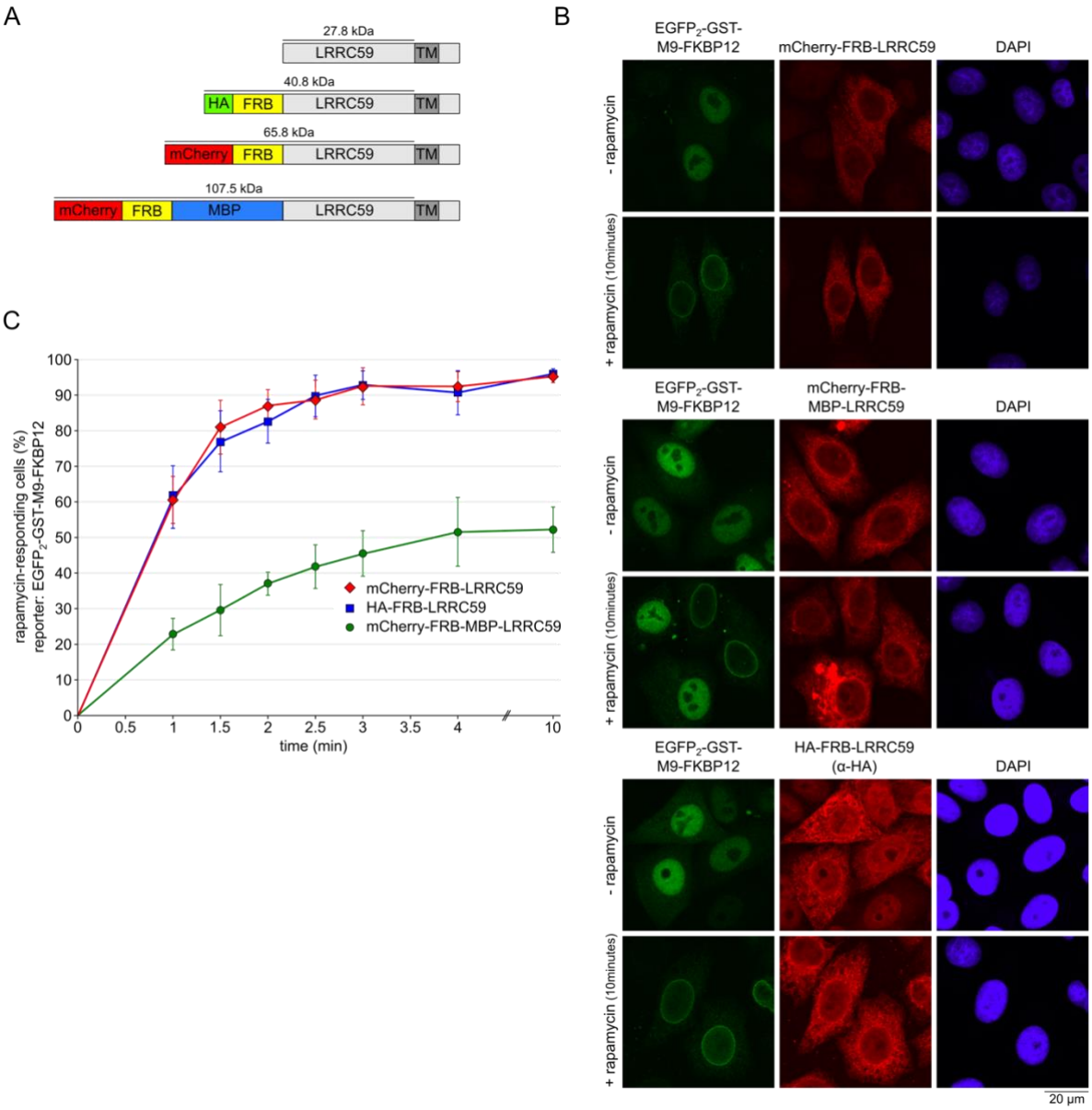

Figure 21: The size of the extraluminal region of LRRC59 affects targeting to the INM.
(A) Schematic overview of LRRC59 proteins with different sizes of the cytoplasmic/nucleoplasmic region used together with the reporter $EGFP_2$-GST-M9-FKBP12 in the rapamycin-induced dimerization assay. (B). The proteins mCherry-FRB-LRRC59, mCherry-FRB-MBP-LRRC59 and HA-FRB-LRRC59, respectively, were expressed in HeLa cells together with $EGFP_2$-GST-M9-FKBP12. For similar expression levels, the plasmid DNA concentrations were adjusted for the different proteins

of LRRC59. Cells were incubated without (-) or with (+) rapamycin for 1, 1.5, 2, 2.5, 3, 4, and 10 minutes. After fixation, the cells were analyzed by confocal microscopy. The images represent the rapamycin incubation time of 10 minutes. DAPI marked the nucleic acids in fluorescence microscopy. (C) Quantification of the experiment as described in (B). The mean of the percentage of cells responding to rapamycin treatment was plotted against the rapamycin incubation time. The standard deviation of the mean of at least four individual experiments (100 cells analyzed each time point) is indicated by error bars. For values, see table S 5, for overview of counted cell numbers see table S 6. Also see Blenski and Kehlenbach, 2019.

Next, the cytoplasmic domain was further increased in size by inserting a GST-tag into pmCherry-FRB-LRRC59 resulting in a plasmid coding for mCherry-FRB-GST-LRRC59. This protein had a cytoplasmic size of 91.4 kDa, but as GST is known to dimerize (Bell et al., 2013), expression of mCherry-FRB-GST-LRRC59 resulted in expected dimers with an extraluminal domain of 182.8 kDa (figure 22A). Due to the dimerization property of GST, the reporter $EGFP_2$-GST-M9-FKBP12 had to be exchanged into a reporter lacking the GST-tag. Therefore, a plasmid coding for $EGFP_2$-MBP-M9-FKBP12 was created, which located to the nucleus (figure 22B). In the rapamycin-induced dimerization assay, the proteins mCherry-FRB-LRRC59, mCherry-FRB-MBP-LRRC59 and mCherry-FRB-GST-LRRC59 located similar to the ER and in a rim at the NE (figure 22B). Cells overexpressing these proteins were examined in a rapamycin-induced dimerization assay with rapamycin-incubation times of 1, 1.5, 2, 2.5, 3, 4, and 10 minutes. For cells overexpressing mCherry-FRB-LRRC59 and mCherry-FRB-MBP-LRRC59, a similar percentage of rapamycin-responding cells was observed for the reporter $EGFP_2$-MBP-M9-FKBP12 as for $EGFP_2$-GST-M9-FKBP12 (compare figure 21C and 22C). The increase of the cytoplasmic domain by the insertion of the MBP-tag reduced the rapamycin-responding cells by approximately 40% (figure 22C). For mCherry-FRB-GST-LRRC59 expressing cells, the reporter $EGFP_2$-MBP-M9-FKBP12 was almost not recruited to the NE (figure 22B and C). On average for all tested rapamycin incubation times for mCherry-FRB-GST-LRRC59, approximately 92% of the cells did not show a reporter-recruitment to the NE. This result indicates that the further increase of the cytoplasmic domain to 182.8 kDa almost completely blocked INM targeting of mCherry-FRB-GST-LRRC59 in the rapamycin-induced dimerization assay.

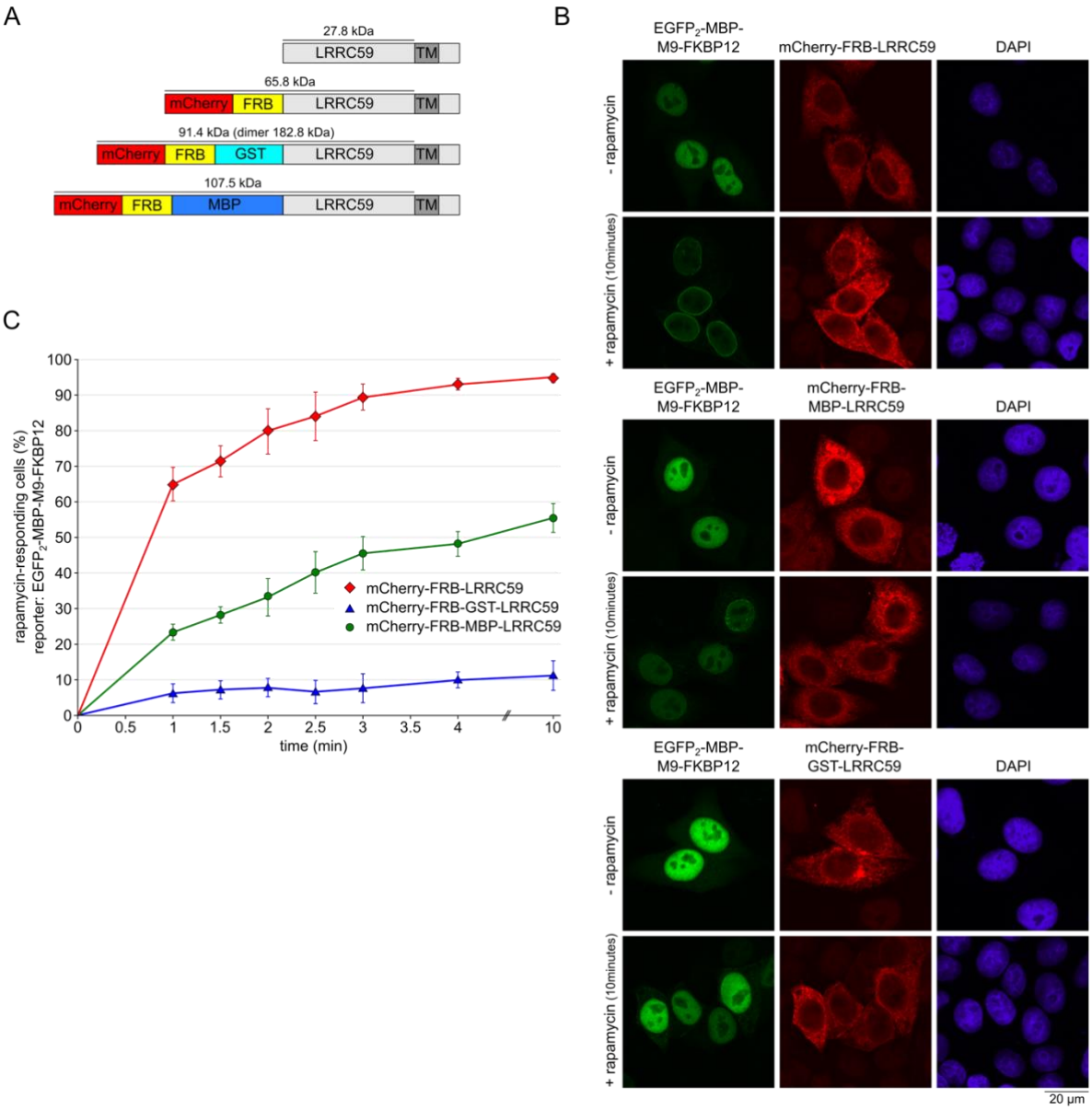

Figure 22: Increase of the size of the cytoplasmic domain of LRRC59 inhibits its INM targeting. (A) Schematic overview of LRRC59 constructs of different extraluminal regions used together with the reporter EGFP$_2$-MBP-M9-FKBP12. (B) HeLa cells were transiently transfected with plasmids coding for EGFP$_2$-MBP-M9-FKBP12 and mCherry-FRB-LRRC59, mCherry-FRB-MBP-LRRC59 and mCherry-FRB-GST-LRRC59, respectively. For similar expression levels of the LRRC59-proteins, the plasmid DNA concentrations were adjusted. Cells were treated without (-) or with (+) rapamycin for 1, 1.5, 2, 2.5, 3, 4, and 10 minutes, fixed and analyzed by fluorescence microscopy. The microscopic images represent cells of 10 minutes rapamycin incubation time. (C) Quantification of the experiment as described in (B). The graph plots the percentage of cells responding to rapamycin against the drug incubation time. The error bars indicate the standard deviation from the mean of five independent experiments, counting 100 cells per time point and condition. For values see table S 7. See also Blenski and Kehlenbach, 2019.

Taken together, these results indicate a dependency of INM targeting on the size of the extraluminal domain of LRRC59. The exchange of mCherry in mCherry-FRB-LRRC59 to the smaller HA-tag did not change the number of rapamycin-responding cells in the rapamycin-induced dimerization assay. However, the increase of the cytoplasmic domain to 107.5 kDa of mCherry-FRB-MBP-LRRC59 reduced the recruitment of both used reporters to the NE by approximately 40%. By further increase of the cytoplasmic domain to 182.8 kDa of the dimerizing protein mCherry-FRB-GST-LRRC59, the reporter was almost not recruited to the NE. This indicates that the protein mCherry-FRB-GST-LRRC59 was inhibited in its INM targeting by the increase of the extraluminal domain. This size-dependency in INM-targeting suggests that LRRC59 reaches the INM by diffusion, not by active transport.

3.3 Rapamycin- and APEX-dependent identification of proteins by SILAC (RAPIDS): analysis of LRRC59 by proximity

3.3.1 Experimental procedure

Very little is known about the biological function of LRRC59 (see section 1.4). A method for the identification of binding and/or proximity partners of membrane proteins was established by Dr. Marret Müller in the laboratory of Prof. Dr. Ralph H. Kehlenbach, Göttingen. For the analysis of LRRC59 by proximity, the original assay was applied to LRRC59 with some experimental modifications.

To identify proteins in close proximity of a protein of interest, three experimental components were combined in one approach (figure 23). First, the rapamycin-induced dimerization assay using cells expressing the membrane protein of interest tagged with FRB and the reporter FKBP12-EGFP-APEX2 was applied. Second, a biotinylation assay followed by enrichment of biotinylated proteins was performed, and third, mass spectrometry was done to analyze the biotinylated proteins in the context of a SILAC (stable isotope labeling by amino acids in cell culture) approach. This assay was called rapamycin- and APEX-dependent identification of proteins by SILAC (RAPIDS).

The rapamycin-induced dimerization assay was performed with HeLa cells expressing mCherry-FRB-LRRC59 and the soluble reporter FKBP12-EGFP-APEX2, which localized all over the cell. Upon the addition of rapamycin, the soluble reporter is recruited to mCherry-FRB-LRRC59 due to the dimerization of FKBP12/rapamycin with FRB. For further and general information about the rapamycin-induced dimerization assay, see section 3.2.2 and 2.5.

The biotinylation of proteins in the RAPIDS experiments is mediated by APEX2, an engineered ascorbate peroxidase, which is part of the reporter used for the rapamycin-induced dimerization assay. APEX2 oxidizes biotinphenol into phenoxyl radicals in the presence of H_2O_2. These biotin-phenoxyl radicals covalently react with electron-rich amino acids of proteins in close proximity to APEX2 (<20 nm), resulting in biotinylation of endogenous proteins, which can be enriched by NeutrAvidin beads (Martell et al., 2012; Lam et al., 2015).

Mass spectrometry analysis was performed to identify biotinylated, endogenous proteins in close proximity to mCherry-FRB-LRRC59. Transfected cells were incubated with medium supplemented with rapamycin and biotinphenol, followed by treatment with H_2O_2 for the biotinylation reaction. Upon the addition of rapamycin, the APEX2-containing reporter was recruited to mCherry-FRB-LRRC59. Because of the recruitment, the biotinylation of proteins close to mCherry-FRB-LRRC59 by APEX2 increases upon H_2O_2 treatment. In the absence of rapamycin, APEX2 located all over the cell and biotinylates random proteins in close proximity to itself upon H_2O_2 treatment. To distinguish between these two conditions in mass spectrometry, cells were cultivated in medium containing heavy or light isotopes of arginine and lysine (SILAC: Ong et al. (2002)). In a forward experiment, cells grown in light isotope labeled medium were treated with rapamycin and biotinphenol, resulting in an increased biotinylation of proteins close to mCherry-FRB-LRRC59. Cells grown in heavy isotope labeled medium were only incubated with biotinphenol. After the biotinylation reaction, cells were lysed, the protein concentrations were determined and adjusted. For mass spectrometry analysis, the lysates of cells coming from heavy or light isotope labeled medium were mixed in a protein concentration ratio of 1:1. Biotinylated proteins were enriched with NeutrAvidin beads. The eluted proteins were sent for mass spectrometry analysis or analyzed by Western blot (figure 23).

To exclude the possible influence of the isotope labeling itself on the experimental setup, RAPIDS experiments were performed in a forward and a reverse experiment switching the rapamycin-treatment depending on the isotope labeled medium. In the forward experiments, cells grown in light isotope labeled medium were supplemented with rapamycin, while in the reverse experiments the rapamycin treatment was performed with cells of heavy isotope labeled medium. In total, two forward and two reverse experiments were performed and the results of mass spectrometry analysis were united for statistical evaluation. (For information about workflow in Perseus Software, see table S 8).

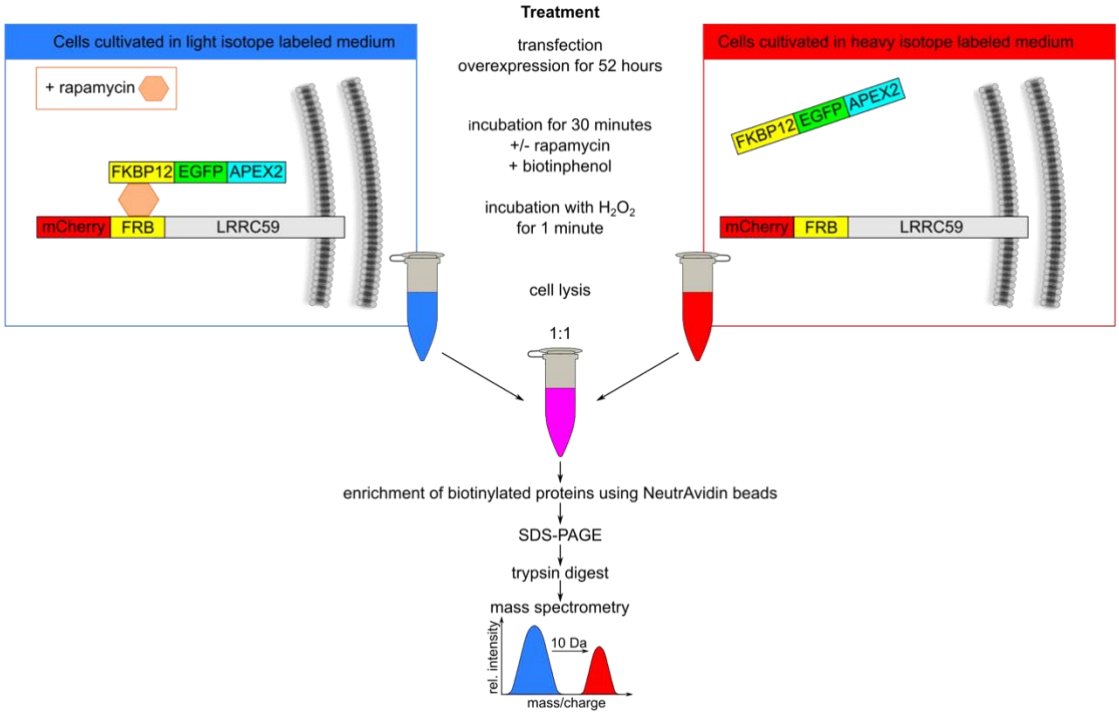

Figure 23: Workflow of RAPIDS experiments for identification of proteins in close proximity to mCherry-FRB-LRRC59.
For forward experiments, HeLa cells were grown in heavy or light isotope labeled medium and transfected with plasmids coding for mCherry-FRB-LRRC59 and FKBP12-EGFP-APEX2. Cells cultivated in light isotope labeled medium (blue box) were incubated with biotinphenol and rapamycin, increasing the biotinylation of proteins in close proximity to mCherry-FRB-LRRC59 by the recruitment of the FKBP12-tagged APEX2. Cells grown in heavy isotope labeled medium (red box) were not treated with rapamycin. For the biotinylation reaction of endogenous proteins by APEX2, H_2O_2 was added. After cell lysis, the lysates were mixed in a 1:1 protein concentration ratio and biotinylated proteins were enriched by incubation with NeutrAvidin beads. For mass spectrometry analysis, the eluate was separated by SDS-PAGE and proteins were digested by trypsin. The increase of biotinylation of proteins in close proximity to mCherry-FRB-LRRC59 due to rapamycin treatment in cells grown in light isotope labeled medium led to an increase in their relative intensity (blue peak). Biotinylated proteins of cells cultivated in heavy isotope labeled medium showed an increase in the mass to charge ratio of 10 Da (red peak). The 10 Da shift enables a discrimination of proteins being biotinylated in the presence or absence of rapamycin. The reverse experiments were performed in an identical workflow with rapamycin treatment for cells grown in heavy isotope labeled medium.

Microscopic analysis of RAPIDS experiments

In RAPIDS experiments, the recruitment of FKBP12-EGFP-APEX2 to mCherry-FRB-LRRC59 upon rapamycin treatment was controlled by microscopic analysis. For cells grown in heavy or light isotope labeled medium, mCherry-FRB-LRRC59 localized to the ER and the NE. In the absence of rapamycin, the reporter FKBP12-EGFP-APEX2 was observed all over the cell (figure 24). In cells treated with rapamycin, the reporter was targeted to mCherry-FRB-LRRC59 due to the dimerization of FRB and FKBP12. Both overexpressed proteins colocalized at the ER and in a rim at the NE (figure 24). The cultivation in differently isotope labeled medium had no observable influence on the localization of the overexpressed proteins or the rapamycin-induced recruitment of the reporter.

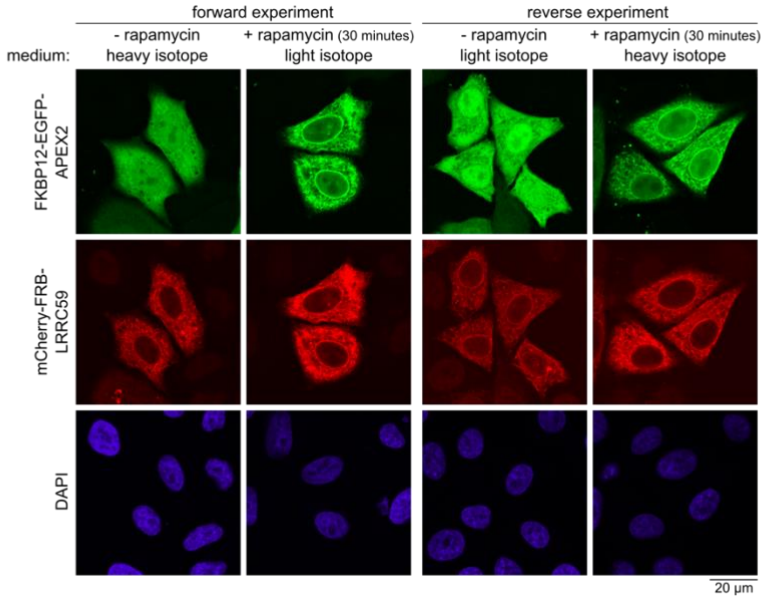

Figure 24: The reporter FKBP12-EGFP-APEX2 is recruited to mCherry-FRB-LRRC59 in RAPIDS experiments upon the addition of rapamycin.
HeLa cells for RAPIDS experiments were cultivated in heavy or light isotope labeled medium prior to seeding into 10 cm cell culture dishes for RAPIDS experiments containing a coverslip for fluorescence microscopy. Cells were transfected with plasmids coding for mCherry-FRB-LRRC59 and FKBP12-EGFP-APEX2 for 52 hours and incubated with biotinphenol in the presence (+) or absence (-) of rapamycin for 30 minutes. After the treatment of the cells with H_2O_2 but before cell lysis, the coverslips were removed. Cells were fixed and directly analyzed by confocal microscopy. DAPI marked the nucleic acids in fluorescence microscopy. For forward experiments (left panel), rapamycin was added to cells cultivated in light isotope labeled medium, while in reverse experiments, cells grown in heavy isotope labeled medium were supplemented with rapamycin (right panel).

Western blot analysis of RAPIDS experiments

In addition to microscopic analysis, Western blot analysis was performed to monitor the enrichment of biotinylated proteins using NeutrAvidin beads and to compare the transfection efficiency of cells grown in heavy or light isotope labeled medium.

For the analysis of enrichment of biotinylated proteins with NeutrAvidin beads, total cell lysate and eluate coming from forward and reverse experiments, respectively, were separated by SDS-PAGE prior to Western blotting and detection using HRP-coupled Streptavidin. It was shown that biotinylated proteins could be isolated from the total lysate and eluted from the beads for the forward and reverse experiments (figure 25A).

Next, it was examined whether the rapamycin addition led to an increase in biotinylation of mCherry-FRB-LRRC59, as the APEX2-containing reporter was recruited to FRB upon drug treatment. As seen in figure 25B, a weak increase in biotinylation of mCherry-FRB-LRRC59 could be shown in the presence of rapamycin for both forward and reverse experiments. Interestingly, endogenous LRRC59 was also biotinylated in the presence of rapamycin, indicating a potential dimer assembly between endogenous LRRC59 and mCherry-FRB-LRRC59.

Comparable signals for FKBP12-EGFP-APEX2 could be detected in lysates of cells cultivated in heavy or light isotope labeled medium for forward and reverse experiments. This result indicates a comparable efficiency for transfection and expression of the cells (figure 25C).

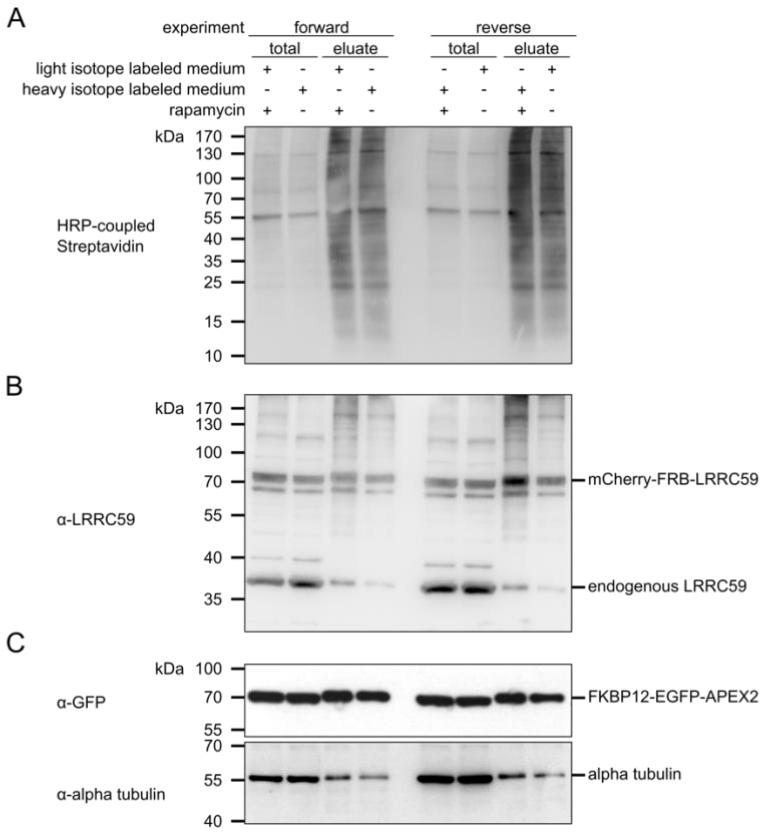

Figure 25: Western blot analysis of forward and reverse experiments of RAPIDS approach. Cell lysates from cells cultivated in heavy or light isotope labeled medium were adjusted to each other in protein concentration (total). Biotinylated proteins were enriched by usage of NeutrAvidin beads. After elution (eluate), biotinylated proteins were analyzed by SDS-PAGE and Western blotting in comparison to the total cell lysate. (A) Detection of biotinylated proteins using HRP-coupled Streptavidin for forward and reverse experiments. (B) Immunodetection of LRRC59 using a LRRC59-antibody for forward and reverse experiments. (C) Immunodetection of FKBP12-EGFP-APEX2 using an antibody against GFP. The signal of the antibody against alpha-tubulin served as a loading control.

The microscopy analysis showed a recruitment of FKBP12-EGFP-APEX2 to mCherry-FRB-LRRC59 in the presence of rapamycin. In the Western blot analysis, the successful enrichment of biotinylated proteins could be confirmed. In addition, an increase in biotinylation of mCherry-FRB-LRRC59 in presence of rapamycin could be demonstrated, as well as a comparable transfection efficiency for the reporter FKBP12-EGFP-APEX2. Based on these results, the samples were subjected to mass spectrometry analysis.

3.3.2 Mass spectrometry

The enriched biotinylated proteins of the RAPIDS experiments were analyzed by mass spectrometry. The results were processed in a significance analysis resulting in a Scatter plot containing all identified proteins (figure S 7). In the Scatter plot, the logarithmic values of the heavy/light normalized LRRC59 of the forward experiments were plotted on the x-axis against the values of the reverse experiments on the y-axis. Proteins identified as significantly enriched were marked within the Scatter plot. In the forward experiments, cells grown in light isotope labeled medium were treated with rapamycin. APEX2 was recruited to mCherry-FRB-LRRC59 in these cells leading to an increase in the biotinylation of proteins in close proximity to mCherry-FRB-LRRC59. The values of relative intensity of increased biotinylated proteins grown in light isotope labeled medium is therefore expected to be higher than the values of the same proteins of cells grown in heavy isotope labeled medium. As the values are given in a ratio of heavy to light, a smaller value is divided by a bigger value leading to a negative value in the logarithmic calculation. Proteins which were not affected by the rapamycin treatment would not cause a difference between the heavy or light normalized LRRC59 values resulting in a $\log_2$-ratio around zero. For the reverse experiments, an enrichment of biotinylation of proteins in close proximity to

mCherry-FRB-LRRC59 was expected in cells cultivated in heavy isotope labeled medium, as these cells were treated with rapamycin. This led to an increase of the relative intensity of proteins of cells of heavy isotope medium. Therefore, a high value was divided by a smaller value in the ratio of heavy to light, yielding a positive value for the log_2. Within the Scatter plot, the interesting candidates expected to be in close proximity to mCherry-FRB-LRRC59 are located in the fourth quadrant (negative value for forward and positive value for reverse experiments of ratio log_2 heavy/light normalized LRRC59). In this quadrant, 13 candidates were identified as significantly enriched in the forward and the reverse experiments as well as LRRC59 itself (figure 26, red font color). By rapamycin treatment, 6 proteins were significantly enriched in the forward experiments (figure 26, blue font color), while 10 (figure 26, green font color) were identified as significantly enriched in the reverse experiments. The significantly enriched proteins of quadrant IV are listed with the gene and protein names, information of localization within the cell and function assigned to UniProt in table 26. The majority of proteins were not identified as significant. Proteins not affected by the rapamycin treatment clustered around zero for the ratio log_2 heavy/light normalized LRRC59 for forward and reverse experiments (figure 26, gray dots). The proteins MCCC2, MCCC1, ACABA, ACACA, PCCA and PCCB are endogenously biotinylated and served as internal controls, as their biotinylation should not be changed by rapamycin treatment. This was true for five of the six proteins. MCCC1 was identified as significantly enriched by rapamycin treatment in the forward experiments, but with a positive ratio log_2 heavy/light normalized LRRC59 value. For further details of values see table S 9 and S 10.

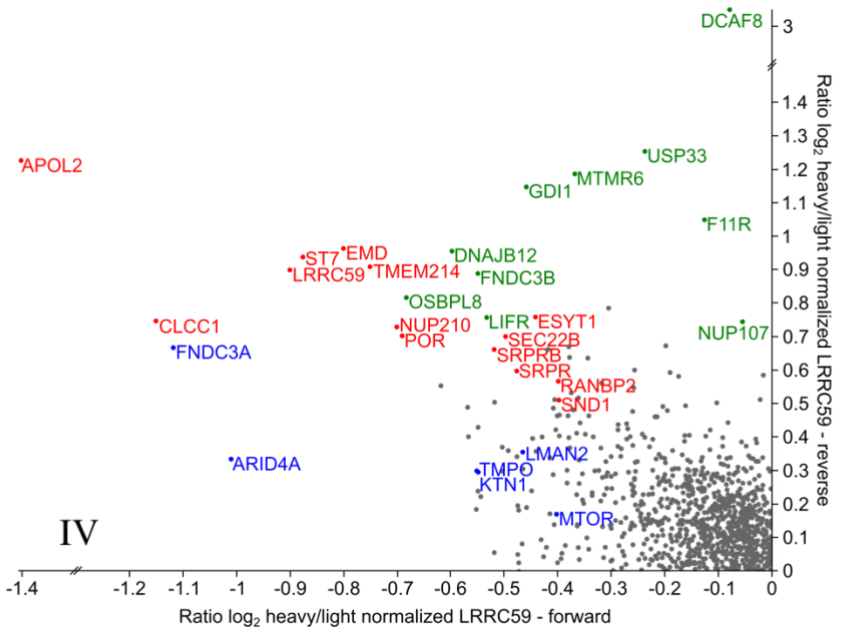

Figure 26: Mass spectrometry analysis of four RAPIDS experiments identifies significantly enriched candidates in close proximity to mCherry-FRB-LRRC59.
Data of mass spectrometry was analyzed using Perseus Software and a matrix resulting in a two-sided Significance B test with Benjamini Hochberg False Discovery Rate and a Scatter plot scaling the ratio log_2 heavy/light normalized LRRC59 of the forward experiments on the x-axis and this ratio for the reverse experiments on the y-axis. The fourth quadrant (IV) contains proteins enriched upon the addition of rapamycin. Significantly enriched proteins in forward and reverse experiments are highlighted with red gene names. Proteins identified as significantly enriched in the forward experiments are highlighted with blue gene names, while green font indicates significant enrichment in the reverse experiments. For details see table S 9. For all quadrants of the Scatter plot see figure S 7.

Table 26: Overview of the significantly enriched proteins of quadrant IV with localization and function information referred to UniProt

Gene names	Protein names	UniProt ID	localization	Protein function and further information
APOL2	Apolipoprotein L2	Q9BQE5	cytoplasm	potential role in lipid movement and lipid binding to organelles
CLCC1	Chloride channel CLIC-like protein 1	A96S66	ER-membrane, Golgi apparatus and nucleus	three TMDs, Potential function as chloride ion channel
LRRC59	Leucine-rich repeat-containing protein 59	Q96AG4	ER-membrane and nucleus	for information see section 1.4
ST7; ST7L	Suppressor of tumorigenicity 7 protein (-like)	Q9NRC1	membranes	three TMDs, potential function as tumor suppressor
EMD	Emerin	P50402	ONM and INM	single C-terminal TMD, several functions as e.g. contribution to nuclear architecture
TMEM214	Transmembrane protein 214	Q6NUQ4	ER-membrane	two TMDs, involvement in ER-stress mediated apoptosis
NUP210	Nuclear pore membrane glycoprotein 210	Q8TEM1	nuclear membrane	has one TMD and is important for NPC assembly and anchoring to the nuclear membrane
POR	NADPH--cytochrome P450 reductase	P16435	ER-membrane	one TMD, function in electron transfer from NADP to cytochrome P450
SRPRB	Signal recognition particle receptor subunit beta	Q9Y5M8	ER-membrane	one TMD, component of the SRP complex. See section 1.2
SEC22B	Vesicle-trafficking protein SEC22b	O75396	ER-membrane, INM*	one TMD, involvement in the vesicle transport between ER and Golgi. See section 3.4
SRPR	Signal recognition particle receptor subunit alpha	P08240	ER-membrane associated	component of the SRP complex. See section 1.2
ESYT1	Extended synaptotagmin-1	Q9BSJ8	ER-membrane, plasma-membrane	two TMDs, potential involvement in lipid transport
RANBP2	E3 SUMO-protein ligase RanBP2 Alternative name: Nup358	P49792	nucleus, NPC	involvement in nuclear transport mediated by interaction of the transport factors with the FG-repeat containing domain of Nup358. See section 1.1
SND1	Staphylococcal nuclease domain-containing protein 1	Q7KZF4	nucleus	involvement in miRNA decay
FNDC3A	Fibronectin type III domain-containing protein 3A	Q9Y2H6	Golgi apparatus	one TMD, involvement in spermatogenesis
ARID4A	AT-rich interactive domain-containing protein 4A	P29374	nucleus	binding to DNA and activity control of several transcription factors

Gene names	Protein names	UniProt ID	localization	Protein function and further information
TMPO	Lamina-associated polypeptide 2 (LAP2β), isoforms β/γ; Thymopoietin; Thymopentin	P42167	INM	one TMD, involvement in nuclear lamina assembly contributing to the maintain of the structural NE organization
KTN1	Kinectin	Q86UP2	ER-membrane	one TMD, receptor for kinesin, involvement in kinesin-driven vesicle mobility
LMAN2	Vesicular integral-membrane protein VIP36	Q12907	ER-membrane, Golgi apparatus membrane, INM*	one TMD, involvement in the secretory pathway. See section 3.4
MTOR	Serine/threonine-protein kinase mTOR	P42345	ER-membrane, Golgi apparatus membrane, mitochondrial outer membrane, lysosome	involvement in the regulation of cellular metabolism, hormone response and other cellular processes. The FRB domain of mTOR is bound by rapamycin-FKBP12. See section 3.2.2
OSBPL8	Oxysterol-binding protein-related protein 8; Oxysterol-binding protein	Q9BZF1	ER-membrane, nuclear membrane	one TMD, involvement in lipid transport between ER- and plasma membrane
DNAJB12	DnaJ homolog subfamily B member 12	Q9NXW2	ER-membrane, nuclear membrane	one TMD, involvement in protein folding and trafficking as co-chaperone with Hsc70
FNDC3B	Fibronectin type III domain-containing protein 3B	Q53EP0	membranes	one TMD, potential positive regulator of adipogenesis
LIFR	Leukemia inhibitory factor receptor	P42702	plasma membrane and extracellular region (isoform 1)	one TMD (isoform 1), function as signal-transducing molecule
GDI1	Rab GDP dissociation inhibitor alpha	P31150	Golgi apparatus, cytoplasm	involvement in the GDP/GTP exchange of most Rab proteins by inhibiting the dissociation of GDP from these proteins
MTMR6	Myotubularin-related protein 6	MTMR6	NE	phosphatase acting on lipids
USP33	Ubiquitin carboxyl-terminal hydrolase 33	Q8TEY7	cytoskeleton, perinuclear region	deubiquitinase, involvement in different cellular processes as centrosome duplication
F11R	Junctional adhesion molecule A	Q9Y624	plasma membrane	one TMD, potential involvement in epithelial tight junction formation
DCAF8	DDB1- and CUL4-associated factor 8	Q5TAQ9	nucleus, cytoplasm	potential substrate receptor for the E3 ubiquitin ligase complex CUL4-DDB1
NUP107	Nuclear pore complex protein Nup107	P57740	nuclear membrane, NPC	part of the NPC, involvement in NPC assembly and maintenance. See section 1.1

* for further information about INM localization, see section 3.4

3.3.3 Analysis of potential interaction of LRRC59 with Nup210

In the RAPIDS experiments, Nup210 was identified as a significantly enriched protein in close proximity to mCherry-FRB-LRRC59. Nup210 is a nucleoporin, a protein of the NPC. It has 1887 amino acids with a single TMD close to its C-terminus (TMD: 1809-1829 aa (Greber et al., 1990; Wozniak et al., 1989)). Nup210, also known as gp210, is one of three TMD-containing proteins assembled in the NPC. In metazoan, Nup210 and the other two TMD-containing proteins POM121 and NDC1 are suggested to anchor the NPC in the pore membrane (Weberruss and Antonin, 2016). It was suggested that TMD-containing proteins reaching the INM by diffusion, overcome the NPC by using peripheral channels. These are inner lateral channels adjacent to the pore membrane (Maimon et al., 2012). Due to the proximity of Nup210 to these peripheral channels, this protein is the focus of further analysis.

A pulldown experiment was performed with the protein corresponding to the region of LRRC59 facing the cytoplasm (aa1-244) and the short C-terminal domain of Nup210 after the TMD (aa1830-1887) located in the cytoplasm. The recombinant expressed proteins MBP-LRRC59 aa1-244-His, His-GST-Nup210 aa1830-1887 and His-MBP-His were purified for this pulldown assay (figure S 8). As shown in figure 27, His-GST-Nup210 aa1830-1887 and GST could be immobilized on glutathione beads, while MBP-LRRC59 aa1-244-His and His-MBP-His were immobilized on amylose beads. No binding of His-GST-Nup210 aa1830-1889 to MBP-LRRC59 aa1-244-His could be detected. Weak binding of MBP-LRRC59 aa1-244-His could be shown with immobilized His-GST-Nup210 aa1830-1887, but also with the immobilized GST-tag itself. This shows that the binding between LRRC59 aa1-244 and Nup210 aa1830-1887 was not specific because it was mediated by the GST-tag (figure 27).

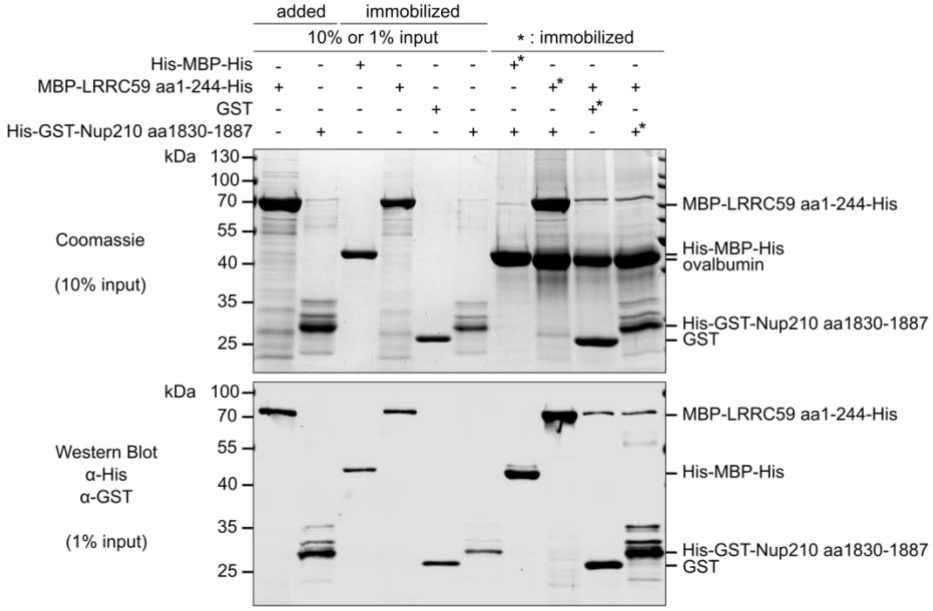

Figure 27: LRRC59 aa1-244 does not bind to Nup210 aa1830-1887.
For the binding assay, MBP-LRRC59 aa1-244-His or His-MBP-His were immobilized using Amylose Resin High Flow and His-GST-Nup210 aa1830-1887 or GST using Glutathione Sepharose High Performance for 60 minutes, respectively. After washing, His-GST-Nup210 aa1830-1887 was added to the immobilized His-MBP-His or MBP-LRRC59 aa1-244-His, while MBP-LRRC59 aa1-244-His was added to the immobilized GST or His-GST-Nup210 aa1830-1887 for 60 minutes. After washing, the binding was analyzed by SDS-PAGE followed by Coomassie staining (upper panel, 60% loading of the reaction) or immunodetection after Western blotting using antibodies against His- and GST-tags (lower panel, 20% loading of the reaction). For Coomassie staining, 10% of immobilized or added protein was loaded as an input, while 1% of used protein was loaded onto SDS-PAGE used for Western blotting. Asterisks indicate the protein immobilized onto the beads in the corresponding binding reaction.

The regions of LRRC59 and Nup210 facing the cytoplasm were analyzed for binding using the pulldown experiment. Even though Nup210 was identified as protein in close proximity to mCherry-FRB-LRRC59, no direct binding between LRRC59 aa1-244 and Nup210 aa1830-1887 could be detected.

3.4 Analysis of inner nuclear membrane localization of classical ER proteins

In 2016, Smoyer and colleagues established a split-GFP microscopy-based live cell assay in *S. cerevisiae* to identify unknown membrane proteins of the INM. More than 400 membrane proteins able to reach the INM were found with this approach. 230 of these proteins have a human ortholog (Smoyer et al., 2016). From these, five single TMD-containing proteins Sec61β, DDOST, LMAN2, Ube2j1, Ube2j2 and the protein Sec22b identified by RAPIDS experiments (as well as LMAN2) were chosen for further analysis of INM localization using the rapamycin-induced dimerization assay.

3.4.1 Overview of the examined single transmembrane domain containing proteins

The N-terminus of **Sec61β** (Protein transport protein Sec61 subunit beta, yeast ortholog is SBH2, figure 28A) faces the cytoplasm. The C-terminus contains a TMD followed by a five amino acid short tail in the ER-lumen (Hartmann et al., 1994) (UniProt ID P60468). Sec61β is one of three transmembrane proteins (with Sec61α and Sec61γ) forming the Sec61 translocon which localizes in the ER-membrane (Osborne et al., 2005). It can, however, also occur as a stable protein on its own (Panzner et al., 1995; Esnault et al., 1994). The translocon is known to insert proteins containing a TMD into the ER-membrane as well as to import proteins for the secretory pathway into the ER-lumen, but can also export misfolded proteins from the ER into the cytoplasm (Osborne et al., 2005; Tsai et al., 2002). For the export, the translocon is part of the endoplasmic reticulum-associated degradation (ERAD) pathway, in which misfolded proteins are exported from the ER, marked with ubiquitin-chains and targeted for degradation to the proteasome (Schnell and Hebert, 2003; Romisch, 2005). Sec61β was shown to associate with the epidermal growth factor (EGF) receptor and retro-translocate it from the ER to the cytoplasm (Liao and Carpenter, 2007). Later it was found that the cytoplasmic, but membrane associated EGF receptor is imported into the nucleus by importin β. Surprisingly, Sec61β was also identified to locate to the INM, where it associates with the EGF receptor to release it from the INM into the nucleus (Wang et al., 2010). This gave a first hint for a potential INM function of Sec61β.

Sec22b, also called vesicle-trafficking protein SEC22B (figure 28B), has a single TMD at its very C-terminus. The N-terminus of the protein faces the cytoplasm and contains a longin domain followed by a v-SNARE coiled-coil homology domain (Mancias and Goldberg, 2007) (UniProt ID O75396). Sec22b is involved in the vesicle transport between the ER-membrane and the Golgi apparatus. The vesicular transport mechanism can be divided into three different steps. First, the vesicle forms at a donor compartment to pack the cargo proteins. This step is mediated by coat proteins, e.g. COPI and COPII, together with GTPases. Second, the vesicle has to be transported from its place of origin to its destination by movement via the cytoskeleton. This step is mediated by motor proteins. Third, the vesicle has to fuse to the membrane meant for destination mediated by the SNARE (Soluble N-ethylmaleimide-sensitive-factor Attachment Protein Receptor) complex. For this complex assembly, one v-SNARE protein pairs with three t-SNARE proteins. Proteins of v-SNARE come from the vesicular membrane, while t-SNARE stands for proteins of the SNARE complex present in the target membrane. The membrane and the vesicle are fused by the formation of these four SNARE proteins. So far, 38 members of the SNARE protein family have been identified. This protein variability controls the fusion of vesicles with the membrane of destination in a variety of membranes (Wang et al., 2017). Sec22b shuttles integrated into the vesicle membrane and is involved in fusion events at the Golgi and the ER-membrane in anterograde and retrograde transport (Liu and Barlowe, 2002; Spang and Schekman, 1998).

Ube2j1 and **Ube2j2** (UniProt IDs Q9Y385 and Q8N2K1, figure 28C and D), also called Ubiquitin-conjugating enzyme E2 J1 and J2, respectively, are TA proteins of the ER-membrane (figure 28C and D). Both proteins are involved in the endoplasmic reticulum-associated protein degradation (ERAD) pathway. Proteins, which are not correctly folded, are marked by ubiquitin for degradation via the proteasome. For the transfer of ubiquitin to these proteins, an enzymatic cascade is necessary. A ubiquitin-activating enzyme E1 activates ubiquitin in an ATP-dependent manner, then the activated ubiquitin is transferred from E1 to the ubiquitin-conjugating enzyme E2 and finally, ubiquitin is

transferred onto the substrate, which is bound by the ubiquitin ligase E3. The E3 ligase binds to E2 and the substrate protein at the same time and mediates the ubiquitin transfer onto the target protein (Glickman and Ciechanover, 2002; Pickart, 2004). Ube2j1 and Ube2j2 are ubiquitin-conjugating E2 enzymes, which are located in the ER-membrane. It has been shown that Ube2j1, but not Ube2j2 is involved in the cell recovery from ER-stress (Lester et al., 2000; Elangovan et al., 2017). The yeast ortholog of Ube2j1 is Ubc6.

LMAN2, also called vesicular integral-membrane protein VIP36, has a C-terminal TMD with a short tail facing the cytoplasm. It has an N-terminal signal peptide, which is cleaved after ER-membrane insertion (UniProt ID Q12907, figure 28E). LMAN2 localizes to the ER-membrane and the Golgi apparatus (Fullekrug et al., 1999). This protein is a mannose-binding lectin protein with a specificity for high-mannose-type glycans and is involved in export of glycoproteins from the ER (Vagin et al., 2009). Its yeast ortholog is EMP47.

DDOST (synonym OST48, figure 28F) has a C-terminal short tail in the cytoplasm after its TMD. The protein is inserted in the ER-membrane via a signal peptide, which is located at the N-terminus (UniProt ID P39656). DDOST, also called Dolichyl-diphosphooligosaccharide-protein glycosyltransferase 48 kDa subunit, is an oligosaccharyltransferase (Yamagata et al., 1997). Most proteins, which are targeted by the secretory pathway, are modified by N-linked glycosylation, the addition of oligosaccharides to asparagine residues. This N-linked glycosylation marks proteins for the secretory pathway. The glycosylation reaction is catalyzed by an oligosaccharyltransferase, a protein complex of several subunits. The proteins STT3A or STT3B are the active catalytic subunit of the OST complex, while several non-catalytic proteins contribute to the complex, one of them being DDOST (Roboti and High, 2012; Aebi et al., 2010). The yeast ortholog of DDOST is WBP1.

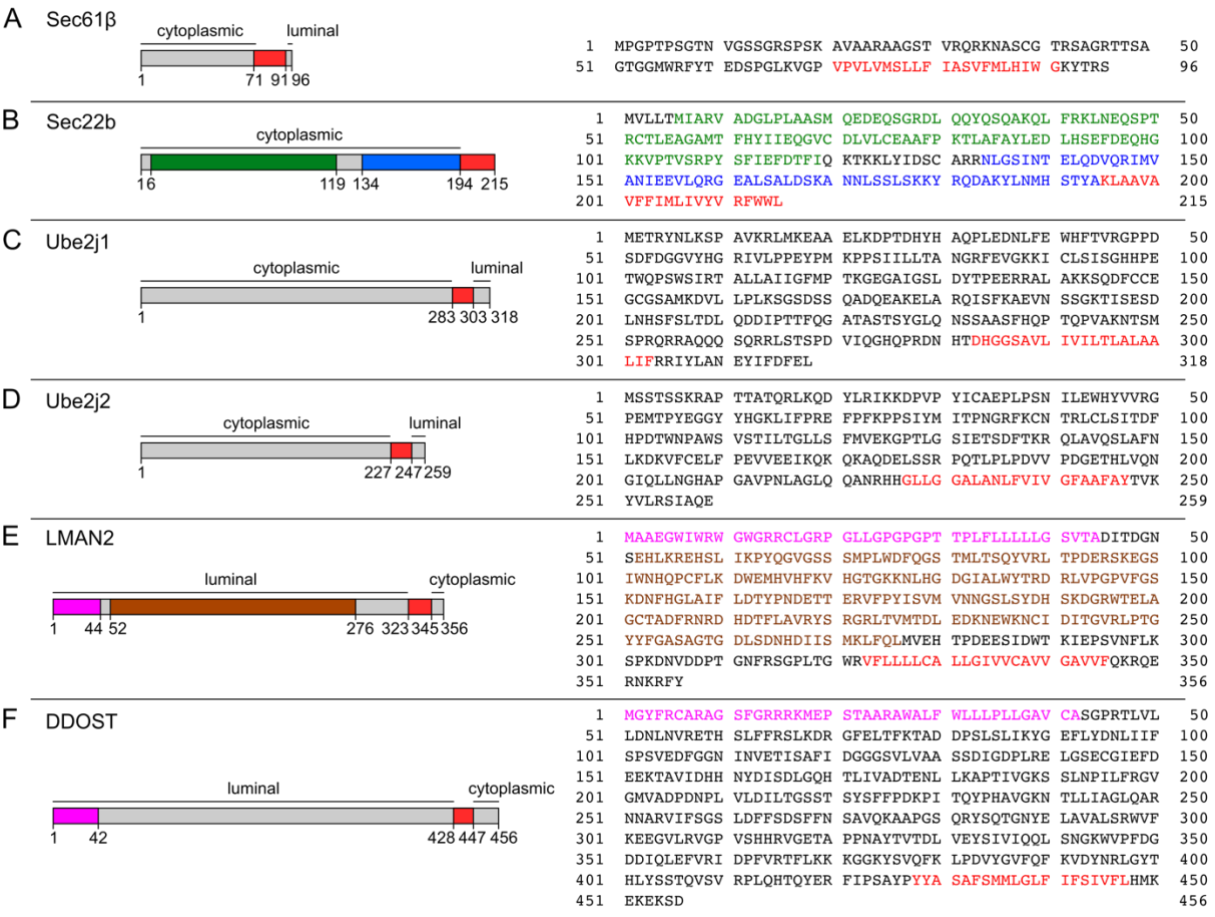

Figure 28: Schemes and amino acid sequences of the proteins tested for INM localization using the rapamycin-induced dimerization assay.

Sec61β, Sec22b, Ube2j1 and Ube2j2 have a C-terminus facing the lumen of the ER, while the C-terminus of LMAN2 and DDOST is located in the cytoplasm. The transmembrane domain (TMD) is indicated in red. (A) For Sec61β (protein transport protein Sec61 subunit beta), no domains or regions are identified except for the TMD. (B) The vesicle-trafficking protein SEC22B (Sec22b) has a longin domain (green) followed by a v-SNARE coiled-coil homology domain (blue) before the TMD. For Ube2j1 (C), ubiquitin-conjugating enzyme E2 J1 and Ube2j2 (D), ubiquitin-conjugating enzyme E2 J2, a single TMD is identified. (E) In addition to the signal peptide (purple) and the TMD, LMAN2 (vesicular integral-membrane protein VIP36) has a L-type lectin-like domain (brown). (F) Dolichyl-diphosphooligosaccharide-protein glycosyltransferase 48 kDa subunit (DDOST) has a signal peptide at its N-terminus.

3.4.2 Rapamycin-induced dimerization assay of potential inner nuclear membrane candidates

In order to examine the INM localization of Sec61β, Sec22b, Ube2j1, Ube2j2, LMAN2 and DDOST, mRNA was isolated from HeLa cells and reverse transcribed into cDNA. Specific cDNAs were cloned into an mCherry- and FRB-containing vector. As the N-terminus of Sec61β, Sec22b, Ube2j1 and Ube2j2 is located in the cytoplasm, mCherry-FRB was added to the N-terminus, resulting in mCherry-FRB-Sec61β, mCherry-FRB-Sec22b, mCherry-FRB-Ube2j1 and mCherry-FRB-Ube2j2. For LMNA2 and DDOST, the cytoplasmic C-terminus was tagged with FRB-mCherry: LMAN2-FRB-mCherry and DDOST-FRB-mCherry. In the rapamycin-induced dimerization assay, the protein of interest was overexpressed together with the nuclear reporter $EGFP_2$-GST-M9-FKBP12 in HeLa cells and analyzed by fluorescence microscopy.

For **mCherry-FRB-Sec61β**, an ER- and NE-localization of the overexpressed protein could be observed (figure 29A). Already after one minute of rapamycin incubation, more than 70% of the overexpressing cells showed a reporter recruitment to the NE. After 2 minutes, a plateau in rapamycin-responding cells of approximately 97% was reached (figure 29B). This strong response of the overexpressing cells to rapamycin-treatment could confirm the already published INM localization of Sec61β. This also confirms the result of Smoyer et al. (2016) for the yeast ortholog SBH2, which was identified as an INM protein.

The protein **mCherry-FRB-Sec22b** localized to the ER and the NE, but for some cells, a punctuated pattern at the ER could be observed (figure 29C). Upon rapamycin-addition, the reporter was recruited to the NE. By increasing the time of rapamycin-treatment, an increasing number of cells responding to rapamycin was observed until a plateau of approximately 70-80% was reached after 3 minutes of incubation (figure 29D). This experiment confirms Sec22b as a protein of the INM.

mCherry-FRB-Ube2j1 localized to the ER and the NE. Upon the addition of rapamycin, the reporter was targeted to the NE, indicating an INM localization of Ube2j1 (figure 29E). The maximum of rapamycin-responding cells was approximately 70% and was reached after 5 minutes of rapamycin treatment (figure 29F). Ube2j1 seems to be able to reach the INM, but not in every cell examined in the rapamycin-induced dimerization assay.

Next, the INM localization of **mCherry-FRB-Ube2j2** was tested in the rapamycin-induced dimerization assay. mCherry-FRB-Ube2j2 localized at the ER and the NE. Upon rapamycin-addition, the nuclear reporter was targeted to the NE, indicating the INM localization of mCherry-FRB-Ube2j2 (figure 29G). A plateau of 60% rapamycin-responding cells was reached after 4 minutes of rapamycin treatment (figure 29H). This shows that Ube2j2 could localize to the INM, however, this was not observed in every cell analyzed in the rapamycin-induced dimerization assay.

The signal of overexpressed **LMAN2-FRB-mCherry** indicated a localization of this protein to the ER. In addition, a rim at the NE was observed, pointing to a potential ONM and INM localization of LMAN2 (figure 29I). Indeed, the INM localization of LMAN2-FRB-mCherry could be confirmed by the recruitment of $EGFP_2$-GST-M9-FKBP12 from the nucleoplasm to the NE upon rapamycin treatment.

The number of cells responding to rapamycin slowly increased with incubation time (figure 29J). Approximately 70% of the cells expressing both constructs showed a reporter recruitment to the NE after 6 minutes of rapamycin treatment. This result shows that LMAN2 can locate to the INM, but this did not happen in all cells.

The last tested potential INM candidate was DDOST. The overexpressed protein **DDOST-FRB-mCherry** was located at the ER-membrane and the NE. Upon rapamycin-treatment, the reporter $EGFP_2$-GST-M9-FKBP12 was targeted to the NE, showing an INM localization of DDOST-FRB-mCherry (figure 29K). By increasing the incubation time of rapamycin treatment, more and more cells showed this reporter recruitment to the NE until a plateau of approximately 98% rapamycin-responding cells was reached after 3 minutes of treatment (figure 29L). This experiment identifies DDOST as a protein of the INM.

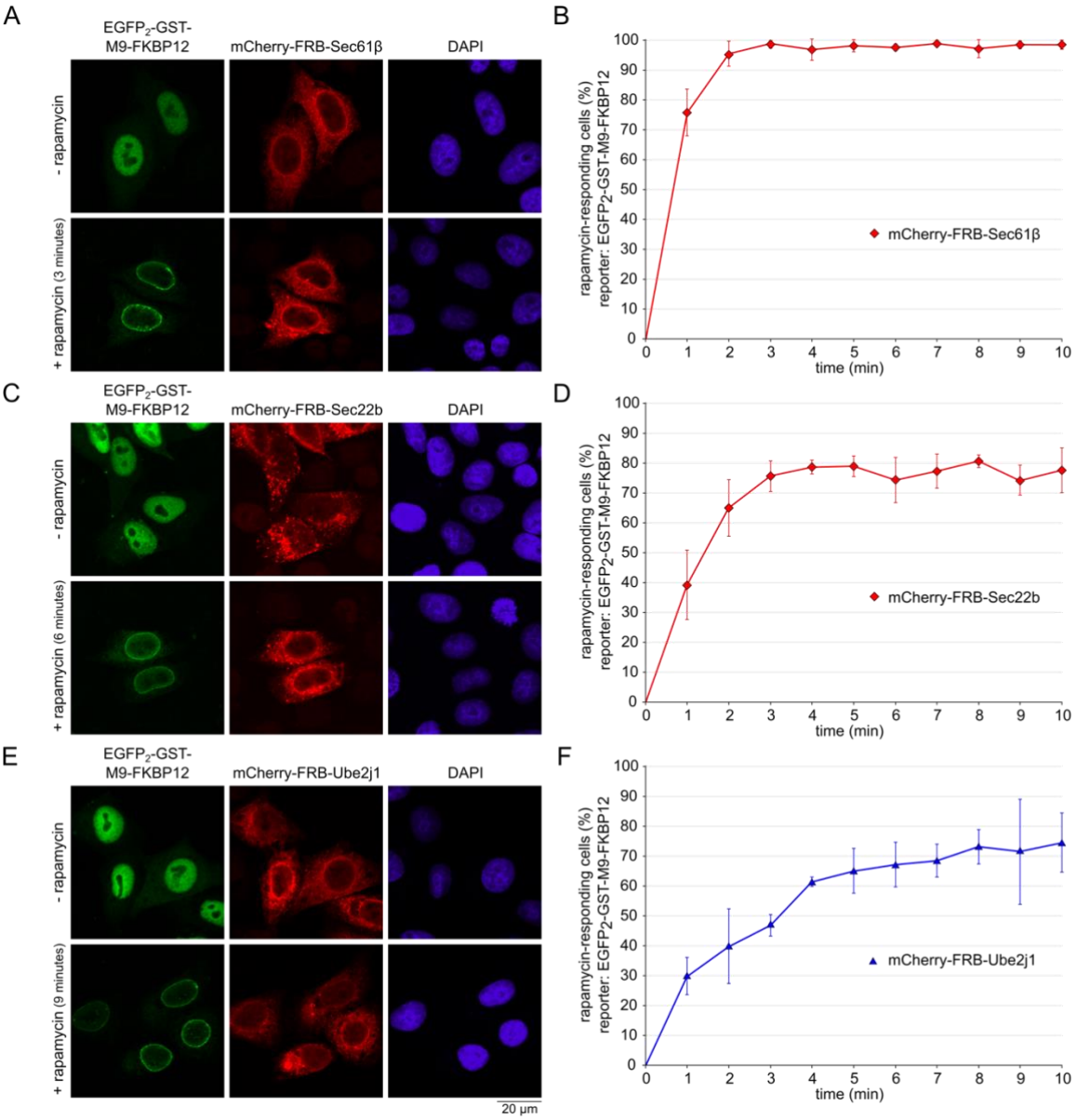

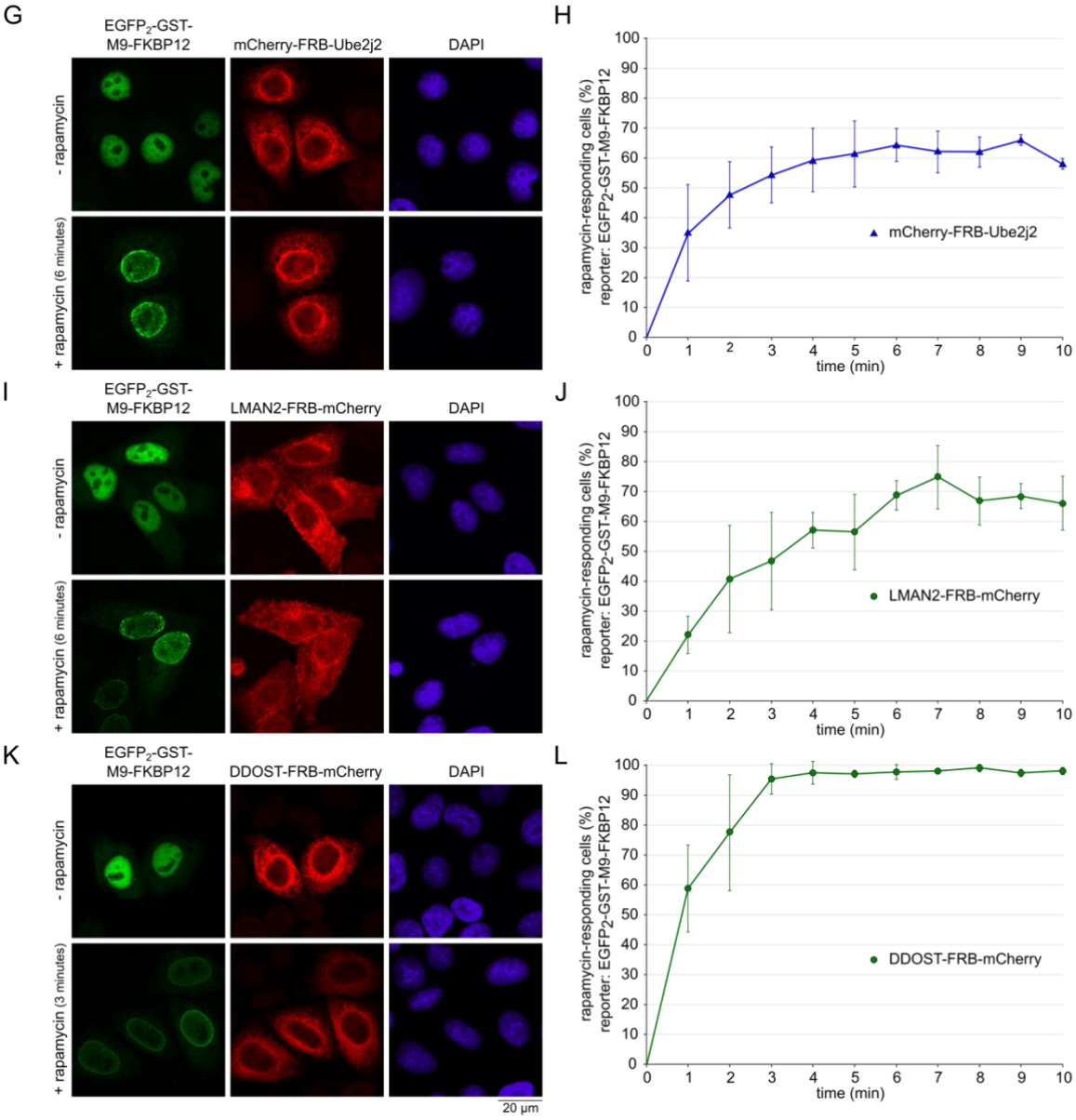

Figure 29: Sec61β, Sec22b, Ube2j1, Ube2j2, LMAN2 and DDOST are located in the INM.
For the rapamycin-induced dimerization assay, HeLa cells were transfected with the reporter EGFP$_2$-GST-M9-FKBP12 and the mCherry- and FRB-tagged protein of interest. After 48 hours, the cells were treated with rapamycin for 1-10 minutes, fixed and directly analyzed by confocal microscopy. DAPI marked the nucleic acids in fluorescence microscopy. (A) Representative microscopic image of mCherry-FRB-Sec61β. (B) Quantification of (A) shows mean and standard deviation for each incubation time with rapamycin of three individual experiments counting 100 cells each. (C) Representative microscopic image of mCherry-FRB-Sec22b. (D) As (B) for mCherry-FRB-Sec22b. (E) Representative microscopic image of mCherry-FRB-Ube2j1. (F) As (B) for mCherry-FRB-Ube2j1. (G) Representative microscopic image of mCherry-FRB-Ube2j2. (H) As (B) for mCherry-FRB-Ube2j2. (I) Representative microscopic image of LMAN2-FRB-mCherry. (J) As (B) for LMAN2-FRB-mCherry. (K) Representative microscopic image of DDOST-FRB-mCherry. (L) As (B) for DDOST-FRB-mCherry. For values see table S 11.

For the six tested potential INM proteins Sec61β, Sec22b, Ube2j1, Ube2j2, LMAN2 and DDOST, a localization to the INM could be shown by the rapamycin-induced dimerization assays.

3.4.3 Size dependency of inner nuclear membrane targeting of candidates on the extraluminal domain

For further examination of INM targeting, Sec61β, Ube2j1 and DDOST became the focus of interest. These three proteins in their mCherry- and FRB-tagged form localized to the ER and NE without punctuated pattern. By the increase of the size of their cytoplasmic domains, the INM targeting of these

proteins was analyzed, as it was performed for LRRC59 (see section 3.2.4). New constructs with tags of MBP and GST, respectively, in addition to the mCherry- and the FRB-tags for the three proteins were cloned.

For the endogenous **Sec61β** protein, the cytoplasmic domain has a molecular mass of 7 kDa. This domain was already increased in the rapamycin-induced dimerization assay for validation of INM localization to 44.9 kDa for mCherry-FRB-Sec61β. To further increase the cytoplasmic domain size, a GST- or an MBP-tag was inserted into the mCherry-FRB-Sec61β construct between FRB and Sec61β. The cytoplasmic domain of the new protein mCherry-FRB-MBP-Sec61β is 86.6 kDa from the starter methionine of mCherry until the last amino acid before the TMD. By the insertion of a GST-tag, the cytoplasmic domain increased to 70.6 kDa in mCherry-FRB-GST-Sec61β. GST is known to assemble into dimers (Bell et al., 2013), so that mCherry-FRB-GST-Sec61β should have a cytoplasmic domain of 141.2 kDa (figure 30A).

Figure 30B gives an overview of the sizes of the cytoplasmic domains of the new constructs of **Ube2j1** for the rapamycin-induced dimerization assay. The addition of mCherry-FRB to Ube2j1 increased the cytoplasmic domain by 38 kDa. mCherry-FRB-MBP-Ube2J1 further increased the extraluminal region to 110.8 kDa, while the dimerizing protein mCherry-FRB-GST-Ube2j1 has a cytoplasmic domain of 189.6 kDa.

For endogenous **DDOST**, its very short C-terminus of 1.1 kDa is facing the cytoplasm. This was increased by the addition of FRB-mCherry to 39.6 kDa. The additional MBP-tag increased the cytoplasmic facing C-terminus by 80.3 kDa compared to endogenous DDOST. In DDOST-GST-FRB-mCherry, the size of the extraluminal region in the dimerized form was 130.8 kDa (figure 30C).

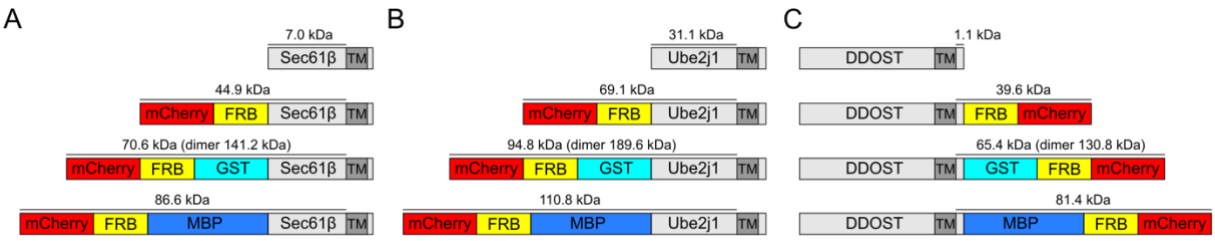

Figure 30: Overview of constructs of Sec61β, Ube2j1 and DDOST with increasing size of the extraluminal domains by addition of different tags.
Scheme of the size of the cytoplasmic domain of Sec61β (A) and Ube2j1 (B), for which the tags mCherry, FRB, GST and MBP are added to the N-terminus of the protein. For DDOST (C), the tags were added to the C-terminus, facing the cytoplasm and/or nucleus.

For the different Sec61β-proteins, a localization to the ER and the NE could be observed without any obvious differences (figure 31A-C). For the rapamycin-induced dimerization assay using the reporter $EGFP_2$-GST-M9-FKBP12 (figure 29A and B) described above, 97% of the cells expressing mCherry-FRB-Sec61β showed a reporter response upon rapamycin-treatment for 10 minutes. This was also true for the same Sec61β-construct tested in the experiment with the reporter $EGFP_2$-MBP-M9-FKBP12 (figure 31D). With the increase of the size of the cytoplasmic domain to 86.6 kDa, 55.7% ± 7.2 of the cells responded with a reporter recruitment to the NE due to rapamycin treatment. For mCherry-FRB-GST-Sec61β (141.2 kDa for cytoplasmic domain), 44.7% ± 11.4 showed a reporter response upon the addition of rapamycin. This indicates that by increase of the cytoplasmic domain of Sec61β by 96.3 kDa the number of rapamycin-responding cells was reduced by 50%.

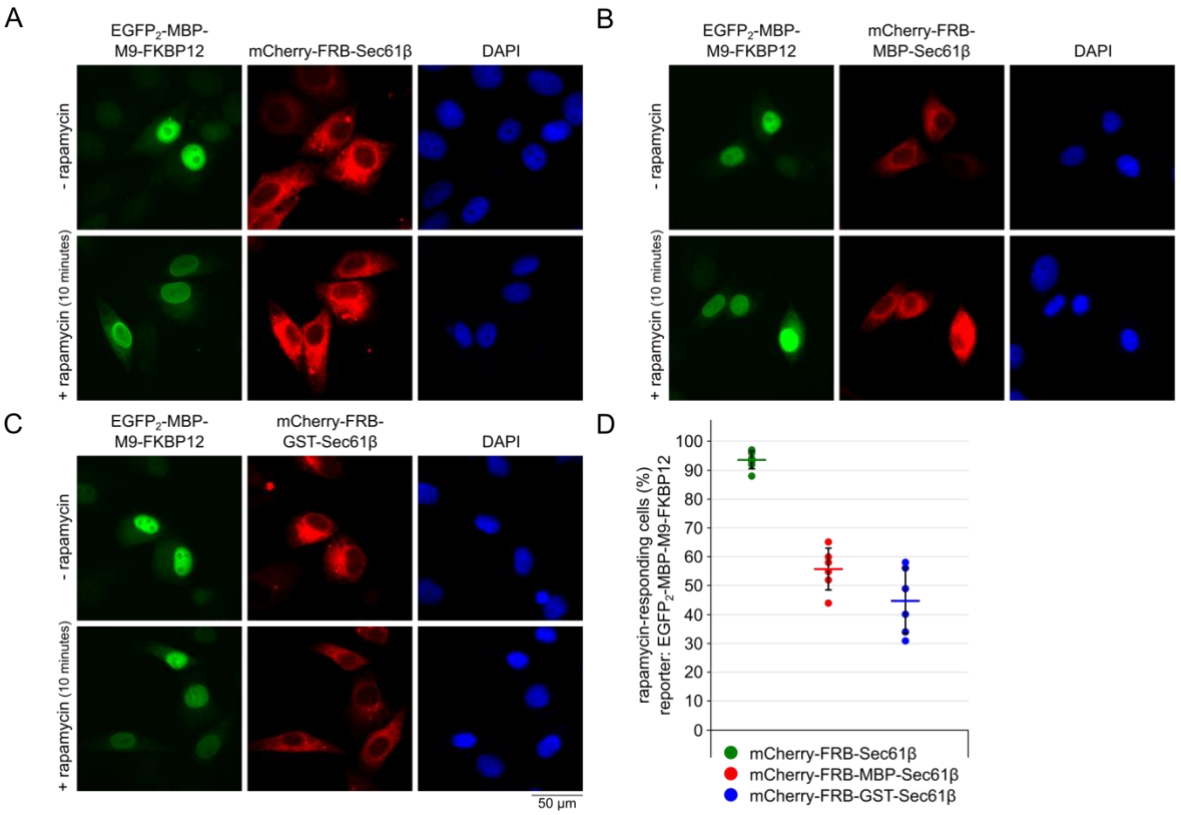

Figure 31: Size-dependency of INM targeting of Sec61β on the extraluminal region.
(A) HeLa cells were transfected with plasmids coding for mCherry-FRB-Sec61β and $EGFP_2$-MBP-M9-FKBP12 for 48 hours followed by an incubation with rapamycin for 10 minutes, fixation and direct analysis using the Axioskop2 mot plus. DAPI marked the nucleic acids in fluorescence microscopy. (B) As (A) with mCherry-FRB-MBP-Sec61β and $EGFP_2$-MBP-M9-FKBP12. (C) As (A) with mCherry-FRB-GST-Sec61β and $EGFP_2$-MBP-M9-FKBP12. (D) Quantification (A-C) shows the mean and the standard deviation of three individual experiments with two replicates each, counting 600 cells of every condition in total.

The overexpression of the three differently tagged Ube2j1-proteins resulted in a similar distribution over the cell. The proteins localized to the ER and the NE (figure 32A-C). After 10 minutes of rapamycin-treatment, 68% ± 5.7 of the cells showed a recruitment of the reporter $EGFP_2$-MBP-M9-FKBP12 to the NE. This result was comparable to the rapamycin-induced dimerization assay using the reporter $EGFP_2$-GST-M9-FKBP12 (74.6% ± 9.9 responding cells, figure 29E and F). When the protein mCherry-FRB-MBP-Ube2j1 was analyzed in the rapamycin-induced dimerization assay, the number of rapamycin-responding cells massively decreased: 23% ± 4.7 showed a reporter targeting to the NE when the cytoplasmic size was increased from 44.9 kDa (mCherry-FRB-Ube2j1) to 86.6 kDa (mCherry-FRB-MBP-Ube2j1). This effect was even more dramatic for cells overexpressing the GST-tagged protein: only 3.3% ± 0.5 of the cells responded to the rapamycin treatment (figure 32D). These results demonstrate that the increase of the size of the cytoplasmic domain of Ube2j1 had an inhibiting effect on its INM targeting. The increase of the size of the cytoplasmic domain by 120.5 kDa decreased the number of rapamycin-responding cells by 65%.

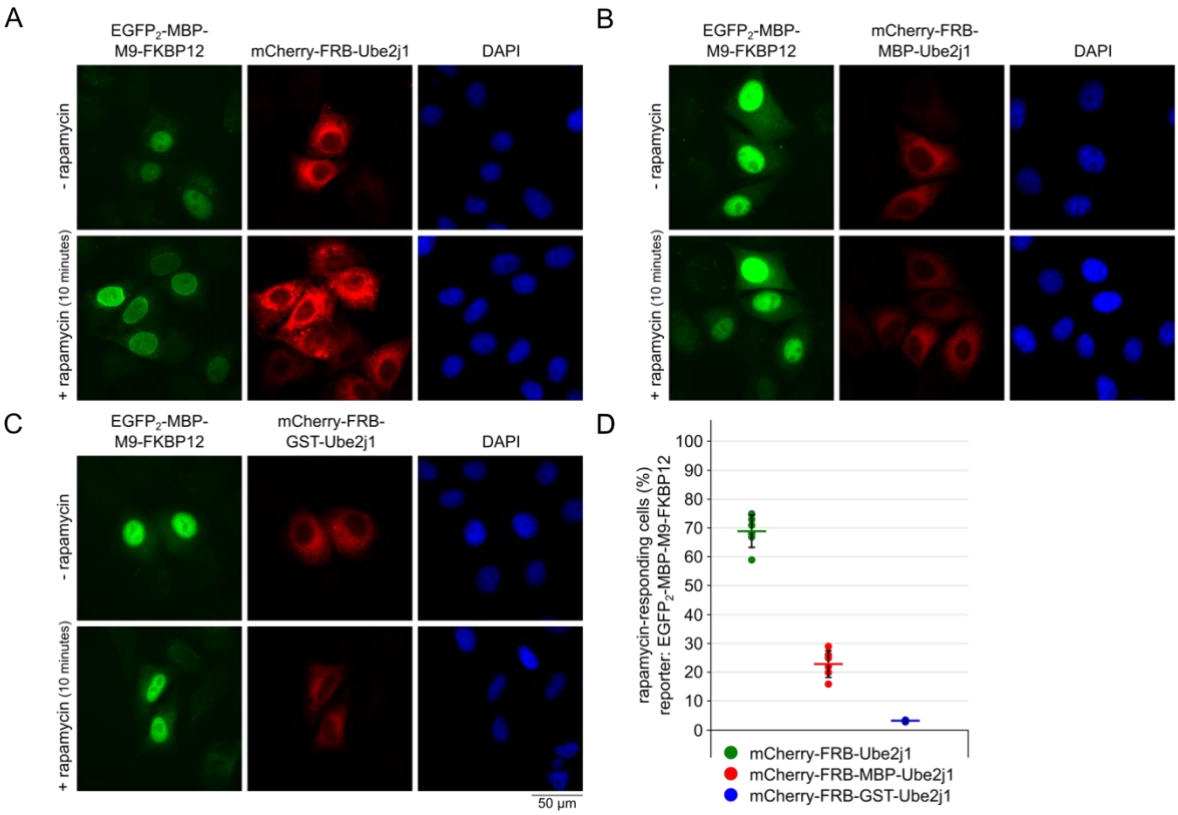

Figure 32: Size-dependency of INM targeting of Ube2j1 on the extraluminal region.
(A) Rapamycin-induced dimerization assay for HeLa cells overexpressing mCherry-FRB-Ube2j1 and $EGFP_2$-MBP-M9-FKBP12 for 48 hours. After 10 minutes of rapamycin addition, cells were fixed and directly analyzed using the Axioskop2 mot plus. DAPI marked the nucleic acids in fluorescence microscopy. (B) As (A) with HeLa cells expressing mCherry-FRB-MBP-Ube2j1 and $EGFP_2$-MBP-M9-FKBP12. (C) As (A) with proteins mCherry-FRB-GST-Ube2j1 and $EGFP_2$-MBP-M9-FKBP12. (D) Quantification of (A-C) shows the mean and standard deviation of three independent experiments with two replicates each, counting 600 cells of every condition in total.

The differently tagged proteins of DDOST located to the ER and the NE in a similar way (figure 33A-C). The testing of DDOST-FRB-mCherry in the rapamycin-induced dimerization assay for 10 minutes of treatment showed comparable results in the number of rapamycin-responding cells for the reporters $EGFP_2$-GST-M9-FKBP12 (figure 29K and L; 98% ± 1) and $EGFP_2$-MBP-M9-FKBP12 (figure 33D; 96.8% ± 1.5). Interestingly, when the domain facing the cytoplasm was increased from 39.6 kDa (DDOST-FRB-mCherry) to 81.4 kDa by an additional MBP-tag, the number of rapamycin-responding cells was reduced to 23.7% ± 5.9. For DDOST-GST-FRB-mCherry, 15.8% ± 6.9 of the cells showed a reporter recruitment to the NE. These results show that the increase of the size of the cytoplasmic domain from 39.6 kDa (DDOST-FRB-mCherry) to 81.4 kDa (DDOST-MBP-FRB-mCherry) reduced the number of rapamycin-responding cells by approximately 73%.

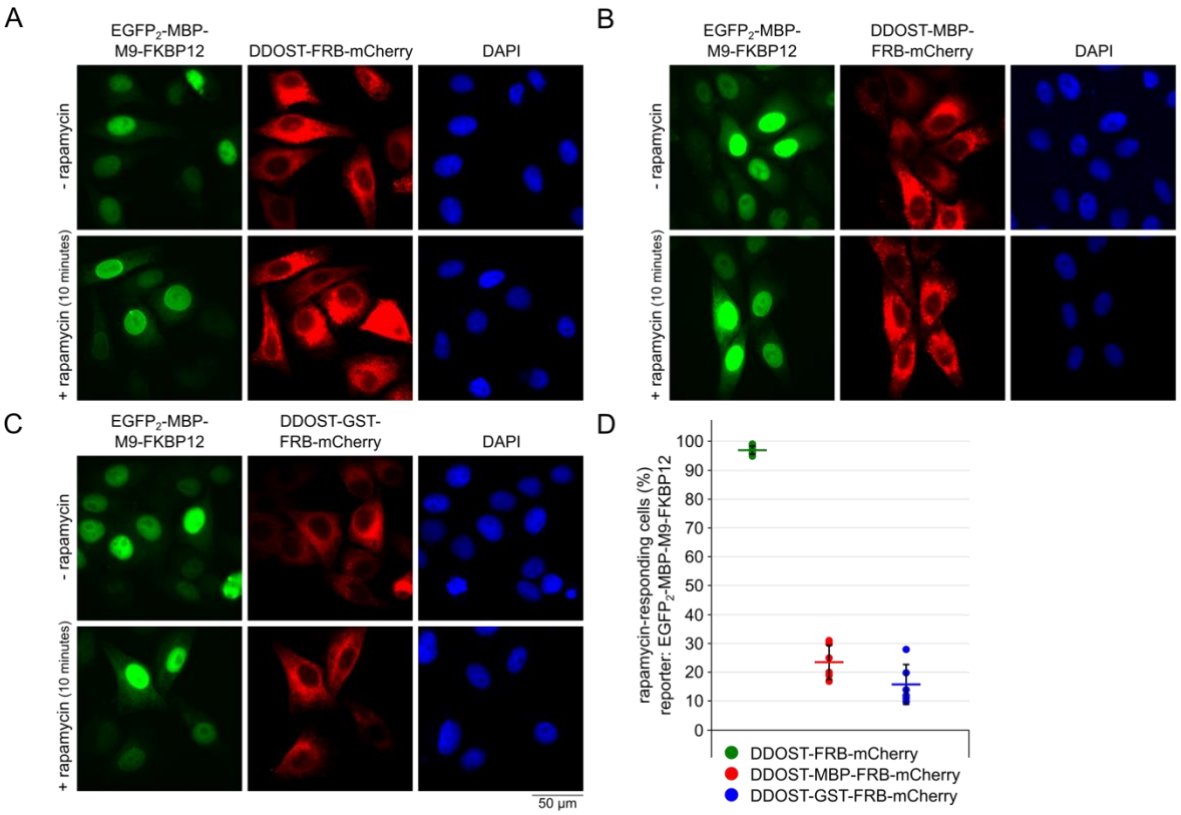

Figure 33: Size-dependency of INM targeting of DDOST on the extraluminal region.
(A) HeLa cells overexpressing DDOST-FRB-mCherry and $EGFP_2$-MBP-M9-FKBP12 for 48 hours prior to rapamycin treatment for 10 minutes, fixation and direct analysis using the Axioskop2 mot plus. DAPI marked the nucleic acids in fluorescence microscopy. (B) As (A) with plasmids coding for DDOST-MBP-FRB-mCherry and $EGFP_2$-MBP-M9-FKBP12. (C) As (A) with plasmids coding for DDOST-GST-FRB-mCherry and $EGFP_2$-MBP-M9-FKBP12. (D) Quantification shows the mean and standard deviation of rapamycin-responding cells for differently tagged DDOST-constructs (A-C) for three individual experiments with two replicates each, counting 600 cells of every condition in total.

The diffusion of proteins to the INM is supposed to be size-dependent. The increase of the size of the extraluminal domains of Sec61β, Ube2j1 and DDOST had an inhibitory effect for their INM targeting, pointing to localization to the INM mediated by diffusion.

4 Discussion

The localization of integral membrane proteins at the INM still raises many questions: First, it is not completely clear, why some membrane proteins reach the INM while others are excluded. How are proteins sorted or which protein properties are required for this restricted access? Further, is there an active transport involving transport factors for some membrane proteins? And if so, how can a transport factor pass the central channel of the NPC while it is bound by a protein which is embedded into the membrane? Does this way of trafficking disrupt the structure of the NPC? If membrane proteins reach the INM by passive diffusion, are the peripheral channels the route into the nucleus to pass the NPC? How flexible are peripheral channels or do they act as bottle neck for diffusion? When membrane proteins reach the INM, are all of these proteins retained by binding events or do some proteins diffuse back into the ER-membrane if they are not retained in the INM? Do all proteins which reach the INM fulfill a function in the nucleus? Do the ONM/ER-membrane and the INM share all membrane proteins containing extraluminal regions which are small enough to pass the peripheral channels by diffusion?

As a contribution solving some of these questions, the protein LRRC59 was chosen as a model protein. LRRC59 is a protein containing a single TMD, which makes the investigation less complex than the analysis of a multi-spanning membrane protein containing several TMDs and intermembrane regions. Furthermore, LRRC59 was suggested to reach the INM in an importin β-dependent manner (Zhen et al., 2012), making LRRC59 an interesting model protein to analyze its INM targeting in more detail.

First, the mechanism of membrane insertion of LRRC59 was investigated by *in vitro* microsome integration assays and cell-based experiments. Then, targeting to the INM of the membrane-embedded, overexpressed mCherry-FRB-LRRC59 protein was studied in rapamycin-induced dimerization assays. Additionally, the extraluminal amino acid sequence of LRRC59 was analyzed with respect to a potential NLS, which could be crucial for the nuclear import of the full-length protein. Not much is known about the biological function of LRRC59. Therefore, LRRC59 was examined by the identification of binding and/or proximity partners by RAPIDS experiments.

In addition to LRRC59, seven proteins, Sec61β, Sec22b, Ube2j1, Ube2j2, LMAN2, DDOST and WRB, were investigated with respect to a potential INM localization. Similar to LRRC59, these proteins, which contain one TMD (except of WRB) and are mainly localized to the ER-membrane, were analyzed for localization of a subpopulation to the INM.

4.1 Membrane insertion of LRRC59

Newly synthesized TMD-containing proteins are inserted into the lipid bilayer of the ER-membrane via co- or post-translational integration mechanisms. After insertion and folding, they are targeted to their final destination (Rapoport, 1992; Kutay et al., 1993).

It was shown that LRRC59 contains a single TMD and a 40 amino acid long C-terminus facing the lumen of the ER (Zhen et al., 2012). As the ribosomal tunnel houses around 40 amino acids during translation (Hegde and Keenan, 2011), this tail could be long enough to enable a co-translational insertion mechanism for LRRC59 using the SRP-dependent pathway. Proteins with shorter luminal C-termini had been shown to be targeted to the ER-membrane by a post-translational insertion mechanism. For instance, the TRC pathway substrate emerin contains 11 amino acids (Pfaff et al., 2016), Sec61β five amino acids (Stefanovic and Hegde, 2007; Favaloro et al., 2008) and syntaxin 5 only one amino acid (Rivera-Monroy et al., 2016) at their C-termini following the TMD.

For the analysis of the insertion mechanism for LRRC59, *in vitro* microsome integration assays were performed (Favaloro et al., 2008; Favaloro et al., 2010; Vilardi et al., 2011; Pfaff et al., 2016; Rivera-Monroy et al., 2016). In the presence of the translation inhibitor puromycin, LRRC59 was still able to insert into rough microsomes when the co-translational insertion mechanism was blocked. This result indicates that LRRC59 can be post-translationally inserted and is therefore classified as a TA protein (figure 9). This post-translational insertion was possible even though the C-terminus of LRRC59

was extended by 13 amino acids by the addition of the opsin-tag. However, with this experimental approach, it cannot formally be excluded that LRRC59 is able to use alternatively a co-translational insertion mechanism, if the post-translational route is blocked.

Further, it was demonstrated that the insertion of LRRC59 cannot happen spontaneously but depends on a receptor (figure 10). Consequently, the involvement of the TRC pathway receptors WRB and CAML for insertion of LRRC59 was further investigated, as the TRC pathway is the main route of post-translational membrane insertion for TA proteins (Vilardi et al., 2011; Yamamoto and Sakisaka, 2012; Vilardi et al., 2014; Borgese and Fasana, 2011). In the presence of dominant negative inhibitory fragments of WRB and CAML (Vilardi et al., 2011; Yamamoto and Sakisaka, 2012; Pfaff et al., 2016), the membrane insertion of LRRC59 was not inhibited at all, while emerin, a TRC pathway-dependent TA protein (Pfaff et al., 2016), could not be inserted (figure 11). Further, the depletion of TRC40 itself did not affect the membrane insertion of LRRC59 in contrast to emerin (figure 12).

When the ATPase-deficient mutant TRC40 D74E (Coy-Vergara et al., 2019), the equivalent of yeast Get3 D57E (Powis et al., 2013), was overexpressed (figure 13), endogenous emerin showed a weaker NE-localization but a diffuse staining in the cytoplasm compared to TRC40 WT expressing or non-transfected cells which both showed a strong NE staining of emerin. This result suggests that emerin was bound by TRC40 D74E but could not be passed on to the receptors WRB and CAML for membrane insertion and further targeting to the NE. Interestingly, Bag6, a component of the pre-targeting complex of the TRC pathway, was not only shown to recruit TRC40 to its substrate, but also to be able to recruit the ubiquitination machinery (Hessa et al., 2011). Proteins which have to be degraded can be marked by polyubiquitin chains resulting in the degradation of the protein by the proteasome (Glickman and Ciechanover, 2002). Therefore, it is possible that emerin bound by TRC40 D74E is degraded by the proteasome which could be tested by the determination and comparison of the signal of emerin in cells overexpressing TRC40 WT or TRC40 D74E.

In contrast to emerin, which needs a functional TRC40 protein for membrane insertion, the localization of endogenous LRRC59 was comparable between TRC40 WT and TRC40 D74E overexpressing and non-transfected cells. This indicates that LRRC59 is either not a substrate of TRC40 at all or that LRRC59 can insert into the ER-membrane by an alternative mechanism if the TRC pathway is compromised.

Conclusion and perspectives

In summary, LRRC59 was demonstrated to be a TA protein, which can be inserted post-translationally into rough microsomes. A dependency for membrane insertion of LRRC59 on the TRC pathway, the best described route of post-translational membrane insertion of TA proteins, could not be shown. The open question is, which alternative pathway could mediate LRRC59 insertion, as an unassisted mechanism was excluded.

Alternatively, LRRC59 could be a substrate of the chaperones Hsp40 and Hsc70, which have been shown to directly interact with the TMD of TA proteins (Abell et al., 2007; Rabu et al., 2008). This possibility could be tested by microsome integration assays using Hsp40 and Hsc70 immunodepleted rabbit reticulocyte lysate similar to the performed TRC40 depletion experiment.

The SND pathway was shown to be an alternative route of TA proteins to the ER-membrane in *S. cerevisiae* if the SRP and GET pathways were not functional (Aviram et al., 2016). So far, only one protein, hSnd2, was identified to be part of the human SND pathway. Interestingly, LRRC59 was co-immunoprecipitated with hSnd2 and identified by mass spectrometry (Hassdenteufel et al., 2017). To further test for an interaction of hSnd2 with LRRC59, chemical crosslinking experiments (Favaloro et al., 2008; Stefanovic and Hegde, 2007) with in rabbit reticulocyte lysate *in vitro* transcribed/translated LRRC59 could be performed.

Another alternative would be membrane targeting in a post-translational manner by SRP, which was shown to bind TA proteins after termination of translation in crosslinking experiments (Abell et al., 2004). As the usage of puromycin in the microsome integration assay only blocks translation itself, it

cannot be excluded that SRP is able to bind and target LRRC59 for membrane insertion after translation termination. Interestingly, RAPIDS experiments identified the SRP receptor subunit alpha and beta (SRPRB, SRPR, figure 26, table 26) to be in close proximity to mCherry-FRB-LRRC59. Ideally, SRP could be blocked by a specific inhibitor as for instance eeyarestatin I (Van Puyenbroeck and Vermeire, 2018). This drug blocks specifically the SRP-dependent pathway by inhibition of the transfer of the signal peptide from SRP to the Sec61 translocon (Cross et al., 2009; Van Puyenbroeck and Vermeire, 2018). However, in this work the efficiency of the drug could not be confirmed with several control proteins (data not shown), even though they were shown or predicted to be eeyarestatin I sensitive (confirmed: preprolactin, P2X2 (Cross et al., 2009); suggested: SUN1 (Laba et al., 2014)).

The experiments performed in this thesis could show that LRRC59 can be inserted post-translationally if the co-translational mechanism is blocked. However, the possibility that LRRC59 is able to insert co-translationally, when this route is not blocked, cannot be excluded by the experimental approach. LRRC59 could be inserted by several mechanism, shifting to an alternative route if one pathway is blocked. To finally answer which route(s) could be used by LRRC59, blocking of several pathways at the same time would be necessary until a total inhibition of membrane insertion in the microsome integration assays is observed. Additionally, chemical crosslinking experiments with the *in vitro* transcribed/translated LRRC59 would be possible (Favaloro et al., 2008; Stefanovic and Hegde, 2007). The performance of siRNA mediated knockdowns of SRP, TRC40 and hSnd2 alone or in combination coupled with the analysis of subcellular localization of endogenous LRRC59 could also be conceivable experiments if compatible with cell survival. In general, further studies are necessary to determine the insertion mechanism of LRRC59 into the ER-membrane.

4.2 Targeting of LRRC59 to the inner nuclear membrane

4.2.1 The rapamycin-induced dimerization assay as a tool for examination of inner nuclear membrane localization

The INM localization of mCherry-FRB-LRRC59 was demonstrated by the rapamycin-induced dimerization assay. In this approach, the presence of an integral membrane protein in the INM is indicated by the recruitment of a soluble nuclear reporter to the NE due to the dimerization of the FKBP12-tagged reporter with the FRB-tagged membrane protein of interest upon rapamycin treatment. As this complex formation was shown to be very stable (Hosoi et al., 1999), it can be excluded that the complex disassembles in the presence of rapamycin. Therefore, mCherry-FRB-LRRC59, which reached the INM, got trapped in the nucleus upon dimerization with rapamycin/$EGFP_2$-GST/MBP-M9-FKBP12. This was indicated by the reporter, which remained in the nucleus and was not distributed to the cytoplasm.

The dimerization of FRB and FKBP12 by rapamycin happens via two hydrophobic pockets (Choi et al., 1996), suggesting a 1:1:1 ratio of dimerization on molecular level. With increasing rapamycin incubation time, the number of cells responding to rapamycin, as indicated by reporter recruitment to the NE, increased for mCherry-FRB-(MBP)-LRRC59. Furthermore, it could be observed that high expression levels of mCherry-FRB-LRRC59 lead to complete reporter recruitment to the NE in less rapamycin incubation time than in cells overexpressing the protein at moderate or low levels. Also, the ratio of overexpression between reporter and protein of interest is important for the reporter recruitment to the NE: when the reporter is highly overexpressed, only a proportion of the reporter could be targeted to the NE. For a complete recruitment of a highly expressed reporter, more plasmid DNA coding for mCherry-FRB-LRRC59 has to be used for transfection (data not shown). The ratio between the concentrations of plasmid DNA coding for reporter and protein of interest is crucial and had to be adjusted for all tested membrane proteins and reporters. This suggests that a targeting process of mCherry-FRB-(MBP)-LRRC59 from the ER-membrane/ONM to the INM can happen during the treatment of the cells with rapamycin. However, the NE recruitment kinetic of the reporter is only an indicator for the amount of integral membrane protein which reaches the INM. The rapamycin-induced

dimerization assay does not reflect the kinetic of movement of the membrane protein of interest to the INM. For kinetic studies of LRRC59 itself, FLIP (Shimi et al., 2004) or FRAP (Zuleger et al., 2011; Wu et al., 2002) experiments could be performed. Furthermore, the kinetic of INM targeting of LRRC59 could be examined by the performance of an established FRAP assay. In this experiment, the extraluminal domain of the membrane protein of interest is tagged with several RFP-tags followed by a tobacco etch virus (TEV) protease site, while the luminal region of the membrane protein is fused to a GFP-tag. Before cleavage, the membrane protein of interest localizes to the ER-membrane as the large extraluminal domain inhibits its diffusion to the INM. Upon the TEV-induced cleavage of the RFP-tags, the membrane protein reaches the INM, which can be observed by the movement of the GFP-tag from the ER to the NE. To analyze the mobility of the membrane protein in the ER before cleavage and at the NE after cleavage of the RFP-tags, FRAP can be performed (Ungricht et al., 2015). With this approach, the kinetic of INM targeting of LRRC59 could be directly observed in contrast to the reporter kinetic of the rapamycin-induced dimerization assay, which indicates the amounts of mCherry-FRB-(MBP)-LRRC59 reaching the INM.

Alternatively, Boni and colleagues used a reporter protein containing a self-cleavage retention system to examine the NE targeting of the N-terminus and the first TMD of LBR in living cells. At the N-terminus of LBR, a NS3 protease, a CMPK domain and a NS3 cleavage site was placed. LBR was tagged with GFP at the C-terminus after the TMD to observe the movement of the protein. The protease cleavage activity is inhibited by the presence of the inhibitor BILN2061 resulting in an ER-membrane localization of the protein. When the inhibitor was washed out, the CMPK domain, which is sufficient to inhibit INM targeting of LBR, was cleaved off and LBR was targeted to the NE. This approach was combined with an RNA interference screen and showed that the depletion of most transport receptors had no effect on the NE targeting of LBR, supporting a diffusion and retention model (Boni et al., 2015). This inducible cleavage could be combined with the rapamycin-induced dimerization assay to examine not only NE targeting and retention but to confirm localization to the INM. For instance, mCherry-FRB-LRRC59 could be N-terminally tagged with the NS3 protease, a GST-tag and the NS3 cleavage site. In the presence of the protease inhibitor, this protein will probably locate to the ER-membrane as it is too big to pass the peripheral channels. Consequently, the nuclear reporter will not be recruited to the NE if the cells are incubated with rapamycin. However, when the protease inhibitor BILN2061 is washed out and rapamycin is added, the INM targeting and retention in the nucleus of the cleaved mCherry-FRB-LRRC59 could be observed in real time by the recruitment of the reporter to the NE. In this thesis, the rapamycin-induced dimerization assay was performed with different incubation times prior to fixation and microscopic analysis of the cells. However, this assay can also be performed in living cells. Therefore, the combination of the inducible cleavage and the rapamycin-induced dimerization assay could be an approach to observe not only NE targeting but confirm INM localization of an integral membrane protein.

The rapamycin-induced dimerization assay could also exclude the possibility that a proportion of mCherry-FRB-LRRC59 was transported into the nucleus as soluble protein and integrated into the INM by a not yet described insertion mechanism within the nucleus. If mCherry-FRB-LRRC59 was transported into the nucleus as a soluble protein, rapamycin/$EGFP_2$-GST/MBP-M9-FKBP12 would probably bind to FRB immediately after the import event, resulting in a complex of two soluble proteins located all over the nucleus. As mCherry-FRB-LRRC59 was at the NE and the reporter was recruited to the NE upon rapamycin treatment, it was assumed that the further analysis observes the INM targeting of a membrane-integrated mCherry-FRB-LRRC59 protein.

Conclusion

The rapamycin-induced dimerization assay is a strong tool to analyze the localization of a membrane-embedded protein to the INM. The presence of the membrane protein of interest is indicated by the reporter recruitment to the NE. The kinetic of reporter recruitment is an indicator for the amounts of FRB-tagged membrane proteins that reach the INM.

4.2.2 Importin β is not required for localization of LRRC59 to the inner nuclear membrane

The *S. cerevisiae* integral membrane proteins Heh1 and Heh2 were suggested to be targeted to the INM dependent on the karyopherin Kap95 (yeast homolog of human importin β), the adaptor protein Kap60 (yeast homolog of human importin α) and the activity of Ran (King et al., 2006). So far, no active transport factor-dependent mechanism could be shown for the nuclear import of a mammalian membrane protein. The human protein LRRC59, however, was suggested to localize to the NE in an importin β-dependent manner (Zhen et al., 2012). In that study, endogenous LRRC59 was shown to lose its NE localization in U2OS cells if the cells were treated with importin β siRNAs (Zhen et al., 2012). However, when this experiment was repeated with the same specific LRRC59-antibody, LRRC59 localized to the ER-membrane and NE similar in control or importin β knockdown cells (figure 17). Experiments with a very high depletion of importin β (14% remaining importin β in Western blot analysis) showed no difference in the localization of endogenous LRRC59 compared to control knockdown cells. As importin β is a crucial component of a functional nucleocytoplasmic transport, which is essential for cell viability (Chook and Suel, 2011), it is likely that in the former study (Zhen et al., 2012) importin β was not depleted in total. Perhaps the loss of the NE localization of LRRC59 was rather caused by off-target effects of the siRNA treatment than by a total importin β knockdown. In the previous study, the importin β knockdown was not controlled by immunofluorescence staining or Western blotting, in contrast to the performed experiments of this thesis. At present, the reason for the conflicting results cannot be easily explained.

To examine the localization of LRRC59 specifically in the INM, the rapamycin-induced dimerization assay was performed in importin β siRNA treated cells. Here, the efficiency of the importin β knockdown was controlled by Western blot with immunodetection and the transfection of the cells with an additional plasmid coding for NES-mTagBFP2-cNLS, which is a substrate of importin β. This protein was shifted from the nucleus to the cytoplasm in importin β siRNA treated cells, indicating that importin β became rate-limiting for nuclear transport. However, in these cells, the recruitment of the reporter to the NE upon rapamycin treatment was not affected in cells overexpressing mCherry-FRB-LRRC59 even in experiments with the highest depletion of importin β (figure 18). The INM localization of mCherry-FRB-LRRC59 was also not affected in the rapamycin-induced dimerization assay when FLAG-Bimax2, a peptide sequence which was shown to block specifically the importin α/importin β pathway (Kosugi et al., 2008), was overexpressed. In contrast, the localization of the importin α/importin β pathway dependent protein NES-mTagBFP2-cNLS was affected (figure 19).

Further, the amino acid sequence of the extraluminal domain of LRRC59 was analyzed for a potential NLS. The soluble protein EGFP-LRRC59 aa1-244 was found exclusively in the nucleus as it was shown before with a similar construct (Zhen et al., 2012). However, this localization was not affected by an importin β knockdown. When the protein was enlarged by an additional EGFP- and a GST-tag, the dimerized protein of 218.6 kDa was found in the cytoplasm (figure 20). The import of a soluble protein containing an NLS would not be limited by this molecular mass, as the NPC is able to transport soluble proteins up to a few megadaltons (Grossman et al., 2012). It is more likely that EGFP-LRRC59 aa1-244 reaches the nucleus by diffusion. The accumulation in the nucleus could be due to unspecific binding to chromatin, which might be mediated by the very basic amino acid sequence of LRRC59 aa1-244 with an isoelectric point of 8.8 (Protein isoelectric point calculator, testing of LRRC59 aa1-244 at isoelectric.org). Importantly, when EGFP-LRRC59 aa1-244 was increased in size by the additional EGFP- and GST-tags, the passive diffusion was inhibited. Consequently, the existence of an NLS within the extraluminal domain of LRRC59 as well as an active nuclear import by importin β or any other transport factor can be excluded for the soluble protein.

Conclusion

In this study, it could be ruled out that LRRC59 is targeted to the INM by an active transport mechanism. The extraluminal domain of LRRC59 does not contain an NLS. In addition, the depletion of

importin β by siRNAs or the inhibition of the importin α/importin β pathway did not affect the localization of LRRC59 to the INM.

4.2.3 LRRC59 reaches the inner nuclear membrane by passive diffusion

For the yeast integral membrane protein Heh2 an active import mechanism into the INM was suggested. However, this finding is still debated as yeast cells lack lamins, which could retain Heh2 in the INM. The observed effect of inhibition in INM targeting of Heh2 by depletion of Kap95 and Kap60 could be the result of blocking the nuclear transport of a soluble binding partner, which retains Heh2 at the INM (Ungricht and Kutay, 2015). The main route to the INM is supposed to be mediated by passive diffusion and retention (Ungricht et al., 2015; Boni et al., 2015; Ungricht and Kutay, 2015). The diffusion to the INM is suggested to occur via peripheral channels of the NPC. These lateral openings are approximately 10 nm in width and restrict the diffusion of membrane proteins with an extraluminal domain of about 60 kDa. As an active transport mechanism depending on importin β could be ruled out for LRRC59, the possibility of free diffusion to the INM was examined. Therefore, the extraluminal domain of LRRC59 was changed for the proteins used in the rapamycin-induced dimerization assay.

The protein mCherry-FRB-LRRC59 has an extraluminal domain of 65.8 kDa and was shown to reach the INM in more than 90% of the cells. When this domain was reduced in size to 40.8 kDa with the exchange of the mCherry- to a HA-tag, the percentage of rapamycin-responding cells was similar over time. However, when the cytoplasmic/nucleoplasmic region was increased to 107.5 kDa with the insertion of an MBP-tag, the percentage of rapamycin responding cells was decreased by approximately 40% for each tested rapamycin incubation time (figure 21, 22). Strikingly, when the extraluminal domain was further increased to 182.8 kDa in the dimerizing protein mCherry-FRB-GST-LRRC59, the INM targeting was almost totally blocked (figure 22). As the size of the extraluminal domain was important for INM localization, these results indicate that LRRC59 reaches the INM by diffusion.

Do these findings fit with the suggested size limit of approximately 60 kDa of diffusing INM proteins (Soullam and Worman, 1993, 1995; Wu et al., 2002; Ohba et al., 2004; Zuleger et al., 2011; Antonin et al., 2011; Katta et al., 2014; Ungricht and Kutay, 2015)? The extraluminal domain of mCherry- and HA-tagged FRB-LRRC59 differ by 25 kDa, but do not show differences in INM targeting of the overexpressed proteins. It was suggested that not only the size of the cytoplasmic/nucleoplasmic domain but also the structure is important for INM targeting of a membrane protein (Soullam and Worman, 1995). Here, a size limit of around 60 kDa for the extraluminal domain is probably not a fixed value, but maybe considered as flexible depending on the geometry of the protein. The 28.8 kDa mCherry β-barrel has a width of approximately 3 nm and a height of about 4 nm (Day and Davidson, 2009). FRB, which is necessary for the experimental approach of the rapamycin-induced dimerization assay, is a helix bundle of four helices with short connections with dimensions of approximately 3 nm x 4.5 nm x 3 nm (Choi et al., 1996). These dimensions are smaller than the suggested width of 10 nm of the peripheral channels. Therefore, it is not surprising that mCherry-FRB-tagged LRRC59 reached the INM even if the considered reference value in INM diffusion of 60 kDa is exceeded by 5.8 kDa.

When the extraluminal domain was further increased by the insertion of an MBP-tag, the INM targeting of LRRC59 was reduced but not blocked. As targeting of proteins occurs during the performance of the rapamycin-induced dimerization assay and rapamycin/reporter-bound FRB-tagged LRRC59 cannot leave the nucleus (discussed in section 4.2.1), more and more mCherry-FRB-MBP-LRRC59 proteins accumulated in the INM over time as indicated by the recruitment of the reporter to the NE. However, the INM targeting of mCherry-FRB-MBP-LRRC59 was delayed compared to INM targeting of mCherry/HA-FRB-tagged LRRC59. It seems that the 42 kDa MBP-tag slowed down the diffusion via the peripheral channels. The MBP-tag has dimensions of approximately 3 nm x 4 nm x 6.5 nm (Spurlino et al., 1991), which should fit into the 10 nm wide peripheral channels. For integral membrane proteins, an inhibition in INM targeting was observed, when the extraluminal domains were increased in size (Boni et al., 2015; Ungricht et al., 2015). It was suggested that the extraluminal domains have to funnel into lateral channels for the diffusion of integral membrane proteins to the INM.

This step seems to be more time-consuming when the cytoplasmic/nucleoplasmic domain is increased in size (Ungricht and Kutay, 2015). Therefore, the MBP-tag slowed down but did not block the INM targeting of LRRC59, as an additional tag had to threat into the lateral channels. However, for defined statements about fast or slow diffusion to the INM, kinetic studies are needed, as the kinetic of the reporter in the rapamycin-induced dimerization assay is only an indicator for the amount of FRB-tagged membrane protein, which reaches the INM.

When the MBP-tag was exchanged for a GST-tag, which is known to assemble into dimers (Bell et al., 2013), the INM targeting of LRRC59 was almost completely inhibited (figure 22). The used GST-tag, which contains several β-sheets and α-helices, has a geometry of approximately 10 nm x 10 nm x 6 nm for the monomer (Lim et al., 1994). When GST assembles in dimers yielding an extraluminal domain of 182.8 kDa for mCherry-FRB-GST-LRRC59, the geometry of GST is suggested to block INM targeting as the protein is too big in dimension to fit into peripheral channels of the NPC. Therefore, mCherry-FRB-GST-LRRC59 was hardly targeted to the INM to mediate a reporter recruitment to the NE, as no differences in the percentage of rapamycin-responding cells over time could be observed (figure 22). For all tested rapamycin incubation times, in average around eight percent of the cells showed a moderate reporter recruitment to the NE. This recruitment could potentially be explained by mCherry-FRB-GST-LRRC59 reaching the INM rather during NE reassembly in mitosis than by passive diffusion during interphase.

For a schematic overview of the results of the rapamycin-induced dimerization assay for LRRC59 see figure 34.

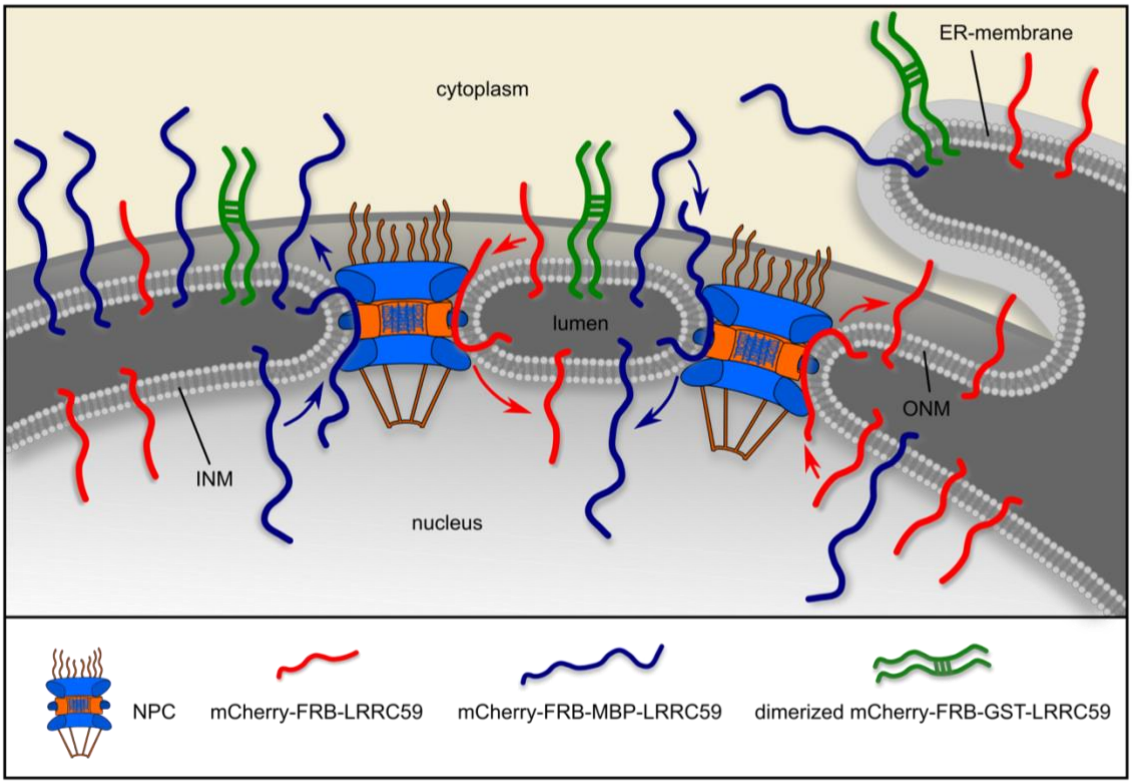

Figure 34: The size and the geometry of the extraluminal domain control the localization of LRRC59 indicating an INM targeting by passive diffusion.
Schematic overview of the results of the rapamycin-induced dimerization assays: mCherry-FRB-LRRC59 (red protein) and mCherry-FRB-MBP-LRRC59 (blue protein) reach the INM by passive diffusion. However, the kinetic of the recruitment of the reporter to the NE (reporter not illustrated in scheme) is much slower for mCherry-FRB-MBP-LRRC59 compared to the protein lacking the MBP-tag. As the reporter kinetic is an indicator for the amounts of proteins, which reach the INM, less mCherry-FRB-MBP-LRRC59 diffuses into the INM compared to mCherry-FRB-LRRC59 for similar incubation times with the drug in the rapamycin-induced dimerization assay. This could be explained by threading into the peripheral channels of the nuclear pore complex (NPC), which could require more time for larger cytoplasmic/nucleoplasmic regions. It is speculated that both proteins are also

able to leave the INM to the ONM/ER-membrane by diffusion. The protein mCherry-FRB-GST-LRRC59 (green protein), which is assembled in dimers, is not able to reach the INM due to the large extraluminal domain and the geometry of the GST-tag.

Endogenous emerin lost its NE localization upon the knockdown of lamin A/C. However, when endogenous LRRC59 reaches the INM, it seems that it is not retained in the nucleus by binding to lamin A/C (figure 16). The absence of an effect of the localization of LRRC59 in lamin A/C siRNA treated cells could be due to two reasons: first, as LRRC59 mainly localizes to the ER-membrane, the loss of the retaining protein in the nucleus would not cause an observable shift to the ER-membrane compared to emerin, which is mainly in the INM in control knockdown cells. The second explanation could be that LRRC59, in contrast to emerin, is not a binding partner of lamin A/C and therefore the knockdown has no effect for the INM localization.

Previously, the nuclear targeting mechanism has been mainly studied by the examination of proteins primarily localizing to the INM as for instance emerin (Manilal et al., 1996), LBR (Worman et al., 1990) or LAP2β (Furukawa et al., 1995). For integral membrane proteins diffusing to the INM, a retention mechanism is suggested, which mediates the accumulation of these proteins in the nucleus. Many INM protein have been shown to bind lamins or chromatin for their INM retention (Katta et al., 2014; Ungricht and Kutay, 2015). In contrast, the majority of the model protein LRRC59 is located in the ER-membrane, whereas only a small subpopulation reaches the INM. The question arises whether LRRC59 is retained in the INM or rather diffuse into and out of the nucleus as its small extraluminal domain does not inhibit passage through peripheral channels. To solve this question, further studies are needed to assign a biological function to LRRC59, which might explain its INM localization, and to rule out that the subpopulation could be retained in the INM by binding to other proteins than lamin A/C. As only a small subpopulation of LRRC59 reaches the INM, this thesis rather suggests that LRRC59 is an ER-membrane protein, which can diffuse into the nucleus via peripheral channels due to its small extraluminal domain, where it is probably not retained in the INM and diffuses back to the ER-membrane.

Conclusion

In this thesis, it could be shown that LRRC59 is targeted to the INM independent of the importin α/importin β pathway (see section 4.2.2). In contrast, by the increase of the size of the extraluminal domain, it could be demonstrated that LRRC59 diffuses into the INM. For the passage of the peripheral channel of the NPC, not only the size of the cytoplasmic/nucleoplasmic domain was important for INM targeting of LRRC59, but also the geometry and dimensions of the used tags, as the 107.5 kDa MBP-tagged LRRC59 protein was able to reach the INM over time, an extraluminal domain size which is much bigger than the suggested limit for passage of peripheral channels of approximately 60 kDa (Ungricht and Kutay, 2015). In the INM, LRRC59 does not seem to get retained by binding to lamin A/C but might rather diffuse out of the nucleus as the majority of the protein is ER-membrane located.

4.3 Protein interaction partners of LRRC59

Proteins in close proximity to LRRC59

Nup210 was identified in RAPIDS experiments as a protein in close proximity to mCherry-FRB-LRRC59. Nup210 is a protein of the NPC that contains a TMD at its C-terminus and anchors the NPC together with the TMD-containing nucleoporins Pom121 and NDC1 to the NE (Weberruss and Antonin, 2016; Grossman et al., 2012). These proteins are suggested to be adjacent to peripheral channels (Knockenhauer and Schwartz, 2016). LRRC59 diffuses into the INM, which is in general suggested to occur via peripheral channels of the NPC (Katta et al., 2014; Ungricht and Kutay, 2015). Therefore, it is not surprising that Nup210 was identified in RAPIDS experiments to be in close proximity to LRRC59 (figure 26, table 26). A direct interaction between the extraluminal domains of LRRC59 (N-terminus) and

Nup210 (C-terminus) could not be identified by pulldown experiments (figure 27). This is in line with the suggestion that passage of LRRC59 by peripheral channels does not require binding to the NPC when LRRC59 is targeted to the INM. The second nucleoporin identified by RAPIDS was RANBP2, also called Nup358. This protein assembles the cytoplasmic filaments together with Nup214 and Nlp1.These filaments extend into the cytoplasm and interact with transport complexes (Beck and Hurt, 2017; Marelli et al., 2001; Suntharalingam and Wente, 2003). As LRRC59 is not actively transported into the INM by a transport factor, which could interact with Nup358, it is likely that the extraluminal domain of LRRC59 extended by mCherry-FRB is adjacent to Nup358, when the protein is on its way to the INM. However, it cannot be easily explained why RAPIDS experiments did not identify further proteins of the NPC except of Nup210, Nup358 and Nup107 to be in close proximity to LRRC59.

In other large-scale studies and yeast two-hybrid screens, LRRC59 was identified as a binding partner for human MT_1 melatonin receptor (Daulat et al., 2007), MPG (DNA-3-methyladenine glycosylase) (Ewing et al., 2007), RRP1B (ribosomal RNA processing 1 homolog B) (Crawford et al., 2009), CIP2A (Pallai et al., 2015) or FGF1 (Skjerpen et al., 2002; Zhen et al., 2012). However, none of these binding partners could be identified by the RAPIDS experiments. Several ER-membrane resident proteins, for instance Sec22b or LMAN2, could be identified, which could be explained by their proximity to LRRC59. Nevertheless, further experiments are needed to analyze a potential direct interaction or proximity between LRRC59 and the remaining identified proteins of the RAPIDS experiments.

The interaction of LRRC59 with FGF1 and CIP2A

In previous studies, it was proposed that the nuclear localization of CIP2A (Pallai et al., 2015) and FGF1 (Zhen et al., 2012) depends on LRRC59. In fractionation studies, exogenous FGF1 was suggested to be imported into the nucleus by the interaction with LRRC59. The INM targeting of LRRC59 was suggested to be importin β-dependent in importin β siRNA treated U2OS cells (Zhen et al., 2012). However, these cells were not controlled for the efficiency of the importin β knockdown as discussed above. As LRRC59 was shown to diffuse into the INM and its nuclear targeting is importin β-independent, the question arises, how the findings of this thesis fit together with the LRRC59-dependency of nuclear localization of CIP2A and FGF1.

CIP2A, an inhibitor of PP2A (Protein phosphatase 2A, involved in tumor suppression), has in total 905 amino acids and contains a single TMD (amino acids 192-212; UniProt ID Q8TCG1). Its N-terminus (amino acids 1-583) was shown to bind to LRRC59 in a yeast two-hybrid screen, an interaction which was validated by immunoprecipitation experiments in prostate cancer cells. CIP2A translocates into the nucleus at G2/M due to the interaction with LRRC59 (Pallai et al., 2015). However, it was not shown whether the N-terminus of CIP2A is oriented to the cytoplasm or the lumen of the ER. In this thesis, it is suspected that the interacting part of CIP2A faces the cytoplasm, as the interaction probably occurs with the N-terminal LRR or the coiled-coil domain of LRRC59 rather than with its short C-terminus in the lumen. For CIP2A, this could either be amino acids 1-192, which is the N-terminal region before the TMD, or amino acids 213-583 after the TMD. If the binding to LRRC59 occurs via amino acids 1-192 of CIP2A, 21.3 kDa of the extraluminal domain of CIP2A would bind to 27.8 kDa of the cytoplasmic/nucleoplasmic region of LRRC59. The molecular mass of both interacting cytoplasmic regions could be small enough to pass the peripheral channels by diffusion. If amino acids 213-583 of CIP2A bind to the N-terminal region of LRRC59, the C-terminus of CIP2A, which has a molecular mass of 78.7 kDa (amino acid 213-905), would probably face the cytoplasm. Therefore, the extraluminal domain of LRRC59 would be increased by binding to CIP2A to a total of 106.5 kDa. As the protein mCherry-FRB-MBP-LRRC59 with its extraluminal domain of 107.5 kDa is able to reach the INM, LRRC59 bound by the C-terminus of CIP2A could probably also reach the INM. However, as mentioned above, the shape and dimension of the extraluminal domains of proteins play a role in the passage of the peripheral channels. Consequently, these speculations have to be proofed by further studies.

FGF1 is a soluble protein of only 17.5 kDa (UniProt ID P05230) which was shown to interact with the coiled-coil domain of LRRC59 (Skjerpen et al., 2002; Zhen et al., 2012). Despite its small molecular mass, exogenous FGF1 is not able to freely diffuse into the nucleus (Imamura et al., 1990; Zhan et al.,

1992; Wesche et al., 2005) but its nuclear localization depends on LRRC59 (Zhen et al., 2012). The suggested import of LRRC59 by importin β could be ruled out in this thesis. It could be possible that FGF1 binds to LRRC59 in the cytoplasm and diffuses together with LRRC59 into the nucleus. However, this targeting would not explain why the knockdown of importin β inhibits the nuclear import of FGF1 (Zhen et al., 2012). If FGF1 is bound by importin β in the cytoplasm and additionally interacts with LRRC59, the targeting via a peripheral channel would probably not be possible. A collective diffusion of FGF1 and LRRC59 to the INM would only be possible, if the transport factor is striped off from FGF1 before entering the peripheral channel (Ungricht and Kutay, 2015).

LRRC59 was shown to be overexpressed in some metastasizing cell lines (Terp et al., 2012) and to interact with FGF1 (Skjerpen et al., 2002; Zhen et al., 2012), an inhibitor of p53-dependent apoptosis and cell growth arrest (Rodriguez-Enfedaque et al., 2009; Bouleau et al., 2005), and CIP2A (Pallai et al., 2015), an inhibitor of a phosphatase involved in tumor suppression (Eichhorn et al., 2009; Junttila et al., 2007). In the rapamycin-induced dimerization assay, it was observed that a higher percentage of cells respond to the rapamycin treatment in a shorter period of time, if the cells were transfected with an increased amount of plasmid DNA coding for mCherry-FRB-LRRC59 (data not shown). This indicates that more LRRC59 diffuses into the INM if the cell expresses more LRRC59 in general. If the expression of endogenous LRRC59 is increased in metastasizing cell lines, it can be speculated that more FGF1 and/or CIP2A could reach the nucleus. This increase in the nucleus could contribute to metastatic potential of a cell and cancer formation.

Conclusion and perspectives

Not much is known about the biological function of LRRC59. In this thesis, several proteins have been shown to be in close proximity to LRRC59. Interestingly, the TMD-containing nucleoporin Nup210, which is adjacent to peripheral channels of the pore, was significantly enriched in RAPIDS experiments indicating a close proximity to LRRC59. Here, it was shown that the N-terminus of LRRC59 cannot interact with the extraluminal region of Nup210. This is in line with the suggestion that LRRC59 passes the peripheral channels on its way to the INM and that a direct binding would not fit to the theory of free diffusion in and out of the nucleus of the mainly ER-membrane localized membrane protein. However, to exclude that LRRC59 is able to bind to Nup210 directly, the luminal domains of both proteins have to be recombinantly purified and tested for binding in pulldown experiments, comparable to the performed testing of the extraluminal regions. The pulldown experiments could also be used to examine further identified proteins in close proximity to mCherry-FRB-LRRC59 of the RAPIDS experiment for direct binding events. In general, to identify additional proteins which directly interact with the extraluminal domain of LRRC59, the purified MBP-tagged LRRC59 aa1-244 could be immobilized on beads and incubated with cell lysate. If interacting proteins can be pulled out of the cell lysate indicated by Coomassie staining after SDS-PAGE, samples could be analyzed by mass spectrometry. To assign a biological function to LRRC59, further studies have to be performed, which can, for instance, start with the analysis of binding partners.

4.4 The analysis of inner nuclear membrane targeting of further membrane proteins

In addition to LRRC59 and emerin, seven more membrane proteins were analyzed in this thesis with respect to an INM localization.

First, **WRB** was examined, a small protein of around 19 kDa, which contains 3 TMDs (UniProt ID O00258). Its N-terminus is luminal while the 4 amino acid short C-terminus faces the cytoplasm. The intermembrane region of 69 amino acids following the N-terminal TMD contains a coiled-coil domain (Vilardi et al., 2011; Anghel et al., 2017). In theory, by the addition of the 11 kDa FRB-tag and the 1.1 kDa small HA-tag, the extraluminal region of the C-terminus of WRB should be small enough to reach the INM, resulting in a recruitment of the reporter to the NE in the presence of rapamycin.

However, even after 30 minutes of rapamycin treatment, no reporter recruitment could be observed (figure S 3 and 15B) indicating that WRB-FRB-HA is unable to reach the INM. Therefore, it served as a negative control for the rapamycin-induced dimerization assay. Nevertheless, the question arises, why WRB was not identified as an INM protein. One explanation could be that WRB exists in a large complex together with CAML. It was shown that the overexpression of both TRC pathway receptor subunits, WRB and CAML, did not inhibit the membrane insertion of Sec61β, while the overexpression of one subunit alone lead to membrane insertion inhibition (Yamamoto and Sakisaka, 2012). Later, it was shown that CAML can be found in 4-fold excess in rat liver microsomes or 7-fold excess in neuroblastoma or human primary fibroblast cell lines compared to WRB. The stoichiometric analysis of the complex indicated that the expression levels of WRB and CAML critically depend on the presence of the other protein. The depletion of CAML, for instance, reduced the WRB levels in HeLa cells (Colombo et al., 2016). However, in this study the stoichiometric imbalance of WRB and CAML was not examined in cells overexpressing one of the receptor subunits. The overexpression of WRB-FRB-HA could therefore lead to two scenarios: as a result, expression levels of CAML could also be changed, probably upregulated, or CAML is not affected in its expression levels as it was shown to be available in excess compared to WRB. In the rapamycin-induced dimerization assay, it is possible that WRB-FRB-HA assembles a complex in the ER-membrane with CAML. The N-terminus of CAML (amino acid 1-189), which faces the cytoplasm, has a molecular mass of 20.8 kDa. If WRB and CAML assemble in a complex, each of the extraluminal domains should be small enough to pass peripheral channels. However, when WRB is tagged with FRB-HA and both extraluminal domains are not in close proximity to each other, the shape and structures of the cytoplasmic regions could inhibit INM targeting. Furthermore, the absence of WRB-FRB-HA in the INM could also be explained by the coiled-coil domain of the cytoplasmic intermembrane region. Even though this region has only a molecular mass of 8.3 kDa, the shape and dimensions of this domain could inhibit INM targeting of WRB via peripheral channels especially when the C-terminus of the protein is tagged by FRB-HA. These hypotheses again suggest an importance not only of the molecular mass but also of the geometry of extraluminal domains in context of INM targeting events via peripheral channels. To confirm this idea, further analyses have to be performed to see whether endogenous WRB would be able to reach the INM alone or in a complex with CAML.

Six additional proteins were analyzed for localization to the INM in the rapamycin-induced dimerization assay. These single TMD-containing candidates were either picked because they were identified ER-membrane proteins in close proximity to mCherry-FRB-LRRC59 in RAPIDS experiments (Sec22b, LMAN2) or they were human orthologs of identified *S. cerevisiae* INM proteins of a systematic split-GFP microscopy-based live cell assay (Smoyer et al., 2016) (HCOP: Orthology Prediction Search: www.genenames.org/tools/hcop; LMAN2: human ortholog of EMP47; SEC61β: human ortholog of SBH2; DDOST: human ortholog of WBP1; Ube2j1: human ortholog of Ubc6; Ube2j2: similar function and 43% sequence identity to Ube2j1 (Protein sequence BLAST tool of NCBI)).

The mCherry- and FRB-tagged proteins **Sec22b**, **LMAN2** and **Ube2j2** were shown to localize to the ER-membrane and the NE. In the rapamycin-induced dimerization assay, an INM localization could be demonstrated for these proteins (figure 29). This result does not explain, why these proteins locate to the INM or whether they fulfill a function in the nucleus. However, it is interesting that proteins, which localized similar to LRRC59 mainly in the ER-membrane and contain a small extraluminal domain, are able to reach the INM. It could be that these proteins reach the nucleus by diffusion as their extraluminal domains could be small enough to pass the peripheral channels. In the INM, it is not obvious that they are bound or retained by nuclear proteins as they mainly locate to the ER-membrane as overexpressed protein. This suggests that Sec22b, LMAN2 and Ube2j2 are not retained in the INM, similar to LRRC59.

For the candidates DDOST, Ube2j1 and Sec61β an INM localization could be shown. To analyze their targeting mechanism to the INM, the extraluminal domains of these proteins were also enlarged, similar to the analysis of LRRC59.

DDOST has a very short C-terminal extraluminal domain of 9 amino acids. When DDOST was C-terminally tagged with FRB-mCherry, it located to the ER-membrane and at the NE. An INM localization could be confirmed in the rapamycin-induced dimerization assay (figure 29). When the extraluminal domain of DDOST was increased in size by the insertion of MBP or GST into the FRB-mCherry-tagged protein, the INM targeting was inhibited, indicating that DDOST reaches the INM by diffusion. However, the insertion of an MBP- or a GST-tag reduced the INM targeting in similar way: DDOST-MBP-FRB-mCherry could recruit the reporter to the NE in around 23% of the examined cells, while around 16% of the cells respond to rapamycin for DDOST-GST-FRB-mCherry (figure 33). The extraluminal domain of the GST-tagged DDOST protein has a molecular mass of 130.8 kDa, which is much more than the cytoplasmic/nucleoplasmic region of MBP-tagged DDOST (81.4 kDa). Due to the enlarged size of the extraluminal domain and the geometry of the GST-tag, the diffusion of DDOST-GST-FRB-mCherry to the INM was expected to be more drastically inhibited. This finding cannot be explained easily, however, the INM targeting of DDOST is reduced with the extension of its extraluminal domain. Further experiments, for instance rapamycin-induced dimerization assays with a shorter drug incubation time than 10 minutes, are needed to explain the small difference in INM targeting inhibition between MBP- and GST-tagged DDOST-FRB-mCherry.

The 283 amino acid long N-terminus (31.1 kDa) of **Ube2j1** faces the cytoplasm/nucleoplasm. When the mCherry-FRB-tagged protein was enlarged by the addition of an MBP-tag, the percentage of rapamycin-responding cells was reduced from around 70% to 23% (figure 32). This result indicates that Ube2j1 diffuses to the INM comparable to LRRC59. The extraluminal domain of mCherry-FRB-MBP-Ube2j1 (110.8 kDa) was similar in size to mCherry-FRB-MBP-LRRC59 (107.5 kDa). As mCherry-FRB-MBP-Ube2j1 could still reach the INM, it is possible that with increasing drug treatment time, more and more of this protein accumulates in the INM mediating an NE recruitment of the reporter. It is conceivable that this larger extraluminal domain needs more time to funnel into the peripheral channels, resulting in a delay of the rapamycin response of the reporter, similar as it was discussed for mCherry-FRB-MBP-LRRC59. With the further increase of the extraluminal domain by the exchange of the MBP-tag to the dimerizing GST-tag, the INM localization of Ube2j1 got almost completely lost. Here, the dimer of GST could also be too big in dimension to fit into the peripheral channels inhibiting the INM targeting of mCherry-FRB-GST-Ube2j1. In general, these results are very similar to the rapamycin-induced dimerization assay with respect to the increase of the size of the extraluminal domain of LRRC59.

Interestingly, an ortholog of human Ube2j1, the *S. cerevisiae* ubiquitin conjugating enzyme Ubc6 was shown to function together with the E3 ubiquitin ligase complex Asi (Asi1, Asi2, and Asi3) at the INM to degrade soluble and integral membrane proteins. This special quality control at the INM differs from but is complementary to the endoplasmic reticulum-associated degradation (ERAD). In ERAD, misfolded proteins are exported from the ER, marked with ubiquitin-chains by a reaction cascade and targeted to the proteasome for degradation (Schnell and Hebert, 2003; Romisch, 2005). For the modification of a protein with ubiquitin, ubiquitin is transferred from the ubiquitin-activating protein E1 to the ubiquitin-conjugating enzyme E2. The E3 ubiquitin ligase binds to E2 and the substrate protein at the same time and mediates the ubiquitin transfer onto the substrate (Glickman and Ciechanover, 2002; Pickart, 2004). It had been shown that the Asi complex acts as an E3 ubiquitin ligase at the INM together with the ubiquitin-conjugating enzyme E2 Ubc6 or Ubc7 and is involved in the degradation of a distinct set of INM proteins (Foresti et al., 2014; Khmelinskii et al., 2014). However, not much is known so far about the degradation of INM proteins but it was suggested that the Asi complex together with Ubc6 is part of an INM-associated degradation (INMAD) pathway which controls the quality of INM proteins (Foresti et al., 2014; Khmelinskii et al., 2014; Smoyer et al., 2019). For the Asi complex subcomponents,

sequence homologs have been found in fungi but not in higher eukaryotes. However, a functional homolog of the Asi complex might be important for the INM quality control in post-mitotic cells, which do not undergo frequent NE breakdown (Foresti et al., 2014). If Ube2j1 is part of an INMAD pathway in human cells similar to Ubc6 in yeast, it has to reach the INM. The possibility of Ube2j1 to reach the INM was demonstrated in this thesis and the protein was shown to reach the INM by diffusion.

Sec61β was examined with an N-terminal mCherry-FRB-tag in the rapamycin-induced dimerization assay. This protein localized at in the ER-membrane and in a rim around the NE. The recruitment of the reporter to the NE confirmed an INM localization of mCherry-FRB-Sec61β. When the extraluminal domain of this protein was increased by the insertion of an MBP-tag, the percentage of rapamycin-responding cells was reduced by around 40% suggesting an INM localization of Sec61β mediated by diffusion. Similar to LRRC59, the insertion of the GST-tag was expected to block the diffusion of Sec61β to the INM. However, when the cytoplasmic/nucleoplasmic domain was increased from 86.6 kDa of the MBP-tagged protein to 141.2 kDa of the GST-tagged protein, the percentage of rapamycin responding cells was only reduced to around 45% (figure 31). This result cannot be easily explained.

Sec61β, which is a subunit of the Sec61 translocon, was supposed to fulfill a function in the INM. Cell surface located EGFR (epidermal growth factor receptor) was suggested to reach the INM in a membrane-embedded manner dependent on importin β after EGF (epidermal growth factor) stimulation. In the INM, Sec61β associates with EGFR. When Sec61β was knocked down, EGFR accumulated in the INM. Sec61β was supposed to mediate the release of EGFR from the INM to the nucleoplasm (Wang et al., 2010), as the translocon mediates import of proteins in the ER-lumen but also retro-translocation of misfolded proteins from the ER to the cytoplasm for degradation (part of the ERAD process) (Schnell and Hebert, 2003; Romisch, 2005). As Sec61β was shown to associate with EGFR also in the ER-membrane in cell fractionation experiments, it was suspected that Sec61β is targeted together with EGFR in an importin β-dependent manner to the INM. However, this theory was not proven experimentally (Wang et al., 2010).

The reduction of INM localization of mCherry-FRB-MBP-Sec61β in the rapamycin-induced dimerization assay points to a diffusion of Sec61β into the nucleus. However, an active transport mechanism cannot be excluded completely, as the exchange of the MBP- to a GST-tag did not result in a full inhibition of INM targeting of Sec61β. So far, an active transport mechanism to the INM dependent on karyopherin Kap95 (yeast homolog of human importin β), the adaptor protein Kap60 (yeast homolog of human importin α) and the activity of Ran was suggested for Heh1 and Heh2 in yeast (King et al., 2006). The fragment of Heh2 containing the bipartite NLS (Lokareddy et al., 2015; Kralt et al., 2015), the first TMD and the linker between these regions, was shown to localize to the NE. This localization was lost, if the region containing the NLSs was removed (Meinema et al., 2011). When the identical fragment containing the NLSs (GFP-Heh2-NLS-linker-TMD) was expressed in leaf epidermal cells of the plant *Nicotiana benthamiana*, a stronger accumulation at the NE was observed compared to the fragment missing the NLSs (GFP-Heh2-linker-TMD) or the full-length protein (Groves et al., 2019). However, when the cNLS of SV40 was N-terminally added in front of the Heh2 sequence (GFP-cNLS-Heh2-linker-TMD), the protein accumulated at the NE. This increase in NE targeting could also be observed when the cNLS in GFP-cNLS-Heh2-linker-TMD was replaced by different monopartite or bipartite NLS compared to the protein missing an NLS. When the linker between cNLS and TMD was reduced from 145 to 10 amino acids, the localization to the NE increased for this fragment of Heh2 compared to GFP-Heh2-linker-TMD. Also, when the linker was increased to 60 kDa, an increase in NE targeting of the protein was observed (Groves et al., 2019). By the performance of Airyscan sub-diffraction limited imaging, which reaches a resolution of 140 nm (Weisshart, 2014; Huff, 2015; Korobchevskaya et al., 2017), it could be demonstrated that the N-terminal fusion of GFP-cNLS enabled the access to the INM of the plant ER-membrane TA protein PICL. Also, the fusion of a GFP-tagged monopartite or a bipartite NLS to the N-terminus of Heh2-linker-TMD was sufficient to mediate INM

localization of the protein as shown by Airyscan sub-diffraction limited imaging (Groves et al., 2019). Not much is known about the INM targeting of membrane proteins in plants. However, the findings in plants that the NE accumulation and the INM targeting of an integral membrane protein can be mediated by monopartite or bipartite NLSs of different species gives a first hint about a potential active transport mechanism to the INM. It is possible that the INM targeting of membrane proteins in yeast and plants differs from mammals. However, further studies are necessary to analyze whether some membrane proteins are also targeted to the INM by an active transport mechanism in mammals, in contrast to the so far examined proteins whose INM localization is mainly explained by passive diffusion. One potential candidate for further analysis could be Sec61β, because the results in the rapamycin-induced dimerization assay cannot be explained only by passive diffusion.

Conclusion and perspectives

In this thesis, by rapamycin-induced dimerization assays, an INM localization of the single TMD-containing proteins Sec22b, LMAN2, Ube2j2, Sec61β, DDOST and Ube2j1 could be shown. By an increase of the extraluminal domains, DDOST and Ube2j1 could be shown to diffuse to the INM. For Sec61β, the results do not give a clear answer for an INM targeting mechanism. The three proteins Sec22b, LMAN2 and Ube2j2 remain for analysis of their INM targeting mechanism in an identical experimental approach. Similar to LRRC59, Sec61β, DDOST and Ube2j1 are mainly ER-located proteins which are able to reach the INM. For Sec61β and Ube2j1, a potential function in the INM has been suggested. However, if the main function of the proteins is fulfilled in the INM, a retention mechanism would be expected to keep this protein in the nucleus, comparable to emerin. However, these two overexpressed proteins did not accumulate at the NE. Immunofluorescence or electron microscopy studies are needed to analyze the localization of endogenous Sec61β, DDOST and Ube2j1. A similar localization of overexpressed and endogenous proteins could suggest a function rather in the ER-membrane than in the INM. Sec61β is part of the ER-membrane embedded translocon, while Ube2j1 is required for ERAD, the degradation pathway at the ER-membrane. Therefore, it is suggested that Sec61β, DDOST and Ube2j1 diffuse into the INM but also leave the nucleus, similar to LRRC59. However, the subpopulation of Ube2j1 and Sec61β in the INM could be constantly exchanged due to the diffusion process, but could be large enough to fulfill their function in the nucleus. To prove this hypothesis, further studies on these proteins are necessary.

4.5 Summary and Outlook

The aim of this thesis was to gain a deeper understanding for the INM targeting mechanism of LRRC59 and other single TMD-containing proteins.

First, the insertion of LRRC59 into rough microsomes was examined showing that the TA protein LRRC59 can insert via a post-translational integration mechanism. However, the post-translational TRC pathway was not required for insertion of LRRC59. This makes LRRC59 an interesting TA protein to be studied further. It could be possible that LRRC59 can switch from one insertion pathway to another, if a pathway is not functional. In addition to the TRC pathway, several recently described ways into the ER-membrane have been shown to enable a post-translational insertion of TA proteins. As both subunits of the SRP receptor were shown to be in close proximity to LRRC59 in RAPIDS experiments, the possibility of a post-translational insertion via SRP should be further analyzed.

In addition to these studies, an examination of the insertion mechanism of the five tested INM proteins Sec22b, Ube2j1, Ube2j2, DDOST and LMAN2 would be interesting. Membrane insertion of Sec61β has already been shown to depend on the TRC pathway (Stefanovic and Hegde, 2007). The yeast protein Sec22, the orthologue of human Sec22b, was shown to interact with Get3 in a yeast two-hybrid screen (Schuldiner et al., 2008) and structural analysis (Yamagata et al., 2010). This interaction could be examined for the human homolog. Sec22b has its TMD at the very C-terminus, while Ube2j1 and Ube2j2 have 15 and 12 amino acids, respectively, following the TMD. Therefore, these proteins could be membrane inserted in a post-translational manner as termination of translation probably occurs before the TMD emerges from the ribosome. The proteins DDOST and LMAN2 each contain a signal peptide at their N-terminus, which could be co-translationally targeted by SRP for membrane insertion. Microsome integration assays with SRP-immunodepleted rabbit reticulocyte lysate could be used to confirm this.

Further, the INM targeting mechanism of LRRC59 is independent of the importin α/importin β pathway and the extraluminal region of LRRC59 does not contain an NLS. However, by the increase of the size of the extraluminal domain in rapamycin-induced dimerization assays, it could be shown that LRRC59 reaches the INM by passive diffusion. It was suggested that not only the molecular mass of the cytoplasmic/nucleoplasmic region is crucial for the passage of the peripheral channels but also the geometry of the domains. Additionally, it was proposed that the mainly ER-membrane located protein LRRC59 diffuses into the INM by peripheral channels, but might not be retained in the nucleus and subsequently leaves the nucleus by a diffusion process. To confirm this theory, kinetic studies need to focus not only on the INM targeting mechanism but also on the way of the protein back to the ER-membrane.

For DDOST, Ube2j1 and Sec61β, it could be shown that the majority of the proteins resides in the ER-membrane, while a subpopulation is able to reach the INM. The INM localization of DDOST and Ube2j1 was shown to depend on the size of the extraluminal domains suggesting a diffusion into the nucleus. However, the INM localization of Sec61β did not depend on the size of the extraluminal region to the same extent as it does for LRRC59, DDOST and Ube2j1. Further studies are needed to analyze whether Sec61β reaches the INM only by diffusion.

The ER-membrane/ONM and the INM could in principle share all proteins with an extraluminal domain able to pass the peripheral channels by diffusion. Only proteins with binding sites would consequently be retained and accumulated in the INM (Ungricht and Kutay, 2017; Zuleger et al., 2011). In yeast, around 35% of the proteins able to reach the INM are proteins of the ER-membrane with small extraluminal regions (Smoyer et al., 2016). This thesis contributes to the understanding of the INM targeting in mammals of the mainly ER located integral membrane proteins LRRC59, Sec61β, DDOST and Ube2j1, which might or might not have a function in the nucleus. The proteins LRRC59, DDOST and Ube2j1 seem to reach the INM by diffusion but are probably not retained in the INM in contrast to proteins like emerin, which resides primarily in the INM.

References

Current Protocols in Molecular Biology. Wiley Online Library

https://currentprotocols.onlinelibrary.wiley.com/loi/19343647 (accessed 18.02.2019).

Abell, B.M., Jung, M., Oliver, J.D., Knight, B.C., Tyedmers, J., Zimmermann, R., and High, S. (2003). Tail-anchored and signal-anchored proteins utilize overlapping pathways during membrane insertion. J Biol Chem *278*, 5669-5678.

Abell, B.M., Pool, M.R., Schlenker, O., Sinning, I., and High, S. (2004). Signal recognition particle mediates post-translational targeting in eukaryotes. Embo J *23*, 2755-2764.

Abell, B.M., Rabu, C., Leznicki, P., Young, J.C., and High, S. (2007). Post-translational integration of tail-anchored proteins is facilitated by defined molecular chaperones. J Cell Sci *120*, 1743-1751.

Adam, S.A. (2016). Nuclear Protein Transport in Digitonin Permeabilized Cells. Methods Mol Biol *1411*, 479-487.

Adam, S.A., Marr, R.S., and Gerace, L. (1990). Nuclear protein import in permeabilized mammalian cells requires soluble cytoplasmic factors. J Cell Biol *111*, 807-816.

Adamus, G., Arendt, A., and Hargrave, P.A. (1991). Genetic control of antibody response to bovine rhodopsin in mice: epitope mapping of rhodopsin structure. J Neuroimmunol *34*, 89-97.

Aebi, M., Bernasconi, R., Clerc, S., and Molinari, M. (2010). N-glycan structures: recognition and processing in the ER. Trends Biochem Sci *35*, 74-82.

Aitchison, J.D., Blobel, G., and Rout, M.P. (1996). Kap104p: a karyopherin involved in the nuclear transport of messenger RNA binding proteins. Science *274*, 624-627.

Akey, C.W., and Radermacher, M. (1993). Architecture of the Xenopus nuclear pore complex revealed by three-dimensional cryo-electron microscopy. J Cell Biol *122*, 1-19.

Akopian, D., Shen, K., Zhang, X., and Shan, S.O. (2013). Signal recognition particle: an essential protein-targeting machine. Annu Rev Biochem *82*, 693-721.

Alber, F., Dokudovskaya, S., Veenhoff, L.M., Zhang, W., Kipper, J., Devos, D., Suprapto, A., Karni-Schmidt, O., Williams, R., Chait, B.T.*, et al.* (2007). The molecular architecture of the nuclear pore complex. Nature *450*, 695-701.

Anderson, D.J., Vargas, J.D., Hsiao, J.P., and Hetzer, M.W. (2009). Recruitment of functionally distinct membrane proteins to chromatin mediates nuclear envelope formation in vivo. J Cell Biol *186*, 183-191.

Anghel, S.A., McGilvray, P.T., Hegde, R.S., and Keenan, R.J. (2017). Identification of Oxa1 Homologs Operating in the Eukaryotic Endoplasmic Reticulum. Cell Rep *21*, 3708-3716.

Antonin, W., Ungricht, R., and Kutay, U. (2011). Traversing the NPC along the pore membrane: targeting of membrane proteins to the INM. Nucleus *2*, 87-91.

Aramburu, I.V., and Lemke, E.A. (2017). Floppy but not sloppy: Interaction mechanism of FG-nucleoporins and nuclear transport receptors. Semin Cell Dev Biol *68*, 34-41.

Arkin, I.T. (2002). Structural aspects of oligomerization taking place between the transmembrane alpha-helices of bitopic membrane proteins. Biochim Biophys Acta *1565*, 347-363.

Ast, T., Cohen, G., and Schuldiner, M. (2013). A network of cytosolic factors targets SRP-independent proteins to the endoplasmic reticulum. Cell *152*, 1134-1145.

Ast, T., and Schuldiner, M. (2013). All roads lead to Rome (but some may be harder to travel): SRP-independent translocation into the endoplasmic reticulum. Crit Rev Biochem Mol Biol *48*, 273-288.

Atanassov, I., and Urlaub, H. (2013). Increased proteome coverage by combining PAGE and peptide isoelectric focusing: comparative study of gel-based separation approaches. Proteomics *13*, 2947-2955.

Aviram, N., Ast, T., Costa, E.A., Arakel, E.C., Chuartzman, S.G., Jan, C.H., Hassdenteufel, S., Dudek, J., Jung, M., Schorr, S.*, et al.* (2016). The SND proteins constitute an alternative targeting route to the endoplasmic reticulum. Nature *540*, 134-138.

Banaszynski, L.A., Liu, C.W., and Wandless, T.J. (2005). Characterization of the FKBP.rapamycin.FRB ternary complex. J Am Chem Soc *127*, 4715-4721.

Beck, M., and Hurt, E. (2017). The nuclear pore complex: understanding its function through structural insight. Nat Rev Mol Cell Biol *18*, 73-89.

Beck, M., Lucic, V., Forster, F., Baumeister, W., and Medalia, O. (2007). Snapshots of nuclear pore complexes in action captured by cryo-electron tomography. Nature *449*, 611-615.

Beck, M., Schmidt, A., Malmstroem, J., Claassen, M., Ori, A., Szymborska, A., Herzog, F., Rinner, O., Ellenberg, J., and Aebersold, R. (2011). The quantitative proteome of a human cell line. Mol Syst Biol *7*, 549.

Becker, J., Melchior, F., Gerke, V., Bischoff, F.R., Ponstingl, H., and Wittinghofer, A. (1995). RNA1 encodes a GTPase-activating protein specific for Gsp1p, the Ran/TC4 homologue of Saccharomyces cerevisiae. J Biol Chem *270*, 11860-11865.

Beckmann, R., Bubeck, D., Grassucci, R., Penczek, P., Verschoor, A., Blobel, G., and Frank, J. (1997). Alignment of conduits for the nascent polypeptide chain in the ribosome-Sec61 complex. Science *278*, 2123-2126.

Beilharz, T., Egan, B., Silver, P.A., Hofmann, K., and Lithgow, T. (2003). Bipartite signals mediate subcellular targeting of tail-anchored membrane proteins in Saccharomyces cerevisiae. J Biol Chem *278*, 8219-8223.

Bell, M.R., Engleka, M.J., Malik, A., and Strickler, J.E. (2013). To fuse or not to fuse: what is your purpose? Protein Sci *22*, 1466-1477.

Bierer, B.E., Mattila, P.S., Standaert, R.F., Herzenberg, L.A., Burakoff, S.J., Crabtree, G., and Schreiber, S.L. (1990). Two distinct signal transmission pathways in T lymphocytes are inhibited by complexes formed between an immunophilin and either FK506 or rapamycin. Proc Natl Acad Sci U S A *87*, 9231-9235.

Bigalke, J.M., and Heldwein, E.E. (2015). Structural basis of membrane budding by the nuclear egress complex of herpesviruses. Embo J *34*, 2921-2936.

Bione, S., Maestrini, E., Rivella, S., Mancini, M., Regis, S., Romeo, G., and Toniolo, D. (1994). Identification of a novel X-linked gene responsible for Emery-Dreifuss muscular dystrophy. Nat Genet *8*, 323-327.

Birnboim, H.C., and Doly, J. (1979). A rapid alkaline extraction procedure for screening recombinant plasmid DNA. Nucleic Acids Res *7*, 1513-1523.

Bischoff, F.R., Klebe, C., Kretschmer, J., Wittinghofer, A., and Ponstingl, H. (1994). RanGAP1 induces GTPase activity of nuclear Ras-related Ran. Proc Natl Acad Sci U S A *91*, 2587-2591.

Bischoff, F.R., Krebber, H., Kempf, T., Hermes, I., and Ponstingl, H. (1995a). Human RanGTPase-activating protein RanGAP1 is a homologue of yeast Rna1p involved in mRNA processing and transport. Proc Natl Acad Sci U S A *92*, 1749-1753.

Bischoff, F.R., Krebber, H., Smirnova, E., Dong, W., and Ponstingl, H. (1995b). Co-activation of RanGTPase and inhibition of GTP dissociation by Ran-GTP binding protein RanBP1. Embo J *14*, 705-715.

Bischoff, F.R., and Ponstingl, H. (1991a). Catalysis of guanine nucleotide exchange on Ran by the mitotic regulator RCC1. Nature *354*, 80-82.

Bischoff, F.R., and Ponstingl, H. (1991b). Mitotic regulator protein RCC1 is complexed with a nuclear ras-related polypeptide. Proc Natl Acad Sci U S A *88*, 10830-10834.

Blenski, M., and Kehlenbach, R.H. (2019). Targeting of LRRC59 to the Endoplasmic Reticulum and the Inner Nuclear Membrane. Int J Mol Sci *20*.

Bocharov, E.V., Mineev, K.S., Pavlov, K.V., Akimov, S.A., Kuznetsov, A.S., Efremov, R.G., and Arseniev, A.S. (2017). Helix-helix interactions in membrane domains of bitopic proteins: Specificity and role of lipid environment. Biochim Biophys Acta Biomembr *1859*, 561-576.

Boettcher, B., and Barral, Y. (2013). The cell biology of open and closed mitosis. Nucleus *4*, 160-165.

Bogenhagen, D.F., Rousseau, D., and Burke, S. (2008). The layered structure of human mitochondrial DNA nucleoids. J Biol Chem *283*, 3665-3675.

Boni, A., Politi, A.Z., Strnad, P., Xiang, W., Hossain, M.J., and Ellenberg, J. (2015). Live imaging and modeling of inner nuclear membrane targeting reveals its molecular requirements in mammalian cells. J Cell Biol *209*, 705-720.

Bonne, G., Di Barletta, M.R., Varnous, S., Becane, H.M., Hammouda, E.H., Merlini, L., Muntoni, F., Greenberg, C.R., Gary, F., Urtizberea, J.A.*, et al.* (1999). Mutations in the gene encoding lamin A/C cause autosomal dominant Emery-Dreifuss muscular dystrophy. Nat Genet *21*, 285-288.

Bonne, G., and Quijano-Roy, S. (2013). Emery-Dreifuss muscular dystrophy, laminopathies, and other nuclear envelopathies. Handb Clin Neurol *113*, 1367-1376.

Borgese, N., Colombo, S., and Pedrazzini, E. (2003). The tale of tail-anchored proteins: coming from the cytosol and looking for a membrane. J Cell Biol *161*, 1013-1019.

Borgese, N., and Fasana, E. (2011). Targeting pathways of C-tail-anchored proteins. Biochim Biophys Acta *1808*, 937-946.

Borgese, N., and Righi, M. (2010). Remote origins of tail-anchored proteins. Traffic *11*, 877-885.

Bouleau, S., Grimal, H., Rincheval, V., Godefroy, N., Mignotte, B., Vayssiere, J.L., and Renaud, F. (2005). FGF1 inhibits p53-dependent apoptosis and cell cycle arrest via an intracrine pathway. Oncogene *24*, 7839-7849.

Brambillasca, S., Yabal, M., Makarow, M., and Borgese, N. (2006). Unassisted translocation of large polypeptide domains across phospholipid bilayers. J Cell Biol *175*, 767-777.

Brambillasca, S., Yabal, M., Soffientini, P., Stefanovic, S., Makarow, M., Hegde, R.S., and Borgese, N. (2005). Transmembrane topogenesis of a tail-anchored protein is modulated by membrane lipid composition. Embo J *24*, 2533-2542.

Braunagel, S.C., Williamson, S.T., Ding, Q., Wu, X., and Summers, M.D. (2007). Early sorting of inner nuclear membrane proteins is conserved. Proc Natl Acad Sci U S A *104*, 9307-9312.

Brown, E.J., Albers, M.W., Shin, T.B., Ichikawa, K., Keith, C.T., Lane, W.S., and Schreiber, S.L. (1994). A mammalian protein targeted by G1-arresting rapamycin-receptor complex. Nature *369*, 756-758.

Buchanan, S.G., and Gay, N.J. (1996). Structural and functional diversity in the leucine-rich repeat family of proteins. Prog Biophys Mol Biol *65*, 1-44.

Burke, B. (2012). It takes KASH to hitch to the SUN. Cell *149*, 961-963.

Burke, B., and Stewart, C.L. (2002). Life at the edge: the nuclear envelope and human disease. Nat Rev Mol Cell Biol *3*, 575-585.

Burke, B., and Stewart, C.L. (2013). The nuclear lamins: flexibility in function. Nat Rev Mol Cell Biol *14*, 13-24.

Burns, L.T., and Wente, S.R. (2012). Trafficking to uncharted territory of the nuclear envelope. Curr Opin Cell Biol *24*, 341-349.

Caly, L., Ghildyal, R., and Jans, D.A. (2015). Respiratory virus modulation of host nucleocytoplasmic transport; target for therapeutic intervention? Front Microbiol *6*, 848.

Capelson, M., Doucet, C., and Hetzer, M.W. (2010). Nuclear pore complexes: guardians of the nuclear genome. Cold Spring Harb Symp Quant Biol *75*, 585-597.

Casson, J., McKenna, M., Hassdenteufel, S., Aviram, N., Zimmerman, R., and High, S. (2017). Multiple pathways facilitate the biogenesis of mammalian tail-anchored proteins. J Cell Sci *130*, 3851-3861.

Cautain, B., Hill, R., de Pedro, N., and Link, W. (2015). Components and regulation of nuclear transport processes. Febs j *282*, 445-462.

Cavazza, T., and Vernos, I. (2015). The RanGTP Pathway: From Nucleo-Cytoplasmic Transport to Spindle Assembly and Beyond. Front Cell Dev Biol *3*, 82.

Chang, Y.W., Chuang, Y.C., Ho, Y.C., Cheng, M.Y., Sun, Y.J., Hsiao, C.D., and Wang, C. (2010). Crystal structure of Get4-Get5 complex and its interactions with Sgt2, Get3, and Ydj1. J Biol Chem *285*, 9962-9970.

Charneau, P., Mirambeau, G., Roux, P., Paulous, S., Buc, H., and Clavel, F. (1994). HIV-1 reverse transcription. A termination step at the center of the genome. J Mol Biol *241*, 651-662.

Chartron, J.W., Clemons, W.M., Jr., and Suloway, C.J. (2012). The complex process of GETting tail-anchored membrane proteins to the ER. Curr Opin Struct Biol *22*, 217-224.

Chatzifrangkeskou, M., Bonne, G., and Muchir, A. (2015). Nuclear envelope and striated muscle diseases. Curr Opin Cell Biol *32*, 1-6.

Chen, C., and Okayama, H. (1987). High-efficiency transformation of mammalian cells by plasmid DNA. Mol Cell Biol *7*, 2745-2752.

Chen, J., Zheng, X.F., Brown, E.J., and Schreiber, S.L. (1995). Identification of an 11-kDa FKBP12-rapamycin-binding domain within the 289-kDa FKBP12-rapamycin-associated protein and characterization of a critical serine residue. Proc Natl Acad Sci U S A *92*, 4947-4951.

Chen, X., Zaro, J.L., and Shen, W.C. (2013). Fusion protein linkers: property, design and functionality. Adv Drug Deliv Rev *65*, 1357-1369.

Chi, N.C., Adam, E.J., and Adam, S.A. (1995). Sequence and characterization of cytoplasmic nuclear protein import factor p97. J Cell Biol *130*, 265-274.

Chio, U.S., Cho, H., and Shan, S.O. (2017). Mechanisms of Tail-Anchored Membrane Protein Targeting and Insertion. Annu Rev Cell Dev Biol *33*, 417-438.

Chitwood, P.J., Juszkiewicz, S., Guna, A., Shao, S., and Hegde, R.S. (2018). EMC Is Required to Initiate Accurate Membrane Protein Topogenesis. Cell *175*, 1507-1519.e1516.

Chiu, M.I., Katz, H., and Berlin, V. (1994). RAPT1, a mammalian homolog of yeast Tor, interacts with the FKBP12/rapamycin complex. Proc Natl Acad Sci U S A *91*, 12574-12578.

Chizhik, A.M., Ruhlandt, D., Pfaff, J., Karedla, N., Chizhik, A.I., Gregor, I., Kehlenbach, R.H., and Enderlein, J. (2017). Three-Dimensional Reconstruction of Nuclear Envelope Architecture Using Dual-Color Metal-Induced Energy Transfer Imaging. ACS Nano *11*, 11839-11846.

Choi, J., Chen, J., Schreiber, S.L., and Clardy, J. (1996). Structure of the FKBP12-rapamycin complex interacting with the binding domain of human FRAP. Science *273*, 239-242.

Chook, Y.M., and Suel, K.E. (2011). Nuclear import by karyopherin-betas: recognition and inhibition. Biochim Biophys Acta *1813*, 1593-1606.

Chou, K.C., and Cai, Y.D. (2005). Prediction of membrane protein types by incorporating amphipathic effects. J Chem Inf Model *45*, 407-413.

Chou, K.C., and Elrod, D.W. (1999). Prediction of membrane protein types and subcellular locations. Proteins *34*, 137-153.

Christie, M., Chang, C.W., Rona, G., Smith, K.M., Stewart, A.G., Takeda, A.A., Fontes, M.R., Stewart, M., Vertessy, B.G., Forwood, J.K.*, et al.* (2016). Structural Biology and Regulation of Protein Import into the Nucleus. J Mol Biol *428*, 2060-2090.

Colombo, S.F., Cardani, S., Maroli, A., Vitiello, A., Soffientini, P., Crespi, A., Bram, R.F., Benfante, R., and Borgese, N. (2016). Tail-anchored Protein Insertion in Mammals: FUNCTION AND RECIPROCAL INTERACTIONS OF THE TWO SUBUNITS OF THE TRC40 RECEPTOR. J Biol Chem *291*, 15292-15306.

Colombo, S.F., Longhi, R., and Borgese, N. (2009). The role of cytosolic proteins in the insertion of tail-anchored proteins into phospholipid bilayers. J Cell Sci *122*, 2383-2392.

Cook, A., Bono, F., Jinek, M., and Conti, E. (2007). Structural biology of nucleocytoplasmic transport. Annu Rev Biochem *76*, 647-671.

Cordes, V.C., Reidenbach, S., Rackwitz, H.R., and Franke, W.W. (1997). Identification of protein p270/Tpr as a constitutive component of the nuclear pore complex-attached intranuclear filaments. J Cell Biol *136*, 515-529.

Cox, J., and Mann, M. (2008). MaxQuant enables high peptide identification rates, individualized p.p.b.-range mass accuracies and proteome-wide protein quantification. Nat Biotechnol *26*, 1367-1372.

Coy-Vergara, J., Rivera-Monroy, J., Urlaub, H., Lenz, C., and Schwappach, B. (2019). A trap mutant reveals the physiological client spectrum of TRC40. J Cell Sci.

Crawford, N.P., Yang, H., Mattaini, K.R., and Hunter, K.W. (2009). The metastasis efficiency modifier ribosomal RNA processing 1 homolog B (RRP1B) is a chromatin-associated factor. J Biol Chem *284*, 28660-28673.

Cronshaw, J.M., Krutchinsky, A.N., Zhang, W., Chait, B.T., and Matunis, M.J. (2002). Proteomic analysis of the mammalian nuclear pore complex. J Cell Biol *158*, 915-927.

Cross, B.C., McKibbin, C., Callan, A.C., Roboti, P., Piacenti, M., Rabu, C., Wilson, C.M., Whitehead, R., Flitsch, S.L., Pool, M.R.*, et al.* (2009). Eeyarestatin I inhibits Sec61-mediated protein translocation at the endoplasmic reticulum. J Cell Sci *122*, 4393-4400.

D'Angelo, M.A., Raices, M., Panowski, S.H., and Hetzer, M.W. (2009). Age-dependent deterioration of nuclear pore complexes causes a loss of nuclear integrity in postmitotic cells. Cell *136*, 284-295.

Dauer, W.T., and Worman, H.J. (2009). The nuclear envelope as a signaling node in development and disease. Dev Cell *17*, 626-638.

Daulat, A.M., Maurice, P., Froment, C., Guillaume, J.L., Broussard, C., Monsarrat, B., Delagrange, P., and Jockers, R. (2007). Purification and identification of G protein-coupled receptor protein complexes under native conditions. Mol Cell Proteomics *6*, 835-844.

Day, R.N., and Davidson, M.W. (2009). The fluorescent protein palette: tools for cellular imaging. Chem Soc Rev *38*, 2887-2921.

de Las Heras, J.I., Meinke, P., Batrakou, D.G., Srsen, V., Zuleger, N., Kerr, A.R., and Schirmer, E.C. (2013). Tissue specificity in the nuclear envelope supports its functional complexity. Nucleus *4*, 460-477.

Denic, V. (2012). A portrait of the GET pathway as a surprisingly complicated young man. Trends Biochem Sci *37*, 411-417.

Denic, V., Dotsch, V., and Sinning, I. (2013). Endoplasmic reticulum targeting and insertion of tail-anchored membrane proteins by the GET pathway. Cold Spring Harb Perspect Biol *5*, a013334.

Denks, K., Vogt, A., Sachelaru, I., Petriman, N.A., Kudva, R., and Koch, H.G. (2014). The Sec translocon mediated protein transport in prokaryotes and eukaryotes. Mol Membr Biol *31*, 58-84.

Dingwall, C., and Laskey, R.A. (1991). Nuclear targeting sequences--a consensus? Trends Biochem Sci *16*, 478-481.

Dingwall, C., Robbins, J., Dilworth, S.M., Roberts, B., and Richardson, W.D. (1988). The nucleoplasmin nuclear location sequence is larger and more complex than that of SV-40 large T antigen. J Cell Biol *107*, 841-849.

Dreger, M., Bengtsson, L., Schoneberg, T., Otto, H., and Hucho, F. (2001). Nuclear envelope proteomics: novel integral membrane proteins of the inner nuclear membrane. Proc Natl Acad Sci U S A *98*, 11943-11948.

Drivas, G.T., Shih, A., Coutavas, E., Rush, M.G., and D'Eustachio, P. (1990). Characterization of four novel ras-like genes expressed in a human teratocarcinoma cell line. Mol Cell Biol *10*, 1793-1798.

Dultz, E., Zanin, E., Wurzenberger, C., Braun, M., Rabut, G., Sironi, L., and Ellenberg, J. (2008). Systematic kinetic analysis of mitotic dis- and reassembly of the nuclear pore in living cells. J Cell Biol *180*, 857-865.

Eichhorn, P.J., Creyghton, M.P., and Bernards, R. (2009). Protein phosphatase 2A regulatory subunits and cancer. Biochim Biophys Acta *1795*, 1-15.

Elangovan, M., Chong, H.K., Park, J.H., Yeo, E.J., and Yoo, Y.J. (2017). The role of ubiquitin-conjugating enzyme Ube2j1 phosphorylation and its degradation by proteasome during endoplasmic stress recovery. J Cell Commun Signal *11*, 265-273.

Ellenberg, J., Siggia, E.D., Moreira, J.E., Smith, C.L., Presley, J.F., Worman, H.J., and Lippincott-Schwartz, J. (1997). Nuclear membrane dynamics and reassembly in living cells: targeting of an inner nuclear membrane protein in interphase and mitosis. J Cell Biol *138*, 1193-1206.

Emery, A.E. (1989). Emery-Dreifuss syndrome. J Med Genet *26*, 637-641.

Emery, A.E., and Dreifuss, F.E. (1966). Unusual type of benign x-linked muscular dystrophy. J Neurol Neurosurg Psychiatry *29*, 338-342.

Esnault, Y., Feldheim, D., Blondel, M.O., Schekman, R., and Kepes, F. (1994). SSS1 encodes a stabilizing component of the Sec61 subcomplex of the yeast protein translocation apparatus. J Biol Chem *269*, 27478-27485.

Evans, E.A., Gilmore, R., and Blobel, G. (1986). Purification of microsomal signal peptidase as a complex. Proc Natl Acad Sci U S A *83*, 581-585.

Ewing, R.M., Chu, P., Elisma, F., Li, H., Taylor, P., Climie, S., McBroom-Cerajewski, L., Robinson, M.D., O'Connor, L., Li, M.*, et al.* (2007). Large-scale mapping of human protein-protein interactions by mass spectrometry. Mol Syst Biol *3*, 89.

Fabre, E., and Hurt, E. (1997). Yeast genetics to dissect the nuclear pore complex and nucleocytoplasmic trafficking. Annu Rev Genet *31*, 277-313.

Favaloro, V., Spasic, M., Schwappach, B., and Dobberstein, B. (2008). Distinct targeting pathways for the membrane insertion of tail-anchored (TA) proteins. J Cell Sci *121*, 1832-1840.

Favaloro, V., Vilardi, F., Schlecht, R., Mayer, M.P., and Dobberstein, B. (2010). Asna1/TRC40-mediated membrane insertion of tail-anchored proteins. J Cell Sci *123*, 1522-1530.

Feldherr, C.M., Kallenbach, E., and Schultz, N. (1984). Movement of a karyophilic protein through the nuclear pores of oocytes. J Cell Biol *99*, 2216-2222.

Fire, A., Xu, S., Montgomery, M.K., Kostas, S.A., Driver, S.E., and Mello, C.C. (1998). Potent and specific genetic interference by double-stranded RNA in Caenorhabditis elegans. Nature *391*, 806-811.

Foresti, O., Rodriguez-Vaello, V., Funaya, C., and Carvalho, P. (2014). Quality control of inner nuclear membrane proteins by the Asi complex. Science *346*, 751-755.

Fornerod, M., Ohno, M., Yoshida, M., and Mattaj, I.W. (1997). CRM1 is an export receptor for leucine-rich nuclear export signals. Cell *90*, 1051-1060.

Frey, S., and Görlich, D. (2007). A saturated FG-repeat hydrogel can reproduce the permeability properties of nuclear pore complexes. Cell *130*, 512-523.

Frey, S., and Görlich, D. (2009). FG/FxFG as well as GLFG repeats form a selective permeability barrier with self-healing properties. Embo J *28*, 2554-2567.

Frey, S., Rees, R., Schunemann, J., Ng, S.C., Funfgeld, K., Huyton, T., and Görlich, D. (2018). Surface Properties Determining Passage Rates of Proteins through Nuclear Pores. Cell *174*, 202-217.e209.

Frey, S., Richter, R.P., and Görlich, D. (2006). FG-rich repeats of nuclear pore proteins form a three-dimensional meshwork with hydrogel-like properties. Science *314*, 815-817.

Fried, H., and Kutay, U. (2003). Nucleocytoplasmic transport: taking an inventory. Cell Mol Life Sci *60*, 1659-1688.

Froger, A., and Hall, J.E. (2007). Transformation of plasmid DNA into E. coli using the heat shock method. J Vis Exp, 253.

Frohnert, C., Hutten, S., Walde, S., Nath, A., and Kehlenbach, R.H. (2014). Importin 7 and Nup358 promote nuclear import of the protein component of human telomerase. PLoS One *9*, e88887.

Frosst, P., Guan, T., Subauste, C., Hahn, K., and Gerace, L. (2002). Tpr is localized within the nuclear basket of the pore complex and has a role in nuclear protein export. J Cell Biol *156*, 617-630.

Fukuda, M., Asano, S., Nakamura, T., Adachi, M., Yoshida, M., Yanagida, M., and Nishida, E. (1997). CRM1 is responsible for intracellular transport mediated by the nuclear export signal. Nature *390*, 308-311.

Fullekrug, J., Scheiffele, P., and Simons, K. (1999). VIP36 localisation to the early secretory pathway. J Cell Sci *112 (Pt 17)*, 2813-2821.

Furukawa, K., Pante, N., Aebi, U., and Gerace, L. (1995). Cloning of a cDNA for lamina-associated polypeptide 2 (LAP2) and identification of regions that specify targeting to the nuclear envelope. Embo J *14*, 1626-1636.

Gallagher, S., Winston, S.E., Fuller, S.A., and Hurrell, J.G.R. (2004). Immunoblotting and Immunodetection. Current Protocols in Molecular Biology.

Gerace, L., and Blobel, G. (1980). The nuclear envelope lamina is reversibly depolymerized during mitosis. Cell *19*, 277-287.

Glickman, M.H., and Ciechanover, A. (2002). The ubiquitin-proteasome proteolytic pathway: destruction for the sake of construction. Physiol Rev *82*, 373-428.

Goldberg, M.W., and Allen, T.D. (1992). High resolution scanning electron microscopy of the nuclear envelope: demonstration of a new, regular, fibrous lattice attached to the baskets of the nucleoplasmic face of the nuclear pores. J Cell Biol *119*, 1429-1440.

Gomez-Cavazos, J.S., and Hetzer, M.W. (2012). Outfits for different occasions: tissue-specific roles of Nuclear Envelope proteins. Curr Opin Cell Biol *24*, 775-783.

Gonzalez, J.M., and Andres, V. (2011). Synthesis, transport and incorporation into the nuclear envelope of A-type lamins and inner nuclear membrane proteins. Biochem Soc Trans *39*, 1758-1763.

Gorjanacz, M., Klerkx, E.P., Galy, V., Santarella, R., Lopez-Iglesias, C., Askjaer, P., and Mattaj, I.W. (2007). Caenorhabditis elegans BAF-1 and its kinase VRK-1 participate directly in post-mitotic nuclear envelope assembly. Embo J *26*, 132-143.

Görlich, D., Kostka, S., Kraft, R., Dingwall, C., Laskey, R.A., Hartmann, E., and Prehn, S. (1995). Two different subunits of importin cooperate to recognize nuclear localization signals and bind them to the nuclear envelope. Curr Biol *5*, 383-392.

Görlich, D., and Kutay, U. (1999). Transport between the cell nucleus and the cytoplasm. Annu Rev Cell Dev Biol *15*, 607-660.

Görlich, D., Prehn, S., Laskey, R.A., and Hartmann, E. (1994). Isolation of a protein that is essential for the first step of nuclear protein import. Cell *79*, 767-778.

Goss, V.L., Hocevar, B.A., Thompson, L.J., Stratton, C.A., Burns, D.J., and Fields, A.P. (1994). Identification of nuclear beta II protein kinase C as a mitotic lamin kinase. J Biol Chem *269*, 19074-19080.

Greber, U.F., Senior, A., and Gerace, L. (1990). A major glycoprotein of the nuclear pore complex is a membrane-spanning polypeptide with a large lumenal domain and a small cytoplasmic tail. Embo J *9*, 1495-1502.

Grossman, E., Medalia, O., and Zwerger, M. (2012). Functional architecture of the nuclear pore complex. Annu Rev Biophys *41*, 557-584.

Groves, N.R., McKenna, J.F., Evans, D.E., Graumann, K., and Meier, I. (2019). A nuclear localization signal targets tail-anchored membrane proteins to the inner nuclear envelope in plants. J Cell Sci.

Grudnik, P., Bange, G., and Sinning, I. (2009). Protein targeting by the signal recognition particle. Biol Chem *390*, 775-782.

Gruenbaum, Y. (2015). Nuclear organization. Annu Rev Biochem *84*, 61-64.

Grünwald, D., Singer, R.H., and Rout, M. (2011). Nuclear export dynamics of RNA-protein complexes. Nature *475*, 333-341.

Guna, A., Volkmar, N., Christianson, J.C., and Hegde, R.S. (2018). The ER membrane protein complex is a transmembrane domain insertase. Science *359*, 470-473.

Hagen, C., Dent, K.C., Zeev-Ben-Mordehai, T., Grange, M., Bosse, J.B., Whittle, C., Klupp, B.G., Siebert, C.A., Vasishtan, D., Bauerlein, F.J.*, et al.* (2015). Structural Basis of Vesicle Formation at the Inner Nuclear Membrane. Cell *163*, 1692-1701.

Halic, M., Becker, T., Pool, M.R., Spahn, C.M., Grassucci, R.A., Frank, J., and Beckmann, R. (2004). Structure of the signal recognition particle interacting with the elongation-arrested ribosome. Nature *427*, 808-814.

Hampoelz, B., Andres-Pons, A., Kastritis, P., and Beck, M. (2019). Structure and Assembly of the Nuclear Pore Complex. Annu Rev Biophys.

Hanein, D., Matlack, K.E., Jungnickel, B., Plath, K., Kalies, K.U., Miller, K.R., Rapoport, T.A., and Akey, C.W. (1996). Oligomeric rings of the Sec61p complex induced by ligands required for protein translocation. Cell *87*, 721-732.

Haraguchi, T., Kojidani, T., Koujin, T., Shimi, T., Osakada, H., Mori, C., Yamamoto, A., and Hiraoka, Y. (2008). Live cell imaging and electron microscopy reveal dynamic processes of BAF-directed nuclear envelope assembly. J Cell Sci *121*, 2540-2554.

Harlow, E., and Lane, D. (1988). Immunoblotting. Antibodies: A Laboratory Manual *CSH Laboratory, Cold Spring Harbor, New York*, pp. 471-510.

Hartmann, E., Sommer, T., Prehn, S., Görlich, D., Jentsch, S., and Rapoport, T.A. (1994). Evolutionary conservation of components of the protein translocation complex. Nature *367*, 654-657.

Haruki, H., Nishikawa, J., and Laemmli, U.K. (2008). The anchor-away technique: rapid, conditional establishment of yeast mutant phenotypes. Mol Cell *31*, 925-932.

Hassdenteufel, S., Sicking, M., Schorr, S., Aviram, N., Fecher-Trost, C., Schuldiner, M., Jung, M., Zimmermann, R., and Lang, S. (2017). hSnd2 protein represents an alternative targeting factor to the endoplasmic reticulum in human cells. FEBS Lett *591*, 3211-3224.

Hayama, R., Rout, M.P., and Fernandez-Martinez, J. (2017). The nuclear pore complex core scaffold and permeability barrier: variations of a common theme. Curr Opin Cell Biol *46*, 110-118.

Heald, R., and McKeon, F. (1990). Mutations of phosphorylation sites in lamin A that prevent nuclear lamina disassembly in mitosis. Cell *61*, 579-589.

Hegde, R.S., and Keenan, R.J. (2011). Tail-anchored membrane protein insertion into the endoplasmic reticulum. Nat Rev Mol Cell Biol *12*, 787-798.

Hellberg, T., Passvogel, L., Schulz, K.S., Klupp, B.G., and Mettenleiter, T.C. (2016). Nuclear Egress of Herpesviruses: The Prototypic Vesicular Nucleocytoplasmic Transport. Adv Virus Res *94*, 81-140.

Hessa, T., Sharma, A., Mariappan, M., Eshleman, H.D., Gutierrez, E., and Hegde, R.S. (2011). Protein targeting and degradation are coupled for elimination of mislocalized proteins. Nature *475*, 394-397.

High, S., and Laird, V. (1997). Membrane protein biosynthesis - all sewn up? Trends Cell Biol *7*, 206-210.

Hinshaw, J.E., Carragher, B.O., and Milligan, R.A. (1992). Architecture and design of the nuclear pore complex. Cell *69*, 1133-1141.

Hockenbery, D., Nunez, G., Milliman, C., Schreiber, R.D., and Korsmeyer, S.J. (1990). Bcl-2 is an inner mitochondrial membrane protein that blocks programmed cell death. Nature *348*, 334-336.

Hoelz, A., Glavy, J.S., and Beck, M. (2016). Toward the atomic structure of the nuclear pore complex: when top down meets bottom up. Nat Struct Mol Biol *23*, 624-630.

Holmer, L., and Worman, H.J. (2001). Inner nuclear membrane proteins: functions and targeting. Cell Mol Life Sci *58*, 1741-1747.

Hopper, A.K., Traglia, H.M., and Dunst, R.W. (1990). The yeast RNA1 gene product necessary for RNA processing is located in the cytosol and apparently excluded from the nucleus. J Cell Biol *111*, 309-321.

Hosoi, H., Dilling, M.B., Shikata, T., Liu, L.N., Shu, L., Ashmun, R.A., Germain, G.S., Abraham, R.T., and Houghton, P.J. (1999). Rapamycin causes poorly reversible inhibition of mTOR and induces p53-independent apoptosis in human rhabdomyosarcoma cells. Cancer Res *59*, 886-894.

Huff, J. (2015). The Airyscan detector from ZEISS: confocal imaging with improved signal-to-noise ratio and super-resolution. Nat Methods *12*.

Hutten, S., Flotho, A., Melchior, F., and Kehlenbach, R.H. (2008). The Nup358-RanGAP complex is required for efficient importin alpha/beta-dependent nuclear import. Mol Biol Cell *19*, 2300-2310.

Ichimura, T., Shindo, Y., Uda, Y., Ohsumi, T., Omata, S., and Sugano, H. (1993). Anti-(p34 protein) antibodies inhibit ribosome binding to and protein translocation across the rough microsomal membrane. FEBS Lett *326*, 241-245.

Imamoto, N., Shimamoto, T., Takao, T., Tachibana, T., Kose, S., Matsubae, M., Sekimoto, T., Shimonishi, Y., and Yoneda, Y. (1995). In vivo evidence for involvement of a 58 kDa component of nuclear pore-targeting complex in nuclear protein import. Embo J *14*, 3617-3626.

Imamura, T., Engleka, K., Zhan, X., Tokita, Y., Forough, R., Roeder, D., Jackson, A., Maier, J.A., Hla, T., and Maciag, T. (1990). Recovery of mitogenic activity of a growth factor mutant with a nuclear translocation sequence. Science *249*, 1567-1570.

Jagus, R., and Beckler, G.S. (2003). Overview of eukaryotic in vitro translation and expression systems. Curr Protoc Cell Biol *Chapter 11*, Unit 11.11.

Johnson, N., Powis, K., and High, S. (2013). Post-translational translocation into the endoplasmic reticulum. Biochim Biophys Acta *1833*, 2403-2409.

Jonikas, M.C., Collins, S.R., Denic, V., Oh, E., Quan, E.M., Schmid, V., Weibezahn, J., Schwappach, B., Walter, P., Weissman, J.S.*, et al.* (2009). Comprehensive characterization of genes required for protein folding in the endoplasmic reticulum. Science *323*, 1693-1697.

Junttila, M.R., Puustinen, P., Niemela, M., Ahola, R., Arnold, H., Bottzauw, T., Ala-aho, R., Nielsen, C., Ivaska, J., Taya, Y.*, et al.* (2007). CIP2A inhibits PP2A in human malignancies. Cell *130*, 51-62.

Kabachinski, G., and Schwartz, T.U. (2015). The nuclear pore complex--structure and function at a glance. J Cell Sci *128*, 423-429.

Kalbfleisch, T., Cambon, A., and Wattenberg, B.W. (2007). A bioinformatics approach to identifying tail-anchored proteins in the human genome. Traffic *8*, 1687-1694.

Kalderon, D., Roberts, B.L., Richardson, W.D., and Smith, A.E. (1984). A short amino acid sequence able to specify nuclear location. Cell *39*, 499-509.

Kalies, K.U., Görlich, D., and Rapoport, T.A. (1994). Binding of ribosomes to the rough endoplasmic reticulum mediated by the Sec61p-complex. J Cell Biol *126*, 925-934.

Kang, D., Gho, X.S., Suh, M., and Kang, C. (2002). Highly Sensitive and Fast Protein Detection with Coomassie Brilliant Blue

in Sodium Dodecyl Sulfate-Polyacrylamide Gel Electrophoresis. Bull Korean Chem Soc *23, No. 11*.

Katahira, J., Strasser, K., Podtelejnikov, A., Mann, M., Jung, J.U., and Hurt, E. (1999). The Mex67p-mediated nuclear mRNA export pathway is conserved from yeast to human. Embo J *18*, 2593-2609.

Katta, S.S., Smoyer, C.J., and Jaspersen, S.L. (2014). Destination: inner nuclear membrane. Trends Cell Biol *24*, 221-229.

Kelleher, D.J., Kreibich, G., and Gilmore, R. (1992). Oligosaccharyltransferase activity is associated with a protein complex composed of ribophorins I and II and a 48 kd protein. Cell *69*, 55-65.

Keminer, O., and Peters, R. (1999). Permeability of single nuclear pores. Biophys J *77*, 217-228.

Khmelinskii, A., Blaszczak, E., Pantazopoulou, M., Fischer, B., Omnus, D.J., Le Dez, G., Brossard, A., Gunnarsson, A., Barry, J.D., Meurer, M.*, et al.* (2014). Protein quality control at the inner nuclear membrane. Nature *516*, 410-413.

Kim, D., and Rossi, J. (2008). RNAi mechanisms and applications. Biotechniques *44*, 613-616.

Kim, Y.H., Han, M.E., and Oh, S.O. (2017). The molecular mechanism for nuclear transport and its application. Anat Cell Biol *50*, 77-85.

King, M.C., Lusk, C.P., and Blobel, G. (2006). Karyopherin-mediated import of integral inner nuclear membrane proteins. Nature *442*, 1003-1007.

Klebe, C., Bischoff, F.R., Ponstingl, H., and Wittinghofer, A. (1995). Interaction of the nuclear GTP-binding protein Ran with its regulatory proteins RCC1 and RanGAP1. Biochemistry *34*, 639-647.

Klemm, J.D., Beals, C.R., and Crabtree, G.R. (1997). Rapid targeting of nuclear proteins to the cytoplasm. Curr Biol *7*, 638-644.

Klupp, B.G., Granzow, H., Fuchs, W., Keil, G.M., Finke, S., and Mettenleiter, T.C. (2007). Vesicle formation from the nuclear membrane is induced by coexpression of two conserved herpesvirus proteins. Proc Natl Acad Sci U S A *104*, 7241-7246.

Knockenhauer, K.E., and Schwartz, T.U. (2016). The Nuclear Pore Complex as a Flexible and Dynamic Gate. Cell *164*, 1162-1171.

Koley, D., and Bard, A.J. (2010). Triton X-100 concentration effects on membrane permeability of a single HeLa cell by scanning electrochemical microscopy (SECM). Proc Natl Acad Sci U S A *107*, 16783-16787.

Korfali, N., Wilkie, G.S., Swanson, S.K., Srsen, V., Batrakou, D.G., Fairley, E.A., Malik, P., Zuleger, N., Goncharevich, A., de Las Heras, J.*, et al.* (2010). The leukocyte nuclear envelope proteome varies with cell activation and contains novel transmembrane proteins that affect genome architecture. Mol Cell Proteomics *9*, 2571-2585.

Korfali, N., Wilkie, G.S., Swanson, S.K., Srsen, V., de Las Heras, J., Batrakou, D.G., Malik, P., Zuleger, N., Kerr, A.R., Florens, L.*, et al.* (2012). The nuclear envelope proteome differs notably between tissues. Nucleus *3*, 552-564.

Korobchevskaya, K., Lagerholm, B., Colin-York, H., and Fritzsche, M. (2017). Exploring the Potential of Airyscan Microscopy for Live Cell Imaging. Photonics *4*.

Kosugi, S., Hasebe, M., Entani, T., Takayama, S., Tomita, M., and Yanagawa, H. (2008). Design of peptide inhibitors for the importin alpha/beta nuclear import pathway by activity-based profiling. Chem Biol *15*, 940-949.

Kralt, A., Jagalur, N.B., van den Boom, V., Lokareddy, R.K., Steen, A., Cingolani, G., Fornerod, M., and Veenhoff, L.M. (2015). Conservation of inner nuclear membrane targeting sequences in mammalian Pom121 and yeast Heh2 membrane proteins. Mol Biol Cell *26*, 3301-3312.

Kriechbaumer, V., Shaw, R., Mukherjee, J., Bowsher, C.G., Harrison, A.M., and Abell, B.M. (2009). Subcellular distribution of tail-anchored proteins in Arabidopsis. Traffic *10*, 1753-1764.

Krull, S., Dorries, J., Boysen, B., Reidenbach, S., Magnius, L., Norder, H., Thyberg, J., and Cordes, V.C. (2010). Protein Tpr is required for establishing nuclear pore-associated zones of heterochromatin exclusion. Embo J *29*, 1659-1673.

Kubitscheck, U., Grünwald, D., Hoekstra, A., Rohleder, D., Kues, T., Siebrasse, J.P., and Peters, R. (2005). Nuclear transport of single molecules: dwell times at the nuclear pore complex. J Cell Biol *168*, 233-243.

Kutay, U., Hartmann, E., and Rapoport, T.A. (1993). A class of membrane proteins with a C-terminal anchor. Trends Cell Biol *3*, 72-75.

Laba, J.K., Steen, A., Popken, P., Chernova, A., Poolman, B., and Veenhoff, L.M. (2015). Active Nuclear Import of Membrane Proteins Revisited. Cells *4*, 653-673.

Laba, J.K., Steen, A., and Veenhoff, L.M. (2014). Traffic to the inner membrane of the nuclear envelope. Curr Opin Cell Biol *28*, 36-45.

Laemmli, U.K. (1970). Cleavage of structural proteins during the assembly of the head of bacteriophage T4. Nature *227*, 680-685.

Lai, T.P., Stauffer, K.A., Murthi, A., Shaheen, H.H., Peng, G., Martin, N.C., and Hopper, A.K. (2009). Mechanism and a peptide motif for targeting peripheral proteins to the yeast inner nuclear membrane. Traffic *10*, 1243-1256.

Lakkaraju, A.K., Mary, C., Scherrer, A., Johnson, A.E., and Strub, K. (2008). SRP keeps polypeptides translocation-competent by slowing translation to match limiting ER-targeting sites. Cell *133*, 440-451.

Lam, S.S., Martell, J.D., Kamer, K.J., Deerinck, T.J., Ellisman, M.H., Mootha, V.K., and Ting, A.Y. (2015). Directed evolution of APEX2 for electron microscopy and proximity labeling. Nat Methods *12*, 51-54.

Lanford, R.E., and Butel, J.S. (1984). Construction and characterization of an SV40 mutant defective in nuclear transport of T antigen. Cell *37*, 801-813.

Laurell, E., Beck, K., Krupina, K., Theerthagiri, G., Bodenmiller, B., Horvath, P., Aebersold, R., Antonin, W., and Kutay, U. (2011). Phosphorylation of Nup98 by multiple kinases is crucial for NPC disassembly during mitotic entry. Cell *144*, 539-550.

Lee, K.K., Haraguchi, T., Lee, R.S., Koujin, T., Hiraoka, Y., and Wilson, K.L. (2001). Distinct functional domains in emerin bind lamin A and DNA-bridging protein BAF. J Cell Sci *114*, 4567-4573.

Lee, P.Y., Costumbrado, J., Hsu, C.Y., and Kim, Y.H. (2012). Agarose gel electrophoresis for the separation of DNA fragments. J Vis Exp.

Lester, D., Farquharson, C., Russell, G., and Houston, B. (2000). Identification of a family of noncanonical ubiquitin-conjugating enzymes structurally related to yeast UBC6. Biochem Biophys Res Commun *269*, 474-480.

Leznicki, P., Clancy, A., Schwappach, B., and High, S. (2010). Bat3 promotes the membrane integration of tail-anchored proteins. J Cell Sci *123*, 2170-2178.

Li, C., Goryaynov, A., and Yang, W. (2016). The selective permeability barrier in the nuclear pore complex. Nucleus *7*, 430-446.

Liang, J., Choi, J., and Clardy, J. (1999). Refined structure of the FKBP12-rapamycin-FRB ternary complex at 2.2 A resolution. Acta Crystallogr D Biol Crystallogr *55*, 736-744.

Liao, H.J., and Carpenter, G. (2007). Role of the Sec61 translocon in EGF receptor trafficking to the nucleus and gene expression. Mol Biol Cell *18*, 1064-1072.

Lim, K., Ho, J.X., Keeling, K., Gilliland, G.L., Ji, X., Ruker, F., and Carter, D.C. (1994). Three-dimensional structure of Schistosoma japonicum glutathione S-transferase fused with a six-amino acid conserved neutralizing epitope of gp41 from HIV. Protein Sci *3*, 2233-2244.

Lim, R.Y., Fahrenkrog, B., Koser, J., Schwarz-Herion, K., Deng, J., and Aebi, U. (2007). Nanomechanical basis of selective gating by the nuclear pore complex. Science *318*, 640-643.

Lipp, J., Dobberstein, B., and Haeuptle, M.T. (1987). Signal recognition particle arrests elongation of nascent secretory and membrane proteins at multiple sites in a transient manner. J Biol Chem *262*, 1680-1684.

Liu, Y., and Barlowe, C. (2002). Analysis of Sec22p in endoplasmic reticulum/Golgi transport reveals cellular redundancy in SNARE protein function. Mol Biol Cell *13*, 3314-3324.

Lodish, H., Berk, A., Zipursky, S.L.M., P. Baltimore, D., and Darnell, J. (2000). Molecular Cell Biology. 4th edition. Section 3.4, Membrane Proteins.

Lokareddy, R.K., Hapsari, R.A., van Rheenen, M., Pumroy, R.A., Bhardwaj, A., Steen, A., Veenhoff, L.M., and Cingolani, G. (2015). Distinctive Properties of the Nuclear Localization Signals of Inner Nuclear Membrane Proteins Heh1 and Heh2. Structure *23*, 1305-1316.

Lupas, A. (1996). Coiled coils: new structures and new functions. Trends Biochem Sci *21*, 375-382.

Lusk, C.P., Blobel, G., and King, M.C. (2007). Highway to the inner nuclear membrane: rules for the road. Nat Rev Mol Cell Biol *8*, 414-420.

Luttmann, W., Bratke, K., Küpper, M., and Myrtek, D. (2014). Der Experimentator: Immunologie. Springer Spektrum *4. Auflage*.

Ma, Y., Cai, S., Lv, Q., Jiang, Q., Zhang, Q., Sodmergen, Zhai, Z., and Zhang, C. (2007). Lamin B receptor plays a role in stimulating nuclear envelope production and targeting membrane vesicles to chromatin during nuclear envelope assembly through direct interaction with importin beta. J Cell Sci *120*, 520-530.

Macara, I.G., Lounsbury, K.M., Richards, S.A., McKiernan, C., and Bar-Sagi, D. (1996). The Ras superfamily of GTPases. Faseb j *10*, 625-630.

Maddaluno, L., Urwyler, C., and Werner, S. (2017). Fibroblast growth factors: key players in regeneration and tissue repair. Development *144*, 4047-4060.

Mahajan, R., Delphin, C., Guan, T., Gerace, L., and Melchior, F. (1997). A small ubiquitin-related polypeptide involved in targeting RanGAP1 to nuclear pore complex protein RanBP2. Cell *88*, 97-107.

Maimon, T., Elad, N., Dahan, I., and Medalia, O. (2012). The human nuclear pore complex as revealed by cryo-electron tomography. Structure *20*, 998-1006.

Malik, P., Korfali, N., Srsen, V., Lazou, V., Batrakou, D.G., Zuleger, N., Kavanagh, D.M., Wilkie, G.S., Goldberg, M.W., and Schirmer, E.C. (2010). Cell-specific and lamin-dependent targeting of novel transmembrane proteins in the nuclear envelope. Cell Mol Life Sci *67*, 1353-1369.

Mancias, J.D., and Goldberg, J. (2007). The transport signal on Sec22 for packaging into COPII-coated vesicles is a conformational epitope. Mol Cell *26*, 403-414.

Mandon, E.C., Trueman, S.F., and Gilmore, R. (2013). Protein translocation across the rough endoplasmic reticulum. Cold Spring Harb Perspect Biol *5*.

Manilal, S., Nguyen, T.M., Sewry, C.A., and Morris, G.E. (1996). The Emery-Dreifuss muscular dystrophy protein, emerin, is a nuclear membrane protein. Hum Mol Genet *5*, 801-808.

Marelli, M., Dilworth, D.J., Wozniak, R.W., and Aitchison, J.D. (2001). The dynamics of karyopherin-mediated nuclear transport. Biochem Cell Biol *79*, 603-612.

Mariappan, M., Li, X., Stefanovic, S., Sharma, A., Mateja, A., Keenan, R.J., and Hegde, R.S. (2010). A ribosome-associating factor chaperones tail-anchored membrane proteins. Nature *466*, 1120-1124.

Mariappan, M., Mateja, A., Dobosz, M., Bove, E., Hegde, R.S., and Keenan, R.J. (2011). The mechanism of membrane-associated steps in tail-anchored protein insertion. Nature *477*, 61-66.

Martell, J.D., Deerinck, T.J., Sancak, Y., Poulos, T.L., Mootha, V.K., Sosinsky, G.E., Ellisman, M.H., and Ting, A.Y. (2012). Engineered ascorbate peroxidase as a genetically encoded reporter for electron microscopy. Nat Biotechnol *30*, 1143-1148.

Martoglio, B., Hofmann, M.W., Brunner, J., and Dobberstein, B. (1995). The protein-conducting channel in the membrane of the endoplasmic reticulum is open laterally toward the lipid bilayer. Cell *81*, 207-214.

Mason, N., Ciufo, L.F., and Brown, J.D. (2000). Elongation arrest is a physiologically important function of signal recognition particle. Embo J *19*, 4164-4174.

Mateja, A., and Keenan, R.J. (2018). A structural perspective on tail-anchored protein biogenesis by the GET pathway. Curr Opin Struct Biol *51*, 195-202.

Mateja, A., Szlachcic, A., Downing, M.E., Dobosz, M., Mariappan, M., Hegde, R.S., and Keenan, R.J. (2009). The structural basis of tail-anchored membrane protein recognition by Get3. Nature *461*, 361-366.

Matunis, M.J., Coutavas, E., and Blobel, G. (1996). A novel ubiquitin-like modification modulates the partitioning of the Ran-GTPase-activating protein RanGAP1 between the cytosol and the nuclear pore complex. J Cell Biol *135*, 1457-1470.

McIntosh, J.R. (2016). Mitosis. Cold Spring Harb Perspect Biol *8*.

Meinema, A.C., Laba, J.K., Hapsari, R.A., Otten, R., Mulder, F.A., Kralt, A., van den Bogaart, G., Lusk, C.P., Poolman, B., and Veenhoff, L.M. (2011). Long unfolded linkers facilitate membrane protein import through the nuclear pore complex. Science *333*, 90-93.

Meinema, A.C., Poolman, B., and Veenhoff, L.M. (2013). Quantitative analysis of membrane protein transport across the nuclear pore complex. Traffic *14*, 487-501.

Mekhail, K., and Moazed, D. (2010). The nuclear envelope in genome organization, expression and stability. Nat Rev Mol Cell Biol *11*, 317-328.

Melchior, F., Paschal, B., Evans, J., and Gerace, L. (1993a). Inhibition of nuclear protein import by nonhydrolyzable analogues of GTP and identification of the small GTPase Ran/TC4 as an essential transport factor. J Cell Biol *123*, 1649-1659.

Melchior, F., Weber, K., and Gerke, V. (1993b). A functional homologue of the RNA1 gene product in Schizosaccharomyces pombe: purification, biochemical characterization, and identification of a leucine-rich repeat motif. Mol Biol Cell *4*, 569-581.

Miyamoto, Y., Yamada, K., and Yoneda, Y. (2016). Importin alpha: a key molecule in nuclear transport and non-transport functions. J Biochem *160*, 69-75.

Molitor, T.P., and Traktman, P. (2014). Depletion of the protein kinase VRK1 disrupts nuclear envelope morphology and leads to BAF retention on mitotic chromosomes. Mol Biol Cell *25*, 891-903.

Moog, D., and Maier, U.G. (2017). Cellular compartmentation follows rules: The Schnepf theorem, its consequences and exceptions: A biological membrane separates a plasmatic from a non-plasmatic phase. Bioessays *39*.

Moore, J.D. (2001). The Ran-GTPase and cell-cycle control. Bioessays *23*, 77-85.

Moore, M.S., and Blobel, G. (1993). The GTP-binding protein Ran/TC4 is required for protein import into the nucleus. Nature *365*, 661-663.

Mudumbi, K.C., Schirmer, E.C., and Yang, W. (2016). Single-point single-molecule FRAP distinguishes inner and outer nuclear membrane protein distribution. Nat Commun *7*, 12562.

Mülhardt, C. (2013). Der Experimentator: Molekularbiologie/Genomics. Springer Spektrum *7. Auflage*.

Mullis, K.B., and Faloona, F.A. (1987). Specific synthesis of DNA in vitro via a polymerase-catalyzed chain reaction. Methods Enzymol *155*, 335-350.

Muranyi, W., Haas, J., Wagner, M., Krohne, G., and Koszinowski, U.H. (2002). Cytomegalovirus recruitment of cellular kinases to dissolve the nuclear lamina. Science *297*, 854-857.

Murthi, A., and Hopper, A.K. (2005). Genome-wide screen for inner nuclear membrane protein targeting in Saccharomyces cerevisiae: roles for N-acetylation and an integral membrane protein. Genetics *170*, 1553-1560.

Nagano, A., Koga, R., Ogawa, M., Kurano, Y., Kawada, J., Okada, R., Hayashi, Y.K., Tsukahara, T., and Arahata, K. (1996). Emerin deficiency at the nuclear membrane in patients with Emery-Dreifuss muscular dystrophy. Nat Genet *12*, 254-259.

Nagy, V., Hsia, K.C., Debler, E.W., Kampmann, M., Davenport, A.M., Blobel, G., and Hoelz, A. (2009). Structure of a trimeric nucleoporin complex reveals alternate oligomerization states. Proc Natl Acad Sci U S A *106*, 17693-17698.

Neuhoff, V., Arold, N., Taube, D., and Ehrhardt, W. (1988). Improved staining of proteins in polyacrylamide gels including isoelectric focusing gels with clear background at nanogram sensitivity using Coomassie Brilliant Blue G-250 and R-250. Electrophoresis *9*, 255-262.

Ng, D.T., Brown, J.D., and Walter, P. (1996). Signal sequences specify the targeting route to the endoplasmic reticulum membrane. J Cell Biol *134*, 269-278.

Ohba, T., Schirmer, E.C., Nishimoto, T., and Gerace, L. (2004). Energy- and temperature-dependent transport of integral proteins to the inner nuclear membrane via the nuclear pore. J Cell Biol *167*, 1051-1062.

Ohsumi, T., Ichimura, T., Sugano, H., Omata, S., Isobe, T., and Kuwano, R. (1993). Ribosome-binding protein p34 is a member of the leucine-rich-repeat-protein superfamily. Biochem J *294 (Pt 2)*, 465-472.

Ohtsubo, M., Kai, R., Furuno, N., Sekiguchi, T., Sekiguchi, M., Hayashida, H., Kuma, K., Miyata, T., Fukushige, S., Murotsu, T.*, et al.* (1987). Isolation and characterization of the active cDNA of the human cell cycle gene (RCC1) involved in the regulation of onset of chromosome condensation. Genes Dev *1*, 585-593.

Ohtsubo, M., Okazaki, H., and Nishimoto, T. (1989). The RCC1 protein, a regulator for the onset of chromosome condensation locates in the nucleus and binds to DNA. J Cell Biol *109*, 1389-1397.

Oka, M., and Yoneda, Y. (2018). Importin alpha: functions as a nuclear transport factor and beyond. Proc Jpn Acad Ser B Phys Biol Sci *94*, 259-274.

Ong, S.E., Blagoev, B., Kratchmarova, I., Kristensen, D.B., Steen, H., Pandey, A., and Mann, M. (2002). Stable isotope labeling by amino acids in cell culture, SILAC, as a simple and accurate approach to expression proteomics. Mol Cell Proteomics *1*, 376-386.

Ornitz, D.M., and Itoh, N. (2015). The Fibroblast Growth Factor signaling pathway. Wiley Interdiscip Rev Dev Biol *4*, 215-266.

Osborne, A.R., Rapoport, T.A., and van den Berg, B. (2005). Protein translocation by the Sec61/SecY channel. Annu Rev Cell Dev Biol *21*, 529-550.

Ossareh-Nazari, B., Bachelerie, F., and Dargemont, C. (1997). Evidence for a role of CRM1 in signal-mediated nuclear protein export. Science *278*, 141-144.

Ostlund, C., Ellenberg, J., Hallberg, E., Lippincott-Schwartz, J., and Worman, H.J. (1999). Intracellular trafficking of emerin, the Emery-Dreifuss muscular dystrophy protein. J Cell Sci *112 (Pt 11)*, 1709-1719.

Ott, C.M., and Lingappa, V.R. (2002). Integral membrane protein biosynthesis: why topology is hard to predict. J Cell Sci *115*, 2003-2009.

Pallai, R., Bhaskar, A., Barnett-Bernodat, N., Gallo-Ebert, C., Pusey, M., Nickels, J.T., Jr., and Rice, L.M. (2015). Leucine-rich repeat-containing protein 59 mediates nuclear import of cancerous inhibitor of PP2A in prostate cancer cells. Tumour Biol *36*, 6383-6390.

Pante, N., and Kann, M. (2002). Nuclear pore complex is able to transport macromolecules with diameters of about 39 nm. Mol Biol Cell *13*, 425-434.

Panzner, S., Dreier, L., Hartmann, E., Kostka, S., and Rapoport, T.A. (1995). Posttranslational protein transport in yeast reconstituted with a purified complex of Sec proteins and Kar2p. Cell *81*, 561-570.

Park, R., and Baines, J.D. (2006). Herpes simplex virus type 1 infection induces activation and recruitment of protein kinase C to the nuclear membrane and increased phosphorylation of lamin B. J Virol *80*, 494-504.

Pelham, H.R., and Jackson, R.J. (1976). An efficient mRNA-dependent translation system from reticulocyte lysates. Eur J Biochem *67*, 247-256.

Peter, M., Nakagawa, J., Doree, M., Labbe, J.C., and Nigg, E.A. (1990). In vitro disassembly of the nuclear lamina and M phase-specific phosphorylation of lamins by cdc2 kinase. Cell *61*, 591-602.

Pfaff, J., Rivera Monroy, J., Jamieson, C., Rajanala, K., Vilardi, F., Schwappach, B., and Kehlenbach, R.H. (2016). Emery-Dreifuss muscular dystrophy mutations impair TRC40-mediated targeting of emerin to the inner nuclear membrane. J Cell Sci *129*, 502-516.

Pickart, C.M. (2004). Back to the future with ubiquitin. Cell *116*, 181-190.

Pollard, V.W., Michael, W.M., Nakielny, S., Siomi, M.C., Wang, F., and Dreyfuss, G. (1996). A novel receptor-mediated nuclear protein import pathway. Cell *86*, 985-994.

Port, S.A., Mendes, A., Valkova, C., Spillner, C., Fahrenkrog, B., Kaether, C., and Kehlenbach, R.H. (2016). The Oncogenic Fusion Proteins SET-Nup214 and Sequestosome-1 (SQSTM1)-Nup214 Form Dynamic Nuclear Bodies and Differentially Affect Nuclear Protein and Poly(A)+ RNA Export. J Biol Chem *291*, 23068-23083.

Powell, L., and Burke, B. (1990). Internuclear exchange of an inner nuclear membrane protein (p55) in heterokaryons: in vivo evidence for the interaction of p55 with the nuclear lamina. J Cell Biol *111*, 2225-2234.

Powis, K., Schrul, B., Tienson, H., Gostimskaya, I., Breker, M., High, S., Schuldiner, M., Jakob, U., and Schwappach, B. (2013). Get3 is a holdase chaperone and moves to deposition sites for aggregated proteins when membrane targeting is blocked. J Cell Sci *126*, 473-483.

Prinz, A., Behrens, C., Rapoport, T.A., Hartmann, E., and Kalies, K.U. (2000). Evolutionarily conserved binding of ribosomes to the translocation channel via the large ribosomal RNA. Embo J *19*, 1900-1906.

Ptak, C., Aitchison, J.D., and Wozniak, R.W. (2014). The multifunctional nuclear pore complex: a platform for controlling gene expression. Curr Opin Cell Biol *28*, 46-53.

Purves, W.K., Sadava, D., Orians, G.H., and Heller, H.C. (2006a). Biologie. Spektrum Akademischer Verlag *7. Auflage*.

Purves, W.K., Sadava, D., Orians, G.H., and Heller, H.C. (2006b). Biologie. Spektrum Akademischer Verlag *7. Auflage*.

Rabu, C., Schmid, V., Schwappach, B., and High, S. (2009). Biogenesis of tail-anchored proteins: the beginning for the end? J Cell Sci *122*, 3605-3612.

Rabu, C., Wipf, P., Brodsky, J.L., and High, S. (2008). A precursor-specific role for Hsp40/Hsc70 during tail-anchored protein integration at the endoplasmic reticulum. J Biol Chem *283*, 27504-27513.

Radu, A., Blobel, G., and Moore, M.S. (1995a). Identification of a protein complex that is required for nuclear protein import and mediates docking of import substrate to distinct nucleoporins. Proc Natl Acad Sci U S A *92*, 1769-1773.

Radu, A., Moore, M.S., and Blobel, G. (1995b). The peptide repeat domain of nucleoporin Nup98 functions as a docking site in transport across the nuclear pore complex. Cell *81*, 215-222.

Rapoport, T.A. (1992). Transport of proteins across the endoplasmic reticulum membrane. Science *258*, 931-936.

Rehm, H., and Letzel, T. (2010). Der Experimentator: Proteinbiochemie/Proteomics. Spektrum Akademischer Verlag *6. Auflage*.

Reichelt, R., Holzenburg, A., Buhle, E.L., Jr., Jarnik, M., Engel, A., and Aebi, U. (1990). Correlation between structure and mass distribution of the nuclear pore complex and of distinct pore complex components. J Cell Biol *110*, 883-894.

Reynolds, A.E., Ryckman, B.J., Baines, J.D., Zhou, Y., Liang, L., and Roller, R.J. (2001). U(L)31 and U(L)34 proteins of herpes simplex virus type 1 form a complex that accumulates at the nuclear rim and is required for envelopment of nucleocapsids. J Virol *75*, 8803-8817.

Ribbeck, K., and Görlich, D. (2001). Kinetic analysis of translocation through nuclear pore complexes. Embo J *20*, 1320-1330.

Ribbeck, K., and Görlich, D. (2002). The permeability barrier of nuclear pore complexes appears to operate via hydrophobic exclusion. Embo J *21*, 2664-2671.

Ribbeck, K., Lipowsky, G., Kent, H.M., Stewart, M., and Gorlich, D. (1998). NTF2 mediates nuclear import of Ran. Embo J *17*, 6587-6598.

Richards, S.A., Lounsbury, K.M., and Macara, I.G. (1995). The C terminus of the nuclear RAN/TC4 GTPase stabilizes the GDP-bound state and mediates interactions with RCC1, RAN-GAP, and HTF9A/RANBP1. J Biol Chem *270*, 14405-14411.

Riddick, G., and Macara, I.G. (2005). A systems analysis of importin-{alpha}-{beta} mediated nuclear protein import. J Cell Biol *168*, 1027-1038.

Rivera-Monroy, J. (2017). Role of WRB protein in cardiac function. PhD Thesis.

Rivera-Monroy, J., Musiol, L., Unthan-Fechner, K., Farkas, A., Clancy, A., Coy-Vergara, J., Weill, U., Gockel, S., Lin, S.Y., Corey, D.P.*, et al.* (2016). Mice lacking WRB reveal differential biogenesis requirements of tail-anchored proteins in vivo. Sci Rep *6*, 39464.

Robbins, J., Dilworth, S.M., Laskey, R.A., and Dingwall, C. (1991). Two interdependent basic domains in nucleoplasmin nuclear targeting sequence: identification of a class of bipartite nuclear targeting sequence. Cell *64*, 615-623.

Roboti, P., and High, S. (2012). The oligosaccharyltransferase subunits OST48, DAD1 and KCP2 function as ubiquitous and selective modulators of mammalian N-glycosylation. J Cell Sci *125*, 3474-3484.

Rodriguez-Enfedaque, A., Bouleau, S., Laurent, M., Courtois, Y., Mignotte, B., Vayssiere, J.L., and Renaud, F. (2009). FGF1 nuclear translocation is required for both its neurotrophic activity and its p53-dependent apoptosis protection. Biochim Biophys Acta *1793*, 1719-1727.

Romisch, K. (2005). Endoplasmic reticulum-associated degradation. Annu Rev Cell Dev Biol *21*, 435-456.

Sabatini, D.M., Erdjument-Bromage, H., Lui, M., Tempst, P., and Snyder, S.H. (1994). RAFT1: a mammalian protein that binds to FKBP12 in a rapamycin-dependent fashion and is homologous to yeast TORs. Cell *78*, 35-43.

Saiki, R.K., Gelfand, D.H., Stoffel, S., Scharf, S.J., Higuchi, R., Horn, G.T., Mullis, K.B., and Erlich, H.A. (1988). Primer-directed enzymatic amplification of DNA with a thermostable DNA polymerase. Science *239*, 487-491.

Saksena, S., Summers, M.D., Burks, J.K., Johnson, A.E., and Braunagel, S.C. (2006). Importin-alpha-16 is a translocon-associated protein involved in sorting membrane proteins to the nuclear envelope. Nat Struct Mol Biol *13*, 500-508.

Salinovich, O., and Montelaro, R.C. (1986). Reversible staining and peptide mapping of proteins transferred to nitrocellulose after separation by sodium dodecylsulfate-polyacrylamide gel electrophoresis. Anal Biochem *156*, 341-347.

Sambrook, J., and Russell, D.W. (2006). SDS-Polyacrylamide Gel Electrophoresis of Proteins. CSH Protoc *2006*.

Sanger, F., Nicklen, S., and Coulson, A.R. (1977). DNA sequencing with chain-terminating inhibitors. Proc Natl Acad Sci U S A *74*, 5463-5467.

Schirmer, E.C., Florens, L., Guan, T., Yates, J.R., 3rd, and Gerace, L. (2003). Nuclear membrane proteins with potential disease links found by subtractive proteomics. Science *301*, 1380-1382.

Schirmer, E.C., and Gerace, L. (2005). The nuclear membrane proteome: extending the envelope. Trends Biochem Sci *30*, 551-558.

Schmitz, S. (2011). Der Experimentator: Zellkultur. Spektrum Akademischer Verlag *3. Auflage*.

Schnell, D.J., and Hebert, D.N. (2003). Protein translocons: multifunctional mediators of protein translocation across membranes. Cell *112*, 491-505.

Schneppenheim, R., Budde, U., Dahlmann, N., and Rautenberg, P. (1991). Luminography--a new, highly sensitive visualization method for electrophoresis. Electrophoresis *12*, 367-372.

Schooley, A., Vollmer, B., and Antonin, W. (2012). Building a nuclear envelope at the end of mitosis: coordinating membrane reorganization, nuclear pore complex assembly, and chromatin de-condensation. Chromosoma *121*, 539-554.

Schuldiner, M., Metz, J., Schmid, V., Denic, V., Rakwalska, M., Schmitt, H.D., Schwappach, B., and Weissman, J.S. (2008). The GET complex mediates insertion of tail-anchored proteins into the ER membrane. Cell *134*, 634-645.

Schwartz, T.U. (2016). The Structure Inventory of the Nuclear Pore Complex. J Mol Biol *428*, 1986-2000.

Schwoebel, E.D., Talcott, B., Cushman, I., and Moore, M.S. (1998). Ran-dependent signal-mediated nuclear import does not require GTP hydrolysis by Ran. J Biol Chem *273*, 35170-35175.

Seidman, C.E., and Struhl, K. (2001). Introduction of plasmid DNA into cells. Curr Protoc Protein Sci *Appendix 4*, 4d.

Shackleton, S., Collas, P., and Schirmer, E. (2016). The Nuclear Envelope: Methods and Protocols. Humana Press.

Shao, S., and Hegde, R.S. (2011a). A calmodulin-dependent translocation pathway for small secretory proteins. Cell *147*, 1576-1588.

Shao, S., and Hegde, R.S. (2011b). Membrane protein insertion at the endoplasmic reticulum. Annu Rev Cell Dev Biol *27*, 25-56.

Shimi, T., Butin-Israeli, V., Adam, S.A., and Goldman, R.D. (2010). Nuclear lamins in cell regulation and disease. Cold Spring Harb Symp Quant Biol *75*, 525-531.

Shimi, T., Koujin, T., Segura-Totten, M., Wilson, K.L., Haraguchi, T., and Hiraoka, Y. (2004). Dynamic interaction between BAF and emerin revealed by FRAP, FLIP, and FRET analyses in living HeLa cells. J Struct Biol *147*, 31-41.

Shumaker, D.K., Lee, K.K., Tanhehco, Y.C., Craigie, R., and Wilson, K.L. (2001). LAP2 binds to BAF.DNA complexes: requirement for the LEM domain and modulation by variable regions. Embo J *20*, 1754-1764.

Siegel, V., and Walter, P. (1986). Removal of the Alu structural domain from signal recognition particle leaves its protein translocation activity intact. Nature *320*, 81-84.

Singh, K., Sun, S., and Vezina, C. (1979). Rapamycin (AY-22,989), a new antifungal antibiotic. IV. Mechanism of action. J Antibiot (Tokyo) *32*, 630-645.

Skjerpen, C.S., Wesche, J., and Olsnes, S. (2002). Identification of ribosome-binding protein p34 as an intracellular protein that binds acidic fibroblast growth factor. J Biol Chem *277*, 23864-23871.

Smith, A., Brownawell, A., and Macara, I.G. (1998). Nuclear import of Ran is mediated by the transport factor NTF2. Curr Biol *8*, 1403-1406.

Smoyer, C.J., Katta, S.S., Gardner, J.M., Stoltz, L., McCroskey, S., Bradford, W.D., McClain, M., Smith, S.E., Slaughter, B.D., Unruh, J.R.*, et al.* (2016). Analysis of membrane proteins localizing to the inner nuclear envelope in living cells. J Cell Biol *215*, 575-590.

Smoyer, C.J., Smith, S.E., Gardner, J.M., McCroskey, S., Unruh, J.R., and Jaspersen, S.L. (2019). Distribution of Proteins at the Inner Nuclear Membrane Is Regulated by the Asi1 E3 Ligase in Saccharomyces cerevisiae. Genetics.

Solovei, I., Thanisch, K., and Feodorova, Y. (2016). How to rule the nucleus: divide et impera. Curr Opin Cell Biol *40*, 47-59.

Solsbacher, J., Maurer, P., Bischoff, F.R., and Schlenstedt, G. (1998). Cse1p is involved in export of yeast importin alpha from the nucleus. Mol Cell Biol *18*, 6805-6815.

Soullam, B., and Worman, H.J. (1993). The amino-terminal domain of the lamin B receptor is a nuclear envelope targeting signal. J Cell Biol *120*, 1093-1100.

Soullam, B., and Worman, H.J. (1995). Signals and structural features involved in integral membrane protein targeting to the inner nuclear membrane. J Cell Biol *130*, 15-27.

Spang, A., and Schekman, R. (1998). Reconstitution of retrograde transport from the Golgi to the ER in vitro. J Cell Biol *143*, 589-599.

Speese, S.D., Ashley, J., Jokhi, V., Nunnari, J., Barria, R., Li, Y., Ataman, B., Koon, A., Chang, Y.T., Li, Q.*, et al.* (2012). Nuclear envelope budding enables large ribonucleoprotein particle export during synaptic Wnt signaling. Cell *149*, 832-846.

Spurlino, J.C., Lu, G.Y., and Quiocho, F.A. (1991). The 2.3-A resolution structure of the maltose- or maltodextrin-binding protein, a primary receptor of bacterial active transport and chemotaxis. J Biol Chem *266*, 5202-5219.

Stade, K., Ford, C.S., Guthrie, C., and Weis, K. (1997). Exportin 1 (Crm1p) is an essential nuclear export factor. Cell *90*, 1041-1050.

Stan, R., McLaughlin, M.M., Cafferkey, R., Johnson, R.K., Rosenberg, M., and Livi, G.P. (1994). Interaction between FKBP12-rapamycin and TOR involves a conserved serine residue. J Biol Chem *269*, 32027-32030.

Starr, D.A., and Fridolfsson, H.N. (2010). Interactions between nuclei and the cytoskeleton are mediated by SUN-KASH nuclear-envelope bridges. Annu Rev Cell Dev Biol *26*, 421-444.

Stefanovic, S., and Hegde, R.S. (2007). Identification of a targeting factor for posttranslational membrane protein insertion into the ER. Cell *128*, 1147-1159.

Stoffler, D., Fahrenkrog, B., and Aebi, U. (1999). The nuclear pore complex: from molecular architecture to functional dynamics. Curr Opin Cell Biol *11*, 391-401.

Suntharalingam, M., and Wente, S.R. (2003). Peering through the pore: nuclear pore complex structure, assembly, and function. Dev Cell *4*, 775-789.

Tapley, E.C., Ly, N., and Starr, D.A. (2011). Multiple mechanisms actively target the SUN protein UNC-84 to the inner nuclear membrane. Mol Biol Cell *22*, 1739-1752.

Tatematsu, M., Funami, K., Ishii, N., Seya, T., Obuse, C., and Matsumoto, M. (2015). LRRC59 Regulates Trafficking of Nucleic Acid-Sensing TLRs from the Endoplasmic Reticulum via Association with UNC93B1. J Immunol *195*, 4933-4942.

Tazawa, S., Unuma, M., Tondokoro, N., Asano, Y., Ohsumi, T., Ichimura, T., and Sugano, H. (1991). Identification of a membrane protein responsible for ribosome binding in rough microsomal membranes. J Biochem *109*, 89-98.

Terp, M.G., Lund, R.R., Jensen, O.N., Leth-Larsen, R., and Ditzel, H.J. (2012). Identification of markers associated with highly aggressive metastatic phenotypes using quantitative comparative proteomics. Cancer Genomics Proteomics *9*, 265-273.

Terry, L.J., and Wente, S.R. (2009). Flexible gates: dynamic topologies and functions for FG nucleoporins in nucleocytoplasmic transport. Eukaryot Cell *8*, 1814-1827.

Tetenbaum-Novatt, J., and Rout, M.P. (2010). The mechanism of nucleocytoplasmic transport through the nuclear pore complex. Cold Spring Harb Symp Quant Biol *75*, 567-584.

Theerthagiri, G., Eisenhardt, N., Schwarz, H., and Antonin, W. (2010). The nucleoporin Nup188 controls passage of membrane proteins across the nuclear pore complex. J Cell Biol *189*, 1129-1142.

Therizols, P., Fairhead, C., Cabal, G.G., Genovesio, A., Olivo-Marin, J.C., Dujon, B., and Fabre, E. (2006). Telomere tethering at the nuclear periphery is essential for efficient DNA double strand break repair in subtelomeric region. J Cell Biol *172*, 189-199.

Towbin, H., Staehelin, T., and Gordon, J. (1979). Electrophoretic transfer of proteins from polyacrylamide gels to nitrocellulose sheets: procedure and some applications. Proc Natl Acad Sci U S A *76*, 4350-4354.

Tsai, B., Ye, Y., and Rapoport, T.A. (2002). Retro-translocation of proteins from the endoplasmic reticulum into the cytosol. Nat Rev Mol Cell Biol *3*, 246-255.

Tsekrekou, M., Stratigi, K., and Chatzinikolaou, G. (2017). The Nucleolus: In Genome Maintenance and Repair. Int J Mol Sci *18*.

Turgay, Y., Ungricht, R., Rothballer, A., Kiss, A., Csucs, G., Horvath, P., and Kutay, U. (2010). A classical NLS and the SUN domain contribute to the targeting of SUN2 to the inner nuclear membrane. Embo J *29*, 2262-2275.

Ulbert, S., Platani, M., Boue, S., and Mattaj, I.W. (2006). Direct membrane protein-DNA interactions required early in nuclear envelope assembly. J Cell Biol *173*, 469-476.

Ungar, D., and Hughson, F.M. (2003). SNARE protein structure and function. Annu Rev Cell Dev Biol *19*, 493-517.

Ungricht, R., Klann, M., Horvath, P., and Kutay, U. (2015). Diffusion and retention are major determinants of protein targeting to the inner nuclear membrane. J Cell Biol *209*, 687-703.

Ungricht, R., and Kutay, U. (2015). Establishment of NE asymmetry-targeting of membrane proteins to the inner nuclear membrane. Curr Opin Cell Biol *34*, 135-141.

Ungricht, R., and Kutay, U. (2017). Mechanisms and functions of nuclear envelope remodelling. Nat Rev Mol Cell Biol *18*, 229-245.

Vagin, O., Kraut, J.A., and Sachs, G. (2009). Role of N-glycosylation in trafficking of apical membrane proteins in epithelia. Am J Physiol Renal Physiol *296*, F459-469.

Van de Vosse, D.W., Wan, Y., Wozniak, R.W., and Aitchison, J.D. (2011). Role of the nuclear envelope in genome organization and gene expression. Wiley Interdiscip Rev Syst Biol Med *3*, 147-166.

Van den Berg, B., Clemons, W.M., Jr., Collinson, I., Modis, Y., Hartmann, E., Harrison, S.C., and Rapoport, T.A. (2004). X-ray structure of a protein-conducting channel. Nature *427*, 36-44.

Van Puyenbroeck, V., and Vermeire, K. (2018). Inhibitors of protein translocation across membranes of the secretory pathway: novel antimicrobial and anticancer agents. Cell Mol Life Sci *75*, 1541-1558.

Vaughan, A., Alvarez-Reyes, M., Bridger, J.M., Broers, J.L., Ramaekers, F.C., Wehnert, M., Morris, G.E., Whitfield, W.G.F., and Hutchison, C.J. (2001). Both emerin and lamin C depend on lamin A for localization at the nuclear envelope. J Cell Sci *114*, 2577-2590.

Vézina C., K.A., Sehgal S. N. (1975). Rapamycin (AY-22,989), a new antifungal antibiotic. I. Taxonomy of the producing streptomycete and isolation of the active principle. J Antibiotics *28*, 721-726.

Vilardi, F., Lorenz, H., and Dobberstein, B. (2011). WRB is the receptor for TRC40/Asna1-mediated insertion of tail-anchored proteins into the ER membrane. J Cell Sci *124*, 1301-1307.

Vilardi, F., Stephan, M., Clancy, A., Janshoff, A., and Schwappach, B. (2014). WRB and CAML are necessary and sufficient to mediate tail-anchored protein targeting to the ER membrane. PLoS One *9*, e85033.

Vollmer, B., and Antonin, W. (2014). The diverse roles of the Nup93/Nic96 complex proteins - structural scaffolds of the nuclear pore complex with additional cellular functions. Biol Chem *395*, 515-528.

von Appen, A., and Beck, M. (2016). Structure Determination of the Nuclear Pore Complex with Three-Dimensional Cryo electron Microscopy. J Mol Biol *428*, 2001-2010.

Walde, S., and Kehlenbach, R.H. (2010). The Part and the Whole: functions of nucleoporins in nucleocytoplasmic transport. Trends Cell Biol *20*, 461-469.

Walter, P., and Blobel, G. (1980). Purification of a membrane-associated protein complex required for protein translocation across the endoplasmic reticulum. Proc Natl Acad Sci U S A *77*, 7112-7116.

Walter, P., and Blobel, G. (1981). Translocation of proteins across the endoplasmic reticulum III. Signal recognition protein (SRP) causes signal sequence-dependent and site-specific arrest of chain elongation that is released by microsomal membranes. J Cell Biol *91*, 557-561.

Walter, P., and Blobel, G. (1982). Signal recognition particle contains a 7S RNA essential for protein translocation across the endoplasmic reticulum. Nature *299*, 691-698.

Walter, P., and Blobel, G. (1983). Preparation of microsomal membranes for cotranslational protein translocation. Methods Enzymol *96*, 84-93.

Wandke, C., and Kutay, U. (2013). Enclosing chromatin: reassembly of the nucleus after open mitosis. Cell *152*, 1222-1225.

Wang, F., Chan, C., Weir, N.R., and Denic, V. (2014). The Get1/2 transmembrane complex is an endoplasmic-reticulum membrane protein insertase. Nature *512*, 441-444.

Wang, T., Li, L., and Hong, W. (2017). SNARE proteins in membrane trafficking. Traffic *18*, 767-775.

Wang, Y.N., Yamaguchi, H., Huo, L., Du, Y., Lee, H.J., Lee, H.H., Wang, H., Hsu, J.M., and Hung, M.C. (2010). The translocon Sec61beta localized in the inner nuclear membrane transports membrane-embedded EGF receptor to the nucleus. J Biol Chem *285*, 38720-38729.

Wattenberg, B., and Lithgow, T. (2001). Targeting of C-terminal (tail)-anchored proteins: understanding how cytoplasmic activities are anchored to intracellular membranes. Traffic *2*, 66-71.

Weberruss, M., and Antonin, W. (2016). Perforating the nuclear boundary - how nuclear pore complexes assemble. J Cell Sci *129*, 4439-4447.

Weiner, M.P., Costa, G.L., Schoettlin, W., Cline, J., Mathur, E., and Bauer, J.C. (1994). Site-directed mutagenesis of double-stranded DNA by the polymerase chain reaction. Gene *151*, 119-123.

Weisshart, K. (2014). The Basic Principle of Airyscanning. Technology Note, ZEISS.

Wente, S.R., and Rout, M.P. (2010). The nuclear pore complex and nuclear transport. Cold Spring Harb Perspect Biol *2*, a000562.

Wesche, J., Malecki, J., Wiedlocha, A., Ehsani, M., Marcinkowska, E., Nilsen, T., and Olsnes, S. (2005). Two nuclear localization signals required for transport from the cytosol to the nucleus of externally added FGF-1 translocated into cells. Biochemistry *44*, 6071-6080.

Whited, A.M., and Johs, A. (2015). The interactions of peripheral membrane proteins with biological membranes. Chem Phys Lipids *192*, 51-59.

Wilkie, G.S., Korfali, N., Swanson, S.K., Malik, P., Srsen, V., Batrakou, D.G., de las Heras, J., Zuleger, N., Kerr, A.R., Florens, L.*, et al.* (2011). Several novel nuclear envelope transmembrane proteins identified in skeletal muscle have cytoskeletal associations. Mol Cell Proteomics *10*, M110.003129.

Wilson, K.L., and Foisner, R. (2010). Lamin-binding Proteins. Cold Spring Harb Perspect Biol *2*, a000554.

Winey, M., Yarar, D., Giddings, T.H., Jr., and Mastronarde, D.N. (1997). Nuclear pore complex number and distribution throughout the Saccharomyces cerevisiae cell cycle by three-dimensional reconstruction from electron micrographs of nuclear envelopes. Mol Biol Cell *8*, 2119-2132.

Winnefeld, M., Grewenig, A., Schnolzer, M., Spring, H., Knoch, T.A., Gan, E.C., Rommelaere, J., and Cziepluch, C. (2006). Human SGT interacts with Bag-6/Bat-3/Scythe and cells with reduced levels of either protein display persistence of few misaligned chromosomes and mitotic arrest. Exp Cell Res *312*, 2500-2514.

Worman, H.J., Evans, C.D., and Blobel, G. (1990). The lamin B receptor of the nuclear envelope inner membrane: a polytopic protein with eight potential transmembrane domains. J Cell Biol *111*, 1535-1542.

Wozniak, R.W., Bartnik, E., and Blobel, G. (1989). Primary structure analysis of an integral membrane glycoprotein of the nuclear pore. J Cell Biol *108*, 2083-2092.

Wu, J., Matunis, M.J., Kraemer, D., Blobel, G., and Coutavas, E. (1995). Nup358, a cytoplasmically exposed nucleoporin with peptide repeats, Ran-GTP binding sites, zinc fingers, a cyclophilin A homologous domain, and a leucine-rich region. J Biol Chem *270*, 14209-14213.

Wu, W., Lin, F., and Worman, H.J. (2002). Intracellular trafficking of MAN1, an integral protein of the nuclear envelope inner membrane. J Cell Sci *115*, 1361-1371.

Xu, X.M., Rose, A., Muthuswamy, S., Jeong, S.Y., Venkatakrishnan, S., Zhao, Q., and Meier, I. (2007). NUCLEAR PORE ANCHOR, the Arabidopsis homolog of Tpr/Mlp1/Mlp2/megator, is involved in mRNA export and SUMO homeostasis and affects diverse aspects of plant development. Plant Cell *19*, 1537-1548.

Yabal, M., Brambillasca, S., Soffientini, P., Pedrazzini, E., Borgese, N., and Makarow, M. (2003). Translocation of the C terminus of a tail-anchored protein across the endoplasmic reticulum membrane in yeast mutants defective in signal peptide-driven translocation. J Biol Chem *278*, 3489-3496.

Yamagata, A., Mimura, H., Sato, Y., Yamashita, M., Yoshikawa, A., and Fukai, S. (2010). Structural insight into the membrane insertion of tail-anchored proteins by Get3. Genes Cells *15*, 29-41.

Yamagata, T., Tsuru, T., Momoi, M.Y., Suwa, K., Nozaki, Y., Mukasa, T., Ohashi, H., Fukushima, Y., and Momoi, T. (1997). Genome organization of human 48-kDa oligosaccharyltransferase (DDOST). Genomics *45*, 535-540.

Yamamoto, Y., and Sakisaka, T. (2012). Molecular machinery for insertion of tail-anchored membrane proteins into the endoplasmic reticulum membrane in mammalian cells. Mol Cell *48*, 387-397.

Yang, H.J., Iwamoto, M., Hiraoka, Y., and Haraguchi, T. (2017). Function of nuclear membrane proteins in shaping the nuclear envelope integrity during closed mitosis. J Biochem *161*, 471-477.

Yang, L., Guan, T., and Gerace, L. (1997). Integral membrane proteins of the nuclear envelope are dispersed throughout the endoplasmic reticulum during mitosis. J Cell Biol *137*, 1199-1210.

Yang, W., Gelles, J., and Musser, S.M. (2004). Imaging of single-molecule translocation through nuclear pore complexes. Proc Natl Acad Sci U S A *101*, 12887-12892.

Yang, W., and Musser, S.M. (2006). Nuclear import time and transport efficiency depend on importin beta concentration. J Cell Biol *174*, 951-961.

Yokoyama, N., Hayashi, N., Seki, T., Pante, N., Ohba, T., Nishii, K., Kuma, K., Hayashida, T., Miyata, T., Aebi, U.*, et al.* (1995). A giant nucleopore protein that binds Ran/TC4. Nature *376*, 184-188.

Zhan, X., Hu, X., Friedman, S., and Maciag, T. (1992). Analysis of endogenous and exogenous nuclear translocation of fibroblast growth factor-1 in NIH 3T3 cells. Biochem Biophys Res Commun *188*, 982-991.

Zhen, Y., Sorensen, V., Skjerpen, C.S., Haugsten, E.M., Jin, Y., Walchli, S., Olsnes, S., and Wiedlocha, A. (2012). Nuclear import of exogenous FGF1 requires the ER-protein LRRC59 and the importins Kpnalpha1 and Kpnbeta1. Traffic *13*, 650-664.

Zuleger, N., Kelly, D.A., Richardson, A.C., Kerr, A.R., Goldberg, M.W., Goryachev, A.B., and Schirmer, E.C. (2011). System analysis shows distinct mechanisms and common principles of nuclear envelope protein dynamics. J Cell Biol *193*, 109-123.

Zuleger, N., Kerr, A.R., and Schirmer, E.C. (2012). Many mechanisms, one entrance: membrane protein translocation into the nucleus. Cell Mol Life Sci *69*, 2205-2216.

List of Figures

List of Tables

Appendix

A. Synthesized Genes

Sequence of LRRC59_mut_210-243 (5`→3`)

ATGACCAAGGCCGGTAGCAAGGGCGGGAACCTCCGCGACAAGCTGGACGGCAACGAACTGGACCTGAGCCTCAGCGACCTGAA
TGAGGTCCCGGTGAAGGAGCTGGCTGCCCTTCCAAAGGCCACCATCCTGGATCTGTCTTGTAATAAACTGACTACTCTACCGT
CGGATTTCTGTGGCCTCACACACCTGGTGAAGCTAGACCTGAGTAAGAACAAGCTGCAGCAGCTGCCAGCAGACTTTGGCCGT
CTGGTCAACCTCCAGCACCTGGATCTCCTCAACAACAAGCTGGTCACCTTGCCTGTCAGCTTTGCTCAGCTCAAGAACCTGAA
GTGGTTGGACCTGAAGGATAACCCCCTGGATCCTGTCCTGGCCAAGGTGGCAGGTGACTGCTTGGATGAGAAGCAGTGTAAGC
AGTGTGCAAACAAGGTGTTACAGCACATGAAGGCCGTGCAGGCAGATCAGGAGCGGGAGAGGCAGCGGCGGCTGGAAGTAGAA
CGTGAGGCAGAGAAGAAGCGTGAGGCTAAGCAGCGAGCTAAGGAAGCTCAGGAGCGGGAACTGCGGAAGCGGGAGAAGGCGGA
AGAGAAGGAGCGCCGGAGAAAGGAGTATGATGCCCTCAAAGCAGCCGCGGCGGAGCAGGAGGCGGCACCTGCTGCGGAAGCAA
ATCAGGCCCCGAAATCTAAGTCTGGCTCCCGTCCCCGCAAGCCACCACCCGCGGCGCACACTGCTTCCTGGGCTGTGCTGAAG
CTGCTGCTGCTGCTGTTGCTATTTGGTGTGGCGGGAGGGCTGGTTGCTTGTCGGGTGACAGAGCTGCAGCAGCAGCCCCTCTG
CACCAGCGTGAACACCATCTATGACAATGCGGTCCAGGGTCTACGCCGCCATGAGATCCTCCAGTGGGTCCTCCAGACCGACT
CTCAGCAG

Sequence of Nup210_AA1830-1887 (5`→3`)

AAACCATGGAAATGACTGTCTGCACGCCCCGGGATCTTGCTGTGCCTGCAGCCCTCACGCCTCGAGCCAGCCCTGGACACAGC
CCCCACTATTTCGCTGCCTCATCACCCACATCTCCCAATGCATTGCCTCCTGCTCGCAAAGCCAGCCCTCCCTCAGGGCTGTG
GAGCCCAGCCTATGCCTCCCACTGAGAATTCTTTTT

Sequence of EcoRI-P2X2-HindIII (5`→3`)

AAAAAGAATTCATGGTCCGGCGCTTGGCCCGGGGCTGCTGGTCCGCGTTCTGGGACTACGAGACGCCTAAGGTGATCGTGGTG
CGGAATCGGCGCCTGGGATTCGTGCACCGCATGGTGCAGCTTCTCATCCTGCTTTACTTCGTGTGGTACGTCTTCATCGTGCA
GAAAAGCTACCAGGACAGCGAGACCGGACCGGAGAGCTCCATCATCACCAAAGTCAAGGGGATCACCATGTCGGAAGACAAAG
TGTGGGACGTGGAGGAATACGTAAAGCCCCCGGAGGGGGGCAGTGTAGTCAGCATCATCACCAGGATCGAGGTTACCCCTTCC
CAGACCTTGGGAACATGCCCAGAGAGCATGAGGGTTCACAGCTCTACCTGCCATTCAGACGACGACTGTATTGCCGGACAGCT
GGACATGCAAGGCAATGGGATTCGCACAGGGCACTGTGTACCCTATTACCATGGGGACTCCAAGACCTGCGAGGTGTCAGCCT
GGTGCCCGGTGGAGGATGGAACTTCTGACAACCATTTTCTGGGTAAAATGGCCCCAAATTTCACCATCCTCATCAAGAACAGC
ATCCACTACCCCAAGTTCAAGTTCTCAAAGGGCAACATTGCAAGCCAGAAGAGTGACTACCTCAAGCATTGCACATTTGATCA
GGACTCTGACCCATACTGTCCCATCTTCAGGCTGGGTTTCATTGTTGAGAAGGCAGGAGAGAACTTCACAGAACTGGCACACA
AGGGCGGTGTCATTGGAGTCATCATCAACTGGAACTGTGACCTGGACTTGTCTGAATCAGAGTGCAACCCCAAATATTCTTTC
CGGAGGCTCGACCCCAAGTATGACCCTGCCTCCTCAGGCTACAACTTCAGGTTTGCCAAGTATTACAAGATAAACGGCACTAC
CACCACTCGAACTCTCATCAAAGCCTATGGGATTCGAATCGATGTTATCGTGCATGGACAGGCAGGGAAATTCAGTCTCATTC
CCACCATCATCAATCTGGCCACTGCTCTGACCTCCATCGGGGTGGGCTCCTTCCTGTGTGACTGGATTTTGTTAACGTTCATG
AACAAAAACAAGCTCTACAGCCATAAGAAGTTCGACAAGGTGCGTACTCCAAAGCATCCCTCAAGTAGATGGCCTGTGACCCT
TGCCCTTGTCTTGGGCCAGATCCCTCCCCCACCTAGTCACTACTCCCAGGATCAGCCACCCAGCCCTCCATCAGGTGAAGGAC
CAACTTTGGGAGAAGGGGCAGAGCTACCACTGGCTGTCCAGTCTCCTCGGCCTTGCTCCATCTCTGCTCTGACTGAGCAGGTG
GTGGACACACTTGGCCAGCATATGGGACAAAGACCTCCTGTCCCTGAGCCTTCCCAACAGGACTCCACATCCACGGACCCCAA
AGGTTTGGCCCAACTTTGAAAGCTTTTT

B. Supplemental figures

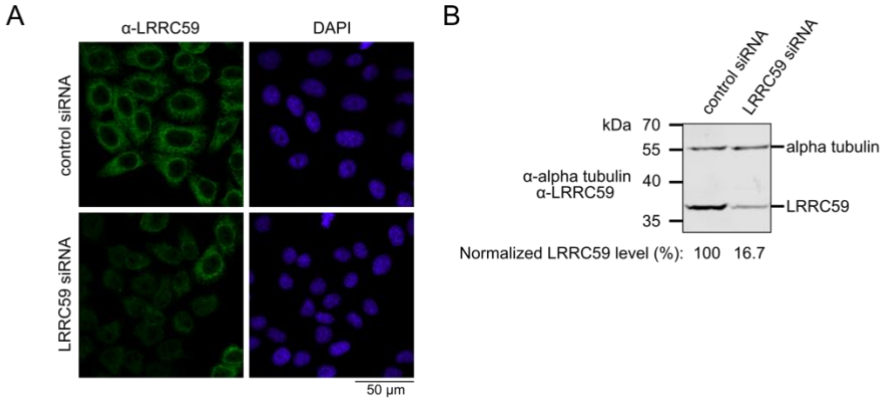

Figure S 1: The LRRC59 antibody is specific.
HeLa cells were transfected with control or LRRC59 siRNAs for 48 hours, fixed and analyzed by indirect immunofluorescence using the LRRC59-antibody (A) or by SDS-PAGE and immunoblotting using antibodies against LRRC59 and alpha tubulin (B). (A) DAPI marked the nucleic acids in fluorescence microscopy. Analysis by confocal microscopy. (B) Levels of LRRC59 were normalized to alpha tubulin. See also Blenski and Kehlenbach, 2019.

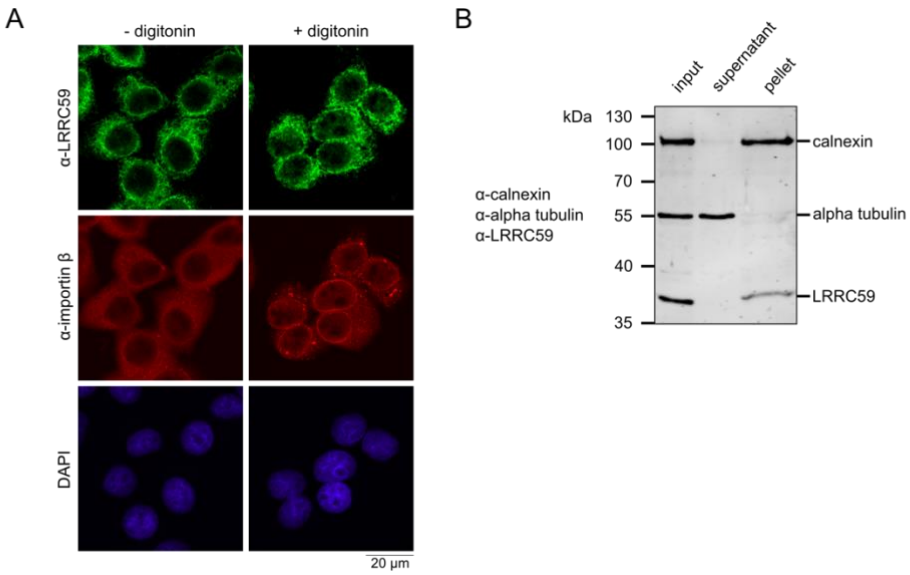

Figure S 2: LRRC59 is a membrane-bound protein.
(A) For the examination of soluble LRRC59, $5x10^6$ HeLa cells were seeded onto a 10 cm cell culture dish containing several coverslips. Cells were treated with (+) or without (-) digitonin. After fixation, cells were immunostained using antibodies against LRRC59 and as permeabilization control importin-β. DAPI marked the nucleic acids in fluorescence confocal microscopy. (B) HeLa cells were detached from the 10 cm cell culture dish. $1x10^6$ cells were resuspended in transport buffer. For the input, $5x10^5$ cells were mixed with SDS sample buffer. The remaining $5x10^5$ cells were permeabilized with digitonin for 5 minutes. After centrifugation, the supernatant was transferred into a new tube and supplemented with SDS sample buffer. The pellet was resuspended in SDS sample buffer. For analysis, proteins of 2,4% of input, supernatant and pellet were analyzed by SDS-PAGE, Western blotting and immunodetection using antibodies against LRRC59, alpha tubulin as control for the soluble fraction and calnexin as control for the membrane-bound fraction.

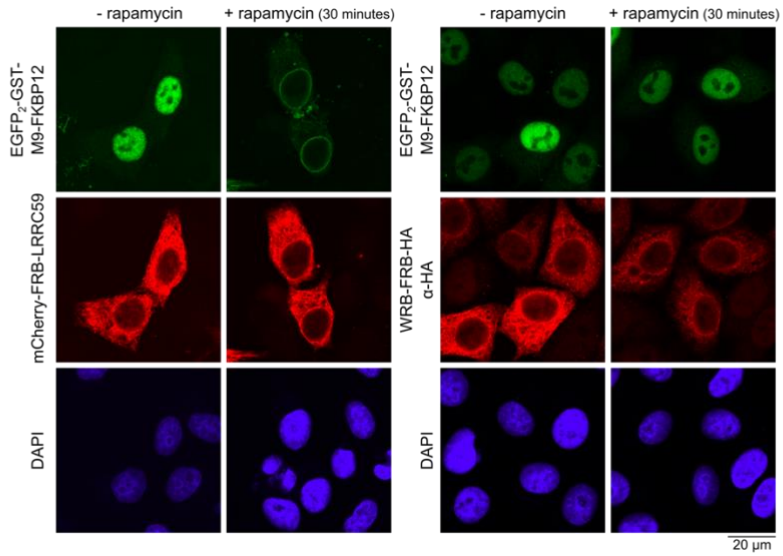

Figure S 3: Upon addition of rapamycin, $EGFP_2$-GST-M9-FKBP12 bound by mCherry-FRB-LRRC59 does not diffuse out of the nucleus.
HeLa cells were seeded on coverslips and co-transfected with plasmids coding for $EGFP_2$-GST-M9-FKBP12 together with mCherry-FRB-LRRC59 or WRB-FRB-HA. After 48 hours, cells were treated with (+) or without (-) rapamycin for 30 minutes. For immunodetection of WRB-FRB-HA, indirect immunostaining using antibodies against HA was performed, while mCherry-FRB-LRRC59 was directly analyzed by confocal microscopy. DAPI marked the nucleic acids in fluorescence microscopy.

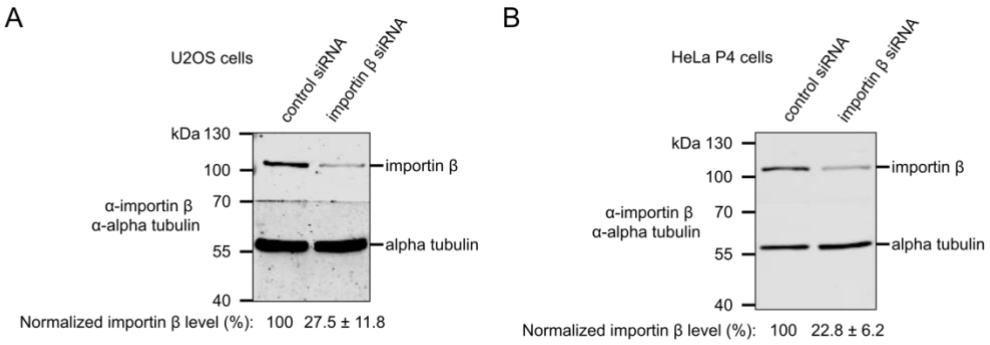

Figure S 4: Knockdown of importin β.
U2OS cells (A) or HeLa P4 cells (B) were treated with control or importin β siRNAs prior to analysis by SDS-PAGE, Western-blotting and detection of importin β and alpha tubulin. The mean and the standard deviations of the importin β levels of four (A) or nine (B) experiments, normalized to alpha tubulin, are indicated. For (A) see table S 2, for (B) see table S 3. See Blenski and Kehlenbach, 2019.

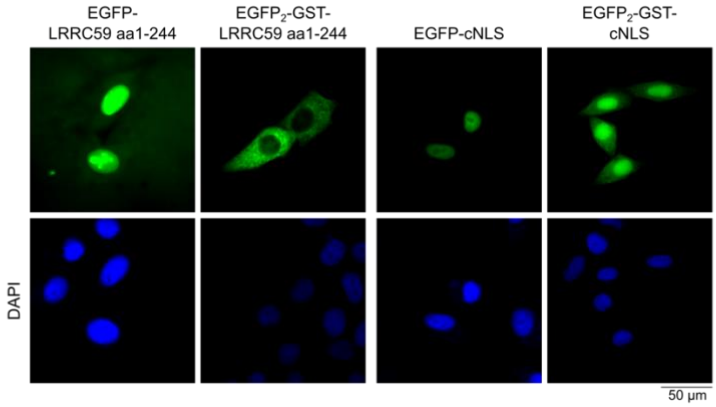

Figure S 5: Comparison of size-dependent localization of LRRC59 lacking a TMD and cNLS.
HeLa cells were transfected with 1 µg plasmids coding for EGFP-LRRC59 aa1-244, $EGFP_2$-GST-LRRC59 aa1-244, EGFP-cNLS or $EGFP_2$-GST-cNLS. After 48 hours, cells were fixed and directly analyzed by fluorescence microscopy using the Axioskop2 mot plus. DAPI marked the nucleic acids in fluorescence microscopy.

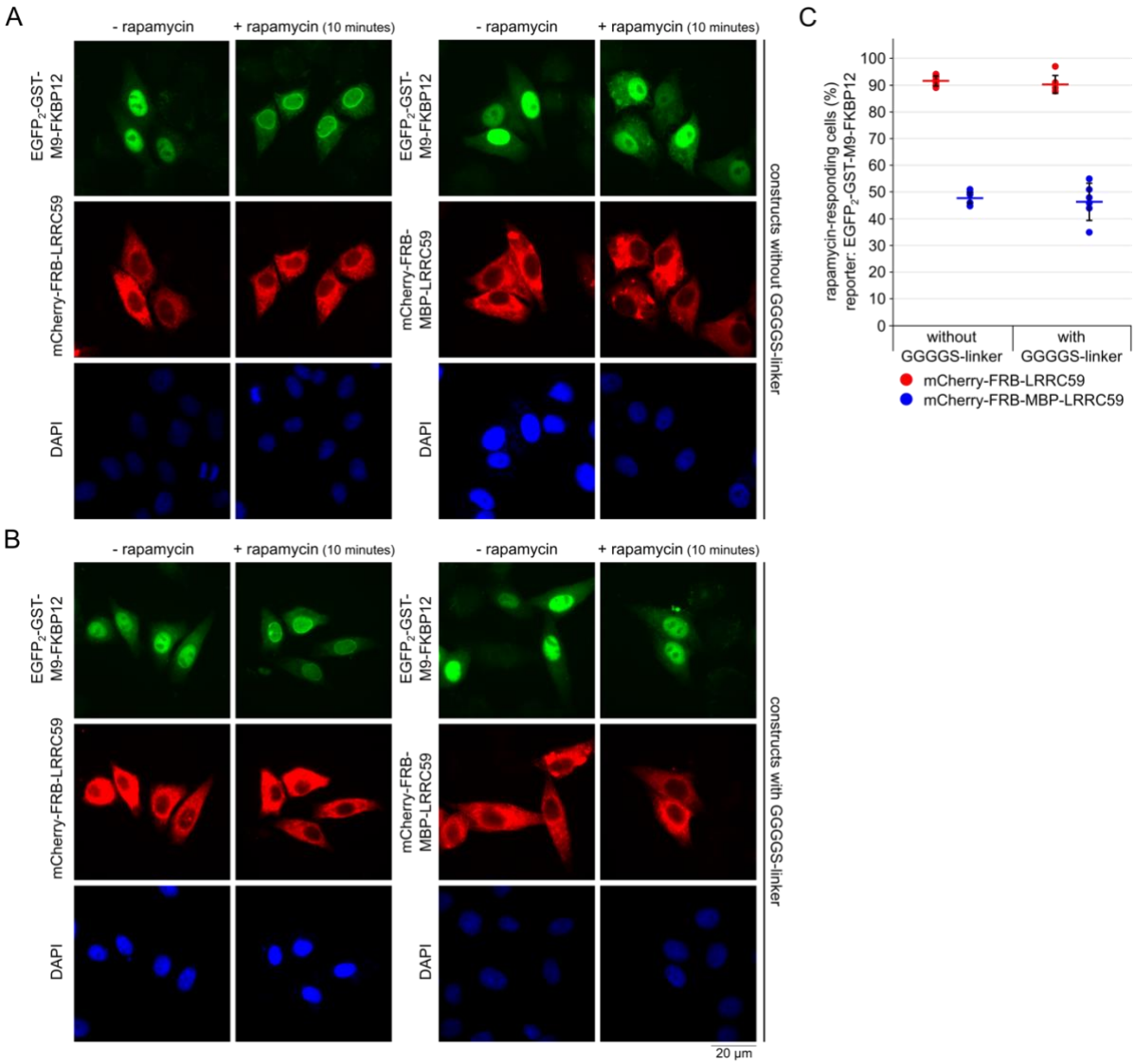

Figure S 6: Additional GGGGS-linker in the construct mCherry-FRB-MBP-LRRC59 do not change the number of rapamycin-responding cells.
HeLa cells were transfected with plasmids coding for $EGFP_2$-GST-M9-FKBP12 and mCherry-FRB-LRRC59 or mCherry-FRB-MBP-LRRC59 without linker between the domains (A) or with additional GGGGS-linker between all domains (B). After 48 hours, the cells were incubated with rapamycin for 10 minutes followed by fixation of the cells and direct analysis using the Zeiss microscope Axioskop2 mot plus. DAPI marked the nucleic acids in fluorescence microscopy. (C) Quantification of mean and the standard deviation of rapamycin-responding cells of (A) and (B) for three independent experiments with two replicates each counting 600 cells in total.

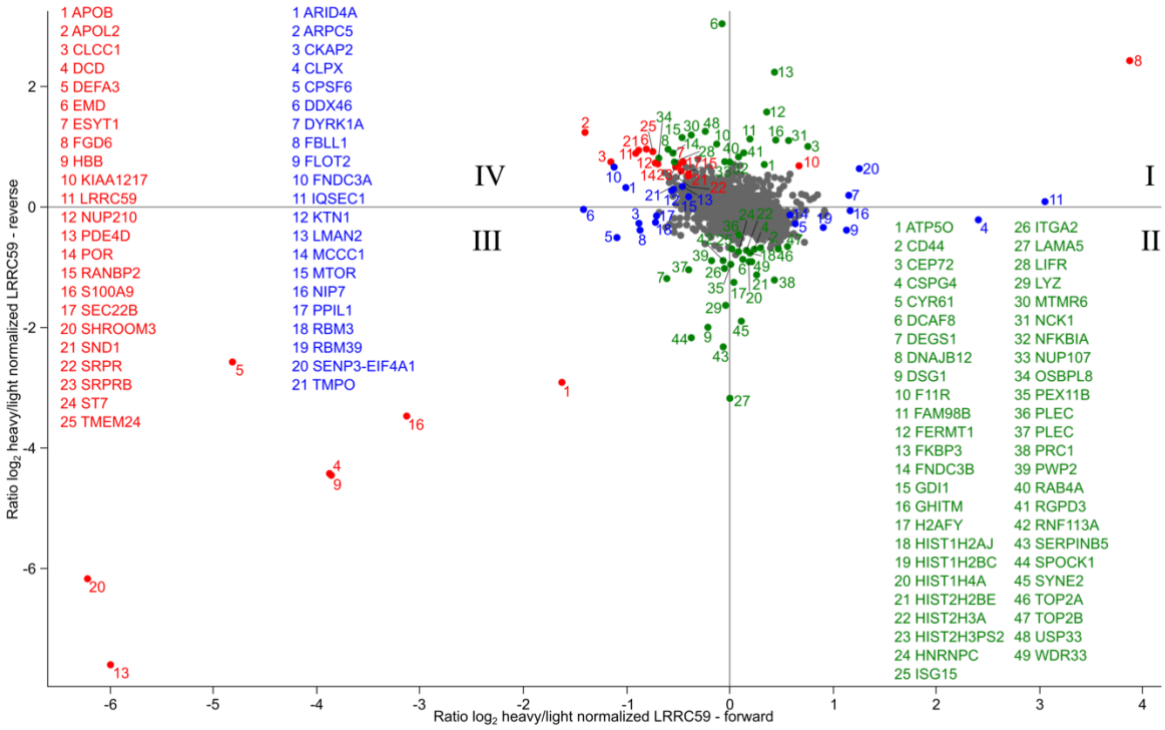

Figure S 7: Overview of all four quadrants of the Scatter plot of the analysis of RAPIDS experiments.
Data of mass spectrometry was analyzed using Perseus Software with matrix indicated in table S 8. The Scatter plot shows the ratio log_2 heavy/light normalized LRRC59 of forward experiments on the x-axis and of reverse experiments on the y-axis. Using Significance B test, significant enriched candidates were identified. Double significant enriched candidates are indicated in red, significantly enriched candidates of the forward experiments in blue and significantly enriched candidates of the reverse experiments in green. For values of proteins located in quadrant IV see table S 9.

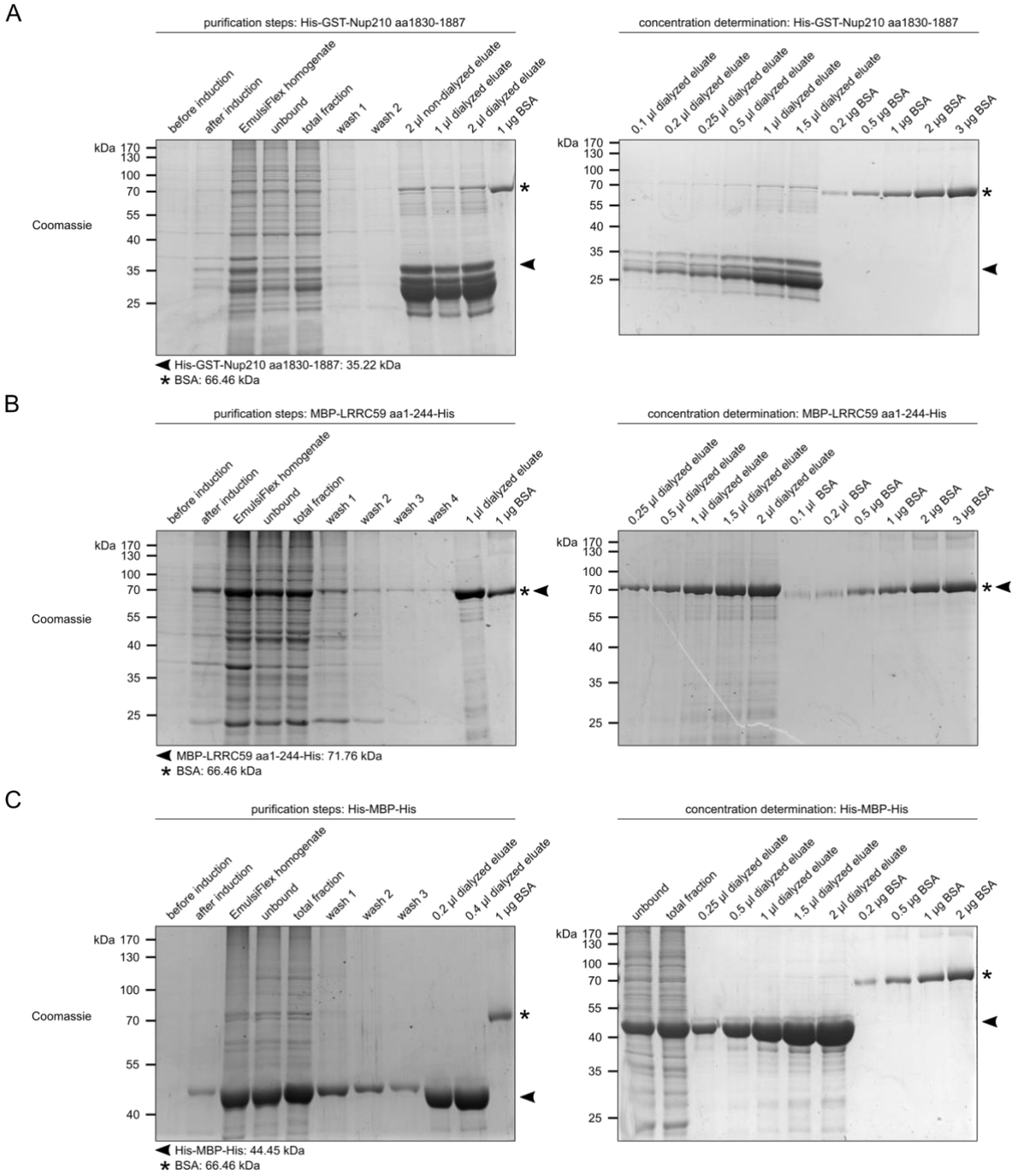

Figure S 8: Protein purification of His-GST-Nup210 aa1830-1887, MBP-LRRC59 aa1-244-His and His-MBP-His from *E. coli* Rosetta 2.
The appropriate plasmid was transformed into *E. coli* Rosetta 2 for expression. His-tagged proteins were purified using Ni-NTA. Purification steps and protein concentration by comparison to a BSA standard (asterisks) were analyzed by SDS-PAGE and Coomassie staining for (A) His-GST-Nup210 aa1830-1887, (B) MBP-LRRC59 aa1-244-His and (C) His-MBP-His.

C. Supplemental data corresponding to section 3.2

Table S 1: Raw data of Western blot of lamin A/C siRNA treated HeLa P4 cells (figure 16)

Date	Western blot	Channel	siRNA	Analyzed protein	signal	Ratio lamin A/C /alpha tubulin	Normalized lamin A/C level
20160307	0008750_01	800	control	lamin A/C	310000	0.04	100.00
20160307	0008750_01	800	control	alpha tubulin	7660000		
20160307	0008750_01	800	lamin A/C	lamin A/C	32800	0.00	9.36
20160307	0008750_01	800	lamin A/C	alpha tubulin	8660000		
20160315	0013778_01	800	control	lamin A/C	158000	2.60	100.00
20160315	0013778_01	800	control	alpha tubulin	60700		
20160315	0013778_01	800	lamin A/C	lamin A/C	21600	0.51	19.71

Date	Western blot	Channel	siRNA	Analyzed protein	signal	Ratio lamin A/C /alpha tubulin	Normalized lamin A/C level
20160315	0013778_01	800	lamin A/C	alpha tubulin	42100		
20160315	0013778_01	800	control	lamin A/C	430000	3.91	100.00
20160315	0013778_01	800	control	alpha tubulin	110000		
20160315	0013778_01	800	lamin A/C	lamin A/C	62000	0.65	16.68
20160315	0013778_01	800	lamin A/C	alpha tubulin	95100		
20161212	0013149_01	800	control	lamin A/C	208000	0.10	100.00
20161212	0013149_01	800	control	alpha tubulin	2020000		
20161212	0013149_01	800	lamin A/C	lamin A/C	18300	0.01	11.18
20161212	0013149_01	800	lamin A/C	alpha tubulin	1590000		
20161212	0013149_01	800	control	lamin A/C	235000	0.19	100.00
20161212	0013149_01	800	control	alpha tubulin	1230000		
20161212	0013149_01	800	lamin A/C	lamin A/C	26800	0.01	6.84
20161212	0013149_01	800	lamin A/C	alpha tubulin	2050000		
20170130	0013149_01	800	control	lamin A/C	57500	0.04	100.00
20170130	0013149_01	800	control	alpha tubulin	1480000		
20170130	0013149_01	800	lamin A/C	lamin A/C	15100	0.01	27.96
20170130	0013149_01	800	lamin A/C	alpha tubulin	1390000		
20171009	0011725_01	700	control	lamin A/C	144000	0.32	100.00
20171009	0011725_01	800	control	alpha tubulin	449000		
20171009	0011725_01	700	lamin A/C	lamin A/C	7860	0.02	5.48
20171009	0011725_01	800	lamin A/C	alpha tubulin	447000		
20181022	0000864_02	800	control	lamin A/C	2320	1.58	100.00
20181022	0000864_02	800	control	alpha tubulin	1470		
20181022	0000864_02	800	lamin A/C	lamin A/C	188	0.19	11.79
20181022	0000864_02	800	lamin A/C	alpha tubulin	1010		
20181105	0000951_02	800	control	lamin A/C	72.3	0.01	100.00
20181105	0000951_02	800	control	alpha tubulin	6800		
20181105	0000951_02	800	lamin A/C	lamin A/C	-18.5	0.00	1.00*
20181105	0000951_02	800	lamin A/C	alpha tubulin	4520		

* value of lamin A/C signal was negative, so put to 1

Table S 2: Raw data of Western blot of importin β siRNA treated U2OS cells (figure S 4A)

Date	Western blot	Channel	siRNA	Analyzed protein	signal	Ratio importin β /alpha tubulin	Normalized importin β level
20180709	0017393_01	800	control	importin β	207000	1.13	100.00
20180709	0017393_01	800	control	alpha tubulin	183000		
20180709	0017393_01	800	importin β	importin β	30600	0.16	14.02
20180709	0017393_01	800	importin β	alpha tubulin	193000		
20180709	0017393_01	800	control	importin β	243000	1.96	100.00
20180709	0017393_01	800	control	alpha tubulin	124000		
20180709	0017393_01	800	importin β	importin β	45900	0.38	19.36
20180709	0017393_01	800	importin β	alpha tubulin	121000		
20180806	0000122_02	800	control	importin β	1830	0.50	100.00
20180806	0000122_02	800	control	alpha tubulin	3670		
20180806	0000122_02	800	importin β	importin β	295	0.14	28.72
20180806	0000122_02	800	importin β	alpha tubulin	2060		
20180813	0000260_02	800	control	importin β	336	0.37	100.00
20180813	0000260_02	800	control	alpha tubulin	906		
20180813	0000260_02	800	importin β	importin β	124	0.11	30.67
20180813	0000260_02	800	importin β	alpha tubulin	1090		
20180820	0000260_02	800	control	importin β	600	0.30	100.00
20180820	0000260_02	800	control	alpha tubulin	1970		
20180820	0000260_02	800	importin β	importin β	120	0.14	44.82
20180820	0000260_02	800	importin β	alpha tubulin	879		

Table S 3: Raw data of Western blot of importin β siRNA treated HeLa P4 cells (figure S 4B)

Date	Western blot	Channel	siRNA	Analyzed protein	signal	Ratio importin β /alpha tubulin	Normalized importin β level
20180312	0016521_01	800	control	importin β	123000	0.14	100.00
20180312	0016521_01	800	control	alpha tubulin	860000		
20180312	0016521_01	800	importin β	importin β	37600	0.05	37.40
20180312	0016521_01	800	importin β	alpha tubulin	703000		
20180319	0016521_01	800	control	importin β	261000	0.25	100.00
20180319	0016521_01	800	control	alpha tubulin	1030000		
20180319	0016521_01	800	importin β	importin β	86300	0.07	29.36
20180319	0016521_01	800	importin β	alpha tubulin	1160000		
20180430	0016806_01	800	control	importin β	370000	0.97	100.00
20180430	0016806_01	800	control	alpha tubulin	382000		
20180430	0016806_01	800	importin β	importin β	125000	0.20	20.29
20180430	0016806_01	800	importin β	alpha tubulin	636000		

Date	Western blot	Channel	siRNA	Analyzed protein	signal	Ratio importin β /alpha tubulin	Normalized importin β level
20180430	0016806_01	800	control	importin β	761000	1.18	100.00
20180430	0016806_01	800	control	alpha tubulin	647000		
20180430	0016806_01	800	importin β	importin β	389000	0.29	25.06
20180430	0016806_01	800	importin β	alpha tubulin	1320000		
20180924	0000654_02	800	control	importin β	2040	0.08	100.00
20180924	0000654_02	800	control	alpha tubulin	24200		
20180924	0000654_02	800	importin β	importin β	753	0.02	26.43
20180924	0000654_02	800	importin β	alpha tubulin	33800		
20180924	0000654_02	800	control	importin β	3830	0.10	100.00
20180924	0000654_02	800	control	alpha tubulin	36700		
20180924	0000654_02	800	importin β	importin β	503	0.02	21.05
20180924	0000654_02	800	importin β	alpha tubulin	22900		
20180522	0017108_01	800	control	importin β	592000	4.11	100.00
20180522	0017108_01	800	control	alpha tubulin	144000		
20180522	0017108_01	800	importin β	importin β	250000	0.59	14.41
20180522	0017108_01	800	importin β	alpha tubulin	422000		
20180528	0017109_01	800	control	importin β	589000	5.61	100.00
20180528	0017109_01	800	control	alpha tubulin	105000		
20180528	0017109_01	800	importin β	importin β	280000	1.26	22.38
20180528	0017109_01	800	importin β	alpha tubulin	223000		
20180604	0017110_01	800	control	importin β	420000	2.64	100.00
20180604	0017110_01	800	control	alpha tubulin	159000		
20180604	0017110_01	800	importin β	importin β	328000	0.51	19.37
20180604	0017110_01	800	importin β	alpha tubulin	641000		
20181015	0000831_02	800	control	importin β	2170	0.58	100.00
20181015	0000831_02	800	control	alpha tubulin	3710		
20181015	0000831_02	800	importin β	importin β	748	0.13	21.42
20181015	0000831_02	800	importin β	alpha tubulin	5970		
20181105	0000951_02	800	control	importin β	1930	1.12	100.00
20181105	0000951_02	800	control	alpha tubulin	1720		
20181105	0000951_02	800	importin β	importin β	599	0.18	16.23
20181105	0000951_02	800	importin β	alpha tubulin	3290		
20181105	0000951_02	800	control	importin β	2440	0.79	100.00
20181105	0000951_02	800	control	alpha tubulin	3070		
20181105	0000951_02	800	importin β	importin β	857	0.16	19.93
20181105	0000951_02	800	importin β	alpha tubulin	5410		

Table S 4: Raw data of rapamycin-induced dimerization assay in importin β siRNA treated cells (figure 18)

Date	siRNA	Rapamycin treatment	responding cells of 100 or 50	responding cells (%)	mean	standard deviation
20180522	control	1 minute	55	55	63.00	5.74
20180528	control	1 minute	60	60		
20180604	control	1 minute	70	70		
20181015	control	1 minute	64	64		
20181105	control	1 minute	66	66		
20180522	control	1.5 minutes	66	66	76.20	6.91
20180528	control	1.5 minutes	85	85		
20180604	control	1.5 minutes	75	75		
20181015	control	1.5 minutes	79	79		
20181105	control	1.5 minutes	76	76		
20180522	control	2 minutes	76	76	83.80	8.73
20180528	control	2 minutes	78	78		
20180604	control	2 minutes	96	96		
20181015	control	2 minutes	90	90		
20181105	control	2 minutes	79	79		
20180522	control	2.5 minutes	85	85	86.80	6.26
20180528	control	2.5 minutes	79	79		
20180604	control	2.5 minutes	95	95		
20181015	control	2.5 minutes	91	91		
20181105	control	2.5 minutes	84	84		
20180522	control	3 minutes	86	86	91.20	4.44
20180528	control	3 minutes	96	96		
20180604	control	3 minutes	94	94		
20181015	control	3 minutes	93	93		
20181105	control	3 minutes	87	87		
20180522	control	4 minutes	94	94	92.60	1.95
20180528	control	4 minutes	91	91		
20180604	control	4 minutes	94	94		
20181015	control	4 minutes	94	94		

Date	siRNA	Rapamycin treatment	responding cells of 100 or 50	responding cells (%)	mean	standard deviation
20181105	control	4 minutes	90	90		
20181015	control	10 minutes	98	98	92.83	3.84
20180312	control	10 minutes	46	92		
20180312	control	10 minutes	46	92		
20180312	control	10 minutes	45	90		
20180312	control	10 minutes	44	88		
20180312	control	10 minutes	45	90		
20180319	control	10 minutes	47	94		
20180319	control	10 minutes	48	96		
20180319	control	10 minutes	43	86		
20180319	control	10 minutes	44	88		
20180319	control	10 minutes	45	90		
20180430	control	10 minutes	45	90		
20180430	control	10 minutes	48	96		
20180430	control	10 minutes	47	94		
20180430	control	10 minutes	49	98		
20180430	control	10 minutes	47	94		
20180430	control	10 minutes	50	100		
20180430	control	10 minutes	44	88		
20180430	control	10 minutes	47	94		
20180430	control	10 minutes	50	100		
20180430	control	10 minutes	47	94		
20180430	control	10 minutes	47	94		
20180430	control	10 minutes	46	92		
20180430	control	10 minutes	48	96		
20180430	control	10 minutes	48	96		
20180430	control	10 minutes	44	88		
20180924	control	10 minutes	43	86		
20180924	control	10 minutes	45	90		
20180924	control	10 minutes	48	96		
20180924	control	10 minutes	44	88		
20180924	control	10 minutes	47	94		
20180924	control	10 minutes	46	92		
20180924	control	10 minutes	47	94		
20180924	control	10 minutes	49	98		
20180924	control	10 minutes	48	96		
20180924	control	10 minutes	45	90		
20180522	importin β	1 minute	47	47	62.80	11.82
20180528	importin β	1 minute	78	78		
20180604	importin β	1 minute	56	56		
20181015	importin β	1 minute	65	65		
20181105	importin β	1 minute	68	68		
20180522	importin β	1.5 minutes	75	75	75.00	3.32
20180528	importin β	1.5 minutes	70	70		
20180604	importin β	1.5 minutes	74	74		
20181015	importin β	1.5 minutes	78	78		
20181105	importin β	1.5 minutes	78	78		
20180522	importin β	2 minutes	83	83	83.80	5.63
20180528	importin β	2 minutes	87	87		
20180604	importin β	2 minutes	76	76		
20181015	importin β	2 minutes	91	91		
20181105	importin β	2 minutes	82	82		
20180522	importin β	2.5 minutes	81	81	83.60	3.58
20180528	importin β	2.5 minutes	83	83		
20180604	importin β	2.5 minutes	80	80		
20181015	importin β	2.5 minutes	89	89		
20181105	importin β	2.5 minutes	85	85		
20180522	importin β	3 minutes	87	87	86.80	5.07
20180528	importin β	3 minutes	78	78		
20180604	importin β	3 minutes	89	89		
20181015	importin β	3 minutes	90	90		
20181105	importin β	3 minutes	90	90		
20180522	importin β	4 minutes	91	91	92.80	2.39
20180528	importin β	4 minutes	96	96		
20180604	importin β	4 minutes	90	90		
20181015	importin β	4 minutes	93	93		
20181105	importin β	4 minutes	94	94		
20181015	importin β	10 minutes	97	97	90.64	7.38
20180312	importin β	10 minutes	39	78		
20180312	importin β	10 minutes	41	82		
20180312	importin β	10 minutes	35	70		

Date	siRNA	Rapamycin treatment	responding cells of 100 or 50	responding cells (%)	mean	standard deviation
20180312	importin β	10 minutes	44	88		
20180312	importin β	10 minutes	36	72		
20180319	importin β	10 minutes	47	94		
20180319	importin β	10 minutes	48	96		
20180319	importin β	10 minutes	45	90		
20180319	importin β	10 minutes	45	90		
20180319	importin β	10 minutes	40	80		
20180430	importin β	10 minutes	44	88		
20180430	importin β	10 minutes	44	88		
20180430	importin β	10 minutes	50	100		
20180430	importin β	10 minutes	45	90		
20180430	importin β	10 minutes	49	98		
20180430	importin β	10 minutes	45	90		
20180430	importin β	10 minutes	50	100		
20180430	importin β	10 minutes	48	96		
20180430	importin β	10 minutes	49	98		
20180430	importin β	10 minutes	50	100		
20180430	importin β	10 minutes	45	90		
20180430	importin β	10 minutes	48	96		
20180430	importin β	10 minutes	48	96		
20180430	importin β	10 minutes	46	92		
20180430	importin β	10 minutes	47	94		
20180924	importin β	10 minutes	43	86		
20180924	importin β	10 minutes	40	80		
20180924	importin β	10 minutes	47	94		
20180924	importin β	10 minutes	45	90		
20180924	importin β	10 minutes	47	94		
20180924	importin β	10 minutes	48	96		
20180924	importin β	10 minutes	45	90		
20180924	importin β	10 minutes	47	94		
20180924	importin β	10 minutes	47	94		
20180924	importin β	10 minutes	46	92		

Constructs: pmCherry-FRB-LRRC59, pEGFP$_2$-GST-M9-FKBP12

Table S 5: Raw data of rapamycin-induced dimerization assay using reporter EGFP$_2$-GST-M9-FKBP12 (figure 21)

Date	Plasmid DNA concentration [µg]	construct	Rapamycin treatment	Respond-ing cells of 100	responding cells (%)	mean	Standard deviation
20180625	0.4	mCherry-FRB-LRRC59	1 minute	58	58		
20180702	0.4	mCherry-FRB-LRRC59	1 minute	63	63		
20180702	0.4	mCherry-FRB-LRRC59	1 minute	50	50		
20180702	0.4	mCherry-FRB-LRRC59	1 minute	58	58	60.43	6.63
20180806	0.4	mCherry-FRB-LRRC59	1 minute	72	72		
20180813	0.4	mCherry-FRB-LRRC59	1 minute	62	62		
20180820	0.4	mCherry-FRB-LRRC59	1 minute	60	60		
20180625	0.4	mCherry-FRB-LRRC59	1.5 minutes	85	85		
20180702	0.4	mCherry-FRB-LRRC59	1.5 minutes	75	75		
20180702	0.4	mCherry-FRB-LRRC59	1.5 minutes	74	74		
20180702	0.4	mCherry-FRB-LRRC59	1.5 minutes	84	84	81.00	7.53
20180806	0.4	mCherry-FRB-LRRC59	1.5 minutes	88	88		
20180813	0.4	mCherry-FRB-LRRC59	1.5 minutes	90	90		
20180820	0.4	mCherry-FRB-LRRC59	1.5 minutes	71	71		
20180625	0.4	mCherry-FRB-LRRC59	2 minutes	80	80		
20180702	0.4	mCherry-FRB-LRRC59	2 minutes	83	83		
20180702	0.4	mCherry-FRB-LRRC59	2 minutes	90	90		
20180702	0.4	mCherry-FRB-LRRC59	2 minutes	90	90		
20180806	0.4	mCherry-FRB-LRRC59	2 minutes	90	90	86.88	4.67
20180813	0.4	mCherry-FRB-LRRC59	2 minutes	91	91		
20180820	0.4	mCherry-FRB-LRRC59	2 minutes	81	81		
20181015	0.4	mCherry-FRB-LRRC59	2 minutes	90	90		
20180625	0.4	mCherry-FRB-LRRC59	2.5 minutes	86	86		
20180702	0.4	mCherry-FRB-LRRC59	2.5 minutes	83	83		
20180702	0.4	mCherry-FRB-LRRC59	2.5 minutes	95	95		
20180702	0.4	mCherry-FRB-LRRC59	2.5 minutes	88	88	88.71	5.41
20180806	0.4	mCherry-FRB-LRRC59	2.5 minutes	92	92		
20180813	0.4	mCherry-FRB-LRRC59	2.5 minutes	95	95		
20180820	0.4	mCherry-FRB-LRRC59	2.5 minutes	82	82		
20180625	0.4	mCherry-FRB-LRRC59	3 minutes	88	88	92.43	5.16
20180702	0.4	mCherry-FRB-LRRC59	3 minutes	96	96		

Date	Plasmid DNA concentration [µg]	construct	Rapamycin treatment	Respond-ing cells of 100	responding cells (%)	mean	Standard deviation
20180702	0.4	mCherry-FRB-LRRC59	3 minutes	96	96		
20180702	0.4	mCherry-FRB-LRRC59	3 minutes	95	95		
20180806	0.4	mCherry-FRB-LRRC59	3 minutes	90	90		
20180813	0.4	mCherry-FRB-LRRC59	3 minutes	98	98		
20180820	0.4	mCherry-FRB-LRRC59	3 minutes	84	84		
20180625	0.4	mCherry-FRB-LRRC59	4 minutes	90	90		
20180702	0.4	mCherry-FRB-LRRC59	4 minutes	95	95		
20180702	0.4	mCherry-FRB-LRRC59	4 minutes	91	91	92.33	4.23
20180806	0.4	mCherry-FRB-LRRC59	4 minutes	94	94		
20180813	0.4	mCherry-FRB-LRRC59	4 minutes	98	98		
20180820	0.4	mCherry-FRB-LRRC59	4 minutes	86	86		
20181015	0.4	mCherry-FRB-LRRC59	10 minutes	95	95		
20181015	0.4	mCherry-FRB-LRRC59	10 minutes	96	96	95.25	1.71
20181015	0.4	mCherry-FRB-LRRC59	10 minutes	97	97		
20181015	0.4	mCherry-FRB-LRRC59	10 minutes	93	93		
20180625	1	mCherry-FRB-MBP-LRRC59	1 minute	28	28		
20180702	1	mCherry-FRB-MBP-LRRC59	1 minute	22	22		
20180702	1	mCherry-FRB-MBP-LRRC59	1 minute	18	18		
20180702	1	mCherry-FRB-MBP-LRRC59	1 minute	30	30	22.86	4.45
20180806	1	mCherry-FRB-MBP-LRRC59	1 minute	20	20		
20180813	1	mCherry-FRB-MBP-LRRC59	1 minute	20	20		
20180820	1	mCherry-FRB-MBP-LRRC59	1 minute	22	22		
20180625	1	mCherry-FRB-MBP-LRRC59	1.5 minutes	32	32		
20180702	1	mCherry-FRB-MBP-LRRC59	1.5 minutes	31	31		
20180702	1	mCherry-FRB-MBP-LRRC59	1.5 minutes	34	34		
20180702	1	mCherry-FRB-MBP-LRRC59	1.5 minutes	41	41	29.57	7.21
20180806	1	mCherry-FRB-MBP-LRRC59	1.5 minutes	19	19		
20180813	1	mCherry-FRB-MBP-LRRC59	1.5 minutes	25	25		
20180820	1	mCherry-FRB-MBP-LRRC59	1.5 minutes	25	25		
20180625	1	mCherry-FRB-MBP-LRRC59	2 minutes	34	34		
20180702	1	mCherry-FRB-MBP-LRRC59	2 minutes	35	35		
20180702	1	mCherry-FRB-MBP-LRRC59	2 minutes	38	38		
20180702	1	mCherry-FRB-MBP-LRRC59	2 minutes	43	43	37.00	3.21
20180806	1	mCherry-FRB-MBP-LRRC59	2 minutes	40	40		
20180813	1	mCherry-FRB-MBP-LRRC59	2 minutes	35	35		
20180820	1	mCherry-FRB-MBP-LRRC59	2 minutes	37	37		
20181015	1	mCherry-FRB-MBP-LRRC59	2 minutes	34	34		
20180625	1	mCherry-FRB-MBP-LRRC59	2.5 minutes	43	43		
20180702	1	mCherry-FRB-MBP-LRRC59	2.5 minutes	40	40		
20180702	1	mCherry-FRB-MBP-LRRC59	2.5 minutes	30	30		
20180702	1	mCherry-FRB-MBP-LRRC59	2.5 minutes	39	39	41.71	6.16
20180806	1	mCherry-FRB-MBP-LRRC59	2.5 minutes	47	47		
20180813	1	mCherry-FRB-MBP-LRRC59	2.5 minutes	48	48		
20180820	1	mCherry-FRB-MBP-LRRC59	2.5 minutes	45	45		
20180625	1	mCherry-FRB-MBP-LRRC59	3 minutes	40	40		
20180702	1	mCherry-FRB-MBP-LRRC59	3 minutes	39	39		
20180702	1	mCherry-FRB-MBP-LRRC59	3 minutes	40	40		
20180702	1	mCherry-FRB-MBP-LRRC59	3 minutes	44	44	45.43	6.43
20180806	1	mCherry-FRB-MBP-LRRC59	3 minutes	50	50		
20180813	1	mCherry-FRB-MBP-LRRC59	3 minutes	49	49		
20180820	1	mCherry-FRB-MBP-LRRC59	3 minutes	56	56		
20180625	1	mCherry-FRB-MBP-LRRC59	4 minutes	70	70		
20180702	1	mCherry-FRB-MBP-LRRC59	4 minutes	42	42		
20180702	1	mCherry-FRB-MBP-LRRC59	4 minutes	46	46	51.50	9.67
20180806	1	mCherry-FRB-MBP-LRRC59	4 minutes	50	50		
20180813	1	mCherry-FRB-MBP-LRRC59	4 minutes	51	51		
20180820	1	mCherry-FRB-MBP-LRRC59	4 minutes	50	50		
20181015	1	mCherry-FRB-MBP-LRRC59	10 minutes	54	54		
20181015	1	mCherry-FRB-MBP-LRRC59	10 minutes	50	50	52.25	6.34
20181015	1	mCherry-FRB-MBP-LRRC59	10 minutes	60	60		
20181015	1	mCherry-FRB-MBP-LRRC59	10 minutes	45	45		
20180716	0.5	HA-FRB-LRRC59	1 minute	75	75		
20180716	0.5	HA-FRB-LRRC59	1 minute	70	70		
20180716	0.5	HA-FRB-LRRC59	1 minute	64	64		
20180716	0.5	HA-FRB-LRRC59	1 minute	60	60		
20180813	0.5	HA-FRB-LRRC59	1 minute	55	55	61.30	8.74
20180813	0.5	HA-FRB-LRRC59	1 minute	54	54		
20180813	0.5	HA-FRB-LRRC59	1 minute	55	55		
20180820	0.5	HA-FRB-LRRC59	1 minute	63	63		
20180820	0.5	HA-FRB-LRRC59	1 minute	70	70		

Date	Plasmid DNA concentration [µg]	construct	Rapamycin treatment	Respond-ing cells of 100	responding cells (%)	mean	Standard deviation
20180820	0.5	HA-FRB-LRRC59	1 minute	47	47		
20180716	0.5	HA-FRB-LRRC59	1.5 minutes	75	75	77.00	8.55
20180716	0.5	HA-FRB-LRRC59	1.5 minutes	90	90		
20180716	0.5	HA-FRB-LRRC59	1.5 minutes	85	85		
20180716	0.5	HA-FRB-LRRC59	1.5 minutes	83	83		
20180813	0.5	HA-FRB-LRRC59	1.5 minutes	78	78		
20180813	0.5	HA-FRB-LRRC59	1.5 minutes	75	75		
20180813	0.5	HA-FRB-LRRC59	1.5 minutes	76	76		
20180820	0.5	HA-FRB-LRRC59	1.5 minutes	80	80		
20180820	0.5	HA-FRB-LRRC59	1.5 minutes	60	60		
20180820	0.5	HA-FRB-LRRC59	1.5 minutes	68	68		
20180716	0.5	HA-FRB-LRRC59	2 minutes	87	87	82.64	6.14
20180716	0.5	HA-FRB-LRRC59	2 minutes	81	81		
20180716	0.5	HA-FRB-LRRC59	2 minutes	89	89		
20180716	0.5	HA-FRB-LRRC59	2 minutes	79	79		
20180813	0.5	HA-FRB-LRRC59	2 minutes	82	82		
20180813	0.5	HA-FRB-LRRC59	2 minutes	80	80		
20180813	0.5	HA-FRB-LRRC59	2 minutes	78	78		
20180820	0.5	HA-FRB-LRRC59	2 minutes	76	76		
20180820	0.5	HA-FRB-LRRC59	2 minutes	76	76		
20180820	0.5	HA-FRB-LRRC59	2 minutes	85	85		
20181015	0.5	HA-FRB-LRRC59	2 minutes	96	96		
20180716	0.5	HA-FRB-LRRC59	2.5 minutes	95	95	89.70	5.83
20180716	0.5	HA-FRB-LRRC59	2.5 minutes	90	90		
20180716	0.5	HA-FRB-LRRC59	2.5 minutes	98	98		
20180716	0.5	HA-FRB-LRRC59	2.5 minutes	96	96		
20180813	0.5	HA-FRB-LRRC59	2.5 minutes	85	85		
20180813	0.5	HA-FRB-LRRC59	2.5 minutes	78	78		
20180813	0.5	HA-FRB-LRRC59	2.5 minutes	90	90		
20180820	0.5	HA-FRB-LRRC59	2.5 minutes	88	88		
20180820	0.5	HA-FRB-LRRC59	2.5 minutes	87	87		
20180820	0.5	HA-FRB-LRRC59	2.5 minutes	90	90		
20180716	0.5	HA-FRB-LRRC59	3 minutes	95	95	92.80	3.99
20180716	0.5	HA-FRB-LRRC59	3 minutes	98	98		
20180716	0.5	HA-FRB-LRRC59	3 minutes	93	93		
20180716	0.5	HA-FRB-LRRC59	3 minutes	97	97		
20180813	0.5	HA-FRB-LRRC59	3 minutes	95	95		
20180813	0.5	HA-FRB-LRRC59	3 minutes	90	90		
20180813	0.5	HA-FRB-LRRC59	3 minutes	95	95		
20180820	0.5	HA-FRB-LRRC59	3 minutes	90	90		
20180820	0.5	HA-FRB-LRRC59	3 minutes	85	85		
20180820	0.5	HA-FRB-LRRC59	3 minutes	90	90		
20180716	0.5	HA-FRB-LRRC59	4 minutes	98	98	90.62	6.19
20180716	0.5	HA-FRB-LRRC59	4 minutes	97	97		
20180716	0.5	HA-FRB-LRRC59	4 minutes	94	94		
20180813	0.5	HA-FRB-LRRC59	4 minutes	90	90		
20180813	0.5	HA-FRB-LRRC59	4 minutes	80	80		
20180813	0.5	HA-FRB-LRRC59	4 minutes	95	95		
20180813	0.5	HA-FRB-LRRC59	4 minutes	80	80		
20180813	0.5	HA-FRB-LRRC59	4 minutes	91	91		
20180820	0.5	HA-FRB-LRRC59	4 minutes	89	89		
20180820	0.5	HA-FRB-LRRC59	4 minutes	85	85		
20180820	0.5	HA-FRB-LRRC59	4 minutes	87	87		
20180820	0.5	HA-FRB-LRRC59	4 minutes	97	97		
20180820	0.5	HA-FRB-LRRC59	4 minutes	95	95		
20181015	0.5	HA-FRB-LRRC59	10 minutes	96	96	96.00	1.41
20181015	0.5	HA-FRB-LRRC59	10 minutes	94	94		
20181015	0.5	HA-FRB-LRRC59	10 minutes	97	97		
20181015	0.5	HA-FRB-LRRC59	10 minutes	97	97		

Table S 6: Overview of counted cell number for rapamycin-induced dimerization assay using reporter $EGFP_2$-GST-M9-FKBP12 (figure 21)

Rapamycin treatment	mCherry-FRB-LRRC59	mCherry-FRB-MBP-LRRC59	HA-FRB-LRRC59
1 minute	700	700	1000
1.5 minutes	700	700	1000
2 minutes	800	800	1100
2.5 minutes	700	700	1000
3 minutes	700	700	1000
4 minutes	600	600	1300
10 minutes	400	400	400

Table S 7: Raw data of rapamycin-induced dimerization assay using reporter $EGFP_2$-MBP-M9-FKBP12 (figure 22)

Date	Plasmid DNA concentration [µg]	construct	Rapamycin treatment	respond-ing cells of 100	respond-ing cells (%)	mean	standard deviation
20181008	0.4	mCherry-FRB-LRRC59	1 minute	61	61	65.00	4.74
20181015	0.4	mCherry-FRB-LRRC59	1 minute	68	68		
20181022	0.4	mCherry-FRB-LRRC59	1 minute	70	70		
20181022	0.4	mCherry-FRB-LRRC59	1 minute	67	67		
20181029	0.4	mCherry-FRB-LRRC59	1 minute	59	59		
20181008	0.4	mCherry-FRB-LRRC59	1.5 minutes	64	64	71.40	4.39
20181015	0.4	mCherry-FRB-LRRC59	1.5 minutes	73	73		
20181022	0.4	mCherry-FRB-LRRC59	1.5 minutes	75	75		
20181022	0.4	mCherry-FRB-LRRC59	1.5 minutes	74	74		
20181029	0.4	mCherry-FRB-LRRC59	1.5 minutes	71	71		
20181008	0.4	mCherry-FRB-LRRC59	2 minutes	73	73	79.80	6.30
20181015	0.4	mCherry-FRB-LRRC59	2 minutes	90	90		
20181022	0.4	mCherry-FRB-LRRC59	2 minutes	80	80		
20181022	0.4	mCherry-FRB-LRRC59	2 minutes	77	77		
20181029	0.4	mCherry-FRB-LRRC59	2 minutes	79	79		
20181008	0.4	mCherry-FRB-LRRC59	2.5 minutes	74	74	84.00	6.78
20181015	0.4	mCherry-FRB-LRRC59	2.5 minutes	91	91		
20181022	0.4	mCherry-FRB-LRRC59	2.5 minutes	89	89		
20181022	0.4	mCherry-FRB-LRRC59	2.5 minutes	81	81		
20181029	0.4	mCherry-FRB-LRRC59	2.5 minutes	85	85		
20181008	0.4	mCherry-FRB-LRRC59	3 minutes	85	85	89.40	3.65
20181015	0.4	mCherry-FRB-LRRC59	3 minutes	95	95		
20181022	0.4	mCherry-FRB-LRRC59	3 minutes	90	90		
20181022	0.4	mCherry-FRB-LRRC59	3 minutes	88	88		
20181029	0.4	mCherry-FRB-LRRC59	3 minutes	89	89		
20181008	0.4	mCherry-FRB-LRRC59	4 minutes	93	93	93.00	1.58
20181015	0.4	mCherry-FRB-LRRC59	4 minutes	94	94		
20181022	0.4	mCherry-FRB-LRRC59	4 minutes	95	95		
20181022	0.4	mCherry-FRB-LRRC59	4 minutes	92	92		
20181029	0.4	mCherry-FRB-LRRC59	4 minutes	91	91		
20181008	0.4	mCherry-FRB-LRRC59	10 minutes	94	94	95.00	0.71
20181015	0.4	mCherry-FRB-LRRC59	10 minutes	96	96		
20181022	0.4	mCherry-FRB-LRRC59	10 minutes	95	95		
20181022	0.4	mCherry-FRB-LRRC59	10 minutes	95	95		
20181029	0.4	mCherry-FRB-LRRC59	10 minutes	95	95		
20181008	1	mCherry-FRB-MBP-LRRC59	1 minute	25	25	23.40	2.19
20181015	1	mCherry-FRB-MBP-LRRC59	1 minute	25	25		
20181022	1	mCherry-FRB-MBP-LRRC59	1 minute	25	25		
20181022	1	mCherry-FRB-MBP-LRRC59	1 minute	21	21		
20181029	1	mCherry-FRB-MBP-LRRC59	1 minute	21	21		
20181008	1	mCherry-FRB-MBP-LRRC59	1.5 minutes	26	26	28.20	2.28
20181015	1	mCherry-FRB-MBP-LRRC59	1.5 minutes	30	30		
20181022	1	mCherry-FRB-MBP-LRRC59	1.5 minutes	31	31		
20181022	1	mCherry-FRB-MBP-LRRC59	1.5 minutes	26	26		
20181029	1	mCherry-FRB-MBP-LRRC59	1.5 minutes	28	28		
20181008	1	mCherry-FRB-MBP-LRRC59	2 minutes	27	27	33.20	5.22
20181015	1	mCherry-FRB-MBP-LRRC59	2 minutes	35	35		
20181022	1	mCherry-FRB-MBP-LRRC59	2 minutes	41	41		
20181022	1	mCherry-FRB-MBP-LRRC59	2 minutes	31	31		
20181029	1	mCherry-FRB-MBP-LRRC59	2 minutes	32	32		
20181008	1	mCherry-FRB-MBP-LRRC59	2.5 minutes	42	42	40.20	5.81
20181015	1	mCherry-FRB-MBP-LRRC59	2.5 minutes	40	40		
20181022	1	mCherry-FRB-MBP-LRRC59	2.5 minutes	49	49		
20181022	1	mCherry-FRB-MBP-LRRC59	2.5 minutes	35	35		
20181029	1	mCherry-FRB-MBP-LRRC59	2.5 minutes	35	35		
20181008	1	mCherry-FRB-MBP-LRRC59	3 minutes	53	53	45.60	4.67
20181015	1	mCherry-FRB-MBP-LRRC59	3 minutes	44	44		
20181022	1	mCherry-FRB-MBP-LRRC59	3 minutes	47	47		
20181022	1	mCherry-FRB-MBP-LRRC59	3 minutes	43	43		
20181029	1	mCherry-FRB-MBP-LRRC59	3 minutes	41	41		
20181008	1	mCherry-FRB-MBP-LRRC59	4 minutes	46	46	48.20	3.50
20181015	1	mCherry-FRB-MBP-LRRC59	4 minutes	48	48		
20181022	1	mCherry-FRB-MBP-LRRC59	4 minutes	54	54		
20181022	1	mCherry-FRB-MBP-LRRC59	4 minutes	48	48		
20181029	1	mCherry-FRB-MBP-LRRC59	4 minutes	45	45		
20181008	1	mCherry-FRB-MBP-LRRC59	10 minutes	55	55	55.40	4.04
20181015	1	mCherry-FRB-MBP-LRRC59	10 minutes	52	52		
20181022	1	mCherry-FRB-MBP-LRRC59	10 minutes	60	60		

Date	Plasmid DNA concentration [µg]	construct	Rapamycin treatment	respond-ing cells of 100	respond-ing cells (%)	mean	standard deviation
20181022	1	mCherry-FRB-MBP-LRRC59	10 minutes	59	59		
20181029	1	mCherry-FRB-MBP-LRRC59	10 minutes	51	51		
20181008	1	mCherry-FRB-GST-LRRC59	1 minute	8	8		
20181015	1	mCherry-FRB-GST-LRRC59	1 minute	4	4		
20181022	1	mCherry-FRB-GST-LRRC59	1 minute	9	9	6.20	2.59
20181022	1	mCherry-FRB-GST-LRRC59	1 minute	7	7		
20181029	1	mCherry-FRB-GST-LRRC59	1 minute	3	3		
20181008	1	mCherry-FRB-GST-LRRC59	1.5 minutes	8	8		
20181015	1	mCherry-FRB-GST-LRRC59	1.5 minutes	5	5		
20181022	1	mCherry-FRB-GST-LRRC59	1.5 minutes	10	10	7.20	2.59
20181022	1	mCherry-FRB-GST-LRRC59	1.5 minutes	9	9		
20181029	1	mCherry-FRB-GST-LRRC59	1.5 minutes	4	4		
20181008	1	mCherry-FRB-GST-LRRC59	2 minutes	10	10		
20181015	1	mCherry-FRB-GST-LRRC59	2 minutes	5	5		
20181022	1	mCherry-FRB-GST-LRRC59	2 minutes	11	11	7.80	2.59
20181022	1	mCherry-FRB-GST-LRRC59	2 minutes	6	6		
20181029	1	mCherry-FRB-GST-LRRC59	2 minutes	7	7		
20181008	1	mCherry-FRB-GST-LRRC59	2.5 minutes	4	4		
20181015	1	mCherry-FRB-GST-LRRC59	2.5 minutes	5	5		
20181022	1	mCherry-FRB-GST-LRRC59	2.5 minutes	7	7	6.60	3.21
20181022	1	mCherry-FRB-GST-LRRC59	2.5 minutes	12	12		
20181029	1	mCherry-FRB-GST-LRRC59	2.5 minutes	5	5		
20181008	1	mCherry-FRB-GST-LRRC59	3 minutes	8	8		
20181015	1	mCherry-FRB-GST-LRRC59	3 minutes	3	3		
20181022	1	mCherry-FRB-GST-LRRC59	3 minutes	12	12	7.60	4.04
20181022	1	mCherry-FRB-GST-LRRC59	3 minutes	11	11		
20181029	1	mCherry-FRB-GST-LRRC59	3 minutes	4	4		
20181008	1	mCherry-FRB-GST-LRRC59	4 minutes	11	11		
20181015	1	mCherry-FRB-GST-LRRC59	4 minutes	8	8		
20181022	1	mCherry-FRB-GST-LRRC59	4 minutes	13	13	10.00	2.12
20181022	1	mCherry-FRB-GST-LRRC59	4 minutes	8	8		
20181029	1	mCherry-FRB-GST-LRRC59	4 minutes	10	10		
20181008	1	mCherry-FRB-GST-LRRC59	10 minutes	18	18		
20181015	1	mCherry-FRB-GST-LRRC59	10 minutes	10	10		
20181022	1	mCherry-FRB-GST-LRRC59	10 minutes	12	12	11.20	4.21
20181022	1	mCherry-FRB-GST-LRRC59	10 minutes	7	7		
20181029	1	mCherry-FRB-GST-LRRC59	10 minutes	9	9		

D. Supplemental data corresponding to section 3.3

Table S 8: Perseus workflow for the identification of proteins in close proximity to mCherry-FRB-LRRC59

Matrix	Processing	Settings	Description
Matrix 1	Generic matrix upload	Main columns Ratio H/L LRRC59-fwd Ratio H/L LRRC59-rev Ratio H/L normalized LRRC59-fwd Ratio H/L normalized LRRC59-rev Numerical columns Intensity LRRC59-fwd Intensity LRRC59-rev Intensity Ratio H/L count LRRC59-fwd Ratio H/L count LRRC59-rev Peptides Razor + unique peptides Sequence coverage [%] Mol. weight [kDa] Categorical columns Only identified by site Reverse Potential contaminant Text/String columns Protein IDs Majority protein IDs Protein names Gene names	Upload of by mass spectrometry identified protein groups with file "proteinGroups – LRRC59.txt"
Matrix 2	Filter rows based on categorical column	**Column:** Only identified by site, Values: + **Mode:** Remove matching rows **Filter mode**: Reduce matrix	Remove proteins only identified by peptides carrying a modified residue

Matrix	Processing	Settings	Description
Matrix 3	Filter rows based on categorical column	**Column:** Reverse; Values: + **Mode:** Remove matching rows **Filter mode:** Reduce matrix	Remove hits that match against a nonsense database
Matrix 4	Filter rows based on categorical column	**Column:** Potential contaminant, Values: + **Mode:** Remove matching rows **Filter mode:** Reduce matrix	Remove common contaminants
Matrix 5	Remove empty columns		Remove empty columns
Matrix 6	Transform	Transformation: log2(x) Columns: Ratio H/L LRRC59-fwd Ratio H/L LRRC59-rev Ratio H/L normalized LRRC59-fwd Ratio H/L normalized LRRC59-rev Intensity LRRC59-fwd Intensity LRRC59-rev	Values in log2(x)
Matrix 7	Numeric Venn diagram	Columns: Ratio H/L LRRC59-fwd Ratio H/L LRRC59-rev Ratio H/L normalized LRRC59-fwd Ratio H/L normalized LRRC59-rev Intensity LRRC59-fwd Intensity LRRC59-rev Intensity Ratio H/L count LRRC59-fwd Ratio H/L count LRRC59-rev Peptides Razor + unique peptides Sequence coverage [%]	Creating Venn diagram with Matrix 6
Matrix 8	Significance B	Ratio columns: Ratio H/L LRRC59-fwd Ratio H/L LRRC59-rev Ratio H/L normalized LRRC59-fwd Ratio H/L normalized LRRC59-rev Intensity columns: Ratio H/L LRRC59-fwd Ratio H/L LRRC59-rev Ratio H/L normalized LRRC59-fwd Ratio H/L normalized LRRC59-rev Intensity LRRC59-fwd Intensity LRRC59-rev Intensity Ratio H/L count LRRC59-fwd Ratio H/L count LRRC59-rev Peptides Razor + unique peptides Sequence coverage [%] Mol. Weight [kDa] Q-value Score Ratio H/L normalized LRRC59-fwd Significance B Ratio H/L normalized LRRC59-rev Significance B **Side:** both **Use for truncation:** Benjamini-Hochberg FDR Threshold value: 0.05	Performance of Significance B test with data of Venn diagram
Matrix 9	Result of Matrix 8	Main columns Ratio H/L LRRC59-fwd Ratio H/L LRRC59-rev Ratio H/L normalized LRRC59-fwd Ratio H/L normalized LRRC59-rev Categorical columns Ratio H/L normalized LRRC59-fwd B significant: + Ratio H/L normalized LRRC59-rev B significant: + String columns Protein IDs Majority protein IDs Protein names Gene names Numerical columns Intensity LRRC59-fwd Intensity LRRC59-rev	Export: Generic matrix export

Matrix	Processing	Settings	Description
		Intensity Ratio H/L count LRRC59-fwd Ratio H/L count LRRC59-rev Peptides Razor + unique peptides Sequence coverage [%] Mol. Weight [kDa] Q-value Score Ratio H/L normalized LRRC59-fwd Significance B Ratio H/L normalized LRRC59-rev	
Matrix 10	Scatter plot	Matrix access: Columns	Creating Scatter plot with data of Matrix 9
Matrix 11	Data for export	Main columns Ratio H/L LRRC59-fwd Ratio H/L LRRC59-rev Ratio H/L normalized LRRC59-fwd Ratio H/L normalized LRRC59-rev Categorical columns Ratio H/L normalized LRRC59-fwd B significant Ratio H/L normalized LRRC59-rev B significant String columns Protein IDs Majority protein IDs Protein names Gene names Numerical columns Intensity LRRC59-fwd Intensity LRRC59-rev Intensity Ratio H/L count LRRC59-fwd Ratio H/L count LRRC59-rev Peptides Razor + unique peptides Sequence coverage [%] Mol. Weight [kDa] Q-value Score Ratio H/L normalized LRRC59-fwd Significance B Ratio H/L normalized LRRC59-rev	Export: Generic matrix export

Abbreviations: fwd: forward, rev: reverse, Mol. weight: molecular weight, ratio H/L: ratio heavy/light, IDs: identifications

Table S 9: Overview of the significant candidates identified in RAPIDS experiments in close proximity to mCherry-FRB-LRRC59 (Scatter plot quadrant IV)

Gene names	Ratio H/L normalized LRRC59-forward		Ratio H/L normalized LRRC59-reverse		Pep-tides	Mol. weight [kDa]	Protein IDs	Majority protein IDs
	value	B significant	value	B significant				
ST7; ST7L	-0.8769695	+	0.938474	+	4	58.07	E7EPW5; G3XAH9; E9PCV1; B7Z4U3; B7Z4L1; E7EPD9; H7BXS2; Q9NRC1-6; Q9NRC1-5; Q9NRC1-4; Q9NRC1-3; Q9NRC1-2; E7ENZ9; C9JU30; Q9NRC1-7; Q9NRC1; Q8TDW4-8; Q8TDW4-6; Q8TDW4-2; Q8TDW4-7; Q8TDW4-5; Q8TDW4-3; Q8TDW4; C9JZV9; C9JRQ0; Q5TEH7; C9JRW1; H0Y7M0; Q8TDW4-4	E7EPW5; G3XAH9; E9PCV1; B7Z4U3; B7Z4L1; E7EPD9; H7BXS2; Q9NRC1-6; Q9NRC1-5; Q9NRC1-4; Q9NRC1-3; Q9NRC1-2; E7ENZ9; C9JU30; Q9NRC1-7; Q9NRC1; Q8TDW4-8; Q8TDW4-6; Q8TDW4-2; Q8TDW4-7; Q8TDW4-5; Q8TDW4-3; Q8TDW4
SEC22B	-0.4972824	+	0.69928515	+	13	24.59	O75396; A0A087X1A9	O75396
SRPR	-0.4761972	+	0.59798396	+	23	69.81	P08240; P08240-2	P08240; P08240-2

Gene names	Ratio H/L normalized LRRC59-forward		Ratio H/L normalized LRRC59-reverse		Pep-tides	Mol. weight [kDa]	Protein IDs	Majority protein IDs
	value	B significant	value	B significant				
POR	-0.6914061	+	0.70336646	+	16	76.69	P16435; H0Y4R2; E7EMD0; E7EWU0; C9JU80	P16435; H0Y4R2; E7EMD0
RANBP2	-0.3993115	+	0.56481713	+	115	358.2	P49792; F8VYC4; P0DJD0; P0DJD1; F8W705; Q99666-2; H7BZ48; H0YBN8; C9J1W9; C9JF75; C9J6W1; Q7Z3J3-2; F8WBP7	P49792
EMD	-0.8016819	+	0.9630301	+	11	28.99	P50402; Q5HY57; F8WEQ1	P50402; Q5HY57
TMEM 214	-0.7508823	+	0.90835178	+	11	77.15	Q6NUQ4; Q6NUQ4-2; H7C085; H7C0H8; H7C008; H7BZI0	Q6NUQ4; Q6NUQ4-2
SND1	-0.3976952	+	0.50853008	+	44	102	Q7KZF4; H7C597	Q7KZF4
NUP210	-0.7014825	+	0.72744125	+	11	205.11	Q8TEM1; Q8TEM1-2	Q8TEM1; Q8TEM1-2
LRRC59	-0.9017692	+	0.89971703	+	21	34.93	Q96AG4; I3L223	Q96AG4
CLCC1	-1.1527086	+	0.74777412	+	10	62.02	Q96S66; Q96S66-2; Q96S66-3; Q96S66-4; Q5T1P5	Q96S66; Q96S66-2; Q96S66-3; Q96S66-4
APOL2	-1.40255	+	1.23235369	+	10	37.09	Q9BQE5; J3KQL8; E9PM95; B0QYK8	Q9BQE5; J3KQL8
ESYT1	-0.4419675	+	0.75634021	+	30	122.85	Q9BSJ8; Q9BSJ8-2; F8VZB1	Q9BSJ8; Q9BSJ8-2
SRPRB	-0.5179571	+	0.66129363	+	16	29.70	Q9Y5M8; H7C4H2; C9J5Z8	Q9Y5M8; H7C4H2
FNDC3A	-1.1193223	+	0.66630214		2	35.29	A0A087X1M6; G5E9X3; Q9Y2H6-2; Q9Y2H6	A0A087X1M6; G5E9X3; Q9Y2H6-2; Q9Y2H6
ARID4A	-1.0110935	+	0.3329657		2	134.95	P29374-3; P29374-2; P29374; H7C485	P29374-3; P29374-2; P29374; H7C485
TMPO	-0.5500425	+	0.29748487		17	50.67	P42167; G5E972	P42167; G5E972
MTOR	-0.4019016	+	0.16748644		12	288.89	P42345; B1AKP8	P42345; B1AKP8
LMAN2	-0.4650221	+	0.35343626		14	40.23	Q12907; D6RBV2; D6RIU4; D6RDX1; D6RBH1	Q12907; D6RBV2; D6RIU4; D6RDX1
KTN1	-0.5491133	+	0.29501763		56	149.61	Q86UP2-2; Q86UP2-4; Q86UP2; Q86UP2-3; G3V4Y7; B7Z6P3; H0YJZ8; G3V5G2; G3V5P0; H0YJP2; H0YJV5; G8JLP4; Q9Y4F3-3; Q9Y4F3-4; Q9Y4F3-5; Q9Y4F3	Q86UP2-2; Q86UP2-4; Q86UP2; Q86UP2-3
DCAF8	-0.0780305		3.05264211	+	3	46.52	V9GY54; G3V3G9; Q5TAQ9; Q5TAQ9-2; Q5TAQ8	V9GY54; G3V3G9; Q5TAQ9; Q5TAQ9-2
GDI1	-0.4588619		1.14802301	+	12	50.58	P31150; G5E9U5	P31150; G5E9U5
LIFR	-0.5325536		0.75830311	+	25	123.74	P42702; D6RF33; H0YAF2	P42702
NUP107	-0.0538381		0.74364418	+	8	106.37	P57740; P57740-3; P57740-2; H0YG15; G3V1T4	P57740; P57740-3; P57740-2
FNDC3B	-0.5491979		0.89001858	+	5	132.89	Q53EP0; Q53EP0-2	Q53EP0; Q53EP0-2
USP33	-0.2367244		1.25344467	+	4	93.96	Q8TEY7-3; Q8TEY7-2; Q8TEY7; H0YCV3; H0YD08	Q8TEY7-3; Q8TEY7-2; Q8TEY7; H0YCV3; H0YD08
OSBPL8	-0.6827191		0.81721389	+	5	96.95	Q9BZF1-3; Q9BZF1-2; Q9BZF1; F8VUA7; F8VQX7	Q9BZF1-3; Q9BZF1-2; Q9BZF1; F8VUA7; F8VQX7
DNAJB12	-0.5971469		0.95546162	+	4	41.82	Q9NXW2; Q9NXW2-2; J3KPS0; V9GY70; V9GYN7	Q9NXW2; Q9NXW2-2; J3KPS0
MTMR6	-0.3672664		1.18618357	+	3	71.97	Q9Y217; Q9Y217-2	Q9Y217; Q9Y217-2
F11R	-0.1256516		1.04830599	+	4	32.58	Q9Y624; A0A087WY82; Q9Y624-2	Q9Y624; A0A087WY82; Q9Y624-2

Abbreviations: Mol. weight: molecular weight, ratio H/L: ratio heavy/light, IDs: identifications

Table S 10: Overview of the values of endogenous biotinylated proteins

Gene names	Protein names	Ratio H/L normalized LRRC59-fwd	Ratio H/L normalized LRRC59-rev	Ratio H/L normalized LRRC59-fwd B significant	Ratio H/L normalized LRRC59-rev B significant
MCCC2	Methylcrotonoyl-CoA carboxylase beta chain, mitochondrial	0.43935713	-0.0723917		
MCCC1	Methylcrotonoyl-CoA carboxylase subunit alpha, mitochondrial	0.57734424	-0.131013	+	
ACACB	Acetyl-CoA carboxylase 2; Biotin carboxylase	-0.0735602	-0.3954162		
ACACA	Acetyl-CoA carboxylase 1; Biotin carboxylase	-0.1019233	-0.0510554		
PCCA	Propionyl-CoA carboxylase alpha chain, mitochondrial	0.37417707	-0.128803		
PCCB	Propionyl-CoA carboxylase beta chain, mitochondrial	0.18256515	-0.1416211		

Abbreviations: fwd: forward, rev: reverse, ratio H/L: ratio heavy/light

E. Supplemental data corresponding to section 3.4

Table S 11: Raw data of rapamycin-induced dimerization assay using reporter $EGFP_2$-GST-M9-FKBP12 (figure 29)

Date	Plasmid DNA concentration [µg]	construct	Rapamycin treatment	responding cells of 100	responding cells (%)	Mean	Standard deviation
20180416	0.5	mCherry-FRB-Sec61β	1 minute	67	67	76.00	7.81
20180423	0.5	mCherry-FRB-Sec61β	1 minute	80	80		
20180420	0.5	mCherry-FRB-Sec61β	1 minute	81	81		
20180416	0.5	mCherry-FRB-Sec61β	2 minutes	91	91	95.67	4.16
20180423	0.5	mCherry-FRB-Sec61β	2 minutes	97	97		
20180420	0.5	mCherry-FRB-Sec61β	2 minutes	99	99		
20180416	0.5	mCherry-FRB-Sec61β	3 minutes	98	98	99.00	1.00
20180423	0.5	mCherry-FRB-Sec61β	3 minutes	99	99		
20180420	0.5	mCherry-FRB-Sec61β	3 minutes	100	100		
20180416	0.5	mCherry-FRB-Sec61β	4 minutes	93	93	97.00	3.61
20180423	0.5	mCherry-FRB-Sec61β	4 minutes	98	98		
20180420	0.5	mCherry-FRB-Sec61β	4 minutes	100	100		
20180416	0.5	mCherry-FRB-Sec61β	5 minutes	96	96	98.33	2.08
20180423	0.5	mCherry-FRB-Sec61β	5 minutes	100	100		
20180420	0.5	mCherry-FRB-Sec61β	5 minutes	99	99		
20180416	0.5	mCherry-FRB-Sec61β	6 minutes	97	97	97.67	0.58
20180423	0.5	mCherry-FRB-Sec61β	6 minutes	98	98		
20180420	0.5	mCherry-FRB-Sec61β	6 minutes	98	98		
20180416	0.5	mCherry-FRB-Sec61β	7 minutes	99	99	99.00	0.00
20180423	0.5	mCherry-FRB-Sec61β	7 minutes	99	99		
20180420	0.5	mCherry-FRB-Sec61β	7 minutes	99	99		
20180416	0.5	mCherry-FRB-Sec61β	8 minutes	94	94	97.33	3.06
20180423	0.5	mCherry-FRB-Sec61β	8 minutes	98	98		
20180420	0.5	mCherry-FRB-Sec61β	8 minutes	100	100		
20180416	0.5	mCherry-FRB-Sec61β	9 minutes	98	98	98.67	1.15
20180423	0.5	mCherry-FRB-Sec61β	9 minutes	100	100		
20180420	0.5	mCherry-FRB-Sec61β	9 minutes	98	98		
20180416	0.5	mCherry-FRB-Sec61β	10 minutes	97	97	98.67	1.53
20180423	0.5	mCherry-FRB-Sec61β	10 minutes	99	99		
20180420	0.5	mCherry-FRB-Sec61β	10 minutes	100	100		
20180416	0.5	mCherry-FRB-Sec22b	1 minute	47	47	39.33	11.59
20180423	0.5	mCherry-FRB-Sec22b	1 minute	45	45		
20180420	0.5	mCherry-FRB-Sec22b	1 minute	26	26		
20180416	0.5	mCherry-FRB-Sec22b	2 minutes	56	56	65.00	9.54
20180423	0.5	mCherry-FRB-Sec22b	2 minutes	64	64		
20180420	0.5	mCherry-FRB-Sec22b	2 minutes	75	75		
20180416	0.5	mCherry-FRB-Sec22b	3 minutes	80	80	75.67	5.13
20180423	0.5	mCherry-FRB-Sec22b	3 minutes	70	70		
20180420	0.5	mCherry-FRB-Sec22b	3 minutes	77	77		
20180416	0.5	mCherry-FRB-Sec22b	4 minutes	80	80	78.67	2.31
20180423	0.5	mCherry-FRB-Sec22b	4 minutes	76	76		
20180420	0.5	mCherry-FRB-Sec22b	4 minutes	80	80		
20180416	0.5	mCherry-FRB-Sec22b	5 minutes	75	75	79.00	3.46
20180423	0.5	mCherry-FRB-Sec22b	5 minutes	81	81		
20180420	0.5	mCherry-FRB-Sec22b	5 minutes	81	81		
20180416	0.5	mCherry-FRB-Sec22b	6 minutes	69	69	74.33	7.57
20180423	0.5	mCherry-FRB-Sec22b	6 minutes	83	83		

Date	Plasmid DNA concentration [µg]	construct	Rapamycin treatment	responding cells of 100	responding cells (%)	Mean	Standard deviation
20180420	0.5	mCherry-FRB-Sec22b	6 minutes	71	71		
20180416	0.5	mCherry-FRB-Sec22b	7 minutes	79	79		
20180423	0.5	mCherry-FRB-Sec22b	7 minutes	82	82	77.33	5.69
20180420	0.5	mCherry-FRB-Sec22b	7 minutes	71	71		
20180416	0.5	mCherry-FRB-Sec22b	8 minutes	80	80		
20180423	0.5	mCherry-FRB-Sec22b	8 minutes	83	83	80.67	2.08
20180420	0.5	mCherry-FRB-Sec22b	8 minutes	79	79		
20180416	0.5	mCherry-FRB-Sec22b	9 minutes	69	69		
20180423	0.5	mCherry-FRB-Sec22b	9 minutes	79	79	74.33	5.03
20180420	0.5	mCherry-FRB-Sec22b	9 minutes	75	75		
20180416	0.5	mCherry-FRB-Sec22b	10 minutes	70	70		
20180423	0.5	mCherry-FRB-Sec22b	10 minutes	85	85	77.67	7.51
20180420	0.5	mCherry-FRB-Sec22b	10 minutes	78	78		
20180416	0.5	LMAN2-FRB-mCherry	1 minute	15	15		
20180423	0.5	LMAN2-FRB-mCherry	1 minute	27	27	22.00	6.24
20180420	0.5	LMAN2-FRB-mCherry	1 minute	24	24		
20180416	0.5	LMAN2-FRB-mCherry	2 minutes	20	20		
20180423	0.5	LMAN2-FRB-mCherry	2 minutes	52	52	40.67	17.93
20180420	0.5	LMAN2-FRB-mCherry	2 minutes	50	50		
20180416	0.5	LMAN2-FRB-mCherry	3 minutes	28	28		
20180423	0.5	LMAN2-FRB-mCherry	3 minutes	58	58	46.67	16.29
20180420	0.5	LMAN2-FRB-mCherry	3 minutes	54	54		
20180416	0.5	LMAN2-FRB-mCherry	4 minutes	51	51		
20180423	0.5	LMAN2-FRB-mCherry	4 minutes	63	63	57.00	6.00
20180420	0.5	LMAN2-FRB-mCherry	4 minutes	57	57		
20180416	0.5	LMAN2-FRB-mCherry	5 minutes	42	42		
20180423	0.5	LMAN2-FRB-mCherry	5 minutes	66	66	56.33	12.66
20180420	0.5	LMAN2-FRB-mCherry	5 minutes	61	61		
20180416	0.5	LMAN2-FRB-mCherry	6 minutes	63	63		
20180423	0.5	LMAN2-FRB-mCherry	6 minutes	71	71	68.67	4.93
20180420	0.5	LMAN2-FRB-mCherry	6 minutes	72	72		
20180416	0.5	LMAN2-FRB-mCherry	7 minutes	65	65		
20180423	0.5	LMAN2-FRB-mCherry	7 minutes	86	86	74.67	10.60
20180420	0.5	LMAN2-FRB-mCherry	7 minutes	73	73		
20180416	0.5	LMAN2-FRB-mCherry	8 minutes	59	59		
20180423	0.5	LMAN2-FRB-mCherry	8 minutes	75	75	66.67	8.02
20180420	0.5	LMAN2-FRB-mCherry	8 minutes	66	66		
20180416	0.5	LMAN2-FRB-mCherry	9 minutes	65	65		
20180423	0.5	LMAN2-FRB-mCherry	9 minutes	73	73	68.33	4.16
20180420	0.5	LMAN2-FRB-mCherry	9 minutes	67	67		
20180416	0.5	LMAN2-FRB-mCherry	10 minutes	57	57		
20180423	0.5	LMAN2-FRB-mCherry	10 minutes	75	75	66.00	9.00
20180420	0.5	LMAN2-FRB-mCherry	10 minutes	66	66		
20180416	0.5	DDOST-FRB-mCherry	1 minute	44	44		
20180423	0.5	DDOST-FRB-mCherry	1 minute	59	59	58.67	14.50
20180420	0.5	DDOST-FRB-mCherry	1 minute	73	73		
20180416	0.5	DDOST-FRB-mCherry	2 minutes	55	55		
20180423	0.5	DDOST-FRB-mCherry	2 minutes	90	90	77.33	19.40
20180420	0.5	DDOST-FRB-mCherry	2 minutes	87	87		
20180416	0.5	DDOST-FRB-mCherry	3 minutes	90	90		
20180423	0.5	DDOST-FRB-mCherry	3 minutes	100	100	95.33	5.03
20180420	0.5	DDOST-FRB-mCherry	3 minutes	96	96		
20180416	0.5	DDOST-FRB-mCherry	4 minutes	93	93		
20180423	0.5	DDOST-FRB-mCherry	4 minutes	100	100	97.33	3.79
20180420	0.5	DDOST-FRB-mCherry	4 minutes	99	99		
20180416	0.5	DDOST-FRB-mCherry	5 minutes	96	96		
20180423	0.5	DDOST-FRB-mCherry	5 minutes	97	97	97.00	1.00
20180420	0.5	DDOST-FRB-mCherry	5 minutes	98	98		
20180416	0.5	DDOST-FRB-mCherry	6 minutes	95	95		
20180423	0.5	DDOST-FRB-mCherry	6 minutes	98	98	97.67	2.52
20180420	0.5	DDOST-FRB-mCherry	6 minutes	100	100		
20180416	0.5	DDOST-FRB-mCherry	7 minutes	98	98		
20180423	0.5	DDOST-FRB-mCherry	7 minutes	98	98	98.00	0.00
20180420	0.5	DDOST-FRB-mCherry	7 minutes	98	98		
20180416	0.5	DDOST-FRB-mCherry	8 minutes	99	99		
20180423	0.5	DDOST-FRB-mCherry	8 minutes	100	100	99.00	1.00
20180420	0.5	DDOST-FRB-mCherry	8 minutes	98	98		
20180416	0.5	DDOST-FRB-mCherry	9 minutes	96	96		
20180423	0.5	DDOST-FRB-mCherry	9 minutes	98	98	97.33	1.15
20180420	0.5	DDOST-FRB-mCherry	9 minutes	98	98		

Date	Plasmid DNA concentration [µg]	construct	Rapamycin treatment	responding cells of 100	responding cells (%)	Mean	Standard deviation
20180416	0.5	DDOST-FRB-mCherry	10 minutes	98	98	98.00	1.00
20180423	0.5	DDOST-FRB-mCherry	10 minutes	99	99		
20180420	0.5	DDOST-FRB-mCherry	10 minutes	97	97		
20180416	1	mCherry-FRB-Ube2j1	1 minute	28	28	30.00	6.24
20180423	1	mCherry-FRB-Ube2j1	1 minute	37	37		
20180420	1	mCherry-FRB-Ube2j1	1 minute	25	25		
20180416	1	mCherry-FRB-Ube2j1	2 minutes	50	50	40.00	12.49
20180423	1	mCherry-FRB-Ube2j1	2 minutes	44	44		
20180420	1	mCherry-FRB-Ube2j1	2 minutes	26	26		
20180416	1	mCherry-FRB-Ube2j1	3 minutes	50	50	47.00	3.61
20180423	1	mCherry-FRB-Ube2j1	3 minutes	48	48		
20180420	1	mCherry-FRB-Ube2j1	3 minutes	43	43		
20180416	1	mCherry-FRB-Ube2j1	4 minutes	62	62	61.67	1.53
20180423	1	mCherry-FRB-Ube2j1	4 minutes	60	60		
20180420	1	mCherry-FRB-Ube2j1	4 minutes	63	63		
20180416	1	mCherry-FRB-Ube2j1	5 minutes	73	73	65.33	7.51
20180423	1	mCherry-FRB-Ube2j1	5 minutes	58	58		
20180420	1	mCherry-FRB-Ube2j1	5 minutes	65	65		
20180416	1	mCherry-FRB-Ube2j1	6 minutes	75	75	67.33	7.51
20180423	1	mCherry-FRB-Ube2j1	6 minutes	67	67		
20180420	1	mCherry-FRB-Ube2j1	6 minutes	60	60		
20180416	1	mCherry-FRB-Ube2j1	7 minutes	75	75	68.67	5.51
20180423	1	mCherry-FRB-Ube2j1	7 minutes	66	66		
20180420	1	mCherry-FRB-Ube2j1	7 minutes	65	65		
20180416	1	mCherry-FRB-Ube2j1	8 minutes	80	80	73.33	5.77
20180423	1	mCherry-FRB-Ube2j1	8 minutes	70	70		
20180420	1	mCherry-FRB-Ube2j1	8 minutes	70	70		
20180416	1	mCherry-FRB-Ube2j1	9 minutes	90	90	71.67	17.56
20180423	1	mCherry-FRB-Ube2j1	9 minutes	70	70		
20180420	1	mCherry-FRB-Ube2j1	9 minutes	55	55		
20180416	1	mCherry-FRB-Ube2j1	10 minutes	86	86	74.67	9.87
20180423	1	mCherry-FRB-Ube2j1	10 minutes	68	68		
20180420	1	mCherry-FRB-Ube2j1	10 minutes	70	70		
20180416	1	mCherry-FRB-Ube2j2	1 minute	40	40	35.00	16.09
20180423	1	mCherry-FRB-Ube2j2	1 minute	48	48		
20180420	1	mCherry-FRB-Ube2j2	1 minute	17	17		
20180416	1	mCherry-FRB-Ube2j2	2 minutes	58	58	47.67	11.06
20180423	1	mCherry-FRB-Ube2j2	2 minutes	49	49		
20180420	1	mCherry-FRB-Ube2j2	2 minutes	36	36		
20180416	1	mCherry-FRB-Ube2j2	3 minutes	65	65	54.33	9.29
20180423	1	mCherry-FRB-Ube2j2	3 minutes	50	50		
20180420	1	mCherry-FRB-Ube2j2	3 minutes	48	48		
20180416	1	mCherry-FRB-Ube2j2	4 minutes	69	69	59.33	10.60
20180423	1	mCherry-FRB-Ube2j2	4 minutes	48	48		
20180420	1	mCherry-FRB-Ube2j2	4 minutes	61	61		
20180416	1	mCherry-FRB-Ube2j2	5 minutes	73	73	61.33	11.06
20180423	1	mCherry-FRB-Ube2j2	5 minutes	51	51		
20180420	1	mCherry-FRB-Ube2j2	5 minutes	60	60		
20180416	1	mCherry-FRB-Ube2j2	6 minutes	70	70	64.33	5.51
20180423	1	mCherry-FRB-Ube2j2	6 minutes	64	64		
20180420	1	mCherry-FRB-Ube2j2	6 minutes	59	59		
20180416	1	mCherry-FRB-Ube2j2	7 minutes	69	69	62.00	7.00
20180423	1	mCherry-FRB-Ube2j2	7 minutes	55	55		
20180420	1	mCherry-FRB-Ube2j2	7 minutes	62	62		
20180416	1	mCherry-FRB-Ube2j2	8 minutes	67	67	62.00	5.00
20180423	1	mCherry-FRB-Ube2j2	8 minutes	62	62		
20180420	1	mCherry-FRB-Ube2j2	8 minutes	57	57		
20180416	1	mCherry-FRB-Ube2j2	9 minutes	67	67	66.00	1.73
20180423	1	mCherry-FRB-Ube2j2	9 minutes	67	67		
20180420	1	mCherry-FRB-Ube2j2	9 minutes	64	64		
20180416	1	mCherry-FRB-Ube2j2	10 minutes	57	57	58.00	1.73
20180423	1	mCherry-FRB-Ube2j2	10 minutes	57	57		
20180420	1	mCherry-FRB-Ube2j2	10 minutes	60	60		

F. Abbreviations

Table S 12: Abbreviations

Abbreviation	Name
α	alpha (in case of antibodies: anti-)
aa	amino acid
ADP	Adenosine-5-diphosphate
ATP	Adenosine-5-phosphate
β	beta
BFP	blue fluorescent protein
BSA	bovine serum albumin
c-Myc	polypeptide protein tag with the sequence EQKLISEEDL
C-terminus	carboxy terminus
CAML	calcium-modulating cyclophilin ligand
cDNA	complementary DNA
CIP2A	Cancerous inhibitor of PP2A
cNLS	classical nuclear localization signal
DAPI	4´,6-diamidino-2-phenylindole
ddH_2O	Deionized distilled water
DDOST	Dolichyl-diphosphooligosaccharide-protein glycosyltransferase 48 kDa subunit
DNA	Deoxyribonucleic acid
dNTP	2`-desoxynucleoside-5´-triphosphate
E. coli	*Escherichia coli*
EDMD	Emery-Dreifuss muscular dystrophy
EDTA	ethylenediaminetetraacetic acid
(E)GFP	(enhanced) green fluorescence protein
EK-RM	EDTA/high salt treated rough microsomes
EMC	ER-membrane protein complex
ER	endoplasmic reticulum
ERAD	endoplasmic reticulum-associated degradation
FBS	fetal bovine serum
FG	phenylalanine - glycine
FGF1/2	fibroblast growth factor 1/2
FKBP12	12 kDa FK506/rapamycin binding protein
FLAG	polypeptide protein tag with the sequence DYKDDDDK
FLIP	fluorescence loss in photobleaching
FRAP	fluorescence recovery after photobleaching
FRB domain	FKBP12-rapamycin binding domain
γ	gamma
GDP	Guanosine-5´-diphosphate
GET	guided entry of tail-anchored proteins
GST	Glutathione S-transferase
GTP	Guanosine-5´-triphosphate
HA	hemagglutinin
His	histidine tag
HRP	horseradish peroxidase
IBB domain	importin β binding domain
INM	inner nuclear membrane
KASH	Klarsicht, ANC-1, Syne homolog
kDa	kilo dalton
LAP2β	Lamina-associated polypeptide 2 beta
LB	Luria-Bertani
LBR	Lamin B receptor
LEM domain	LAP2, emerin, MAN1 domain
LINC	linker of nucleoskeleton and cytoskeleton
LMAN2	Vesicular integral-membrane protein VIP36
LMNA	gene coding for lamin A and C
LRR	leucine rich repeat
LRRC59	leucine rich repeat containing protein 59
M9	PY-NLS initially described for hnRNPA1
MBP	maltose binding protein
MCS	multiple cloning site
mock	control treated sample
mRNA	messenger ribonucleic acid
mTOR or FRAP	FKBP12-rapamycin associated protein
N-terminus	amino terminus

Abbreviation	Name
NE	nuclear envelope
NES	nuclear export signal
NET	nuclear envelope transmembrane protein
NLS	nuclear localization signal
NPC	nuclear pore complex
NPCs	nuclear pore complexes
Nups	nucleoporins
ONM	outer nuclear membrane
op	opsin-tag
op G	glycosylated opsin-tag
PAGE	polyacrylamide gel electrophoresis
PBS	phosphate buffered saline
PCR	polymerase chain reaction
PNGase F	peptide-N-Glycosidase F
PP2A	protein phosphatase 2A
Ran	Ras-related nuclear protein
RanGAP	RanGTPase-activating protein
RanGEF	Ran guanine nucleotide exchange factor
RAPIDS	rapamycin- and APEX-dependent identification of proteins by SILAC
RM	rough microsomes
RNA	ribonucleic acid
rpm	rotations per minute
S. cerevisiae	*Saccharomyces cerevisiae*
SDS	sodium dodecyl sulfate
Sec22b	vesicle-trafficking protein Sec22b
Sec61β	protein transport protein Sec61 subunit beta
SILAC	stable isotope labeling by amino acids in cell culture
siRNA	small interfering RNA
SND	SRP-independent targeting
SRP	signal recognition particle
SV40	simian virus 40
T-RM	trypsin treated rough microsomes
TA	tail-anchored
TMD	transmembrane domain
TRC40	transmembrane domain recognition complex of 40 kDa (ASNA1)
Ube2j1	Ubiquitin-conjugating enzyme E2 J1
Ube2j2	Ubiquitin-conjugating enzyme E2 J2
v/v	volume per volume
w/v	weight per volume
WRB	tryptophan-rich basic protein
WT	wild type
ZZ	protein tag (*S. aureus* protein A IgG-binding domain)

Table S 13: Measurement conventions

Measurements of	Abbreviation	Unit
atomic mass	Da	Dalton
electric current	A	ampere
electricity	V	Volt
enzyme´s catalytic activity	U	Unit
molarity	M	molar
temperature	°C	degree Celsius
time	h	hour
time	min	minute
time	sec	second
volume	l	liter
weight	g	gram
Prefix symbol	**Prefix name**	**Multiplier**
n	nano-	x 10^{-9}
µ	micro-	x 10^{-6}
m	milli-	x 10^{-3}
k	kilo-	x 10^{3}
M	mega-	x 10^{6}

Acknowledgements

Mein Dank gilt Herrn Prof. Dr. Ralph H. Kehlenbach für die Möglichkeit an diesem spannenden und interessanten Projekt mit eigenen Ideen aber auch mit Unterstützung arbeiten zu können.

Das Projekt wurde finanziert durch Zuschüsse der Deutschen Forschungsgemeinschaft und des Sonderforschungsbereiches SFB1190 „Compartmental Gates and Contact Sites in Cells“ an Herrn Prof. Dr. Ralph H. Kehlenbach.

Danken möchte ich außerdem den Mitgliedern meines Thesis Komitees, Herrn Prof. Dr. Michael Meinecke und Herrn Prof. Dr. Steven Johnsen, für ihre Beiträge, Hilfe und Unterstützung.

Besonders danken möchte ich allen ehemaligen und aktuellen Kollegen des Instituts für Molekularbiologie für ihre Hilfsbereitschaft und die positive Arbeitsatmosphäre. Ein Arbeitsklima, das zur eigenen Produktivität beiträgt, Freude an der Arbeit, selbst in harten Zeiten, schafft und positive Gedanken und Motivation ermöglicht, ist von unschätzbarem Wert.

In diesem Zusammenhang möchte ich mich bei den Freunden bedanken, die ich während meiner Doktorarbeit im Institut gefunden habe. Ich bin besonders Priyanka Choudhury, Javier Coy-Vergara, Jimena Dávila Gallesio, Markus Kilisch, Julia Menzel und Jhon Rivera-Monroy für die anregenden Diskussionen über unsere Projekte, die konstruktiven Lösungsvorschläge, den Kaffee zwischendurch, die Unternehmungen außerhalb des Labors, die aufmunternde Worte und die gegenseitige Unterstützung dankbar.

Des Weiteren möchte ich mich bei der Göttinger Graduiertenschule für Neurowissenschaften, Biophysik und Molekulare Biowissenschaften (GGNB) bedanken. Durch die Teilnahme an Kursen und Seminaren konnte ich meine Kenntnisse in Wissenschaft und wichtigen Schlüsselqualifikationen wie Kommunikation und Persönlichkeitsentwicklung erweitern. Außerdem hatte ich eine unvergessliche Zeit bei den Ausflügen, den Retreats und den Stammtischen der Programme „Molecular Biology of Cells“ und „Biomolecules: Structure – Function – Dynamics“.

Darüber hinaus möchte ich mich bei Dr. Paul Charlton bedanken, der mir als Coach für „international communication, career and productivity skills“ wertvolle Eigenschaften und Möglichkeiten zur persönlichen und beruflichen Weiterentwicklung aufgezeigt hat.

Danken möchte ich außerdem meinen Freunden, die mir immer Verständnis und Unterstützung entgegengebracht haben, auch wenn nur wenig Zeit während der Doktorarbeit für sie blieb. Freundschaft ist eine Bereicherung des Lebens, die es wert ist zu pflegen.

Herzlich bedanken möchte ich mich bei meinen Freunden Dr. Claudia Wollny, Dr. Marret Müller, Dr. Evelina De Laurentiis und Dr. Matthias Grunwald, dass sie sich die Zeit genommen haben, meine Dissertation Korrektur zu lesen.

Darüber hinaus, bin ich über die Töpferwerkstatt des Kulturzentrums KAZ Göttingen sehr dankbar, in der ich mich während meiner Doktorarbeit einbringen konnte und die mir einen wichtigen kreativen und handwerklichen Ausgleich ermöglicht.

Mein größter Dank gilt meiner Familie für ihre uneingeschränkte Unterstützung während meiner kompletten schulischen und universitären Ausbildung. Mum und Dad, Sonja und Onkel Michael, ich danke Euch, dass ihr da wart, wenn ich Euch gebraucht habe.

Marina